RESPONSE OF SOIL-PILE SYSTEMS

TO SEISMIC WAVES

RESPONSE OF SOIL-PILE SYSTEMS
TO
SEISMIC WAVES

by

GOPINATHAN PARAMESWARAN NAIR
B.E.(HONS), M.Sc.(ENG)

A Thesis

Submitted to the School of Graduate Studies

in Partial Fulfillment of the requirements

for the degree

Doctor of Philosophy

McMaster University

DOCTOR OF PHILOSOPHY (1975)

(Civil Engineering and Engineering Mechanics)

McMASTER UNIVERSITY,
Hamilton, Ontario.

TITLE: Response of Soil-Pile Systems to Seismic Waves.

AUTHOR: Gopinathan Parameswaran Nair, B.E.(Hons), Madras Univ., India
M.Sc.(Eng), Kerala Univ., India

SUPERVISOR: Dr. John J. Emery

NUMBER OF PAGES: xxii, 252.

ABSTRACT

A finite element method that utilizes boundary conditions from wave propagation considerations is given for predicting the seismic response of a pile embedded in soil. The response of the system and the stress distribution in the soil adjacent to and beneath the pile are resolved, and these provide a means of appraising the behaviour of a soil-pile system during an earthquake. The three directional components of the earthquake excitation are considered. The soil-pile system is idealized as an axisymmetric structure subjected to nonsymmetric loading to simplify the computations.

Records of ground motions during recent earthquakes have clearly demonstrated the significance of local soil conditions on the amplitude and frequency characteristics of seismic motions. For large epicentral distances, the usual assumption of energy transfer by means of vertically propagating shear waves is valid. However, for sites nearer to the source the direction of shear wave propaga~~tion~~ may be inclined and surface waves also contribute to the ground motions. These aspects of the seismic motions are considered.

The spatial variations in seismic motions are computed using wave propagation theory and assuming that the earthquake energy is transferred through the soil layers by shear waves and Rayleigh waves. Spatial variations in motion are compared for various epicentral distances and wave propagation assumptions. It is shown that the surface wave

makes a significant contribution to the response at near sites, while the effect of inclining the shear wave propagation is of secondary importance. The method and programs are general so that they can be used for a variety of problems. Dimensions of the soil-pile system are adopted so that "free field" conditions can be assumed at the boundary. The seismic motion record for each boundary node of the discretized structure is computed and used as the input for the full finite element dynamic analysis which utilizes a step-by-step procedure.

It was found that the single pile foundation considerably reduced the responses transferred to the structure. The method of analysis was used to consider the pore pressures developed in the case of saturated soils around a single pile. The behaviour of a pile-saturated sand system during the San Fernando Earthquake showed that the sand around the pile liquefied. When a pile-saturated clay system was subjected to the same earthquake, there was no sign of liquefaction. These results are in qualitative agreement with field observations.

ACKNOWLEDGEMENTS

In presenting this thesis, the author wishes to record his indebtedness to the Association of Universities and Colleges of Canada for a Commonwealth Fellowship that provided financial support for much of this work, and to McMaster University for providing the excellent computing facilities that made much of the work possible.

The author would also like to thank the following individuals:

- His Supervisor, Dr. J.J. Emery, for his continued encouragement and guidance at every stage of the study.
- Dr. A.C. Heidebrecht, Dr. W.K. Tso and Dr. P.M. Clifford for their valuable suggestions and advice.
- Jack van Nynatten for his assistance in preparing the final drawings.
- Sheelagh Courtney for typing the manuscript.
- and finally, and personally most important, his wife, Dr. Vimala P. Nair, for proofing the manuscript and for her understanding, encouragement and interest in the work.

TABLE OF CONTENTS

Page

Page

Page

LIST OF TABLES

LIST OF FIGURES

LIST OF SYMBOLS

A	-Area of cross section.
A_1, A_{1R}	-Amplification factor for surface response.
$[A]$	-Transformation matrix relating generalized and nodal displacements; also, matrix used in Rayleigh wave propagation, defined by Equation A:44.
$[A_m]$, $[a_m]$	-Matrices relating interface responses due to Rayleigh wave propagation, defined by Equations A:40 to A:43.
A_{ij}, $(A_m)_{ij}$, $(a_m)_{ij}$	-Elements of matrices $[A]$, $[A_m]$, $[a_m]$.
$\{a\}$	-Vector used in the step-by-step method.
$[B]$	-Matrix relating strains and displacements.
$\{b\}$	-Vector used in the step-by-step method.
c	-Rayleigh wave propagational velocity
C, C_1, C_2, C_3, C_4	-Constants.
$[C]$	-Damping matrix.
$[C^{-1}]$	-Transformation matrix relating the generalized displacement coordinates and nodal displacements.
d	-Horizontal distance
D	-Diameter
$[D]$	-Constitutive matrix for stress-strain relations; also, diagonal matrix.
$[D_m]$	-Matrix used in Rayleigh wave propagation, defined by Equation A:36.
e	-Dilatation; volumetric strain

e_N	-Volume change.
E	-Young's modulus.
$\bar{E}$	-Effective Young's modulus
$[E_m]$	-Matrix used in Rayleigh wave propagation, defined by Equation A:38.
f_t	-Splitting tensile stress.
$F(z)$	-Function used in Rayleigh wave propagation.
F_1, F_2, F_3, F_4	-Functions used in Rayleigh wave propagation.
F_k	-Transmitted component of kth interface response.
F_r, F_θ, F_z	-Forces in the radial, circumferential and axial directions respectively.
F_{rn}, $F_{\theta n}$, F_{zn}	-Forces in the radial, circumferential and axial directions respectively in the nth harmonic.
$[F]$	-Matrix used in the step-by-step method.
$\{f\}_t$	-Exciting force vector.
$\{F^*\}$	-Modified load vector.
$\{F\}_N$	-Nodal load vector.
g	-Acceleration due to gravity
G	-Shear modulus; specific gravity
$G(z)$	-Function used in Rayleigh wave propagation.
h_k	-Depth of kth layer.
H_N	-Pore pressure quantity.
$[H]$	-Matrix relating the balancing displacements to the boundary displacements.
i	$-\sqrt{-1}$

$[J]$	-Matrix relating surface response to dilatations and rotations in Rayleigh wave propagation.
k	-Wave number.
k_r, k_θ, k_z	-Stiffness matrix terms for linkage element.
K	-Index depending on the plasticity index in Equation 8:16.
K_B	-Bulk modulus.
$[k]$	-Element stiffness matrix.
$[k_s]$	-Stiffness matrix of linkage element.
$[k']$	-Portion of stiffness matrix $[k]$ due to pore pressure.
$[k^*]$	-Modified stiffness matrix for quadrilaterial ring element.
$[K]$	-Global stiffness matrix.
ℓ, ℓ'	-Length
L	-Number of sublayers in Ray tracing technique; also, the harmonic of the highest order.
$[L]$	-Lower triangular matrix.
m	-Antisymmetric harmonic.
m_1, m_2	-Constants for medium in the matrix product in Equation C:4.
m_i, m_j, m_k	-Contributions of the mass of the triangular ring element to nodes i, j and k.
$[m]$	-Element mass matrix.
$[M]$	-Mass matrix.
n	-Symmetric harmonic.

P_m	-Function used in Rayleigh wave propagation.
$\{p\}$	-Vector of forcing functions in dynamic analysis.
$\{P\}$	-Load vector.
q	-Function used in Rayleigh wave propagation.
Q_m	-Function used in Rayleigh wave propagation.
r	-Radius; radial direction.
r, r_a, r_b r_m, r_{am}, r_{bm}	-Functions used in Rayleigh wave propagation.
R_k	-Reflected component of kth interface response.
R_u, R_d	-Upward and downward reflection coefficients.
s	-Function used in Rayleigh wave propagation.
t	-Time.
t_j	-Time for the jth arrival of signal.
t_ℓ	-Time lag.
$t_{x\ell}, t_{y\ell}$ $t_{h\ell}, t_{v\ell}$	-Time lags in the x, y, horizontal and vertical directions respectively.
T	-Period.
T_m, T_{vm}	-Transfer functions for horizontal and vertical responses of the mth interface due to Rayleigh wave propagation.
T_u, T_d	-Upward and downward transmission coefficients.
u	-Displacement in the radial or x direction.
u_n	-Radial displacement in the nth harmonic.
$\ddot{u}_g$	-Earthquake ground acceleration.
$\ddot{u}_{rn}, \ddot{u}_{\theta n}, \ddot{u}_{zn}$	-Acceleration coefficients in the nth harmonic in the [illegible] and [illegible]

U	-Strain energy.
$\{u\}_N$	-Nodal displacement vector.
$\{u\}_t$	-Dynamic displacement vector.
$\{U\}$	-Total response vector.
$\{U_g\}$	-Boundary response vector.
$\{U_{gg}\}$	-Vector of balancing displacements, defined by Equation 8:8
$\{U_i\}$	-Total response vector for interior nodes.
v	-Circumferential displacement.
v_n	-Circumferential displacement in the nth harmonic.
w	-Axial or vertical displacement.
w_n	-Axial displacement in the nth harmonic.
W	-Work done.
$\ddot{x}_1$, $\ddot{x}_2$	-E-W and N-S components of the ground response respectively.
z	-Depth.
α	-P-wave velocity; also, empirical constant in Proportional damping matrix.
α_1 to α_9	-Generalized displacement coordinates
α_{1n} to α_{9n}	-Generalized displacement coordinates in the nth harmonic.
β	-Shear wave velocity; also, empirical constant in Proportional damping matrix.
γ	-Shear strain.
δ	-Delta function; increment; and also, distance in degrees.

ϵ	-Strain.
ζ	-Pore pressure.
θ	-Angle; angle of incidence.
λ_1 to λ_{11}	-Axisymmetric integrals.
μ	-Impedance ratio.
ν	-Poisson's ratio.
$\bar{\nu}$	-Effective Poisson's ratio.
ξ	-Contribution of shear waves in the response; also, scalar multiplier.
ρ	-Mass density.
σ	-Total stress.
$\bar{\sigma}$	-Effective stress.
τ	-Shear stress.
ω	-Frequency in radians per second.
Δt	-Time interval used in the step-by-step method for computation.
ΔT	-Time interval used in the step-by-step methods for printing results.

<u>Superscripts</u>

$\ddot{}$	-Second derivative with respect to time.
$\dot{}$	-First derivative with respect to time.
T	-Transpose of a matrix or vector.
-1	-Inverse of a matrix.

Subscripts

A, B, C, D	-Stations A, B, C and D.
b,e	-Beginning and end of time interval respectively.
h	-Horizontal direction.
i	-Row number,; also, node i
j	-Column number; also, node j
k	-Node k; also, layer or interface k
ℓ	-Lag.
m	-m^{th} antisymmetric harmonic; layer or interface m
n	-n^{th} symmetric harmonic; layer or interface n
R	-Radial direction; also, rock.
θ	-Circumferential direction.
v	-Vertical direction.
x, y	-E-W and N-S directions.
z	-Axial direction.

CHAPTER I

IMPORTANCE OF SOIL-PILE INTERACTION DURING EARTHQUAKES

1-A INTRODUCTION

Most building codes consider that the dynamic response of a structure depends primarily on the ground motion and on the dynamic characteristics of the structure itself [19]. The structure is assumed to rest on a rigid base and a recorded ground motion is fed in at the base level. Thus, the dynamic characteristics of the foundation as well as any coupling between the structure and the foundation is often neglected. Many codes suggest empirical increases in computed seismic loads for less firm soils [59].

Within the past few years, several researchers have directed their efforts towards studying the importance of soil structure interaction on the response of structures [26,27,66,72,76]. The damage due to shaking on different soils depends not on the soil conditions alone, as many codes suggest, but on the relationship between the dynamic properties of the structure and foundation soils. In the case of more flexible structures, the coupling effects are not significant [25], while a coupled analysis is required for very stiff and heavy structures [28].

For a variety of reasons, structures may not be directly supported on soil; instead, they may rest on a group of piles, which may

be point bearing piles, friction piles or combined point bearing and friction piles. A rational approach for evaluating the seismic response of such a system must include the study of the three-dimensional soil-pile-structure interaction. Significant work in this field has been carried out at Berkeley by Parmalee, et al [67,93]. The seismic effects on a bridge structure supported on long piles extending through deep sensitive clays were reported based on the dynamic response of the system in the direction of the longitudinal axis of the bridge. This work did not consider three-dimensional effects.

Records of ground motions in some recent earthquakes have shown that there are spatial variations in seismic motions [46,80,96]. In general, a seismic wave will propagate upwards through rocks, inclined with respect to a vertical line [87] and there may be spatial variations in all three directions. The response problem should thus be treated as three-dimensional.

A mathematical model capable of predicting the response of the soil-pile-structure interaction system must be of general nature. The finite element method [16,98] seems to be the most suitable method for problems of this nature. However, at the present stage of development, neither the finite element method nor the computers used in its application have progressed enough to economically solve the general three-dimensional problem of a structure on a group of piles.

The available information relating to deep foundations is far from being complete for interpreting the behaviour of a group of piles, even during static loading. A method of explaining the characteristics

of a group of piles with many limitations was developed by Pichumani and D'Appolonia [70]. The extension of this method to more complex systems imposes serious problems.

A logical beginning for a new discrete model is to consider relatively idealized conditions which provide an opportunity to correctly draw some broad conclusions. Once the solution to a single pile-soil interaction problem is feasible, it would be of use in the future to extend the type of solution to a group of piles or a soil-pile-structure interaction system. The development of this thesis is based on this conviction and thus deals with solutions for somewhat ideal situations.

1-B NEED FOR TRAVELLING SEISMIC WAVE SOLUTION

The earthquake motions in the soil at any depth in a particular location depend on the nature of incoming seismic waves in addition to some other conditions [33]. These waves travel through a number of geologic formations and undergo multiple reflections, refractions and dispersions. The types of waves and their relative contributions to the ground motion are dependent on the epicentral distance and the focal depth [17,87,92,96]. At a site in the near-earthquake region the motions will be composed of several waves propagating at various velocities and spanning a wide range of frequencies. In the case of a distant site, the contributions to the motion by the various types of seismic waves may not overlap and then there may not be any need to account for their combined effect. As a result of all these characteristics, there are spatial variations in the

motions in all the three directions. These spatial variations in the motions should be accounted for in order that a better representation of the problem be obtained.

In the case of the soil-pile system, the first step is to evaluate the seismic motions along the boundary of the system. It is reasonable to assume that at some distance from the pile, the ground motions are independent of the pile's influence; that is, "free field" conditions can be considered as boundary values. The dimensions of the soil-pile system are chosen so that this condition is satisfied. The motions along the boundary of the soil-pile system may be computed from a study of the seismic waves and fed in as input for the dynamic analysis. This process satisfies the compatibility conditions at the boundary; the motion at any point on the boundary of the system is the same as that obtained from the travelling seismic wave solution. Without such a study of travelling seismic waves, continuity is not satisfied at the boundaries of the soil-pile system.

1-C AXISYMMETRIC IDEALIZATION

There are many complexities in the incoming seismic waves as well as irregularities and inhomogeneities in the geometric configuration and material properties of the local subsoils. Therefore, it is necessary to commence the theoretical studies with a simple, idealized model. A conventional model for the earth's crust consists of many homogeneous, spherically stratified layers. As far as studies of a single pile and the local subsoils around it are concerned, it is enough to assume a

simpler model consisting of linear, homogeneous, horizontally stratified layers [92, 97]. Then, the layer boundaries are ideal planes extending to infinity in both horizontal directions.

In order to correctly evaluate the behaviour of the soil-pile system, it is imperative to include the three-dimensional components of the earthquake excitation. However, it is possible to simplify the analytical work by assuming that the soil-pile system is an axisymmetric structure that is subjected to non-axisymmetric excitation. This idealization is possible because of the axisymmetric geometry of the pile and the assumption of horizontal layer boundaries. This axisymmetric idealization results in computational advantages and significant reductions in the time required for the analysis.

1-D TYPES OF PILES

There are many types of piles presently being used all over the world. Notwithstanding this, most of these various types of piles come under one of the two basic categories of either drilled or driven piles. As the construction procedures for these two types of piles differ considerably, resulting in different residual stresses, they should be treated separately.

The procedure for constructing a drilled pile is first to excavate the hole for the pile, pour the pile material in the excavated hole, and then let curing take place. This type of construction results in the least disturbance to the soil surrounding the pile and is suitable for areas with a thick layer of stiff clay as no temporary support is

required to hold the hole open between excavating and pouring the concrete. The water content in an annular shaft of soil around the pile is increased during pile construction [85]. The changes in the elastic properties of the soil are insignificant but the adhesion between the pile and the soil is decreased as a result of this local disturbance.

In the case of a driven pile, no soil is removed from the system and the pile displaces an equal volume of soil as it pierces into it. It is difficult to determine the effect of soil disturbance which depends on the type of soil as well as the type of pile and driving equipment. Driven piles are suitable for sites containing sands.

The finite element model for all these types of piles are similar.

1-E PURPOSE AND SCOPE

An understanding of the factors that influence the interaction between an isolated pile and the surrounding soil will aid in formulating solutions for more complex problems of a group of piles and structures supported on such piles. With the present day advancements in the storage and efficiency of computers, it will soon be possible to efficiently deal with very complicated geometries and boundary conditions. The responses of a pile founded in a general soil strata to travelling seismic waves are computed by first determining the motions at the boundary and then making use of these boundary motions as input and accomplishing the dynamic analysis of the soil-pile system.

A method to evaluate the seismic responses of a layered system, taking account of the various types of waves and different assumptions in the direction of wave propagation, is developed in Chapter 2. Chapter 3 presents a solution technique for the spatial variations in seismic motions taking account of the focal depth of the source, the epicentral distance of the station and the various types of waves involved. The method and programs included in these chapters are general so that they can be used for other problems, such as the spatial motion computations required in a two-dimensional or three-dimensional soil structure interaction study, the determination of the amplification of seismic motions due to soil layering, the evaluation of soil layer responses for available earthquake records at ground level or base rock level, etc. A finite element method for an axisymmetric structure subjected to the most general case of non-axisymmetric, static loading is developed in Chapter 4. In order to check the static program, the stresses developed in a cylinder (as typically used in the Standard Split Cylinder Test) are computed and compared with the existing solutions. An extension of the method to account for the pore pressure in the soil during static loading conditions is outlined in Chapter 5. The reliability of the method for problems involving pore pressures is examined by using a triaxial test specimen example.

The extension of the program to dynamic analysis involves the derivation of reliable mass matrices, which may be either consistent or lumped. The validity of these mass matrices for different shapes of elements is studied by computing the first few eigenvalues and the

corresponding vectors for the structure in Chapter 6. For this purpose, a program has been adapted for the CDC 6400 computer that facilitates the computation of the eigenvalues and vectors of large matrices which have symmetric banded form. In Chapter 7, the relationships required to accomplish the dynamic analysis, making use of the step-by-step integration procedure and involving large banded matrices, are established. The correctness of the method has been verified by solving two practical cases that indicate the generality of the program, namely, the response of a ten-story building with masses lumped at floor levels and the seismic motions of an empty circular water tank with its base at ground level. The geometric boundaries of the soil-pile system are established in Chapter 8. The method for spatial seismic motions is extended to facilitate the computations of the motions at the boundary nodes of the system. The step-by-step dynamic analysis procedure is modified to accommodate these boundary motions in the system. Chapter 8 also gives an account of the seismic motions in different types of soil-pile systems.

The methods and computer programs developed in Chapters 2 to 8 are checked by comparing the results to closed form solutions from the literature. The general results and conclusions are summarized in Chapter 9 and suggestions for further research are presented.

CHAPTER II

RESPONSE OF LAYERED SOIL SYSTEMS DURING EARTHQUAKES

2-A SEISMIC WAVES

Whatever be the cause of earthquakes, they release two types of body waves - P and S - and the transfer of energy through the soil layers is caused by the propagation of these waves through the soil. The most extensively favored theory maintains that tectonic earthquakes are caused by slip along geologic faults [61]. As a result of the fault slippage, there occurs a sudden disturbance in the earth's crust or the upper part of the mantle and a large portion of the energy is released within a short period of time as body waves. After travelling a series of paths, these waves finally reach the site where observations are made of the ground motions. A layered half space is appropriate as a model of the earth and then there can be motions which correspond to waves whose activity is confined to a zone near the boundary of the half space [75]. The analysis of several typical accelerograph records indicates that a significant portion of earthquake ground motion consists of surface waves [42,90,91]. Rayleigh waves and Love waves are the most significant among these surface waves. The arrival times of each type of wave and the corresponding contributions to the total ground motion are dependent

on the focal depth of the source, the epicentral distance of the site and the phenomenon of multiple reflections, refractions and dispersions along the various paths.

Because of the nonuniform nature of the materials in the earth's crust and of the seismic waves themselves, the study of the wave propagation through materials near the surface of the earth is complicated. When the epicenter of the earthquake is not far from the site, the surface layers may be excited by the vertically travelling waves. On the other hand, the seismic waves travel a considerable distance horizontally before reaching a distant station. Usually the nature of the seismic waves are not well defined and both the geometric and elastic properties of the surface layers poorly delineated [47,78]. As a result it is essential to make some simplification to the real problem [92]. Figure 2-1 gives a highly idealized system showing the relation between the focal depth of the source, the epicentral distance of the station and the wave motion. Station S_1 is comparatively near to the epicenter and may be at an epicentral distance of the order of 0.65d to 2.25d, d being the focal depth of the source. Though shear waves are the most important components, the contribution of surface waves is significant at this site [64]. At station S_3 which is at a very large distance from the source, the arrival times of surface waves and shear waves are so much apart that there is no possibility of their combined effect. In the case of station S_2 which is of moderate epicentral distance, the surface waves are usually masked by the shear waves and as a result a small portion of the accelerations may be attributed to the surface waves. The surface waves which have any

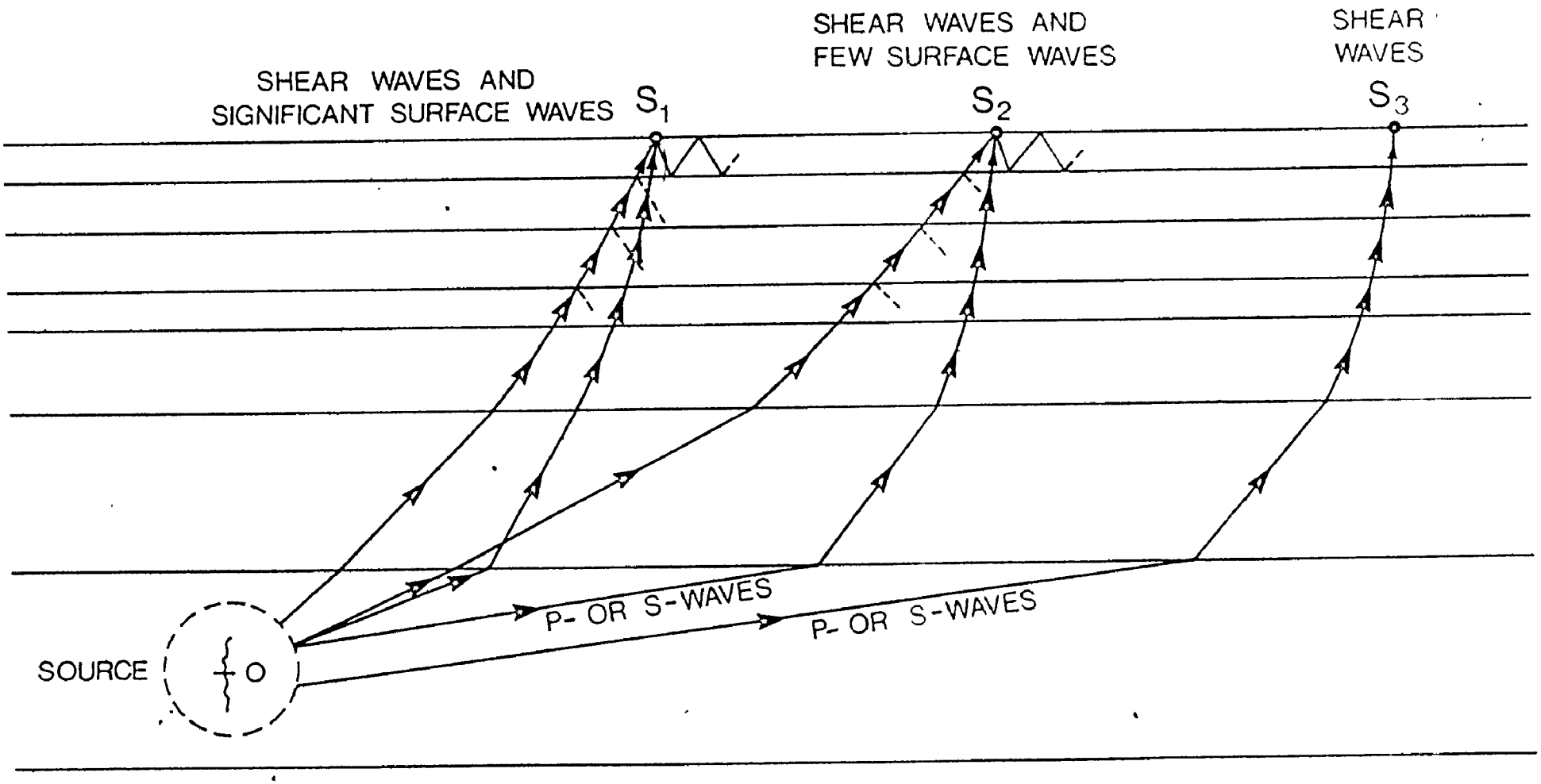

FIG. 2-1 IDEALIZED SYSTEM SHOWING FOCAL DEPTH, EPICENTRAL DISTANCE AND WAVE PATHS [64,92]

significance are Rayleigh waves and Love waves. Among them only Rayleigh waves are important. Love waves are possible only when the surface layer velocity is less than the velocity of the underlying strata; and when the superficial layer is of higher velocity, they do not form [75].

2-B RAYLEIGH WAVE PROPAGATION IN SOIL LAYERS

When the response of a site near the source is to be computed, surface waves also become important. The most significant among all surface waves are Rayleigh waves which are possible in an elastic half-space [74,75]. In accelerograms of destructive earthquakes, a portion of the energy transfer is attributed to Rayleigh waves which are marked only in the surface portion and become indistinct with increasing depth. These Rayleigh waves may be caused by both types of body waves and, unlike body waves, their velocity depends upon the wave frequency and the wave length in addition to the soil properties. These waves propagate as plane waves and thus displacements are independent of the transverse direction.

The relationship for the velocities and stresses in an elastic medium in terms of the phase velocity c and the wave number k of plane Rayleigh waves are established in Appendix A-1 by solving the equations of motion for the medium and imposing the appropriate boundary conditions for a free surface. In the case of a layered soil strata, the problem may be reformulated in terms of matrices using the methods developed by Thomson [88] and Haskell [37]. The Thomson-Haskell matrix formulation [37] is relatively simple and the method involves matrix multiplications and uses the Helmholtz potentials. An outline of this method is given

in Appendix A-2.

The body waves generated at the origin are complex and these waves after travelling through different soil layers give rise to Rayleigh waves. As a result, a series of Rayleigh waves of different wave numbers and propagating at different wave velocities are possible. There is no straightforward method to assign a wave number k or phase velocity c. However, it is possible to specify bounds for the Rayleigh wave propagational velocity in a layered soil strata. If β_L and β_R are the lowest shear wave velocities in the soil layers and the base rock respectively, then the following inequality holds [37]

$$0.93\ \beta_L \leq c \leq \beta_R \tag{2:1}$$

In this range the phase velocity c of the plane Rayleigh wave can assume any value depending on the wave number k. As different trigonometric functions and powers of c appear in the various expressions, usually the computation of the phase velocity c for a given wave number k is more time consuming than the reverse process. Further, the possible values of c are in a known range. For any value of c, the evaluation of k may be accomplished by means of a trial and error procedure as outlined in Appendix A-3.

2-B-1 Evaluation of Transfer Functions for Layer Response

As the phase velocity of Rayleigh waves is dependent on the frequency it is not possible to determine c for the earthquake problem. The possible range for the value of c is given by $0.93 \leq c/\beta_1 \leq \beta_R/\beta_1$.

The various values of c within this range were considered and it was found that only values of c for c/β_1 less than β_n/β_1 gave consistent and meaningful results by exhibiting decay of motions with depth. The method of evaluation of transfer functions for seismic response of layers is approximate and it proceeds as follows:

(1) Compute the possible range for the value of c. Take a set of c-values at regular intervals in its possible range.

(2) For each c-value determine k using the trial and error method as detailed in Appendix A-3. For this k, calculate F_1/F_2 and then in Equation A:48

$$\ddot{w}_o/c = -(F_2/F_1)\ \dot{u}_o/c \qquad (2:2)$$

(3) Using Equations 2:2, A:43 and A:46,

$$\dot{u}_m/c = [(A_m)_{11} - (F_2/F_1)\ (A_m)_{12}]\ \dot{u}_o/c \qquad (2:3)$$

Then the transfer function T_m for the mth interface response in the horizontal direction is

$$T_m = (A_m)_{11} - (F_2/F_1)\ (A_m)_{12} \qquad (2:4)$$

which is always real for the case of Rayleigh waves. The transfer function for base rock is

$$T_n = A_{11} - (F_2/F_1)\ A_{12} \qquad (2:5)$$

Compute all transfer functions $T_0, T_1, T_2, T_3, \ldots, T_n$.

(4) Similarly, for all other values of c in its range, evaluate k and the transfer functions T_0, T_1, T_2, ..., T_n.

(5) For any layer m, the transfer function T_m shall be taken as the average of its values for the various values of c in its range. Thus the transfer functions T_0, T_1, T_2, ..., T_n for the horizontal components of the seismic responses of layers due to the propagation of Rayleigh waves are evaluated.

(6) In the same way the transfer function for the vertical response of the mth interface may be calculated as the average of its values, for the various values of c. The transfer function for the vertical response of the mth interface for any c may be calculated from the relation

$$T_{vm} = (A_m)_{21} - (F_2/F_1)\ (A_m)_{22} \qquad (2:6)$$

(7) The response of the mth interface at any time t is obtained as the product of its transfer function and the surface response at time t. In cases where the base rock motion is known, the surface response is first computed using the function $1/T_n$. Then the response components of soil layers at interface levels may be evaluated using the transfer functions T_0, T_1, T_2, ..., T_n, T_{v0}, T_{v1}, ..., T_{vn}.

2-B-2 Program for Soil Layer Response

In order to compute the response of soil layer interfaces due to the propagation of Rayleigh waves, a computer program RAYRES has been

developed. The program is suitable for both surface response records as well as the records at the base rock level. As the various relationships established in Appendix A involved complex quantities, the program was originally prepared using complex algebra. The complex matrices $[a_m]$, $[A_m]$ and $[A]$ defined in Equations A.41, A:43 and A:44 of Appendix A-2 are such that the term corresponding to the ith row and j^{th} column in any one of them is real when $(i+j)$ is even and imaginary when $(i+j)$ is odd. As a result, the functions F_1 and F_4 are always real while F_2 and F_3 are always imaginary. All the quantities in the computation are either real or imaginary and therefore the numerical value of each quantity is the unknown. By careful programming, the use of complex algebra has been obviated and the modified program makes use of only real quantities. This resulted in a saving of about 60% in the computation time; it takes only about 30 seconds to compute the layer response of a four-layer system for records comprising 1000 time intervals.

The program calls for the dimensions and properties of the soil layers and the earthquake record to be fed in as input. For the different values of c in its range, the wave number k is computed by the iteration method outlined in Appendix A-3. The sequence of operations in the program is shown by the flow chart in Figure 2-2. Once the values of c and k are available, the transfer functions for the horizontal and vertical components of interface responses are computed using Equations 2:4 and 2:6 in Section 2-B-1. The response of the mth interface at any time t may then be obtained by multiplying its transfer function and the surface response at that time. The computed transfer functions for

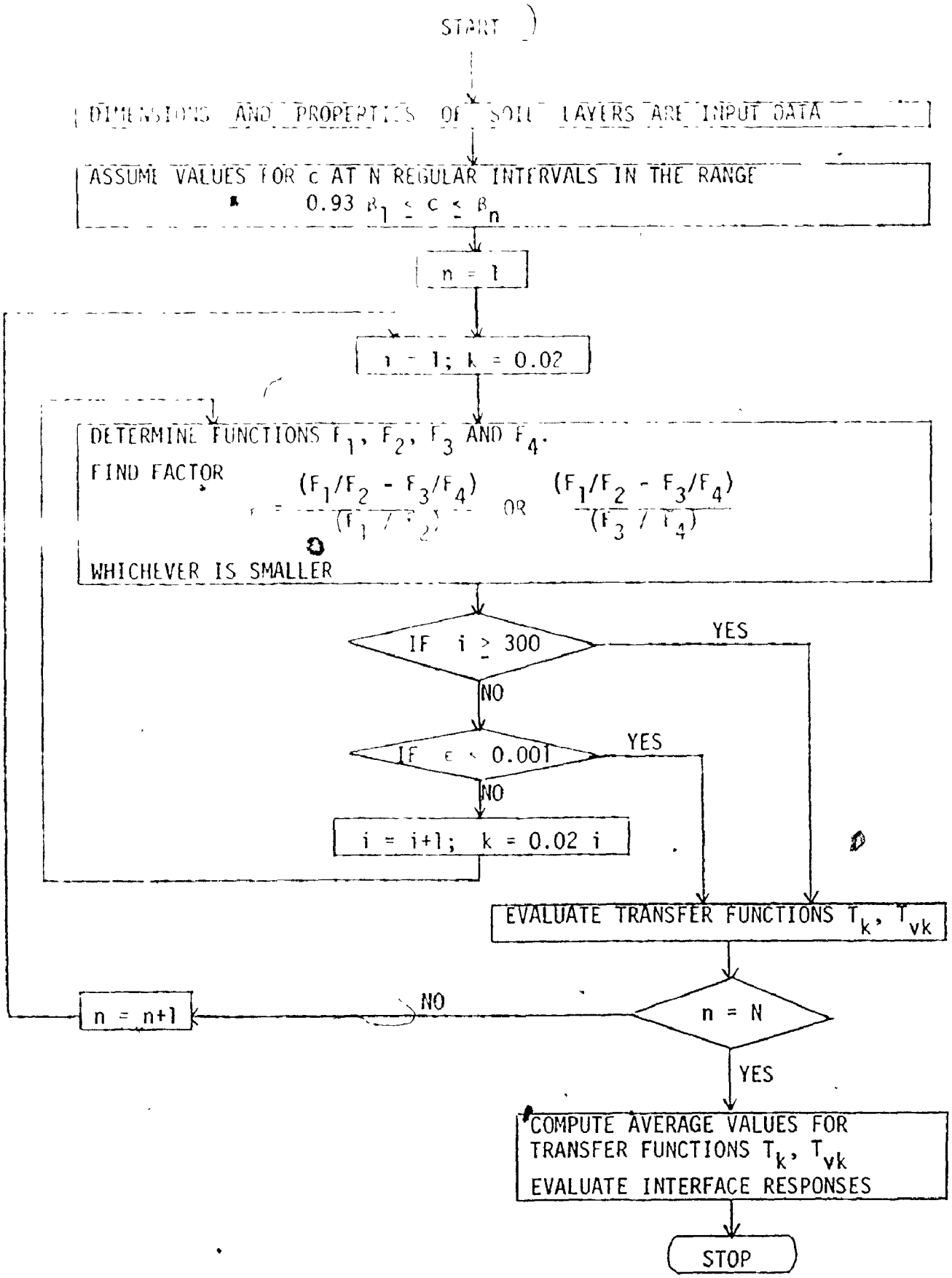

FIG. 2-2 FLOW CHART FOR INTERFACE RESPONSES DUE TO RAYLEIGH WAVE PROPAGATION (RAYRES)

interface responses due to Rayleigh wave propagation are given in Table 2-1 for the four layer system (System 3) in Table 2-2.

2-C VERTICAL PROPAGATION OF SHEAR WAVES

When the site is distant from the earthquake source, the arrival of shear waves at the site is much ahead of the surface waves because of the difference in their velocities. Thus, it may be assumed that there is no need to consider the simultaneous effect of these two types of waves. In such conditions, the shear waves undergo a series of multiple reflections and refractions and the tendency of horizontal stratifications is to make these waves travel close to the vertical direction. As a result of these innumerable reflections and transmissions, the assumption of the vertical propagation of shear waves is an acceptable approximation.

In methods using the multiple reflection-refraction phenomenon of shear waves, the surface response is calculated in the time domain. The first method, known as the "Ray tracing technique" [92], is by far the most efficient method for computer solution. In this method the original soil layer system is divided into L sublayers of constant "time thickness" such that the travelling time of a signal through any sublayer is a constant, Δt. Figure 2-3 shows a diagrammatic scheme for the ray tracing technique which is a plot of sublayers of constant time thickness against time. A wave signal at the base rock level at any time t travels along a path of direct transmission such as $OCBA_1$ and reaches the surface at time $(t+L\ \Delta t)$. Similarly, the same signal after j reflections in any of the layers arrives at the surface at time $[t+L\ \Delta t+2(j-1)\Delta t]$. By summing

TABLE 2-1

TRANSFER FUNCTIONS FOR INTERFACE RESPONSES
DUE TO RAYLEIGH WAVE PROPAGATION

INTERFACE	HORIZONTAL	VERTICAL
Surface (0)	8.31	5.93
1	5.02	1.90
2	0.20	2.65
3	0.99	1.27
Base Rock (4)	1.0	1.30

NOTE: The details are given for the four-layer system (System 3) in Table 2-2.

TABLE 2-2

DATA FOR LAYERED SOIL SYSTEMS

SYSTEM	LAYER NUMBER	LAYER THICKNESS ft	DENSITY lb/ft^3	SHEAR WAVE VELOCITY	RESPONSE AMPLIFICATION FACTOR, USING PROGRAM "LAYRES", A_1			RESPONSE AMPLIFICATION FACTOR, USING RAY TRACING TECHNIQUE [92] A_{1R}
					Case 1	Case 2	Case 3	
1	1 2 Bed Rock	150 325	100 130 145	900 3000 7500	3.72	3.47	3.04	2.66
2	1 2 3 Bed Rock	150 150 175	110 120 140 145	900 2000 4000 7500	3.81	3.38	3.30	3.05
3	1 2 3 4 Bed Rock	150 75 100 150	110 120 130 140 145	900 2000 3000 4000 7500	3.89	3.14	3.21	2.96
4	1 2 3 4 Bed Rock	150 150 100 75	110 140 130 120 145	900 4000 3000 2000 7500	3.38	2.74	1.91	1.79
5	1 2 3 4 Bed Rock	150 150 75 100	110 140 120 130 145	900 4000 2000 3000 7500	3.51	2.93	2.19	2.01

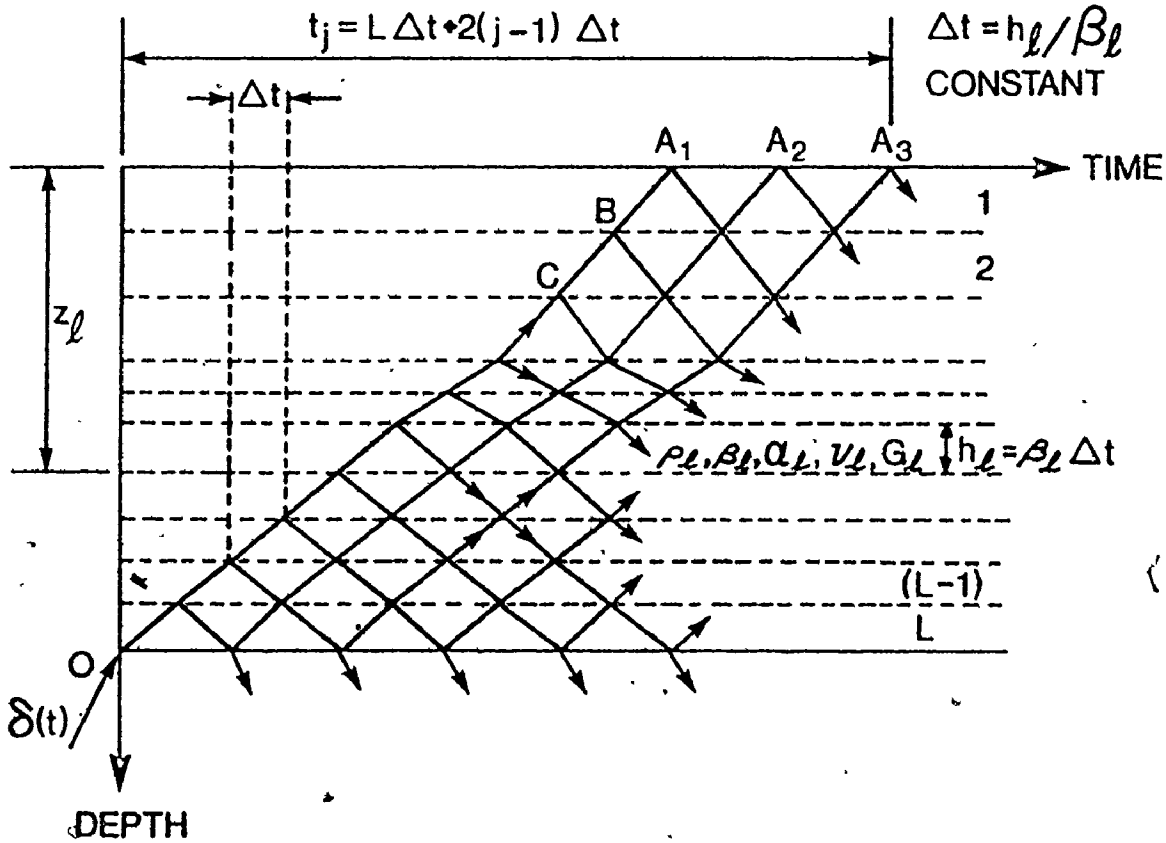

FIG. 2-3 SCHEME FOR RAY TRACING TECHNIQUE [92]

up all such quantities, the surface response at any time t may be written as:

$$\ddot{u}_o(t) = \sum_{j=1}^{\infty} A_j \, \delta(t-t_j) \, \ddot{u}_R(t-t_j) \qquad (2:7)$$

where $\ddot{u}_o$ is the surface response, $\ddot{u}_R$ is the response at the base rock level and $A_j \, \delta(t-t_j)$ is the portion of the surface response due to the jth arrival of a unit signal, and

$$t_j = L \, \Delta t + 2(j-1) \, \Delta t \qquad (2:8)$$

In cases where the response at an interface is to be computed, similar transfer functions may be calculated, but this involves additional work. Thus, the method is advantageous only when the surface response or the base rock response is available and the other quantity needs evaluation. In most cases, it may be necessary to make adjustments of layer parameters to ensure that the relation for travel time in a sublayer equals a constant. This can introduce appreciable errors and to reduce them, the number of sublayers may have to be increased resulting in smaller time-steps and increased computation time. The second method is a numerical analysis of the multiple reflection-refraction phenomena of shear waves in the original soil layer system [50,53]. This process does not bring in errors of the type involved in the ray tracing technique. Further, it has the advantage that the seismic response of the different layers are automatically computed in addition to the surface response. Therefore, the method using the reflections and refractions of shear waves in the original soil layer system has been chosen for all motion computations.

2-C-1 Response of Layered Systems - Method of Time Domain on Original Layers

The method of time domain may be utilized to compute the seismic response of the layered system of soils shown in Figure 2-4a as a result of the vertical propagation of shear waves. The equation of motion for the vertically propagating shear wave is

$$\frac{\partial^2 u}{\partial t^2} = \beta^2 \frac{\partial^2 u}{\partial z^2} \tag{2:9}$$

The general solution of this wave equation is a sum of two waves travelling with velocity β, one in the positive z direction and the other in the negative z direction.

$$u = F(t - z/\beta) + R(t + z/\beta) \tag{2:10}$$

Consider a typical interface between the kth and $k+1^{th}$ layers as shown in Figure 2-4b. The impedance ratio μ_k between these two layers is defined by

$$\mu_k = \frac{\rho_k \beta_k}{\rho_{k+1} \beta_{k+1}} \tag{2:11}$$

When an upward wave signal is incident on this interface there is an upward transmission into the kth layer and a downward reflection back into the $k+1^{th}$ layer. In the same way there is a downward transmission and an upward reflection when the incident signal is downward. The coefficients of upward reflection, downward reflection, upward transmission and downward transmission are respectively:

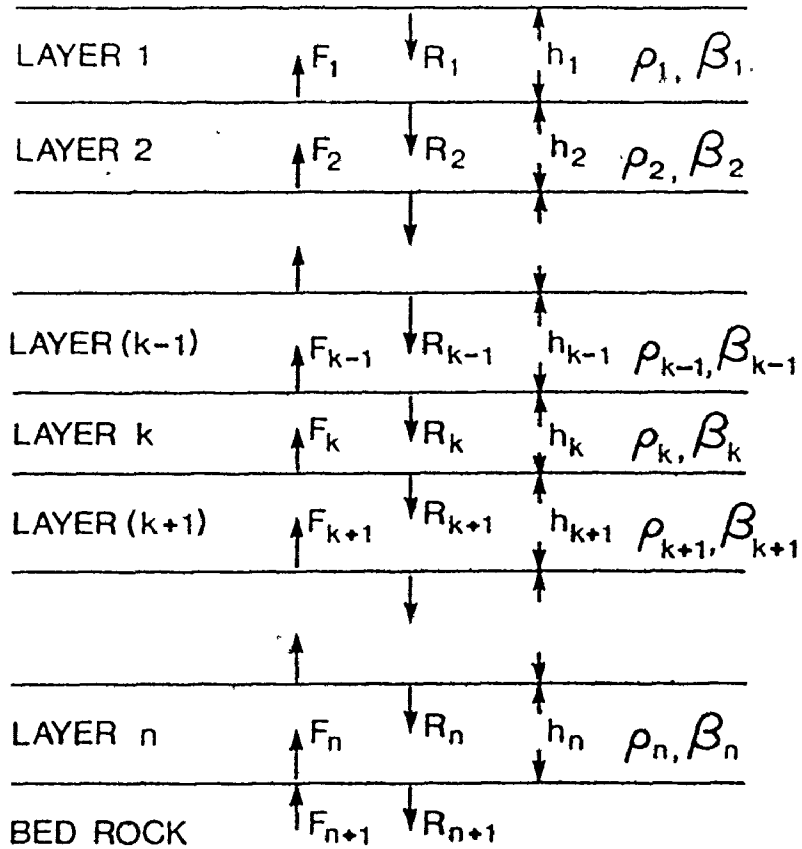

a. BED ROCK TO SURFACE RESPONSE IN LAYERED SOIL

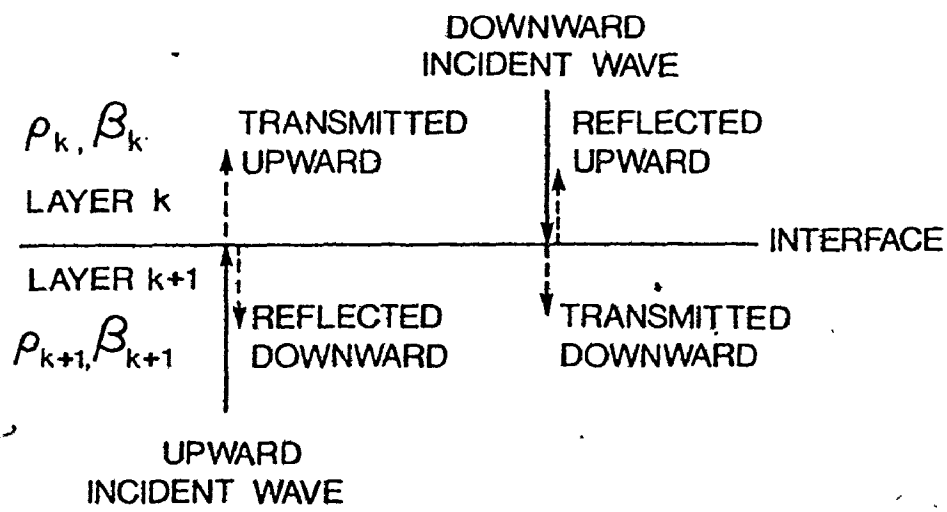

b. INCIDENT AND EMITTED SIGNALS AT A TYPICAL INTERFACE

FIG. 2-4 VERTICAL PROPAGATION OF SHEAR WAVES THROUGH STRATIFIED SOILS

$$(R_u)_k = (\mu_k - 1)/(1 + \mu_k)$$

$$(R_d)_k = (1 - \mu_k)/(1 + \mu_k)$$

$$(T_u)_k = 2/(1 + \mu_k) \qquad (2:12)$$

and

$$(T_d)_k = 2\,\mu_k/(1 + \mu_k)$$

When a wave moves in the vertical direction, it takes some time for the wave to travel from the base rock level to the interfaces of layers. Thus, between two adjacent interfaces there is a time lag. The time lag between the top and the bottom interfaces of the layer k is

$$t_\ell = h_k/\beta_k \qquad (2:13)$$

For the layered soil system in Figure 2-4a the pertinent equations are:

$$R_1(t) = F_1(t-h_1/\beta_1)$$

$$F_1(t) = (T_u)_1\, F_2(t-h_2/\beta_2) + (R_u)_1\, R_1(t-h_1/\beta_1)$$

$$R_2(t) = (R_d)_1\, F_2(t-h_2/\beta_2) + (T_d)_1\, R_1(t-h_1/\beta_1)$$

$$F_2(t) = (T_u)_2\, F_3(t-h_3/\beta_3) + (R_u)_2\, R_2(t-h_2/\beta_2)$$

...

$$R_k(t) = (R_d)_{k-1}\, F_k(t-h_k/\beta_k) + (T_d)_{k-1}\, R_{k-1}(t-h_{k-1}/\beta_{k-1}) \qquad (2:14\text{-a})$$

$$F_k(t) = (T_u)_k \, F_{k+1}(t-h_{k+1}/\beta_{k+1}) + (R_u)_k \, R_k(t-h_k/\beta_k)$$

...

$$R_n(t) = (R_d)_{n-1} \, F_n(t-h_n/\beta_n) + (T_d)_{n-1} \, R_{n-1}(t-h_{n-1}/\beta_{n-1})$$

$$F_n(t) = (T_u)_n \, F_{n+1}(t)$$

and

$$F_{n+1}(t) = \text{Base rock response} \qquad (2:14\text{-b})$$

The values of response components F_k and R_k for the various layers at any time t are evaluated with the aid of their previous values which are known. Thus, the method is a step-by-step procedure. The components F_k and R_k may refer to displacement, velocity or acceleration. If they correspond to displacements, then the displacement at the top of the kth layer is given by the equation

$$u_k(t) = F_k(t-h_k/\beta_k) + R_k(t) \qquad (2:15)$$

If the accelerations in the various soil layers from an earthquake acceleration record are to be computed, then the required equation is:

$$\ddot{u}_k(t) = F_k(t-h_k/\beta_k) + R_k(t) \qquad (2:16)$$

If observed earthquake motions at the bed rock level are available, Equation 2:14 may be repeatedly used to compute the earthquake movements at various interfaces proceeding from bottom to top.

$$F_k(t) = (T_u)_k \, F_{k+1}(t-h_{k+1}/\beta_{k+1}) + (R_u)_k \, R_k(t-h_k/\beta_k)$$

...

$$R_n(t) = (R_d)_{n-1} \, F_n(t-h_n/\beta_n) + (T_d)_{n-1} \, R_{n-1}(t-h_{n-1}/\beta_{n-1})$$

$$F_n(t) = (T_u)_n \, F_{n+1}(t)$$

and

$$F_{n+1}(t) = \text{Base rock response} \qquad (2:14\text{-b})$$

The values of response components F_k and R_k for the various layers at any time t are evaluated with the aid of their previous values which are known. Thus, the method is a step-by-step procedure. The components F_k and R_k may refer to displacement, velocity or acceleration. If they correspond to displacements, then the displacement at the top of the kth layer is given by the equation

$$u_k(t) = F_k(t-h_k/\beta_k) + R_k(t) \qquad (2:15)$$

If the accelerations in the various soil layers from an earthquake acceleration record are to be computed, then the required equation is:

$$\ddot{u}_k(t) = F_k(t-h_k/\beta_k) + R_k(t) \qquad (2:16)$$

If observed earthquake motions at the bed rock level are available, Equation 2:14 may be repeatedly used to compute the earthquake movements at various interfaces proceeding from bottom to top.

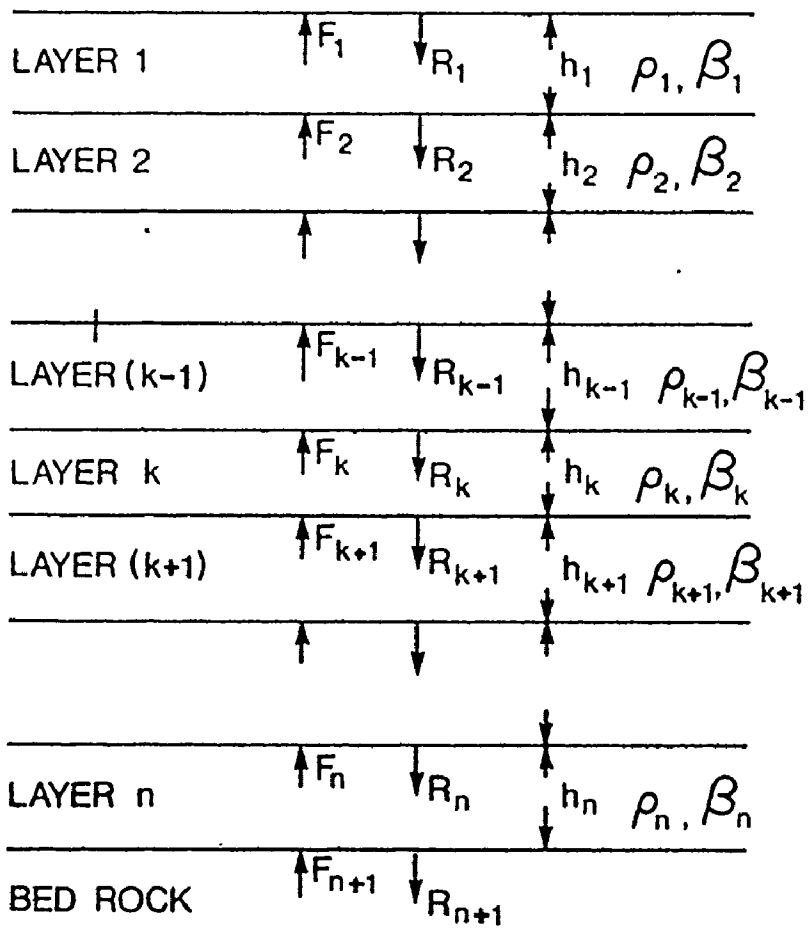

FIG. 2-5 SURFACE TO BED ROCK RESPONSE IN LAYERED SOIL

2-D ANGLE OF INCIDENCE OF EARTHQUAKE MOTION

Extensive research has been carried out on the angle of incidence of earthquake motions [87,8,38,69,73]. The seismograms of certain earthquakes show a typical forerunner of the beginning of the motions. At Hongo, Japan, during the first 1.5 seconds of the North Ida Earthquake, 1930, the horizontal component was small and this was followed by distinct motions. On the other hand, the commencing phase was comparatively large in the case of the vertical component [87]. Similar phenomena were observed during the San Fernando Earthquake of 1971 [43]. The accelerograph AR-240 at the Holiday Inn, 8244 Orion Blvd., Los Angeles and the one at the Jet Propulsion Laboratory, Pasadena, showed typical forerunners of about 2 seconds duration. These observed events can only be attributed to the difference in velocities of dilatational and distortional waves in the upper layer. At Hongo these velocities were 6360 fps and 3740 fps and the corresponding thickness of the upper layer was found to be 2.5 miles.

The angle of incidence may be determined by taking the resultant of the first motions in the three-directional components of the seismogram. An instrument specially designed for this purpose may be used to record the three components. After observing the angle of incidence for about 50 cases, Suzuki [87] concluded that the mean angle of incidence at Hongo was about 4 degrees, its fluctuation being small. Figure 2-6 shows the relationship between the angle of incidence, the epicentral distance and the focal depth.

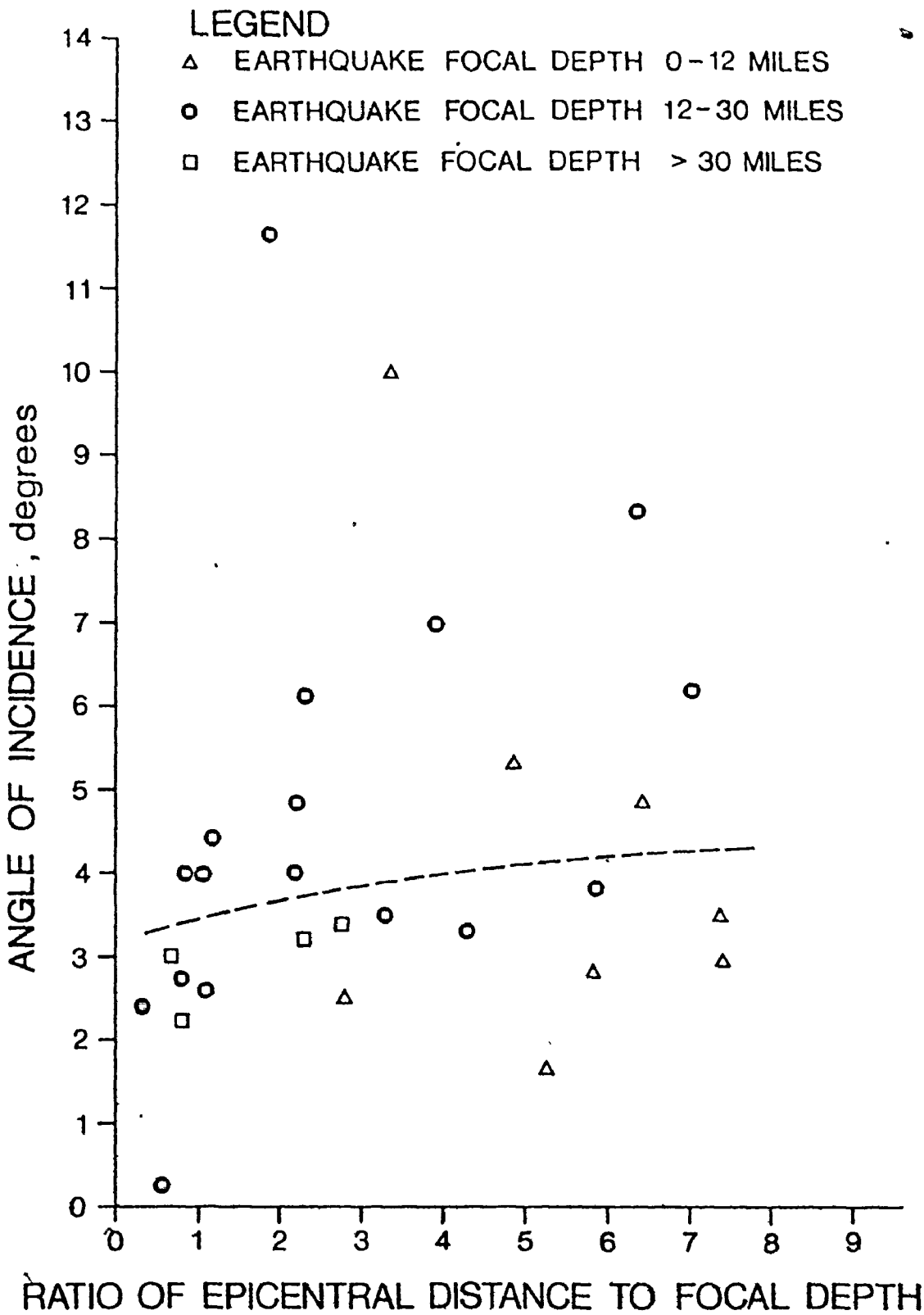

FIG. 2-6 RELATION BETWEEN ANGLE OF INCIDENCE, EPICENTRAL DISTANCE AND FOCAL DEPTH

Seismologists have developed a method for the determination of the incident angles of body waves [8,38,69,73]. Their method is based on a theoretical model of the upper mantle and is suitable for distant stations. The geometry of the earth model is inscribed in Figure 2-7. The distance δ of the station from the source is defined as the angle subtended at the center of the earth by the arc joining the station to the epicenter. According to these findings, the ratio of the sine of the incident angle and the shear wave velocity in the layer is a constant for a station for specified values of focal depth and epicentral distance. Tables of angles of incidence of P-waves and S-waves are presented by Pho and Behe [69] and Chandra [8] respectively. As an example, the incident angle of S-wave at the surface with a near-surface velocity of 11200 fps is 35.67 degrees if the focal depth is 25 miles and the distance δ is 20 degrees (corresponding to an epicentral distance of approximately 1350 miles). The increase in either the focal depth or the epicentral distance resulted in a decrease in this angle, but the more important factor is the epicentral distance. Unfortunately the model is not quite suitable for nearby sites and thus distances less than 20° are omitted in the tables. Qualitatively it may be stated that the angle of incidence is significant for short distances.

In the absence of accurate data it may be required to make some assumption regarding the angle of incidence. An empirical relationship to determine the angle of incidence of the shear wave in the surface layer is detailed in Appendix B-1. The angle of incidence in degrees may be obtained as $\beta_1/240$ for all nearby sites and zero for distant sites, where

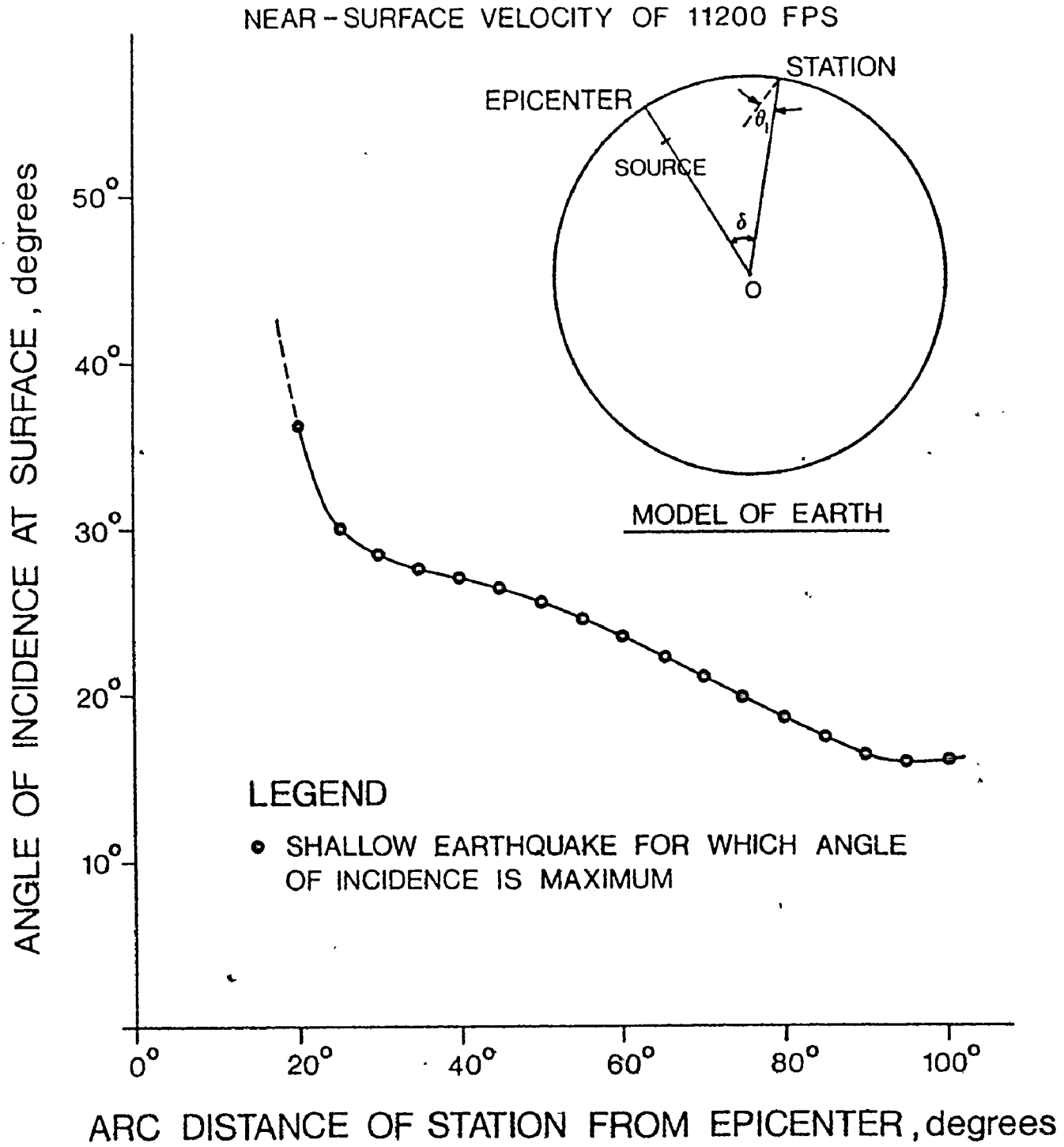

FIG. 2-7 RELATION BETWEEN ANGLE OF INCIDENCE AND DISTANCE OF STATION FROM SOURCE [8,73]

β_1 is the shear wave velocity in the surface layer in ft/sec.

2-E INCLINED PROPAGATION OF SHEAR WAVES

The angle of incidence of the earthquake motion at the surface depends on the shear wave velocity of the surface layer. When a shear wave meets an interface, there are four resultant waves, namely, the transmitted shear wave, the reflected shear wave, the transmitted P-wave and the reflected P-wave. The angles of motions and the amplitudes of the emitted waves are given in Figure B-1b of Appendix B for the case of $\beta_2 = 2\beta_1$.

As the angle of incidence decreases, the amplitudes of the emitted P-waves tend to become unimportant. Therefore, it may be sufficient to consider that only S-waves are emitted at an interface. This is not really an oversimplfication of the problem since there is no significant error introduced.

2-E-1 Soil Layer Response Due to the Inclined Propagation of Shear Waves

When shear waves travel in an inclined direction, there is not only a time lag in the vertical direction, but also one in the horizontal direction. Thus, two locations at the same level and horizontally separated do not have the same motion at any time, t. Therefore, it is required to clearly define the locations at which the computed responses are valid. In a case where only layer responses are considered, the locations shall be taken along a vertical line. Then the response of layer

interface k refers to the response of the point of intersection of the vertical line with the interface k.

The path of shear wave propagation is idealized and the expressions for both the vertical and the horizontal time lags are presented in Sections 3 and 4 of Appendix B. Irrespective of whether it is upward or downward motion, the vertical time lag is a constant. The pertinent equations for the layer response due to inclined propagation of shear waves are obtained by replacing all expressions h_k in Equations 2:14 and 2:17 by $h_k \cos \theta_k$. It should be emphasized that the solutions are valid only at points along a vertical line through the original reference point which may be either at the ground surface level or at the base rock level.

2-F COMPUTER PROGRAM FOR SOIL LAYER RESPONSE DUE TO WAVE PROPAGATION

For facilitating the computation of the response of soil interfaces due to the propagation of shear and Rayleigh waves during an earthquake, a program LAYRES has been formulated. The flow chart of the method of evaluation is shown in Figure 2-8. The layer dimensions and properties and the known earthquake record at either the surface level or the base rock level are given as input. The first operation is to compute the time lag in each layer, its value being dependent on the layer thickness and the angle of incidence. If the shear wave propagation is not vertical, then the angle of incidence of motion is first determined using the relationship given by Equation B:3. The time lag in each layer

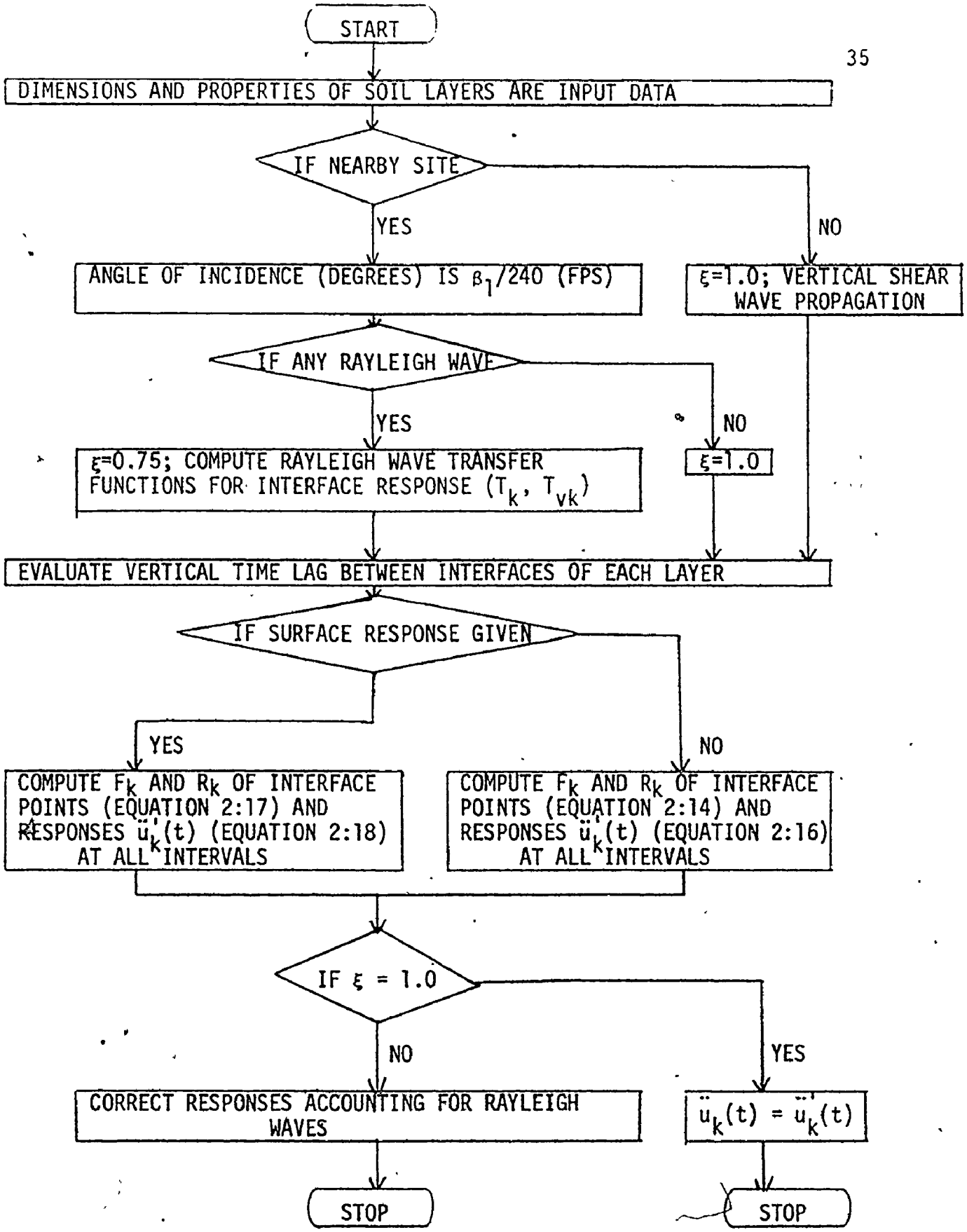

FIG. 2-8 FLOW CHART FOR INTERFACE RESPONSES (LAYRES)

is h_k/β_k or $h_k \cos\theta_k/\beta_k$ depending on whether the shear wave propagation is in a vertical or an inclined direction. When the base rock response is the input, the program proceeds from bottom to top and computes the responses at various interfaces using Equations 2:14 and 2:16. Instead, if the surface responses are available, then the computation advances from top to bottom making use of the relationships given by Equations 2:17 and 2:18.

If there is any contribution due to Rayleigh waves then the program makes the necessary modifications to the computed results. The transfer functions T_k for the interface responses in the horizontal direction due to the propagation of Rayleigh waves are computed using the procedure given in Section 2-B-1. If $\ddot{u}_0'(t)$, $\ddot{u}_1'(t)$, ..., $\ddot{u}_n'(t)$ are the pre-correction values for the responses and ξ denotes the contribution due to shear waves, then the modified interface responses may be computed using the following relationship:

$$\ddot{u}_k(t) = \xi\, \ddot{u}_k'(t) + (1 - \xi)\, T_k\, \ddot{u}_0'(t) \qquad (2:19)$$

2-F-1 Numerical Examples

In order to study the influence of various parameters such as the epicentral distance, the number of layers, the thickness of layers, the arrangement of layers, the mass densities and wave velocities, five layered soil systems were considered. The required data for these systems is given in Table 2-2. The properties of the surface layer and the base rock were kept identical in all these systems. The thickness of the intermediate layer(s) was also kept the same. The effect of soil layering on the

amplification may thus be studied.

The E-W component of the motion for the first 12 seconds during the Olympia Earthquake, 1949 was fed in as the input at the base rock level and the responses of the various interfaces were computed using the computer program LAYRES. Figure 2-9 shows the surface responses of the four-layer system (System 3) in Table 2-2, for three specific cases:

(1) Nearby location; contribution of Rayleigh waves considered as 25% with the remaining contribution from the inclined propagation of shear waves.

(2) Nearby location; inclined propagation of shear waves.

(3) Distant location; vertical propagation of shear waves.

These results show that the response amplification due to soil layering is greater in magnitude when the contribution of Rayleigh waves is accounted for. The difference in the response curves for the nearby and distant sites is small when only the shear waves are considered in the evaluation of layer responses.

Figure 2-10 shows the responses due to the inclined propagation of shear waves for the various interfaces of the three-layer system (System 2) shown in Table 2-2. In order to clearly demonstrate the time lag in the arrival of motions at the various interfaces, the response curves for the first 1 second of the input motion are given. The surface responses in the first three systems (Systems 1 to 3) due to the inclined shear wave propagation and the input base rock response are given in Figure 2-11 and this indicates that the number of layers has only little

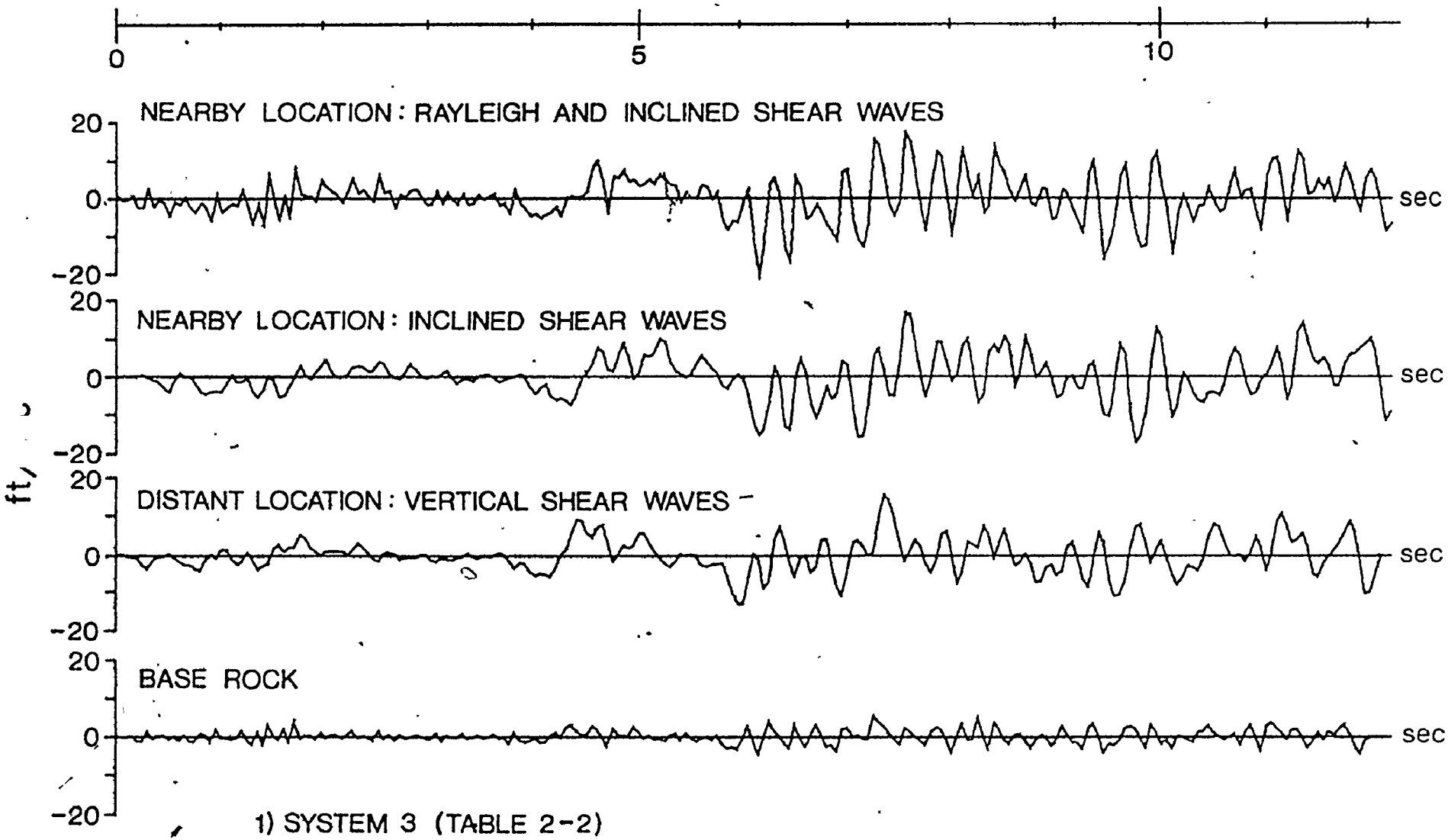

1) SYSTEM 3 (TABLE 2-2)
2) INPUT MOTION AT BASE ROCK LEVEL
3) FOR FIRST 12 SECONDS DURING THE OLYMPIA EARTHQUAKE, 1949

FIG. 2-9 SURFACE RESPONSES OF LOCATIONS UNDER DIFFERENT ASSUMPTIONS,

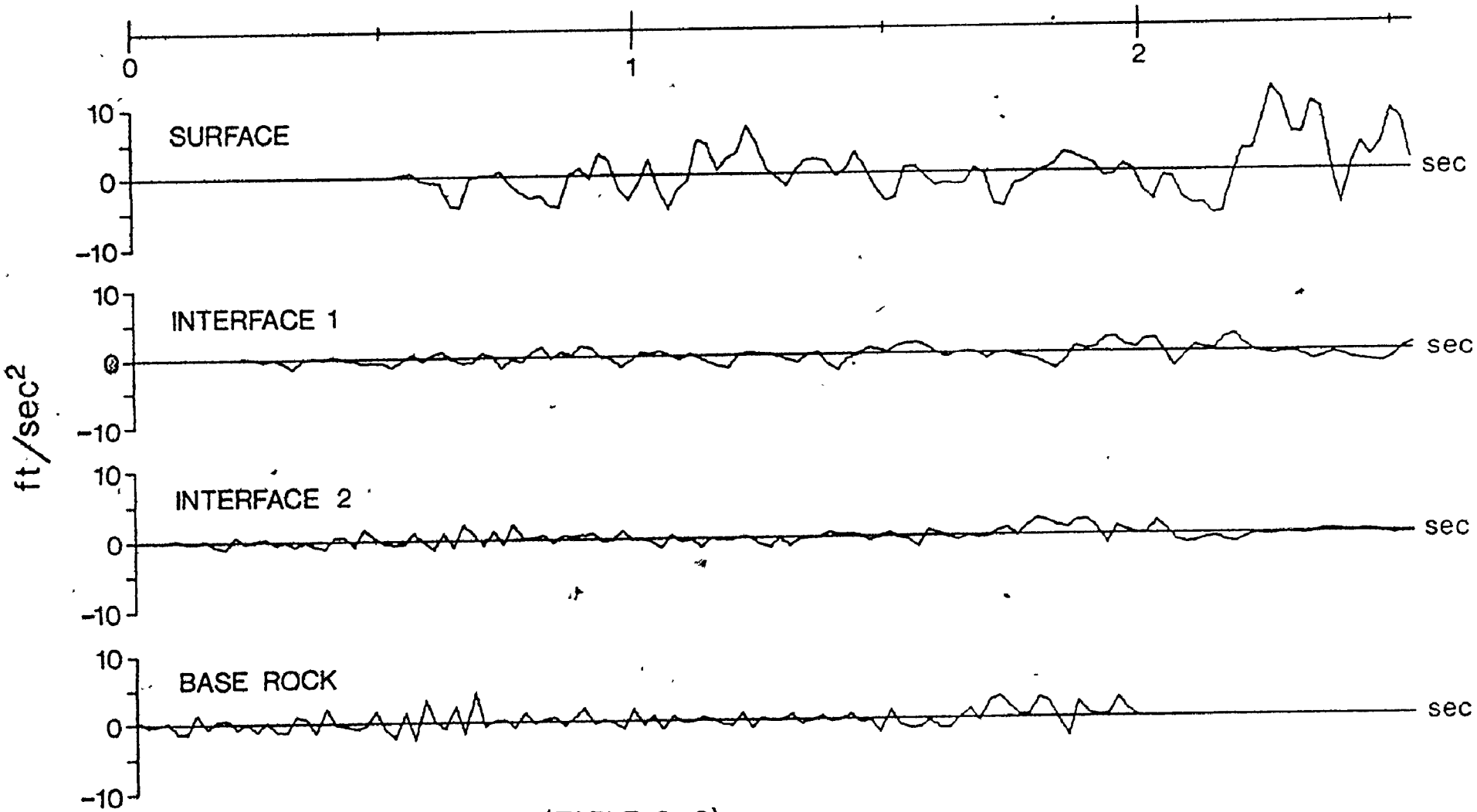

1) SYSTEM 2 (TABLE 2-2)
2) INPUT MOTION AT BASE ROCK LEVEL
3) E-W ACCELERATIONS FOR FIRST 2 SECONDS DURING THE OLYMPIA EARTHQUAKE, 1949

FIG. 2-10 TIME LAG IN INTERFACE MOTIONS DURING EARTHQUAKES

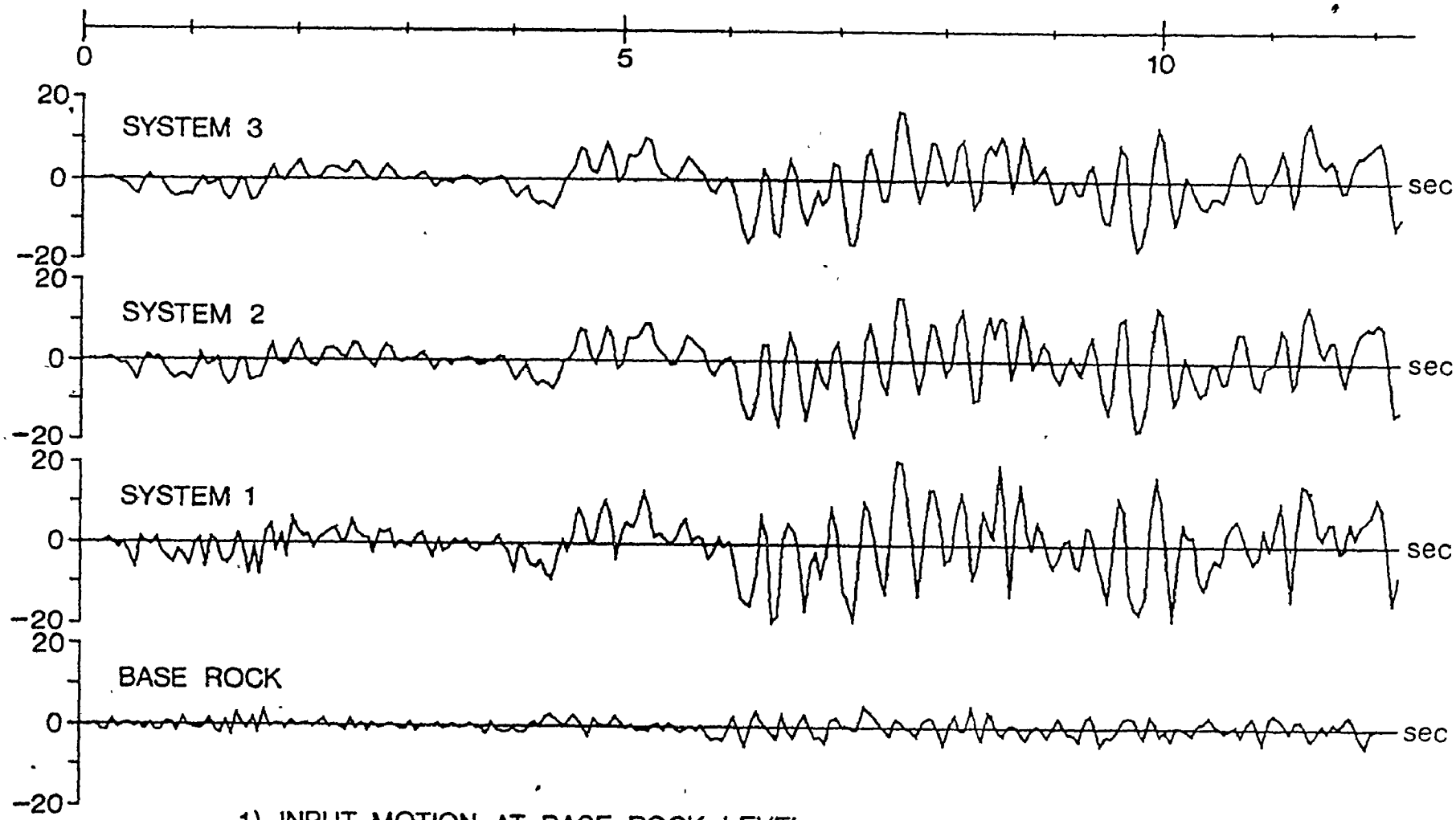

1) INPUT MOTION AT BASE ROCK LEVEL
2) E-W ACCELERATIONS FOR FIRST 12 SECONDS DURING THE OLYMPIA EARTHQUAKE 1949
3) LAYER DIMENSIONS IN TABLE 2-2

FIG. 2-11 EFFECT OF NUMBER OF LAYERS ON EARTHQUAKE AMPLIFICATION

effect on amplification. The response amplification factors for different assumptions are given in Table 2-2. When only vertical shear waves are considered, the values of the amplification factor, A_1, for these three systems fall into a narrow range from 3.04 to 3.30. The values of amplification factors were also worked out for the vertical shear wave propagation using the Ray tracing technique [92] and are included in Table 2-2. These calculations indicate that the number of soil layers has only a moderate influence on the amplification factors so long as the total depth and the average properties of the intermediate layers are unchanged, the properties of the surface layer and the base rock being unchanged.

Figure 2-12 shows the amplification of the responses of four-layer systems (Systems 3 to 5) where the layers are only rearranged. It can be inferred that the amplification factors increased when the soil layers were arranged from the surface downward in increasing order of their impedance (i.e., density x wave velocity) values.

2-F-2 Effect of Saturation

The effect of saturation on the response amplification and time lag in different types of soils was studied. Saturation causes a decrease in the shear wave velocities for both sands and clays [5,75], thereby increasing the time lag. Four soil layer systems were considered, and the types of soil in these systems were dry sand, saturated sand, dry clay and saturated clay respectively. The soil layers in sand refer to the same strata, the only difference in them being in the location of the water table. Similarly the saturated and dry clay systems refer to the

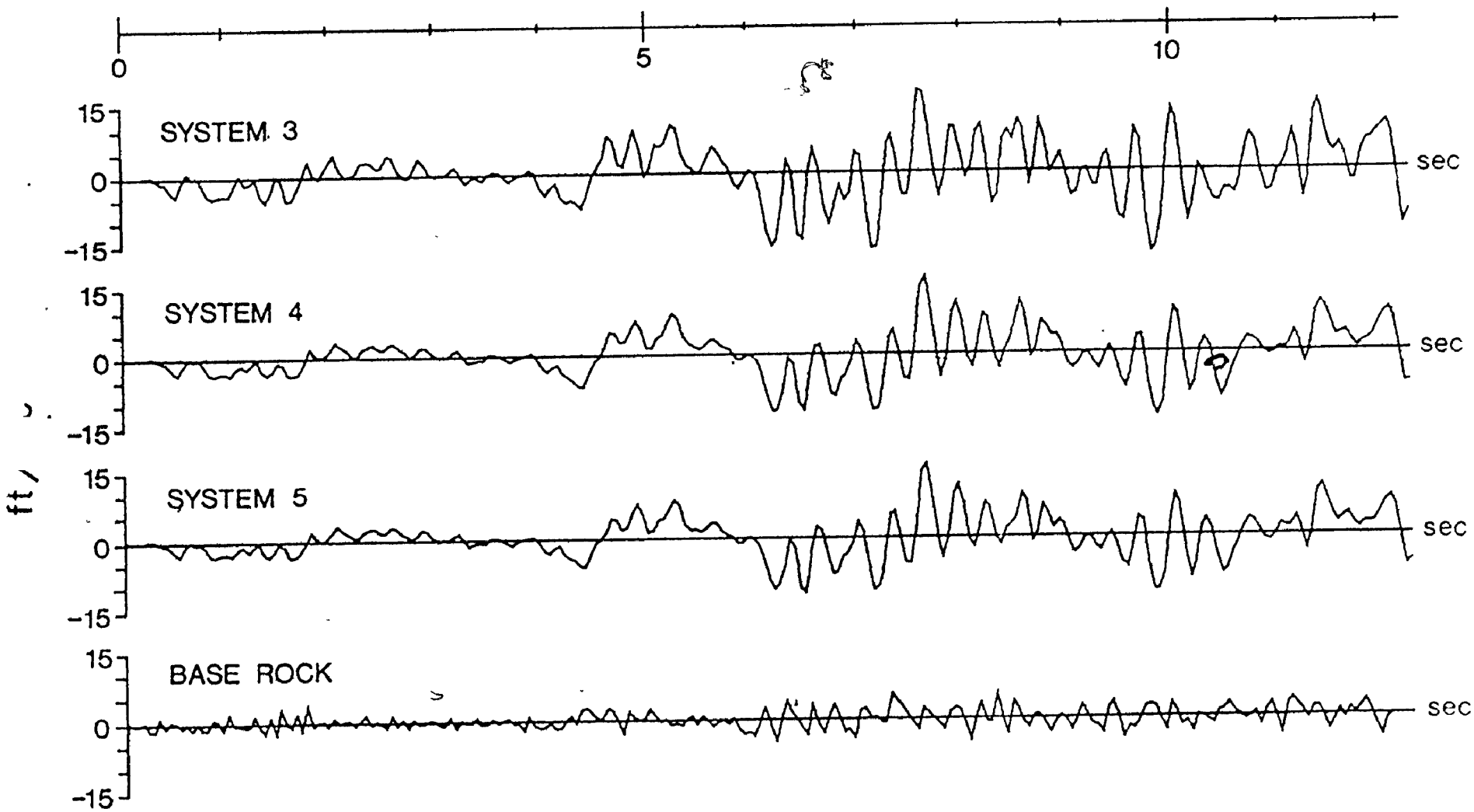

1) INPUT MOTION AT BASE ROCK LEVEL
2) E-W ACCELERATIONS FOR FIRST 12 SECONDS DURING THE OLYMPIA EARTHQUAKE, 1949
3) LAYER DIMENSIONS IN TABLE 2-2

FIG. 2-12 EFFECT OF ARRANGEMENT OF LAYERS ON EARTHQUAKE AMPLIFICATION

same strata.

The responses of these systems at a nearby location due to inclined shear wave propagation to the input motion in the E-W direction at the bed rock level for the first 12 seconds during the Olympia Earthquake, 1949 are shown in Figures 2-13 and 2-14. The amplification factors for the various systems are also given in Table 2-3. In general, the amplification largely depended on the degree of saturation and usually it decreased with saturation in clay layers and increased in sand layers. Changes in degree of saturation alter the impedance ratios and thus indirectly affect the amplification of responses due to layering. As changes in impedance ratios depend on different parameters such as void ratio and specific gravity, the effect of saturation should be considered as different for each type of sand and clay.

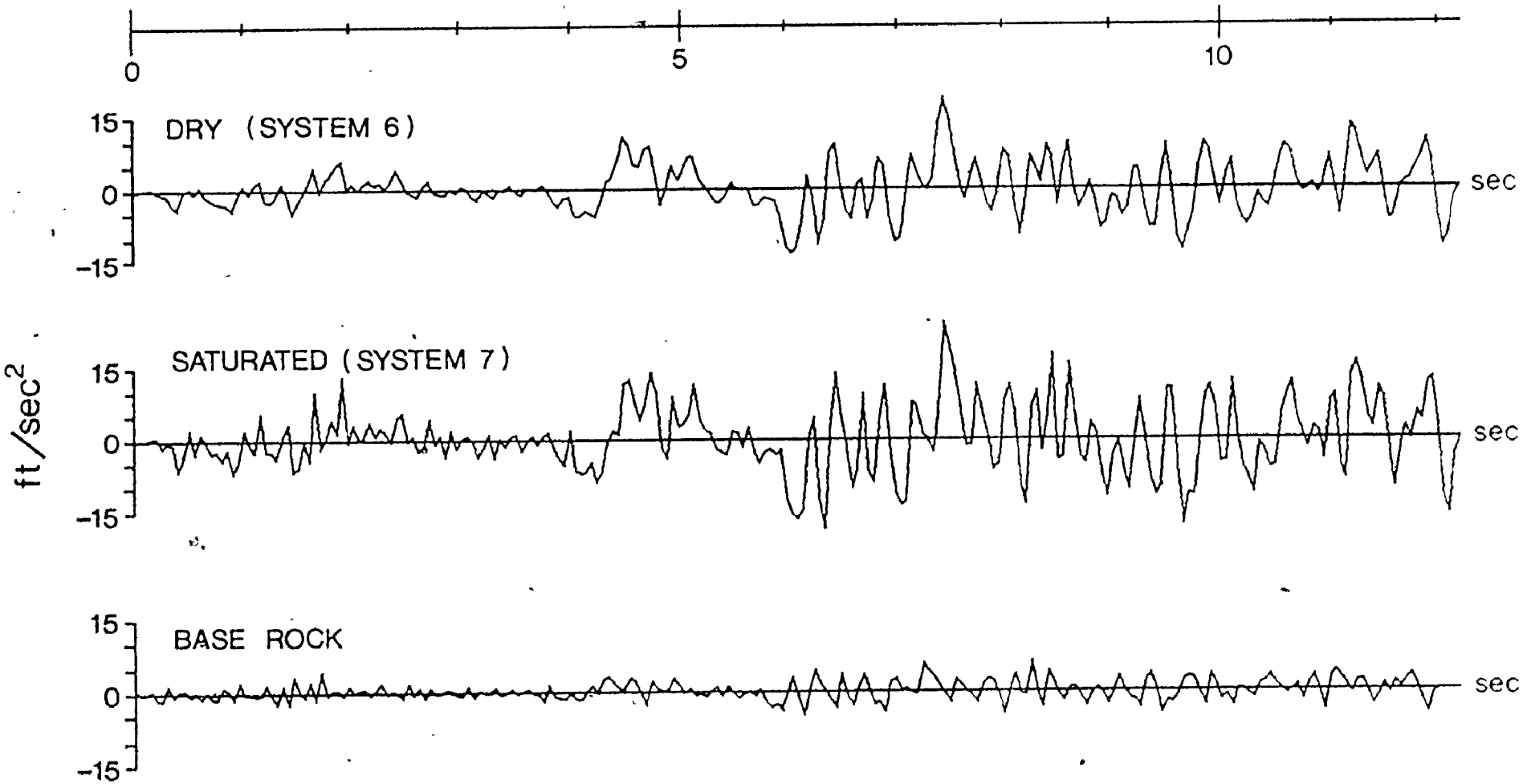

1) INPUT MOTION AT BASE ROCK LEVEL
2) E-W ACCELERATIONS FOR FIRST 12 SECONDS DURING THE OLYMPIA EARTHQUAKE, 1949
3) LAYER DIMENSIONS IN TABLE 2-3

FIG. 2-13 AMPLIFICATION OF EARTHQUAKE MOTIONS IN SAND LAYERS

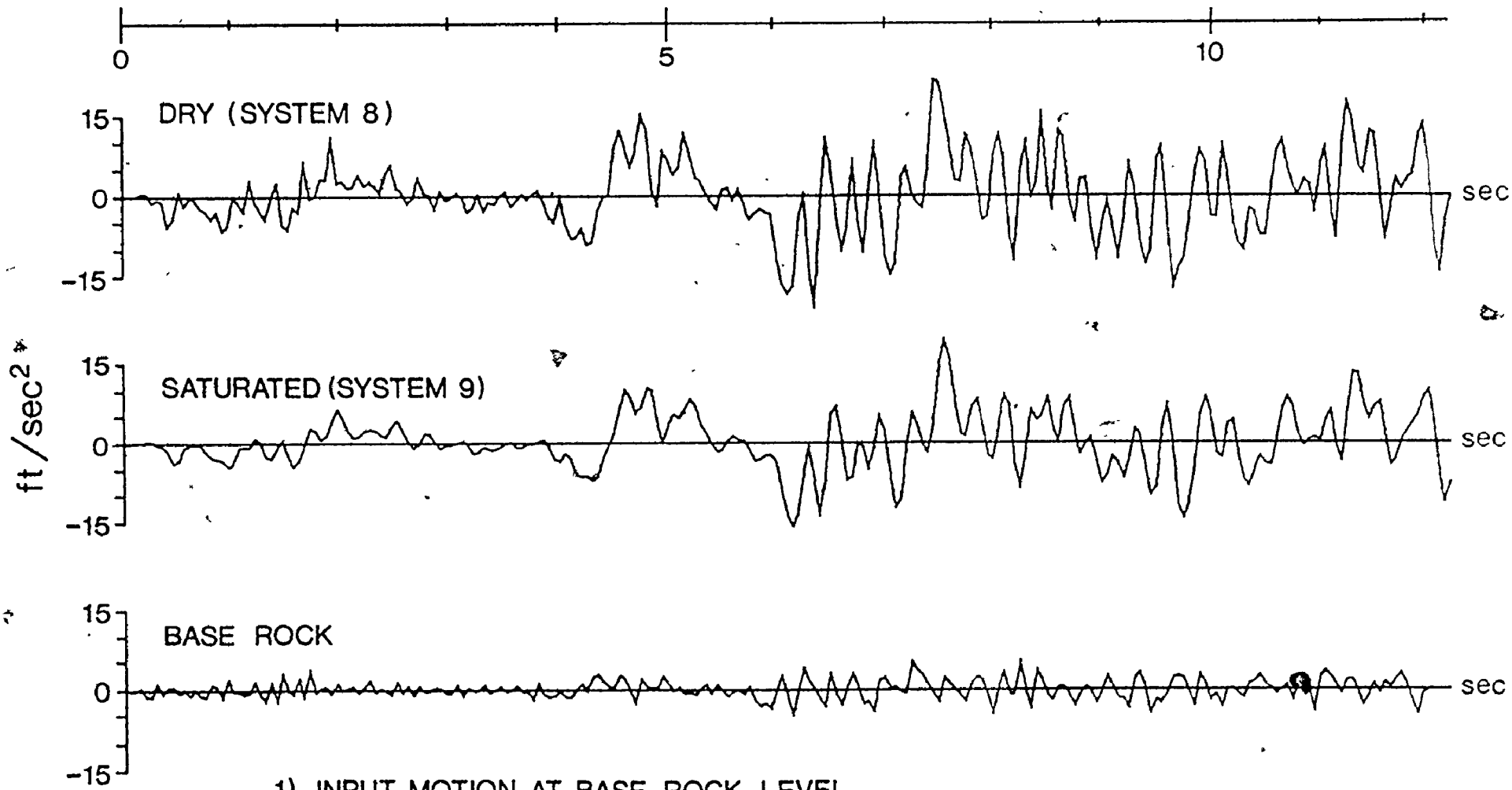

1) INPUT MOTION AT BASE ROCK LEVEL
2) E-W ACCELLERATIONS FOR FIRST 12 SECONDS DURING THE OLYMPIA EARTHQUAKE, 1949
3) LAYER DIMENSIONS IN TABLE 2-3

FIG. 2-14 AMPLIFICATION OF EARTHQUAKE MOTIONS IN CLAY LAYERS

TABLE 2-3

DATA FOR SOIL LAYER SYSTEMS IN SANDS AND CLAYS

SYSTEM	LAYER NUMBER	LAYER THICKNESS ft	DENSITY lb/ft^3	SHEAR WAVE VELOCITY fps	RESPONSE AMPLIFICATION FACTOR DUE TO INCLINED SHEAR WAVE PROPAGATION
6 DRY SAND	1	25	96.7	652	3.27
	2	35	101.1	884	
	3	30	103.7	1050	
	4	50	110.1	1188	
	Bed Rock		145.0	6000	
7 SATURATED SAND	1	25	122.7	515	4.19
	2	35	126.4	704	
	3	30	127.8	842	
	4	50	133.9	961	
	Bed Rock		145.0	6000	
8 DRY CLAY	1	25	65.0	455	3.79
	2	35	70.8	629	
	3	30	86.0	892	
	4	50	80.2	914	
	Bed Rock		145.0	6000	
9 SATURATED CLAY	1	25	104.2	362	3.50
	2	35	107.2	480	
	3	30	116.7	705	
	4	50	112.8	691	
	Bed Rock		145.0	6000	

CHAPTER III

SPATIAL VARIATIONS IN SEISMIC MOTIONS

3-A INTRODUCTION

The common practice for the computation of the soil layer response at distant sites is by assuming that the energy transfer during earthquakes is by means of the vertical propagation of shear waves. If this assumption holds then two locations at the same elevation in a system of horizontally layered soils have the same response at any time t irrespective of the distance between them. In this procedure the time taken for the seismic waves to travel across the distance between these two points is disregarded. Based on field observations during approximately fifty moderate earthquakes, in Japan, Suzuki [87] reported that the earthquake motions had an angle of incidence at the surface. Dezfulian and Seed [17] stressed the importance of considering spatial variations in seismic motions and studied such variations in areas adjacent to sloping rock surfaces. This study did not account for any possible variations in rock motions. Tsai [92] reported that the shear waves propagate in a nearly vertical direction and limited his studies to distant stations where the vertical propagation of shear waves was a reasonable assumption. Yamahara [96] conducted a series of field measurements by placing accelerograms at five different locations on and around Hachinohe Technical College, Tokachioki, Japan and concluded that the motions at

two stations, 117 feet apart, could be out of phase. He observed that these stations at the ground level were almost in phase for a record of motions with longer periods while the phase relation between them was remarkably disturbed during motions of shorter periods. All these findings give convincing evidence of the spatial variations in seismic motions [17, 87, 92, 96]; the assumption of vertical shear wave propagation becomes questionable even when distances of the order of 100 ft are involved.

Observations at Hongo and Mitaka [87] indicated that the mean angle of incidence there was 4° with very little fluctuation. Geophysicists have presented a method to compute the angle of incidence of body waves explicitly, accounting for the focal depth and the epicentral distance [8, 69, 73]. Tables for the angle of incidence of shear waves with surface layer velocities of 3.4 km/sec (11200 fps) were published by Chandra [8]. An accurate analysis for the spatial variations in seismic motions should account for all types of waves, their relative contributions, multiple reflections and refractions, nonhomogeneities of materials and realistic layer stratification. Due to the lack of suitable ground motion records and the complex nature of the problem, it is only possible to base the investigation on some broad assumptions.

It is generally accepted that the major portion of the energy in an earthquake is carried by the inclined propagation of shear waves. In addition it is realized that for comparatively small epicentral distances, the effect of both shear waves and Rayleigh waves may overlap. A method is presented for spatial motion computations which account for

the combined effect of inclined propagation of shear waves and Rayleigh waves.

3-B ASSUMPTIONS

Certain broad assumptions are made in order to facilitate spatial motion computations during an earthquake.

3-B-1 Relative Contributions

There are different types of waves and their relative contributions to the seismic motion depend on the focal depth of the source and the epicentral distance of the station. The most important among them are the shear waves which propagate in an inclined direction. In addition, for small epicentral distances, the combined effect of shear waves and Rayleigh waves are to be considered. It may be assumed that the energy transfer during an earthquake is by means of the inclined propagation of shear waves and also Rayleigh waves, the latter tending to lose their significance as the epicentral distance increases.

3-B-2 Angle of Incidence of Shear Waves

The angle of incidence of the shear wave at the surface depends on the shear wave velocity of the surface layer mainly and also on the focal depth and the epicentral distance. An empirical method for the evaluation of the angle of incidence accounting for these parameters is presented in Appendix B-1. For nearby sites, the angle of incidence in degrees is $\beta_1/240$ where β_1 is the shear wave velocity in the surface

layer in ft/sec, while for distant sites, it may be taken as zero.

3-B-3 Decomposition of Shear Waves at Boundary

As the angle of incidence of shear waves in soil layers is small, the emitting waves may be considered to consist of only the reflecting and transmitting shear waves. Then the coefficients of reflection and transmission may be evaluated using Equation 2:5.

3-B-4 Independence of Waves

Both the shear waves and the Rayleigh waves are considered planar. Then the motions in each of the two perpendicular, horizontal directions are independent of the other horizontal direction. The two types of waves in the x-z plane contribute to motions in x and z directions. Similarly, the motions in the y direction are caused by the waves in the y-z plane. It is assumed that the waves in each plane are independent of the other plane and that in each plane, the two types of waves are not dependent on each other.

3-B-5 Horizontal Time Lag

Consider the horizontally stratified soil layers in three dimensions as shown in Figure 3-1. Stations A and B are at the same level at a horizontal distance d_x apart. Then the accelerograms for x direction motions at A and B are identical except for a time lag. This time lag depends on the distance between stations, the angle of incidence at surface, etc. If waves first reach the station A and the time lag between stations A and B in the x direction is $t_{x\ell}$ then

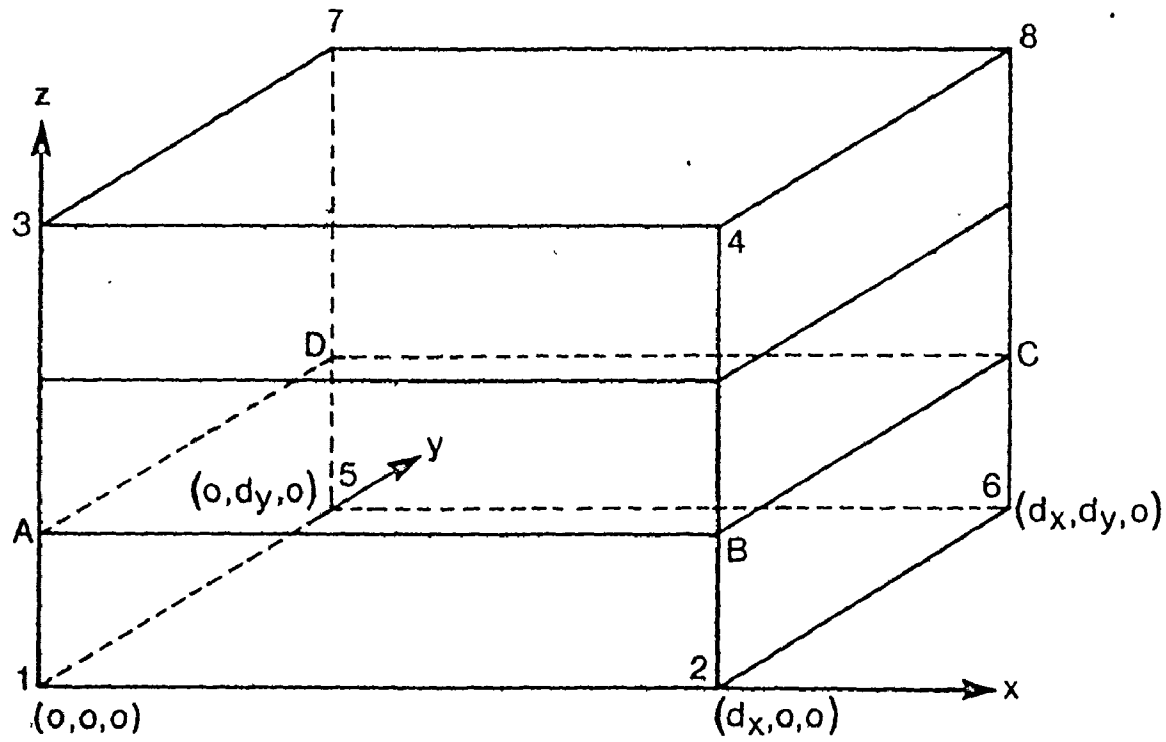

FIG. 3-1 HORIZONTALLY STRATIFIED SOIL LAYERS IN THREE DIMENSIONS

$$\ddot{u}_A(t) = \ddot{u}_B(t + t_{x\ell}) \tag{3:1}$$

In a similar way the motions at B and C hold the following relationship

$$\ddot{v}_B(t) = \ddot{v}_C(t + t_{y\ell}) \tag{3:2}$$

where $t_{y\ell}$ is the time lag between B and C in the y direction.

Stations A, B, C, and D form a rectangle with sides parallel to the x and y axes. Then B and C have a time lag $t_{x\ell}$ with respect to A and D in the x direction and C and D have a time lage $t_{y\ell}$ in the y direction with respect to A and B. There is no time lag in the x direction between two stations which are on the same y-z plane. The relevant equations are:

$$\begin{aligned} \ddot{u}_A(t) &= \ddot{u}_B(t + t_{x\ell}) = \ddot{u}_C(t + t_{x\ell}) = \ddot{u}_D(t) \\ \ddot{v}_A(t) &= \ddot{v}_B(t) = \ddot{v}_C(t + t_{y\ell}) = \ddot{v}_D(t + t_{y\ell}) \end{aligned} \tag{3:3}$$

3-B-6 Time Lag for Vertical Motions

The vertical component of the earthquake motion at any location is separated into two parts; one associated with the motions in the E-W direction and the other corresponding to those in the N-S direction. It is assumed that the time lag for each vertical component is the same as that of the corresponding horizontal motion. These time lags are automatically accounted for in the spatial motion computations.

3-C IDEALIZED PATH OF SHEAR WAVE PROPAGATION

The idealized soil medium in three dimensions is shown in Figure 3-2. It is assumed that the shear waves that cause motions on the x-z plane are plane waves on it and that these motions are independent of the waves which are on the y-z plane. An idealized path of the wave propagation on the x-z plane is in Figure 3-3a. The wave path in the kth layer makes an angle of inclination of θ_k with the vertical and as the wave transmits upward into the $k-1^{th}$ layer, there occurs a deviation in its path at the boundary and the angle of inclination alters to θ_{k-1} in the $k-1^{th}$ layer. A wave signal that moves upward and reaches the location 0_k at any time t continues on its path and reaches the location $0'$ at time $t+\Delta t$, where Δt is the time lag between 0_k and $0'$. The difference in arrival times of the same wave signal at any two locations is termed the time lag between them.

The particle motions due to shear waves are in a direction normal to that of the wave propagation. Then two locations 0_{k-1} and $0'$ in Figure 3-3b get excited simultaneously by the same wave signal. Therefore, there is no time lag between these locations 0_{k-1} and $0'$. In order to mark all locations which have no time lag with respect to 0_{k-1}, the procedure will be to project the line 0_{k-1} - $0'$ both ways such that the direction of this extended line in any layer is normal to the wave path in that layer. Figure 3-3a also shows the locus of all such points which have zero time lag with one another. It is important to note that the amplitudes of motions at these points are not equal because they are at different elevations.

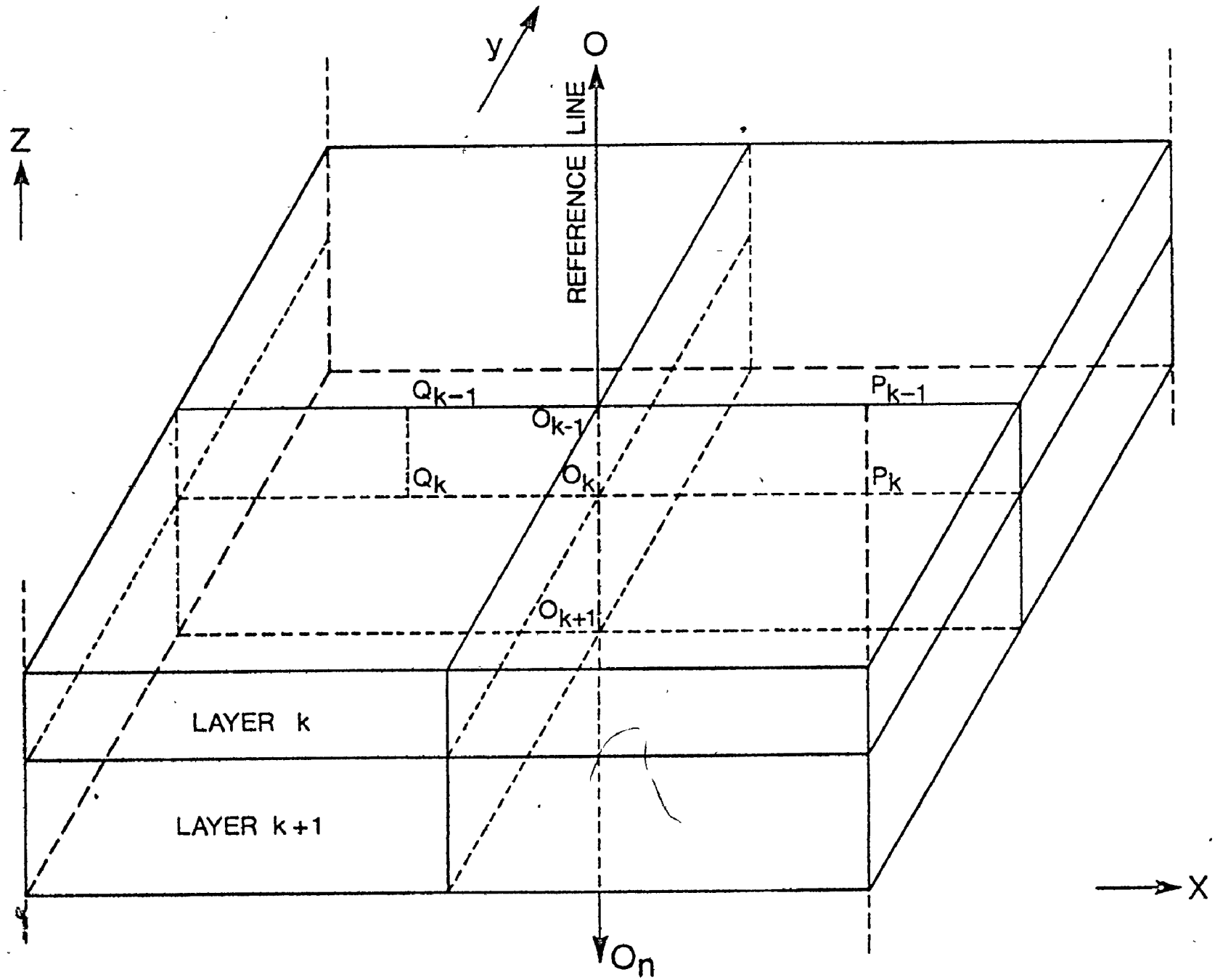

FIG. 3-2 IDEALIZED SOIL MEDIUM IN THREE DIMENSIONS

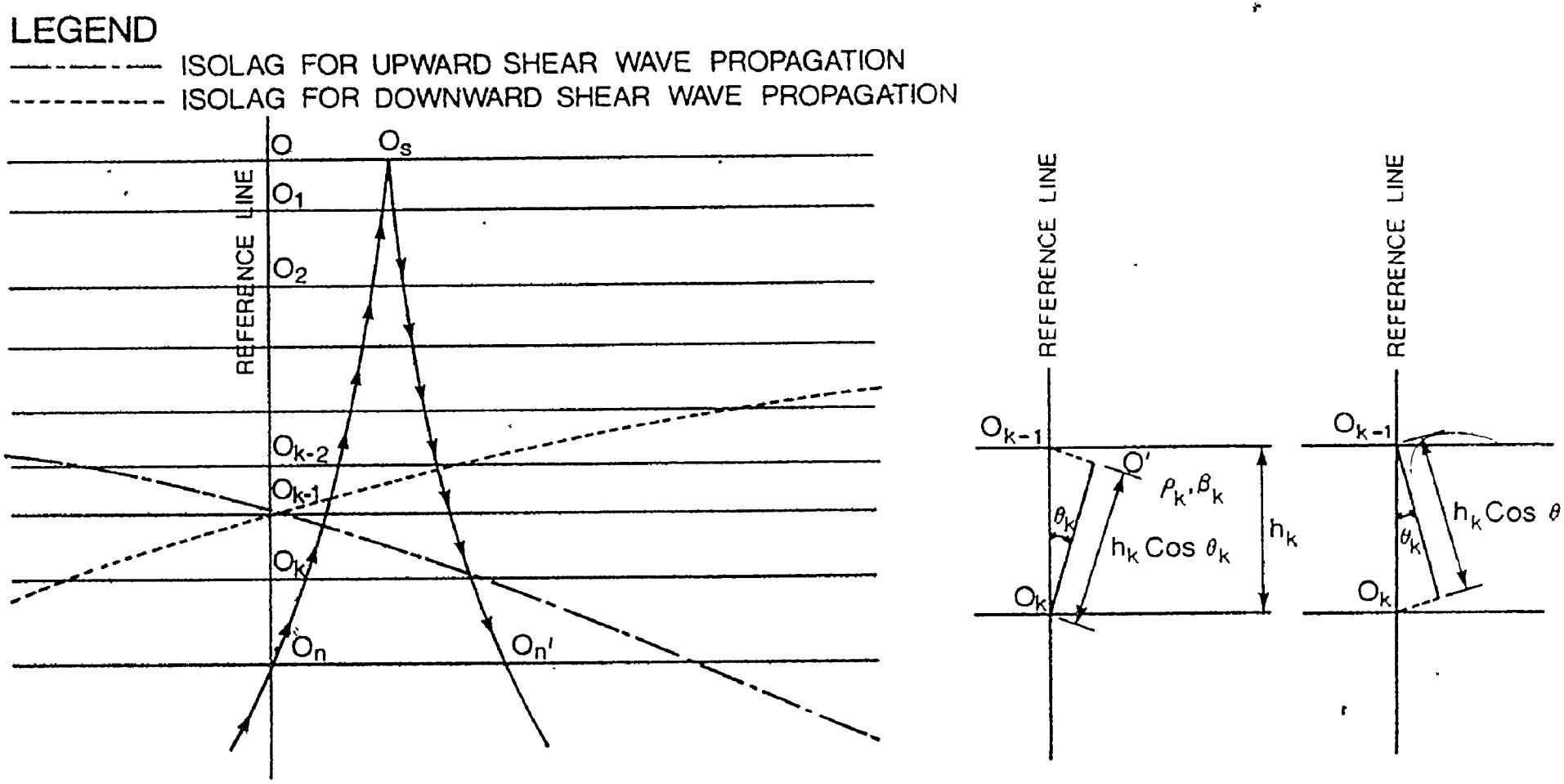

a. IDEALIZED PATH OF INCLINED SHEAR WAVE PROPAGATION IN SOIL LAYERS AND ISOLAGS

b. TIME LAG BETWEEN TOP AND BOTTOM INTERFACES OF LAYER k ALONG A VERTICAL DUE TO UPWAR AND DOWNWARD MOTIONS

FIG. 3-3 INCLINED PROPAGATION OF SHEAR WAVES THROUGH SOIL LAYERS

In general, for any two locations in the soil medium, there is a time lag between them and this may be decomposed into a vertical time lag component and a horizontal time lag component. For example, if t_ℓ is the time lag between 0_n and 0_s in Figure 3-3a, then

$$t_\ell = t_{v\ell} + t_{h\ell} \tag{3:4}$$

where $t_{v\ell}$ is the vertical time lag between 0_n and 0_s and $t_{h\ell}$ is the horizontal time lag between them.

3-D METHOD FOR SPATIAL SEISMIC MOTIONS

The computation of the three components of earthquake motions at certain specified locations may be accomplished by means of a three-dimensional analysis. However, such a procedure is quite complicated and time-consuming and therefore a simpler method involving plane wave motions is developed. The various assumptions in this analysis are presented in Section 3-B. The first step in the procedure is to determine the relative contributions of plane Rayleigh and shear waves to the motions, based on the focal depth and epicentral distance. There are not enough data for the vertical component of seismic motion and the usual available information is in the form of acceleration records in two perpendicular horizontal directions either at the surface level or the base rock level. The axes x and y are chosen to refer to these two directions and the z axis is vertical. First, the record for the x direction motions is considered and the components of accelerations in the x and z directions at the required locations are computed by assuming that these motions are produced by the propagation of plane

Rayleigh and shear waves on the x-z plane. In a similar way the acceleration components in the y and z directions at these locations may be calculated using the record for the y direction motions and the wave propagation on the y-z plane. The z component of the acceleration at these locations is the algebraic sum of the values for the two planar motions. The procedure for the spatial motion computation during earthquakes is outlined in Section 3-D-1.

3-D-1 Computation Procedure

A method of computation for the three components of earthquake motions at a specified location is presented. It is assumed that the transfer of energy during an earthquake is the outcome of two types of plane wave motions, namely, the inclined propagation of shear waves and the horizontal propagation of Rayleigh waves. The soil medium is idealized into a system of horizontally stratified layers. The effect of shear waves is studied using the multiple reflection criterion while the amplification of motions due to Rayleigh waves is calculated in the frequency domain.

As the shear waves travel in an inclined direction, there is a time lag in the arrival of them not only in the vertical direction but also in the horizontal. In the case of horizontally polarized Rayleigh waves the time lag occurs only in the horizontal direction.

Computation procedure calls for a clear identification of the various locations. For this purpose, a vertical line is taken as the

reference as in Figure 3-2 and the horizontal distances (x and y coordinates) are measured from this line. Any point in space is defined by its x and y coordinates and the interface on which it lies. The procedure for the computation for spatial motions is followed systematically.

(1) For each point in the required set, where motions are to be computed, list the x and y coordinates and the interface number corresponding to its location.

(2) Determine the incident angle of the seismic wave at the surface using Equation B:3. For nearby sites, the angle of incidence at the surface in degrees is $\beta_1/240$, where β_1 is the shear wave velocity in ft/sec in the surface layer while it is zero for distant sites. As the ratio of the sine of the incident angle and the shear wave velocity in any layer is constant, these angles in the various layers may be worked out using Equation B:4.

(3) Compute the x directional time lag for each point with respect to the reference line O_n-O. Referring to Figure 3-2, the time lag of P_k is measured with relation to O_k while that of P_{k-1} is ascertained with reference to O_{k-1}. As both P_k and P_{k-1} have the same x coordinate, the x directional time lags for both P_k and P_{k-1} are equal. In a similar way, the y directional time lags for the various points shall be determined.

(4) For short epicentral distances, it may be assumed that the contribution of shear waves is 75%. When the ratio of the epicentral distance to the focal depth reaches 5, only shear waves need be considered. For distances in between these limits, interpolation is required. Let the contribution of shear waves be denoted by ξ.

(5) If there is any contribution due to Rayleigh waves ($\xi \neq 1$), then evaluate the transfer functions for interface responses due to Rayleigh wave propagation using the procedure given in Section 2-B-1. For the kth layer, these transfer functions are T_k and T_{vk} for the horizontal and vertical motions. The response of the kth layer as a result of Rayleigh wave motions at any time t may be computed as the product of $(1-\xi)$, its transfer function and the surface response at time t.

(6) If the surface responses are available as data, then these motions are valid for the point 0 on the reference line (Figure 3-3a). Let S(t) be the excitation due to incident waves when arriving at 0 at any time t. Then it may be resolved into two portions, one due to shear wave propagation and the other due to Rayleigh waves. The portion of the excitation carried by shear waves is ξ S(t) and the remaining portion of $(1-\xi)$ S(t) is taken by Rayleigh waves. If instead of the surface response the base motions are available, then they refer to the point 0_n.

(7) From given data for 0_n or 0, proceed and compute the response calculations for points such as 0_k and 0_{k-1} along the reference line and located at interface levels using only the shear wave propagation theory. The vertical time lag between the two adjacent interface points 0_{k-1} and 0_k is given by $h_k \cos \theta_k/\beta_k$. If motions at 0_n are available, then Equations 2:14 and 2:16 are applicable while Equations 2:17 and 2:18 are to be used for the case of given motions at 0. However, it shall be remembered that in all expressions h_k must be replaced by $h_k \cos \theta_k$ in Equations 2:14 to 2:18. First the x direction motions (E-W direction) are computed for the entire period of the record. Let $\ddot{u}'_0(t)$, $\ddot{u}'_1(t)$, ..., $\ddot{u}'_n(t)$ be the computed x direction motions of interface points 0, 0_1, ..., 0_n at time t. As these motions did not yet account for the Rayleigh waves, a correction is required in the values. Let $\ddot{u}_0(t)$, $\ddot{u}_1(t)$, ..., $\ddot{u}_n(b)$ be the corrected x direction motions at the interface points. Then the following relationships hold:

$$\ddot{u}_0(t) = \ddot{u}'_0(t)$$

$$\ddot{u}_1(t) = \xi\, \ddot{u}'_1(t) + (1-\xi)\, T_1\, \ddot{u}'_0(t)$$

$$\ddot{u}_k(t) = \xi\, \ddot{u}'_k(t) + (1-\xi)\, T_k\, \ddot{u}'_0(t) \qquad (3:5)$$

$$\ddot{u}_n(t) = \xi\, \ddot{u}'_n(t) + (1-\xi)\, T_n\, \ddot{u}'_0(t)$$

There is a computational advantage in storing the pre-correction values of the x direction motions, namely, $\ddot{u}_o'(t)$, $\ddot{u}_1'(t)$, ..., $\ddot{u}_n'(t)$. In a similar way compute and store the y direction (N-S direction) motions $\ddot{v}_o'(t)$, $\ddot{v}_1'(t)$, ..., $\ddot{v}_n'(t)$. The relationships in Equation 3:5 hold for y direction motions if u is replaced by v in all expressions.

(8) The spatial motions at the various required locations are computed one by one. For example, if the responses at O_k and P_k in Figure 3-2 are required, then they may be computed using the following relationships:

$$\ddot{u}_{ok}(t) = \xi\, \ddot{u}_k'(t) + (1-\xi)\, T_k\, \ddot{u}_o'(t)$$

$$\ddot{v}_{ok}(t) = \xi\, \ddot{v}_k'(t) + (1-\xi)\, T_k\, \ddot{v}_o'(t)$$

$$\ddot{w}_{ok}(t) = \xi \tan \theta_k\, [\ddot{u}_k'(t) + \ddot{v}_k'(t)] + (1-\xi)\, T_{vk} [\ddot{u}_o'(t) + \ddot{v}_o'(t)]$$

$$\ddot{u}_{pk}(t) = \xi\, \ddot{u}_k'(t-t_{hp}) + (1-\xi)\, T_k\, \ddot{u}_o'\, (t-t_{hp}) \qquad (3:6)$$

$$\ddot{v}_{pk}(t) = \xi\, \ddot{v}_k'(t-t_{hp}) + (1-\xi)\, T_k\, \ddot{v}_o'\, (t-t_{hp})$$

$$\ddot{w}_{pk}(t) = \xi \tan \theta_k [\ddot{u}_k(t-t_{hp}) + \ddot{v}_k'\, (t-t_{hp})]$$

$$+ (1-\xi)\, T_{vk}\, [\ddot{u}_o'(t-t_{hp}) + \ddot{v}_o'(t-t_{hp})]$$

3-E ILLUSTRATION

The three-layer system (System 2) used to study the response of soil layers in Section 2-F is chosen to illustrate the importance of spatial seismic motions. The properties of the system are given in Table 2-2. The motion considered is the E-W component for the first half second during the El Centro Earthquake of 1940, this being assumed as the record at the base rock level. The station considered was located at a short epicentral distance and for this case, the relative contribution of Rayleigh waves was taken as 25%.

The computation was accomplished using the computer program SPARES. A flow chart giving the sequence of operations in the program SPARES is shown in Figure 3-4. The program follows the procedure for spatial seismic motion computations presented in Section 3-D-1. For the system considered, the angle of incidence of the motion at the surface was found to be 2.6 degrees. To demonstrate the variation in seismic motions along the vertical and horizontal directions, eight locations are considered and these may be visualized as the top and bottom corners of the rectangular three-layer soil box shown in Figure 3-1. The spatial coordinates of these locations are given in Table 3-1. Figure 3-5 shows the responses at these locations and it is obvious from this illustration that motions at the same levels are practically identical except for a time lag between these motions.

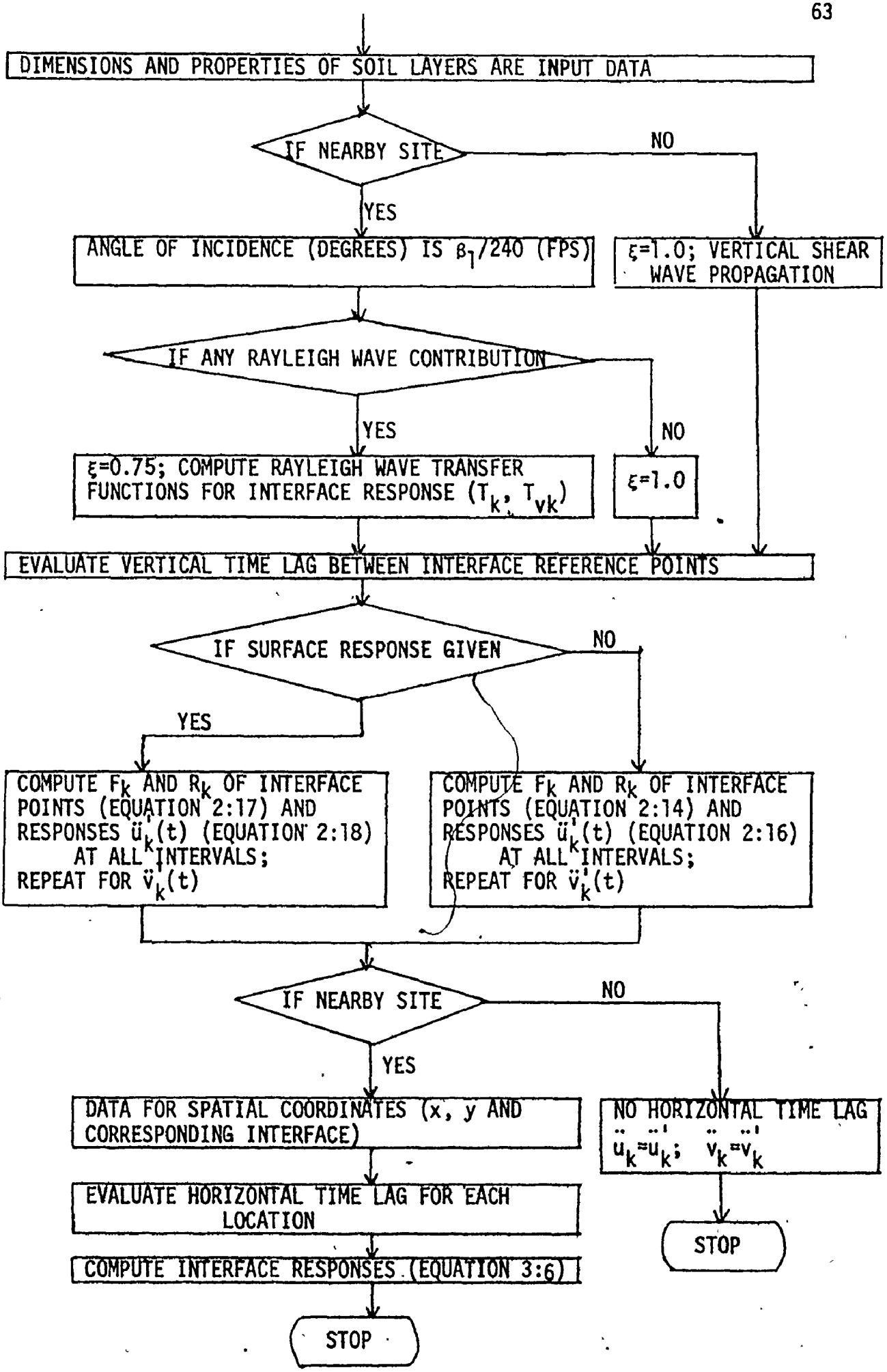
DIMENSIONS AND PROPERTIES OF SOIL LAYERS ARE INPUT DATA
IF NEARBY SITE
NO
YES
ANGLE OF INCIDENCE (DEGREES) IS β_1/240 (FPS)
ξ=1.0; VERTICAL SHEAR WAVE PROPAGATION
IF ANY RAYLEIGH WAVE CONTRIBUTION
YES
NO
ξ=0.75; COMPUTE RAYLEIGH WAVE TRANSFER FUNCTIONS FOR INTERFACE RESPONSE (T_k, T_{vk})
ξ=1.0
EVALUATE VERTICAL TIME LAG BETWEEN INTERFACE REFERENCE POINTS
IF SURFACE RESPONSE GIVEN
NO
YES
COMPUTE F_k AND R_k OF INTERFACE POINTS (EQUATION 2:17) AND RESPONSES $\ddot{u}'_k(t)$ (EQUATION 2:18) AT ALL INTERVALS; REPEAT FOR $\ddot{v}'_k(t)$
COMPUTE F_k AND R_k OF INTERFACE POINTS (EQUATION 2:14) AND RESPONSES $\ddot{u}'_k(t)$ (EQUATION 2:16) AT ALL INTERVALS; REPEAT FOR $\ddot{v}'_k(t)$
IF NEARBY SITE
NO
YES
DATA FOR SPATIAL COORDINATES (x, y AND CORRESPONDING INTERFACE)
NO HORIZONTAL TIME LAG
$\ddot{u}_k=\ddot{u}'_k$; $\ddot{v}_k=\ddot{v}'_k$
EVALUATE HORIZONTAL TIME LAG FOR EACH LOCATION
STOP
COMPUTE INTERFACE RESPONSES (EQUATION 3:6)
STOP

TABLE 3-1

SPATIAL COORDINATES OF LOCATIONS

LOCATION	x (E-W)	y (N-S)	z (Vertical)
1	0.0	0.0	0.0
2	50.0	0.0	0.0
3	0.0	0.0	475.0
4	50.0	0.0	475.0
5	0.0	40.0	0.0
6	50.0	40.0	0.0
7	0.0	40.0	475.0
8	50.0	40.0	475.0

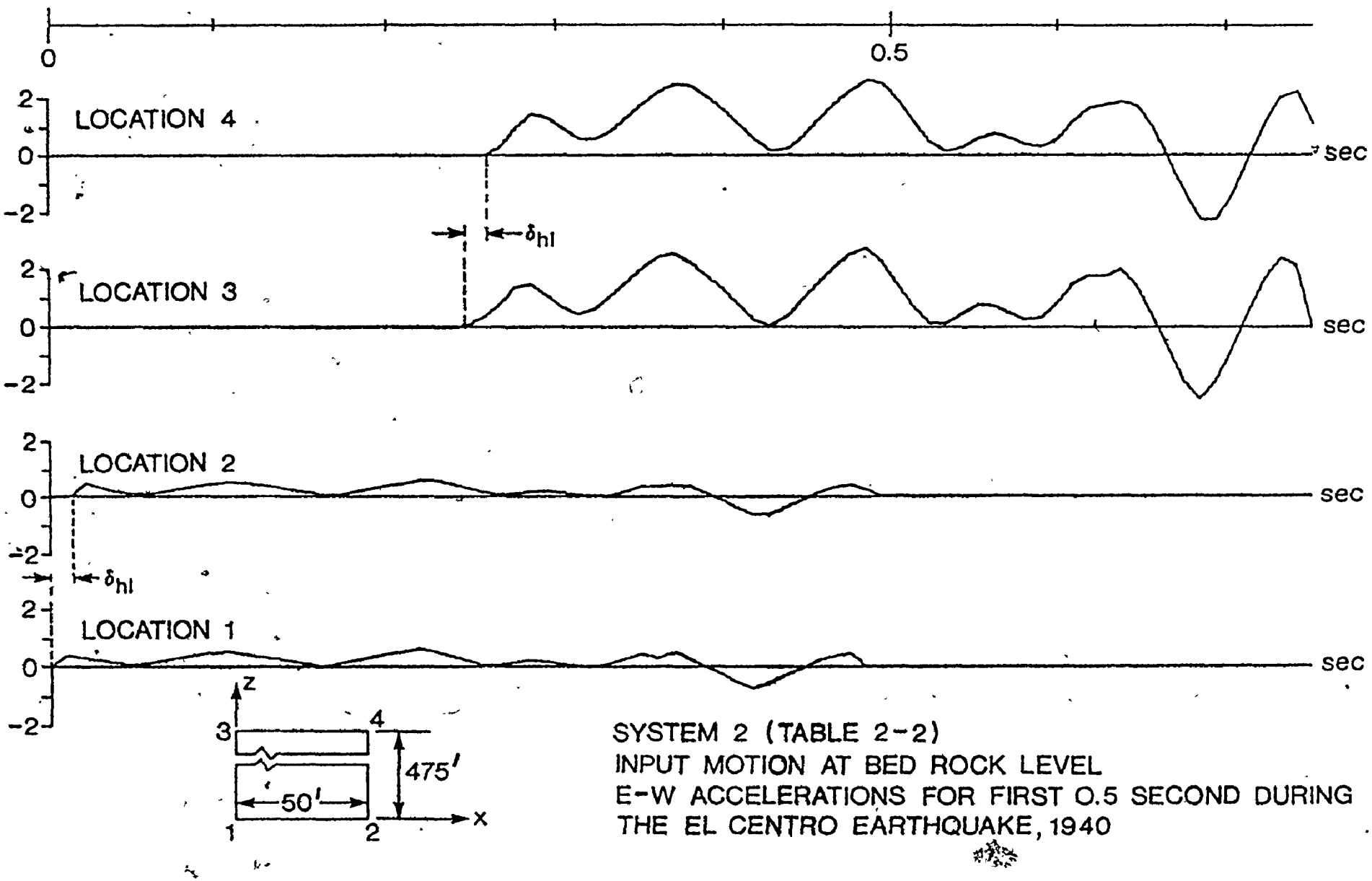

FIG. 3-5 SPATIAL MOTIONS FOR THREE-LAYER SYSTEM

CHAPTER IV

ANALYSIS OF AXISYMMETRIC SOLIDS UNDER NONSYMMETRIC STATIC LOADING

4-A INTRODUCTION

A finite element procedure suitable for the static analysis of axisymmetric solids under axisymmetric loading has been developed by Clough [15], Zienkiewicz [98] and other researchers. For axisymmetric solids, the elastic continuum is replaced by a finite number of axisymmetric ring elements connected at a finite number of circumferential joints or nodes. Figure 4-1 shows the structure idealization and typical triangular and quadrilateral axisymmetric ring elements. When the loading is axisymmetric, the pertinent displacements are those in the radial and the longitudinal directions. The method has also been extended to consider cases of nonsymmetric loadings which are symmetric about a plane containing the axis of revolution [51, 94]. For nonsymmetric loading, the circumferential displacements are also to be considered.

There are a few specific problems of axisymmetric structures, which are subjected to nonsymmetric loads and/or displacements. Here the components of loads and displacements are functions of not only r and z but also of θ, the circumferential direction. To maintain equilibrium, there is a tangential component of the displacement associated with θ.

θ and

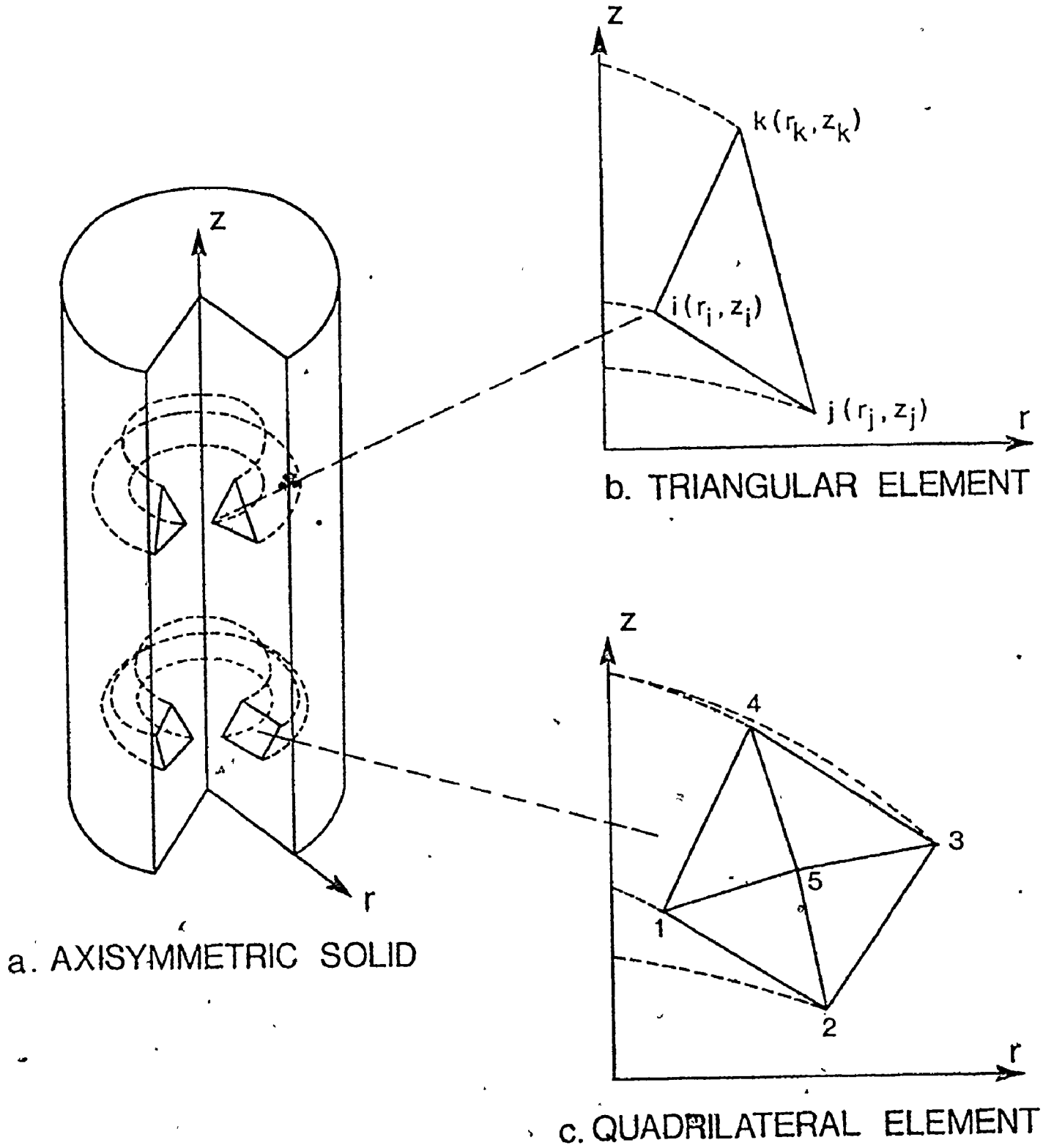

FIG. 4-1 AXISYMMETRIC SOLID AND TYPICAL RING ELEMENTS

this permits the simplification of the problem. The most general case of nonsymmetric loading may be resolved into two components, namely, the loads that are symmetric about a plane containing the $\theta = 0$ axis and those which show antisymmetry about this plane. Only the case of the nonsymmetric loading that has a plane of symmetry has been included in earlier reports [51, 94]. The formulation in this chapter is applicable to the most general problem of nonsymmetric loads and/or displacements in an axisymmetric structure. The analysis of such a structure may be separated into a series of solutions by employing a complete Fourier expansion for each load and displacement. Depending on the accuracy sought and also the rate of convergence of the computed results, the number of harmonics may be limited. The unknowns are solved in each harmonic and then adding corresponding quantities algebraically, the final results are computed.

4-B BASIC PROCEDURE

When the loading on the structure is known and it is required to solve for the nodal ring displacements and element stresses, a systematic procedure is followed as outlined in this section.

(1) Divide the cross section of the structure into a system of finite elements suitable to the geometry and the type of problem. The basic element is the triangular ring as shown in Figure 4-1b and these triangles may be used to make up quadrilateral ring elements. In certain situations, it may

be required to represent a particular property within the structure. As an example, the behaviour of the pile-soil interface is important in the analysis. Special elements may be used for this purpose and it is possible to assign the stiffness of these interface elements.

(2) Evaluate the stiffness matrix for each element in the assemblage. The stiffness matrix defines the relationship for the nodal forces due to unit displacement components at the various nodes of the element.

(3) Assemble the stiffness matrices of all the elements into a global stiffness matrix [K] which represents the entire structure.

(4) Solve the entire system of stiffness equations for nodal displacements.

$$\{F_N\} = [K]\{u_N\} \tag{4:1}$$

(5) Compute the element stresses resulting from the computed nodal displacements.

If mixed boundary conditions are specified, then it is required to compute the unknown forces and displacements for which Equation 4:1 is rewritten as

$$\left\{\begin{array}{c} F_a \\ \hline F_b \end{array}\right\} = \left[\begin{array}{c|c} K_{aa} & K_{ab} \\ \hline K_{ba} & K_{bb} \end{array}\right] \left\{\begin{array}{c} u_a \\ \hline u_b \end{array}\right\} \tag{4:2}$$

where

$\{F_a\}$ are the specified nodal forces,

$\{F_b\}$ are the unknown nodal forces,

$\{u_a\}$ are the unknown nodal displacements, and

$\{u_b\}$ are the specified nodal displacements

4-C FORMULATION OF THE STIFFNESS MATRIX FOR A GENERAL TRIANGULAR RING ELEMENT

Figure 4-1b shows a typical triangular ring element. For the nonsymmetric loading which is most general, the displacement and forces are expanded in Fourier series form:

$$
\begin{aligned}
u &= \sum_{0}^{L} u_n \cos n\theta + \sum_{1}^{L} u_m \sin m\theta \\
v &= \sum_{1}^{L} v_n \sin n\theta + \sum_{1}^{L} v_m \cos m\theta \\
w &= \sum_{0}^{L} w_n \cos n\theta + \sum_{1}^{L} w_m \sin m\theta \\
F_r &= \sum_{0}^{L} F_{rn} \cos n\theta + \sum_{1}^{L} F_{rm} \sin m\theta \\
F_\theta &= \sum_{1}^{L} F_{\theta n} \sin n\theta + \sum_{1}^{L} F_{\theta m} \cos m\theta \\
F_z &= \sum_{0}^{L} F_{zn} \cos n\theta + \sum_{1}^{L} F_{zm} \sin m\theta \ .
\end{aligned}
\tag{4:3}
$$

where u_n, v_n and w_n are the displacements and F_{rn}, $F_{\theta n}$ and F_{zn} are the forces per unit angle (1 radian) length of circumference in the radial, circumferential and axial directions in the nth harmonic. The terms included in the first sum are those which are symmetric about a plane containing $\theta = 0$ axis and the terms in the second sum are antisymmetric about this plane. The axisymmetric loading is included in the symmetric harmonics and for which n = 0. Figure 4-2 shows the loading in the first few harmonics.

With the assumption of the linear displacement field, the displacements u_n, v_n and w_n (n being n or m) are expressed in terms of the nine generalized displacement coordinates, α_{1n}, α_{2n}, ..., α_{9n}.

$$\begin{Bmatrix} u_n \\ v_n \\ w_n \end{Bmatrix} = \begin{Bmatrix} \alpha_{1n} + \alpha_{2n} r + \alpha_{3n} z \\ \alpha_{4n} \quad \alpha_{5n} r + \alpha_{6n} z \\ \alpha_{7n} + \alpha_{8n} r + \alpha_{9n} z \end{Bmatrix} \tag{4:4}$$

The nine equations relating the nodal displacements to the generalized displacement coordinates may be formulated by substituting the corresponding nodal coordinates into Equation 4:4. It is then possible to write the generalized displacement coordinates in terms of the nodal displacements.

$$\{K\} = [C^{-1}]\{u_N\} \tag{4:5}$$

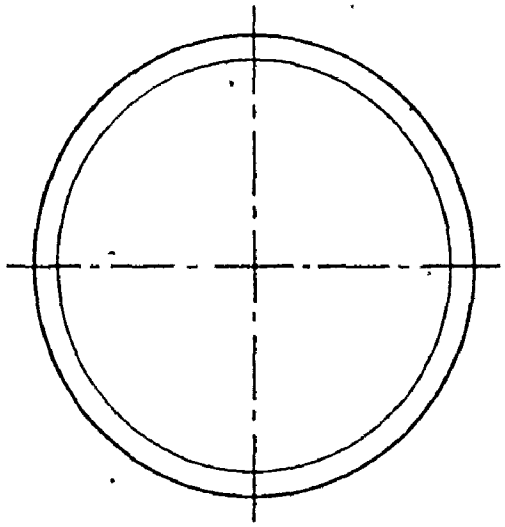

a. N = O (SYMMETRIC)

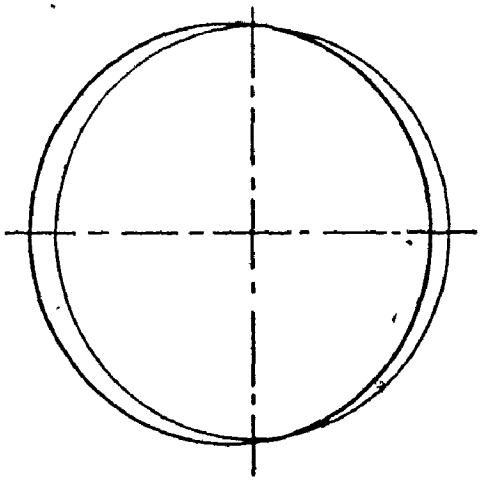

b. N = 1 (SYMMETRIC)

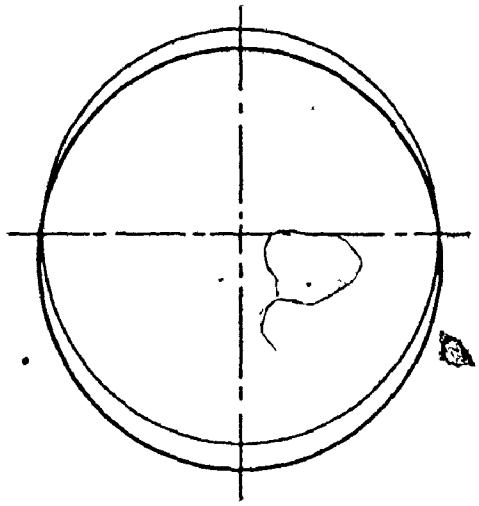

c. N = 1 (ANTISYMMETRIC)

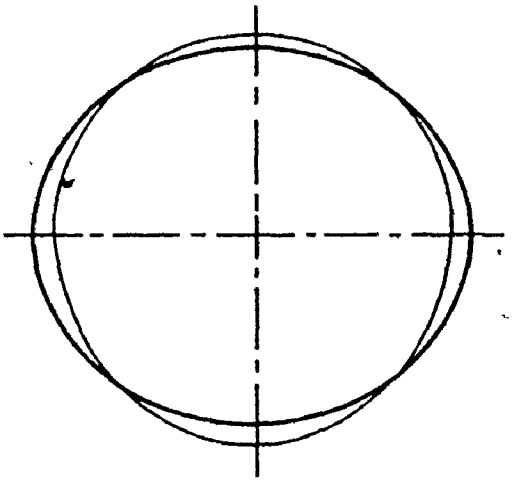

d. N = 2 (SY TRIC)

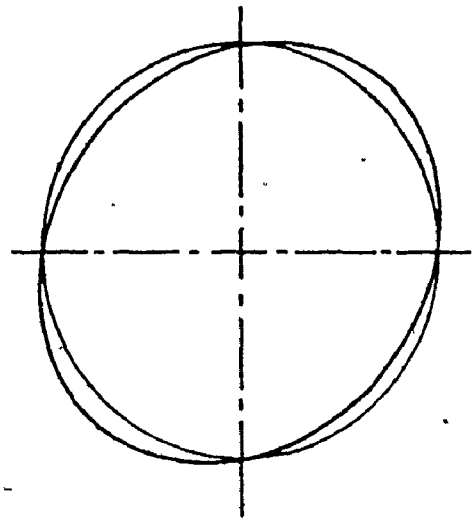

N = 2 (ANT

The strains within the element may be determined by differentiating Equation 4:4 according to the basic relationships between strains and displacements.

$$\varepsilon_{rr} = \frac{\partial u}{\partial r}$$

$$\varepsilon_{\theta\theta} = \frac{1}{r}\left(u + \frac{\partial v}{\partial \theta}\right)$$

$$\varepsilon_{zz} = \frac{\partial w}{\partial z}$$

$$\gamma_{rz} = \frac{\partial u}{\partial z} + \frac{\partial w}{\partial r} \qquad (4:6)$$

$$\gamma_{r\theta} = \frac{1}{r}\frac{\partial u}{\partial \theta} + \frac{\partial v}{\partial r} - \frac{v}{r}$$

$$\gamma_{z\theta} = \frac{\partial v}{\partial z} + \frac{1}{r}\frac{\partial w}{\partial \theta}$$

Equation 4:6 can be written in matrix form

$$\{\varepsilon\} = [B]\,\{\alpha\} \qquad (4:7)$$

Combining Equations 4:5 and 4:7 the relationship between the strains and nodal displacements is expressed as

$$\{\varepsilon\} = [B]\,[C^{-1}]\,\{u_N\} \qquad (4:8)$$

The stresses and strains within the element are related by the constitutive matrix

$$\{\sigma\} = [D]\,\{\varepsilon\} \qquad (4:9)$$

The work done by the nodal forces is expressed as

$$W = \frac{1}{2} \{u_N\}^T \{F_N\} \tag{4:10}$$

and the strain energy stored in the deflected element due to these nodal forces may be written

$$U = \frac{1}{2} \int_{\text{volume}} \{\varepsilon\}^T \{\sigma\} \, dvol \tag{4:11}$$

Then from the principle of minimum potential energy, the work done by the forces and the energy stored in the element may be equated

$$\{u_N\}^T \{F_N\} = \int_{\text{volume}} \{\varepsilon\}^T \{\sigma\} \, dvol \tag{4:12}$$

or

$$\{F_N\} = [k] \{u_N\} \tag{4:13}$$

where [k], the element stiffness matrix is expressed as

$$[k] = [C^{-1}]^T \left(\int_{\text{volume}} [B]^T [D] [B] \, dvol \right) [C^{-1}] \tag{4:14}$$

The expressions for the displacements, loads and strains are different for the two types of harmonics.

4-C-1 Symmetric Harmonic

In this type of harmonic [51,94], the displacements are symmetric about a plane containing the $\theta = 0$ axis. The total forces and

displacements due to these harmonics are

$$u = \sum_{0}^{L} u_n \cos n\theta$$

$$v = \sum_{1}^{L} v_n \sin n\theta$$

$$w = \sum_{0}^{L} w_n \cos n\theta$$

$$F_r = \sum_{0}^{L} F_{rn} \cos n\theta \qquad (4:15)$$

$$F_\theta = \sum_{1}^{L} F_{\theta n} \sin n\theta$$

$$F_z = \sum_{0}^{L} F_{zn} \cos n\theta$$

The strains corresponding to these displacements are expressed as

$$\varepsilon_{rr} = \sum_{0}^{L} \varepsilon_{rrn} \cos n\theta$$

$$\varepsilon_{\theta\theta} = \sum_{1}^{L} \varepsilon_{\theta\theta n} \sin n\theta$$

$$\varepsilon_{zz} = \sum_{0}^{L} \varepsilon_{zzn} \cos n\theta \qquad (4:16\text{-a})$$

$$\gamma_{rz} = \sum_{0}^{L} \gamma_{rzn} \cos n\theta$$

$$\gamma_{r\theta} = \sum_{1}^{L} \gamma_{r\theta n} \sin n\theta \qquad (4:16\text{-b})$$

$$\gamma_{\theta z} = \sum_{1}^{L} \gamma_{\theta zn} \sin n\theta$$

From Equations 4:14 to 4:16, the strains and displacements have the relationship given in Equation 4:7.

The matrices [D], [B], $[C^{-1}]$ and $([B]^T [D] [B])$ used in the formulation of the stiffness matrix $[k_n]$ are given in Appendix C-1. It is assumed in the derivation for [D] that the material is isotropic. Then the stiffness of the element is given by Equation 4:14. The formulation of $[k_n]$ involves some lengthy integrals since the elements are axisymmetric rings. When the matrix product$([B]^T [D] [B])$ is introduced in Equation 4:14, there are distinct integrals λ_1, λ_2, ..., λ_6 which need evaluation. This may be accomplished by means of either numerical integration or explicit multiplication and term by term integration using Green's Lemma. It has been established [48] that the solutions using any numerical integration procedure are valid so long as it accurately determines the volume of the element. The one point integration about the centroidal point $(\bar{r},\bar{z})$ gives simplified forms of these integrals while correctly computing the volume of the element. On the other hand the expressions for these integrals using the exact procedure are very long and as such it is considered accurate enough to

make use of the simplified forms using one point integration. This simplification does not jeopardize the accuracy of the solution and further it has been reported [98] that often these simplified forms are superior to the exact solution when elements at large radial distances are involved. The values obtained for λ_1, λ_2 and λ_3 are unchanged because of the simple procedure, while there is an insignificant alteration in the values of λ_4, λ_5 and λ_6. The simplified and exact forms of the six axisymmetric integrals are included in Appendix C-2.

4-C-2 Antisymmetric Harmonic

The displacements which are antisymmetric about the plane containing the $\theta = 0$ axis are accounted for by this type of harmonics. The formulation of the stiffness matrix for this type of harmonic has not been presented earlier. The total forces and displacements for these harmonics are

$$
\begin{aligned}
u &= \sum_{1}^{L} u_m \sin m\theta \\
v &= \sum_{1}^{L} v_m \cos m\theta \\
w &= \sum_{1}^{L} w_m \sin m\theta \\
F_r &= \sum_{1}^{L} F_{rm} \sin m\theta
\end{aligned}
\qquad (4:17\text{-a})
$$

$$F_\theta = \sum_1^L F_{\theta m} \cos m\theta$$

$$F_z = \sum_1^L F_{zm} \sin m\theta \qquad (4:17\text{-b})$$

The corresponding strains may be stated as

$$\varepsilon_{rr} = \sum_1^L \varepsilon_{rrm} \sin m\theta$$

$$\varepsilon_{\theta\theta} = \sum_1^L \varepsilon_{\theta\theta m} \cos m\theta$$

$$\varepsilon_{zz} = \sum_1^L \varepsilon_{zzm} \sin m\theta$$

$$\gamma_{rz} = \sum_1^L \gamma_{rzm} \sin m\theta \qquad (4:18)$$

$$\gamma_{r\theta} = \sum_1^L \gamma_{r\theta m} \cos m\theta$$

$$\gamma_{\theta z} = \sum_1^L \gamma_{\theta zm} \cos m\theta$$

It is of interest to note that the expressions in Equations 4:17 and 4:18 may be obtained from Equations 4:15 and 4:16 by interchanging sin $n\theta$ and cos $n\theta$ and carrying out summations over harmonics $m = 1$ to $m = L$. The matrices [D] and $[C^{-1}]$ are unchanged while the matrix [B] and the matrix product ($[B]^T$ [D] [B]) for this type of harmonic are the same as that given for the symmetric harmonic in Appendix C-1, with the exception that all underlined terms are changed in sign.

4-D STIFFNESS MATRIX FOR A QUADRILATERAL RING ELEMENT

Figure 4-1c shows the typical quadrilaterial element composed of four triangular ring subelements. For the symmetric as well as the antisymmetric harmonic, the equilibrium equations are first formed for each triangular ring subelement and then systematically added up to form the equilibrium equations for the quadrilateral ring element. There are fifteen equations and these may be written in the form:

$$\begin{Bmatrix} F_1 \\ (12x1) \\ \hline F_2 \\ (3x1) \end{Bmatrix} = \left[\begin{array}{c|c} k_{11} & k_{12} \\ (12x12) & (12x3) \\ \hline k_{21} & k_{22} \\ (3x12) & (3x3) \end{array}\right] \begin{Bmatrix} u_1 \\ (12x1) \\ \hline u_2 \\ (3x1) \end{Bmatrix} \qquad (4:19)$$

where $\{F_1\}$ and $\{u_1\}$ are associated with the exterior nodes 1-4 and $\{F_2\}$ and $\{u_2\}$ are those for the interior node 5. The matrix can be condensed in the form [96]

$$\{F^*\} = [k^*]\ \{u_1\} \qquad (4:20)$$

where

$$[k^*] = [k_{11}] - [k_{12}]\ [k_{22}^{-1}]\ [k_{21}] \qquad (4:21)$$

and

$$\{F^*\} = \{F_1\} - [k_{12}]\ [k_{22}^{-1}]\ \{F_2\}$$

After the evaluation of displacements $\{u_1\}$, the unknown displacements $\{u_2\}$ of the interior node may be obtained from the following relationships:

$$\{u_2\} = [k_{22}^{-1}] (\{F_2\} - [k_{21}] \{F_1\}) \tag{4:22}$$

Usually, the forces at the interior nodes are zero; however, any values may be prescribed in the solution.

4-E LINKAGE ELEMENTS

There exists some skin resistance at the pile-soil interface as a result of which there is a distribution of load transfer between the pile and the soil. The ultimate value of the skin resistance depends on the normal force and friction coefficient at the interface for the portion of a pile embedded in sand. In the case of the portion of a pile embedded in clay, the skin resistance depends on the adhesion between the pile and the soil. When the ultimate skin resistance is exceeded, the pile may slip through the soil in that zone. The linkage between the pile and the soil at the interface may be accounted for by means of linkage elements.

4-E-1 Stiffness Matrix for a Linkage Element

The interface element used is similar to the one developed by Goodman [32,49] and is an extension of the procedure presented by Ellison [20, 21] for symmetric loading on a pile-soil system. In the method formulated by Goodman [32], the behaviour of an interface between two adjacent locations at a distance ℓ apart may be represented by an element having two pairs of nodes as shown in Figure 4-3a. Each pair of nodes have the same spatial coordinates as the corresponding end of the element; i.e., nodes I and L have the same spatial coordinates. The

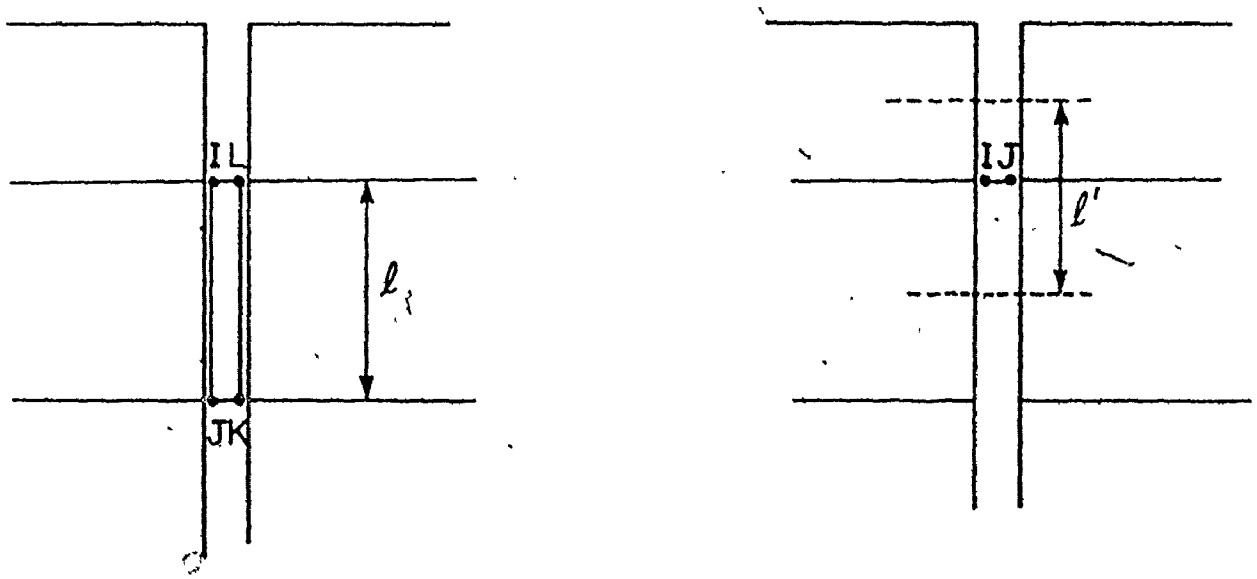

a. FOUR-NODED LINKAGE ELEMENT [32]

b. TWO-NODED LINKAGE ELEMENT [20,21]

FIG. 4-3 LINKAGE ELEMENTS

same type of solution is possible as an extension to the simplified approach independently developed by Ellison et al [21]. In this procedure, the interface behaviour over any distance ℓ' is typified by an element having a pair of nodes as shown in Figure 4-3b. The two nodal circles I and J have the same spartial coordinates and may be located anywhere within the structure without altering the geometry.

The stiffness matrix of the linkage element may be computed by considering the stiffness coefficients k_r, k_θ and k_z for the radial, circumferential and axial directions. A unit displacement in the positive radial direction at node I requires loads of $+k_r$ at node I and $-k_r$ at node J. Similarly loads of $+k_r$ at node J and $-k_r$ at node I are needed in order to cause a unit displacement in the radial direction at J. Proceeding along these lines, the force-displacement relationships for the linkage element may be established in matrix form:

$$\begin{Bmatrix} F_r^i \\ F_\theta^i \\ F_z^i \\ F_r^j \\ F_\theta^j \\ F_z^j \end{Bmatrix} = \begin{bmatrix} k_r & 0 & 0 & -k_r & 0 & 0 \\ 0 & k_\theta & 0 & 0 & -k_\theta & 0 \\ 0 & 0 & k_z & 0 & 0 & -k_z \\ -k_r & 0 & 0 & k_r & 0 & 0 \\ 0 & -k_\theta & 0 & 0 & k_\theta & 0 \\ 0 & 0 & -k_z & 0 & 0 & k_z \end{bmatrix} \begin{Bmatrix} u_i \\ v_i \\ w_i \\ u_j \\ v_j \\ w_j \end{Bmatrix} \qquad (4:23)$$

or

$$\{F\} = [k_s]\{u\} \tag{4:24}$$

where $[k_s]$ is the stiffness matrix of the linkage element. The stiffness of the linkage element is the same in each of the symmetric and antisymmetric harmonics.

4-F SOLUTION FOR NODAL DISPLACEMENTS, STRAINS AND STRESSES

The stiffness matrix of the entire structure is assembled by systematically combining the stiffness of all individual elements. The order of this matrix equals the number of unknown nodal displacements and/or forces. If the displacements are the only unknowns, then Equation 4:1 may be used for the solution, while Equation 4:2 applies for mixed boundary conditions. The stiffness matrix of the structure is banded and symmetric and as a result, special simplified solution techniques may be employed to solve Equation 4:1 or Equation 4:2. Once the nodal displacements are evaluated the strains in the triangular or quadrilateral element are given by Equation 4:8. By combining Equations 4:8 and 4:9, the relationship for stresses in terms of nodal displacements may be written

$$\{\sigma\} = [D]\,[B]\,[C^{-1}]\,\{u_N\} \tag{4:25}$$

Finally, from the definition of the linkage element, the stresses in it may be obtained as

$$\begin{Bmatrix} \sigma_{rr} \\ \sigma_{\theta\theta} \\ \cdot \end{Bmatrix} = \begin{bmatrix} k_r & 0 & 0 \\ 0 & k_\theta & 0 \\ 0 & 0 & k_z \end{bmatrix} \begin{Bmatrix} u_i - u_j \\ v_i - v_j \\ w_i - w_j \end{Bmatrix} \tag{4:26}$$

4-G COMPUTER PROGRAM FOR STATIC ANALYSIS

The static analysis of an axisymmetric structure under non-symmetric loading may be accomplished by means of the program STAX, which is developed using the principles described in Sections 4-C to 4-F. The program uncouples the problem into a series of analyses in different harmonics and algebraically adds up the solutions in the various harmonics to obtain the final results. The program STAX involves a series of operations which are presented in the form of a flow chart in Figure 4-4. The nodes are numbered in such a way that the band width of the stiffness matrix is brought to a minimum. It is possible to use combinations of triangular, quadrilateral and linkage elements in any order and the data for the various elements are given as input. The program considers the various harmonics in a specified order and computes the stiffness matrix of each individual element and assembles these matrices to form the banded global stiffness matrix in each harmonic, the various global matrices being stored on a file. The loads and/or displacements are fed in as input in the same order as the harmonics. For each harmonic, the program reads the stiffness matrix from the tape and the required data on loads and displacements and then computes the unknown displacements and loads using the subroutine BAND, which is based on Choleski's method. If mixed boundary conditions of displacements and loads are specified, the procedure needs some modification in the matrix [K] and the load vector {F}, as explained in Article 5 of Section 4-B. Once the displacements are computed, the strains and stresses in the elements may be worked out using Equations

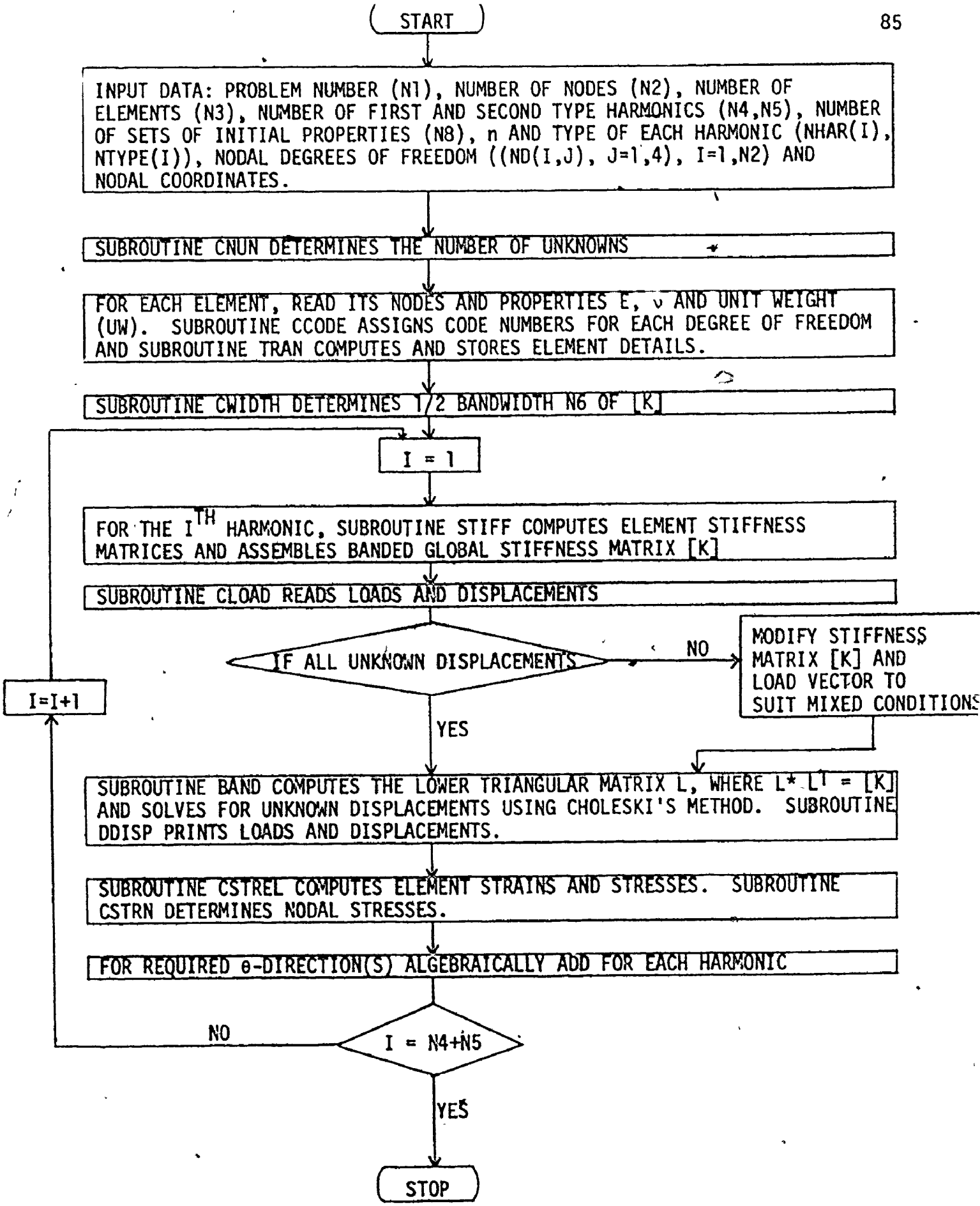

FIG. 4-4 FLOW CHART FOR AXISYMMETRIC STATIC PROGRAM (STAT).

4:8 and 4:9. In order to determine the stresses at the nodes from the element stresses, an averaging procedure is used. The operation is repeated for each remaining harmonic and finally the results are algebraically added up for any desired location(s) specified by the node and the circumferential coordinate, θ.

By systemmatically organizing the program, the computation time and the required storage are kept to a minimum. For the case of 94 nodes and 40 quadrilateral elements (160 triangular subelements), it takes only 280 seconds to solve the problem using 16 harmonics and adding up the results at all the nodes in two perpendicular directions, namely, $\theta=0$ and $\theta=90°$.

4-G-1 Example Problem - Split Cylinder Test

The computer program STAX developed for the analysis of axisymmetric structures under nonsymmetric loading was checked by investigating the stresses in the cylinder used in the Standard Split Cylinder Test (ASTM C496-66). In this test, a 6 in. diameter concrete cylinder (Figure 4-5) is placed with its axis horizontal between the platens of a testing machine and the load is increased until failure occurs by splitting along a vertical diameter [7]. From the load at failure, P, the splitting tensile stress, f_t, is computed using the relationship:

$$f_t = \frac{2P}{\pi LD} \qquad (4:27)$$

where D is the diameter and L is the length of the cylinder. The [illegible] is based on the ass[illegible] that

plane stress conditions exist in the specimen.

The cylinder used in the test has finite dimensions and therefore neither plane stress nor plane strain conditions would be valid. The analysis of the cylinder should be carried out as an axisymmetric structure under nonsymmetric loading. The loading on the cylinder is applied through two bearing strips and depending upon the width of the bearing strip and the distribution of the applied load on the strips. the loadings in the various harmonics vary. The nonsymmetric loading on the cylinder has a plane of symmetry and therefore the load coefficients in all antisymmetric harmonics would be zero. Further it was found that the load coefficients in all odd, symmetric harmonics were zero and thus it was only necessary to consider the loadings in the symmetric harmonics, n = 0, 2, 4, ..., etc.

As the nonsymmetric loading on the cylinder was separated into the loadings in the various harmonics, it was necessary to ensure that equilibrium conditions were satisfied at the boundary; i.e., the force on the boundary of the cylinder in contact with the bearing strip should equal the applied load whereas the free boundaries should be stress free. The load coefficients in the various harmonics were summed up in the ascending order of n and it was found that the error on the boundary conditions was less than 2% when 16 harmonics (n = 0, 2, ..., 30) were considered. By considering a few more harmonics, the error could be made practically zero.

The stresses in the symmetric harmonic for which n= 0 represent the axisymmetric loading. For a solid cylinder, Timoshenko [89] established that there could only be one state of stress distribution symmetric with respect to the axis due to a uniform axisymmetric loading. The radial and circumferential stresses would be equal and uniform in the cylinder. The results obtained using the program STAX were in agreement with this fact and this was an additional check on the program.

The stresses in the various harmonics were computed and algebraically added up to get the final results. It is of interest to note that only 5 (n=0, 2, ..., 8) harmonics are significant in the results. This showed that the results obtained using the series representation converge quickly.

The results indicated that the tensile stresses gradually decreased with increasing radius until about 0.75 times the radius, whereupon it became compressive, as shown in Figure 4-6. The variation of the tensile stresses along the axis is shown in Figure 4-5, with its maximum at the ends of the cylinder. Further, the stresses in the cylinder were found to be dependent on the length of the cylinder. Methods making use of the highly idealized assumptions of plane stress or strain are incapable of accounting for this axial variation in the stresses [81].

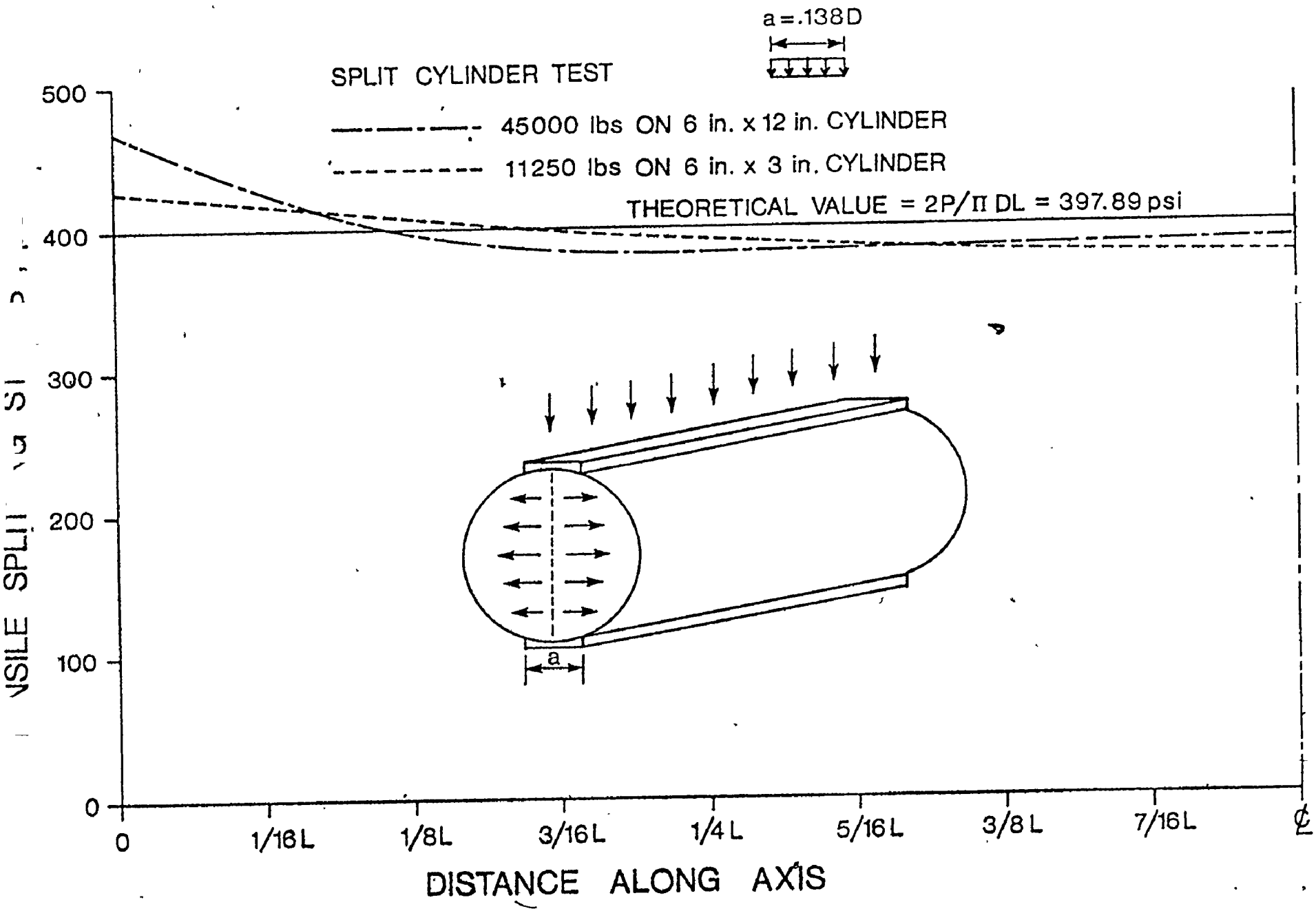

FIG. 4-5 VARIATION OF STRESS ALONG AXIS OF CYLINDER

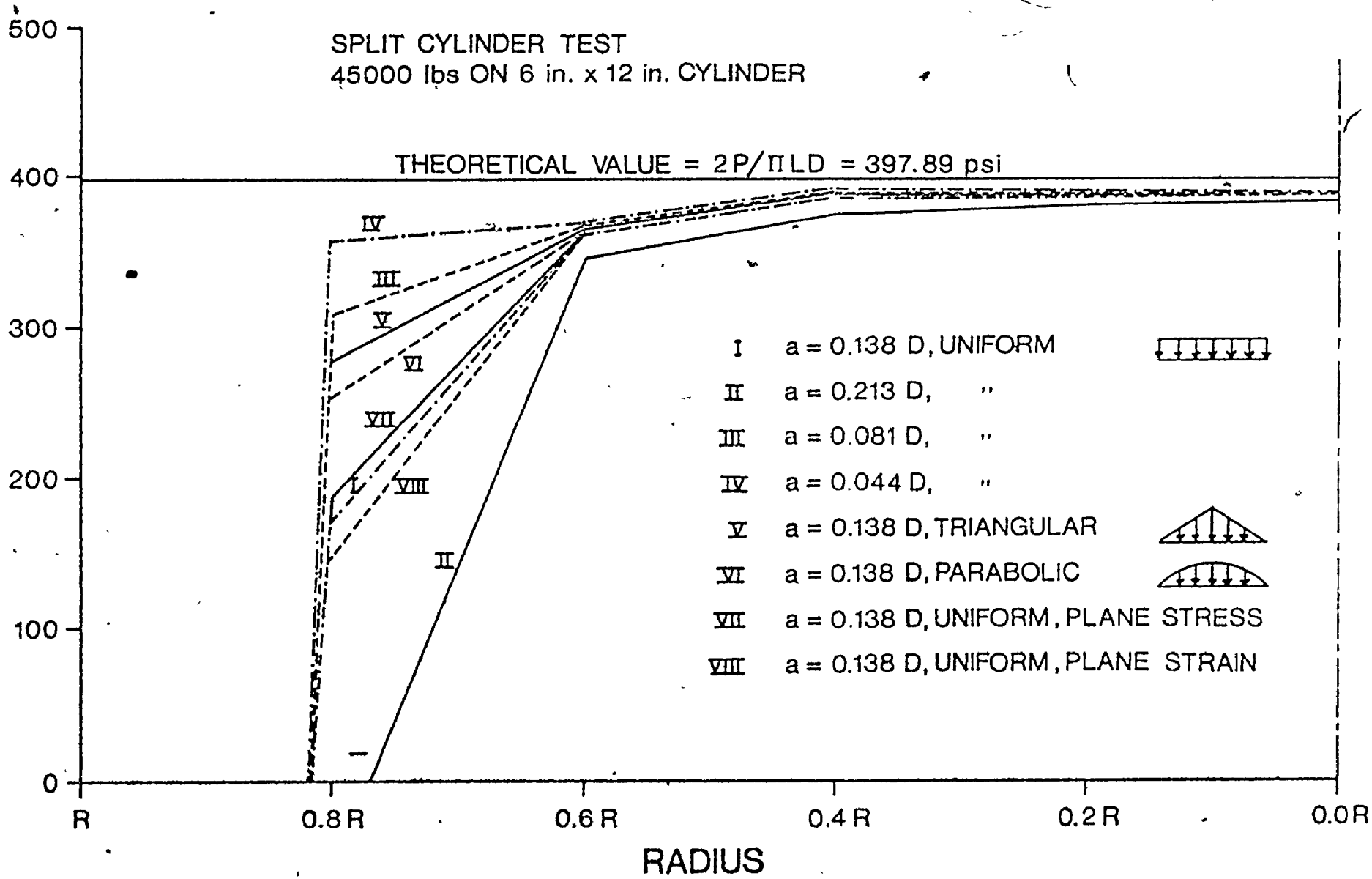

FIG. 4-6 VARIATION OF STRESS ALONG RADIUS OF CYLINDER AT SECTION MIDWAY ALONG AXIS

CHAPTER V

SOLUTION FOR POREPRESSURE PROBLEMS IN AXISYMMETRIC STRUCTURES

5-A INTRODUCTION

The geotechnical engineer often comes across problems in which an initially incompressible soil is loaded or a known volume change occurs in the material. The undrained triaxial test, the consolidation of a cylindrical soil sample and the driving of a pile in an area with a layer of undrained, saturated clay are some examples of axisymmetric structures subjected to such conditions. In problems of this nature it is required to evaluate the porepressures developed in the material so that realistic stress-strain relations can be established. In the finite element method, the stresses are expressed in terms of strains. However, this is not possible when the material is incompressible. For example, the chamber pressure in an undrained triaxial test may be increased without any change in volume of the soil. Thus there is no unique value of stress in terms of ~~the~~ strain. Mathematically speaking, the constitutive matrix includes a term $(1-2\nu)$ in the denominator. For an incompressible material $\nu = 0.5$ and therefore the elements of the constitutive matrix [D] become infinite. Therefore, the method of analysis of axisymmetric structures developed in Chapter 4 are not

of

The analysis of structures involving incompressible materials was first accomplished by Sokolnikoff [86] and Gibson [31]. The total volumetric stress was taken as an unknown and an additional equation specifying no volume change was used in the computations. Herrmann [39] formulated this technique for solving incompressible and nearly incompressible solids and this was extended to the finite element methods by Christian [10, 11, 12]. Both plane stress and strain problems have been solved using this procedure. Herein, an extension of this procedure is developed to analyze axisymmetric structures involving incompressible and nearly incompressible materials subjected to general nonsymmetric, static loadings.

5-B EFFECTIVE STRESS-STRAIN RELATIONSHIPS

When there are problems involving incompressible materials, the usual methods of analysis are not applicable because there are no unique total stress-strain relations. Such problems were solved by Sokolnikoff [86] by introducing total volumetric stress as an unknown and an equation of no volume change. Though the total stress-strain approach is not suitable, it is possible to define the stress-strain relations uniquely in terms of effective stresses. Then the problem reduces to one of finding the porepressures large enough to prevent any compression of the soil. As a result, there will be an additional unknown, namely, the porepressure and a new equation requiring no change in volume. This approach was formulated into a variational principle by [illegible] [39] who [illegible] total stresses in the constitutive relationships.

On the other hand, the methods of solution formulated by Christian [10, 11, 12] made use of effective stresses and are thus adopted readily to realistic stress-strain relations for soil.

The total stress-strain relations for an isotropic and linearly elastic material are in terms of total stress constants, E and ν. In the same way, the effective stresses are related to strains by effective stress constants $\bar{E}$ and $\bar{\nu}$. For an incompressible material, the total stress Poisson's ratio ν shall be one-half. The shear modulus is independent of the porepressure as the pore fluid carries no shear. Therefore, equating the total and effective stress shear moduli, the relationship between effective stress constants and total stress constants is expressed as

$$\frac{\bar{E}}{E} = \frac{1 + \bar{\nu}}{1.5} \tag{5:1}$$

5-C FINITE ELEMENT FORMULATION

The equations developed for the finite element formulation in usual problems involving compressible materials consist of equilibrium equations at the nodes. When the method is applied for the case of incompressible materials or porepressure problems, there are two types of equations, namely, the equilibrium equations at the nodes and the equations restricting the volume change in each element. Each equilibrium equation has the usual relations for displacement at neighboring nodes and additional terms involving porepressure in surrounding elements. The volume change may be set equal to zero for an incompressible material, or

an arbitrary specification of volume change may be allowed.

By choosing appropriate units for stress and volumetric strain, the coefficient matrix for the set of linear algebraic equations for each element is made symmetric. In order that the nodal displacements, u_N and porepressure quantities are nearer in magnitude, the porepressures are divided by the bulk modulus $K_B = \bar{E}/3(1-2\bar{\nu})$. Then the unknowns are the nodal displacements and $H_N = \zeta/K_B$, where ζ is the porepressure. For a triangular element, the resulting equations may be written

$$\left[\begin{array}{c:c} \underset{(9\times9)}{k} & \underset{(9\times1)}{k'} \\ \hdashline k'^{T}_{(1\times9)} & 0 \end{array}\right] \left\{\begin{array}{c} \underset{(9\times1)}{u_N} \\ \hdashline H_N \end{array}\right\} = \left\{\begin{array}{c} \underset{(9\times1)}{F_N} \\ \hdashline K_B \int_{vol} e_N dvol \end{array}\right\} \qquad (5:2)$$

where $[k']$ is given by Equation C:37 in Appendix C-3 and e_N is the specified volume change. As there is a zero on the diagonal, this is a singular set of equations and thus triangular ring elements are not suitable in the case of incompressible materials. The computational problem is avoided by using quadrilateral ring elements. The porepressure is assumed to be constant throughout the quadrilateral element and thus there is only one equation of volume change for each element in addition to the fifteen equilibrium equations at the nodes. These equations may be expressed as

$$\left[\begin{array}{c|c} k_{11} \; (13\times13) & k_{12} \; (13\times3) \\ \hline k_{21} \; (3\times13) & k_{22} \; (3\times3) \end{array}\right] \left\{\begin{array}{c} u_1 \; (12\times1) \\ \hline H_N \\ \hline u_2 \; (3\times1) \end{array}\right\} = \left\{\begin{array}{c} F_1 \; (12\times1) \\ \hline K_B \int_{vol} e_N dvol \\ \hline F_2 \; (3\times1) \end{array}\right\} \qquad (5:3)$$

Using the condensation procedure outlined in Section 4-D, the 16 x 16 element stiffness matrix may be reduced to a 13 x 13 matrix, by eliminating the internal degrees of freedom.

$$\left[k^* \; (13\times13)\right] \left\{\begin{array}{c} u_N \; (12\times1) \\ \hline H_N \end{array}\right\} = \left\{\begin{array}{c} F_1' \; (12\times1) \\ \hline F_2' \end{array}\right\} \qquad (5:4)$$

where $[k^*]$ is the stiffness matrix of the quadrilateral ring element in which there is a specified volume change.

5-D PROGRAM FOR ANALYSIS OF INCOMPRESSIBLE MATERIALS

The principles outlined in Sections 5-A to 5-C are utilized to develop the program PORAX, which is capable of analyzing axisymmetric structures under nonsymmetric, static loading and in which a certain volume change is specified. The program uses axisymmetric ring elements, may be quadrilateral or triangular or linkage elements. Only

quadrilateral elements are suitable when there is any restriction on the volume change or where porepressures are involved. When the loads and/or displacements are nonsymmetric, the analysis is separated into a series of solutions in different harmonics and the final solutions are obtained by algebraic summations. The sequence of operations in the program PORAX is given in the form of a flow chart as shown in Figure 5-1. The various harmonics are considered in a specified order and for each harmonic, first the element stiffness matrix is formed from the equilibrium equations and the equation restricting the volume change, and then the global stiffness matrix is assembled and stored on a file. The loads and/or displacements are given as input data in the same order as the harmonics. The stiffness matrix in each harmonic is read from the tape and the unknown displacements, porepressures and loads are computed using the subroutine BANDI, which is similar to the subroutine BAND used in the program STAX but with modifications to accommodate negative diagonal elements in the stiffness matrix. Once all displacements are available, the strains and stresses in the elements may be determined using Equations 4:8 and 4:9. An averaging procedure is adopted to evaluate the nodal stresses from the element stresses. The operation is repeated for each harmonic and for any location specified by the node and the circumferential coordinate θ, the desired quantities may be obtained as the algebraic sum of the results obtained in the various harmonics.

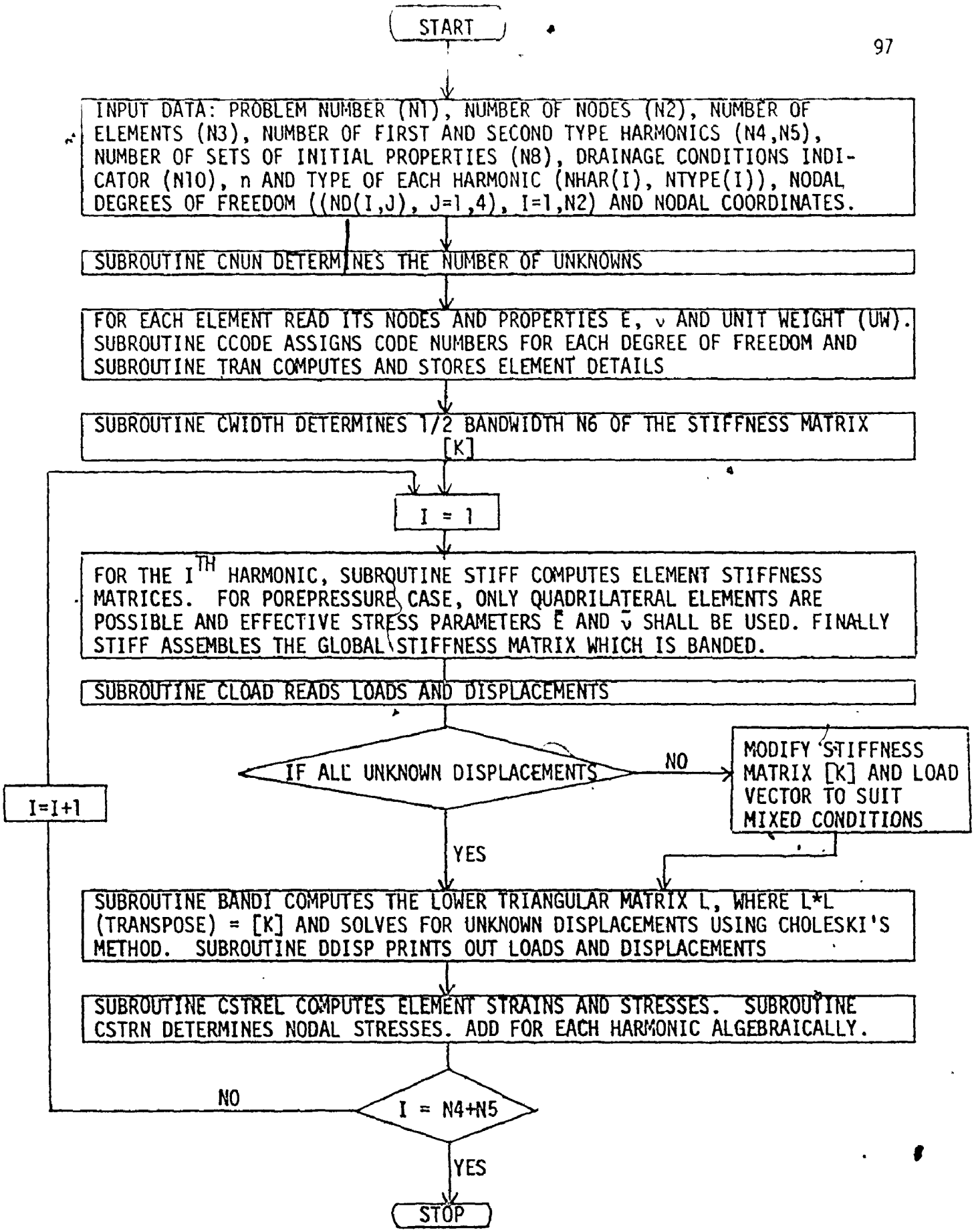
START
INPUT DATA: PROBLEM NUMBER (N1), NUMBER OF NODES (N2), NUMBER OF ELEMENTS (N3), NUMBER OF FIRST AND SECOND TYPE HARMONICS (N4,N5), NUMBER OF SETS OF INITIAL PROPERTIES (N8), DRAINAGE CONDITIONS INDICATOR (N10), n AND TYPE OF EACH HARMONIC (NHAR(I), NTYPE(I)), NODAL DEGREES OF FREEDOM ((ND(I,J), J=1,4), I=1,N2) AND NODAL COORDINATES.
SUBROUTINE CNUN DETERMINES THE NUMBER OF UNKNOWNS
FOR EACH ELEMENT READ ITS NODES AND PROPERTIES E, ν AND UNIT WEIGHT (UW). SUBROUTINE CCODE ASSIGNS CODE NUMBERS FOR EACH DEGREE OF FREEDOM AND SUBROUTINE TRAN COMPUTES AND STORES ELEMENT DETAILS
SUBROUTINE CWIDTH DETERMINES 1/2 BANDWIDTH N6 OF THE STIFFNESS MATRIX [K]
I = 1
FOR THE I^TH HARMONIC, SUBROUTINE STIFF COMPUTES ELEMENT STIFFNESS MATRICES. FOR POREPRESSURE CASE, ONLY QUADRILATERAL ELEMENTS ARE POSSIBLE AND EFFECTIVE STRESS PARAMETERS Ē AND ν̄ SHALL BE USED. FINALLY STIFF ASSEMBLES THE GLOBAL STIFFNESS MATRIX WHICH IS BANDED.
SUBROUTINE CLOAD READS LOADS AND DISPLACEMENTS
IF ALL UNKNOWN DISPLACEMENTS
NO
MODIFY STIFFNESS MATRIX [K] AND LOAD VECTOR TO SUIT MIXED CONDITIONS
YES
SUBROUTINE BANDI COMPUTES THE LOWER TRIANGULAR MATRIX L, WHERE L*L (TRANSPOSE) = [K] AND SOLVES FOR UNKNOWN DISPLACEMENTS USING CHOLESKI'S METHOD. SUBROUTINE DDISP PRINTS OUT LOADS AND DISPLACEMENTS
SUBROUTINE CSTREL COMPUTES ELEMENT STRAINS AND STRESSES. SUBROUTINE CSTRN DETERMINES NODAL STRESSES. ADD FOR EACH HARMONIC ALGEBRAICALLY.
I = N4+N5
NO
I=I+1
YES
STOP

The program PORAX has been organized in such a way that maximum efficiency in both storage and computation time is achieved. For a structural idealization with 94 nodes and 40 quadrilateral elements, only 295 seconds are needed to solve the problem using 16 harmonics and algebraically adding up the results at all the nodes in two perpendicular directions, namely $\theta=0°$ and $\theta=90°$.

5-E CHECKING PROGRAM FOR THE ANALYSIS OF INCOMPRESSIBLE MATERIALS

The program PORAX developed for the static analysis of axisymmetric structures involving specified volume changes was checked by solving two practical problems in soil mechanics for which closed-form solutions are available. The first was the analysis of an undrained specimen of soil, cylindrical in shape and subjected to a uniform axial pressure applied at the ends. In the second problem, the specimen was subjected to the same pressure and the incompressibility condition was enforced.

1. Undrained Specimen

A cylindrical specimen of soil, 4 in. in diameter and 8 in. long and subjected to a uniform axial pressure of 600 psi applied at its ends, was considered as shown in Figure 5-2a. As there was no drainage, the stresses should be entirely carried by the pore phase; the effective stresses would be zero and there should be a uniform pore pressure of 600 psi.

Because of the symmetry of the structure, only a quarter portion

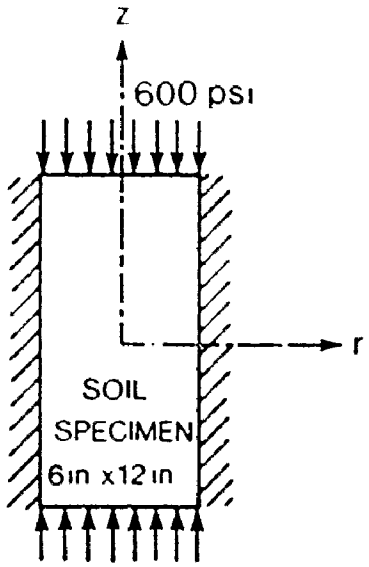

a. CONSTRAINED SPECIMEN

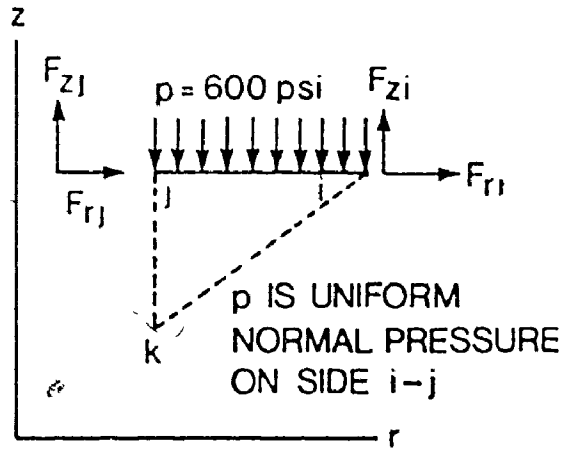

c. NODAL FORCES REPRESENTING AXIAL FORCES

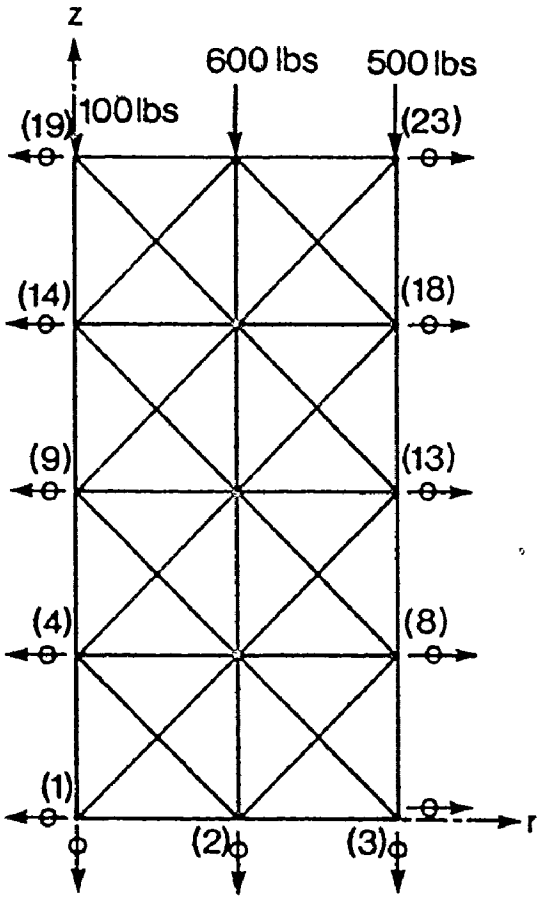

b. DISCRETIZED AXISYMMETRIC STRUCTURE WITH LATERAL CONSTRAINT

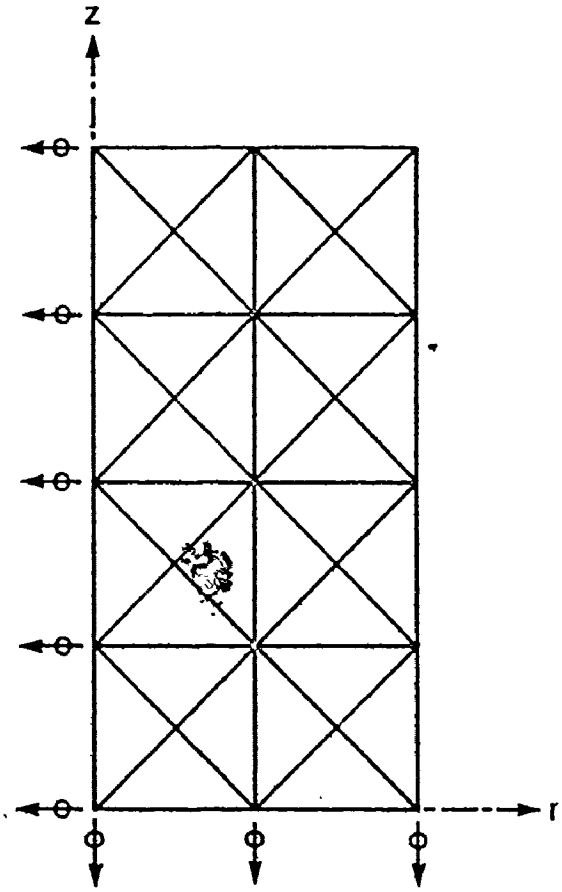

d. DISCRETIZED INCOMPRESSIBLE AXISYMMETRIC STRUCTURE

NODAL DISPLACEMENT IS ZERO
IN OF

lateral constraint, nodes 3, 8, 13, 18 and 23 of the discretized structure undergo no radial displacement. Because of symmetry, the radial displacements at nodes 1, 4, 9, 14 and 19 and the axial displacements at nodes 1, 2 and 3 are zero.

The nodal load vector in the axisymmetric case for an element with a normal surface pressure p from node i to node j as shown in Figure 5-2c is given by

$$\begin{Bmatrix} F_{ri} \\ F_{rj} \\ F_{rk} \\ F_{\theta i} \\ F_{\theta j} \\ F_{\theta k} \\ F_{zi} \\ F_{zj} \\ F_{zk} \end{Bmatrix} = \frac{p}{6} \begin{Bmatrix} 0 \\ 0 \\ 0 \\ 0 \\ 0 \\ 0 \\ 2\,r_i^2 - r_j^2 - r_j\,r_i \\ r_i^2 - 2\,r_j^2 + r_j\,r_i \\ 0 \end{Bmatrix} \qquad (5:5)$$

The uniform axial pressure of 600 psi is replaced by loads of 100, 600 and 500 lbs respectively at nodes 19, 21 and 23 as shown in Figure 5-2b. The program PORAX printed out the values of effective stresses as zero and the uniform pore pressure as 600 psi, thus providing a program check.

2. Incompressible Specimen

A soil specimen 4 in. in diameter and 8 in. in length was subjected to a uniform axial pressure of 600 psi at its ends and it was ensured that there was no volume change. The details of the discretized structure are shown in Figure 5-2d. As the loading was axisymmetric the effective stresses in the radial and circumferential directions would be equal; i.e., $\bar{\sigma}_r = \bar{\sigma}_\theta$. As the soil specimen was incompressible, the volumetric strain $e = \varepsilon_r + \varepsilon_\theta + \varepsilon_z = 0$. Using the constitutive relationship between strains and effective stresses for isotropic materials, the following relationship was obtained

$$\bar{\sigma}_r = \bar{\sigma}_\theta = \frac{-\bar{\sigma}_z}{2} \tag{5:6}$$

The change in volume of the soil skeleton is equal to the change in volume of the pore fluid. When the soil mass is incompressible, for the case of isotropic and elastic materials saturated with an incompressible pore fluid, the pore pressure is obtained using the relationship:

$$\Delta u = \Delta\sigma_3 + \frac{1}{3}(\Delta\sigma_1 - \Delta\sigma_3) \tag{5:7}$$

as the pore pressure parameters B and A are 1 and 1/3 respectively [54]. The pore pressure in the cylindrical soil specimen should be 1/3 of the applied pressure and equal 200 psi. The effective stresses should work out as -200, -200 and 400 psi respectively in the r, θ and z directions.

The results of the analysis using the program PORAX gave uniform effective stresses of -200, -200 and 400 psi respectively in

the radial, circumferential and axial directions. The pore pressure was uniform and equal to 200 psi throughout the specimen.

5-F ILLUSTRATIVE EXAMPLE - ANALYSIS OF A LATERALLY LOADED PILE

A laterally loaded pile founded in sand is chosen for analysis using the program PORAX. The pile considered is a 1.25 ft diameter concrete pile, 60 ft long and driven into a saturated sandy strata of 140 ft depth overlying bed rock. The soil strata is layered and the properties of the various sand layers are shown in Figure 5-3. The pile is subjected to a lateral load of 600 kips at its top which coincides with the ground level.

The finite element arrangement to represent the soil-pile system is decided upon with due consideration of its adequacy, the computation time and the computer storage. These three criteria are not independent of one another. For example, any increase in the number of elements usually improves the accuracy of the solution. However, the storage and computation time increase with the increase in the number of unknowns. The storage required is N(b+1) where N is the number of unknowns and b is the half bandwidth of the stiffness matrix as shown in Equation 5:8

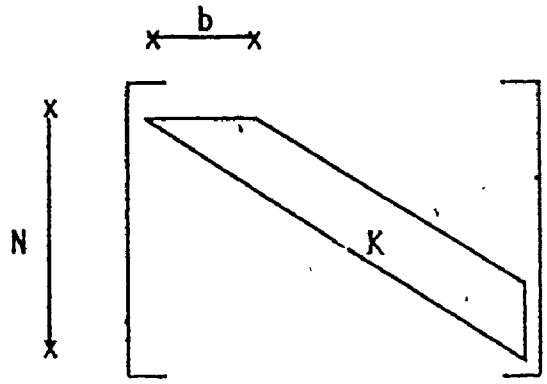

$$\begin{Bmatrix} u \\ (N\times 1) \end{Bmatrix} = \begin{Bmatrix} P \\ (N\times 1) \end{Bmatrix} \quad (5:8)$$

SATURATED SAND	G=2.65 e=0.71 ν=0.30 ϕ=38° γ=122.7 lb/ft^3 E=2.640x10^6 psf
SATURATED SAND CONCRETE PILE γ= 150 lb/ft^2 E=4.32×10^3 psf	G=2.72 e=0.68 ν=0.33 ϕ=41° γ=126.4 lb/ft^3 E=5.168x10^6 psf
SATURATED SAND	G=2.71 e=0.63 ν=0.33 ϕ=41° γ=127.8 lb/ft^3 E=7.485x10^6 psf
SATURATED SAND	G=2.80 e=0.57 ν=0.35 ϕ=42° γ=133.9 lb/ft^3 E=10.37x10^6 psf

FIG. 5-3 PILE AND THE SOIL LAYERS

The computation time is proportional to (Nb^2) [36]. Taking note of all these factors, the finite element arrangement shown in Figure 5-4 is chosen. As pore pressures developed in the soil are to be considered, only quadrilateral ring elements are possible. There exists some bond between the pile and the soil at their interface and this is represented by ring linkage elements. Initially there is an infinite stiffness K_s for these elements, while the stiffness K_s is zero when the pile slips completely with respect to the soil. The elements at the ground level have zero vertical stiffness to simulate the free surface while their horizontal stiffness is K_s [20,21]. For elements along the length of the pile, a stiffness of K_s is assigned for both the horizontal and the vertical directions. The elements under the pile tip are assigned a zero horizontal stiffness as the contact area is comparatively small but a vertical stiffness of K_s. The linkage elements between the soil elements adjacent to the pile tip are specified a stiffness of K_s in horizontal and vertical directions in order to ensure continuity. The lateral load is replaced by equivalent loads of 400 kips at node 66 and 200 kips at node 68.

A parametric study was conducted in order to investigate the importance of considering the interface behaviour and to determine the appropriate values of stiffness to assign to the spring elements in order to simulate a rigid connection between the two nodes of the linkage element. For values of K_s below 1×10^7 lb/ft, the connections are not rigid while there are computational problems for values higher than 1×10^{11} lb/ft. Figure 5-5 shows an arrangement of elements to represent

is not

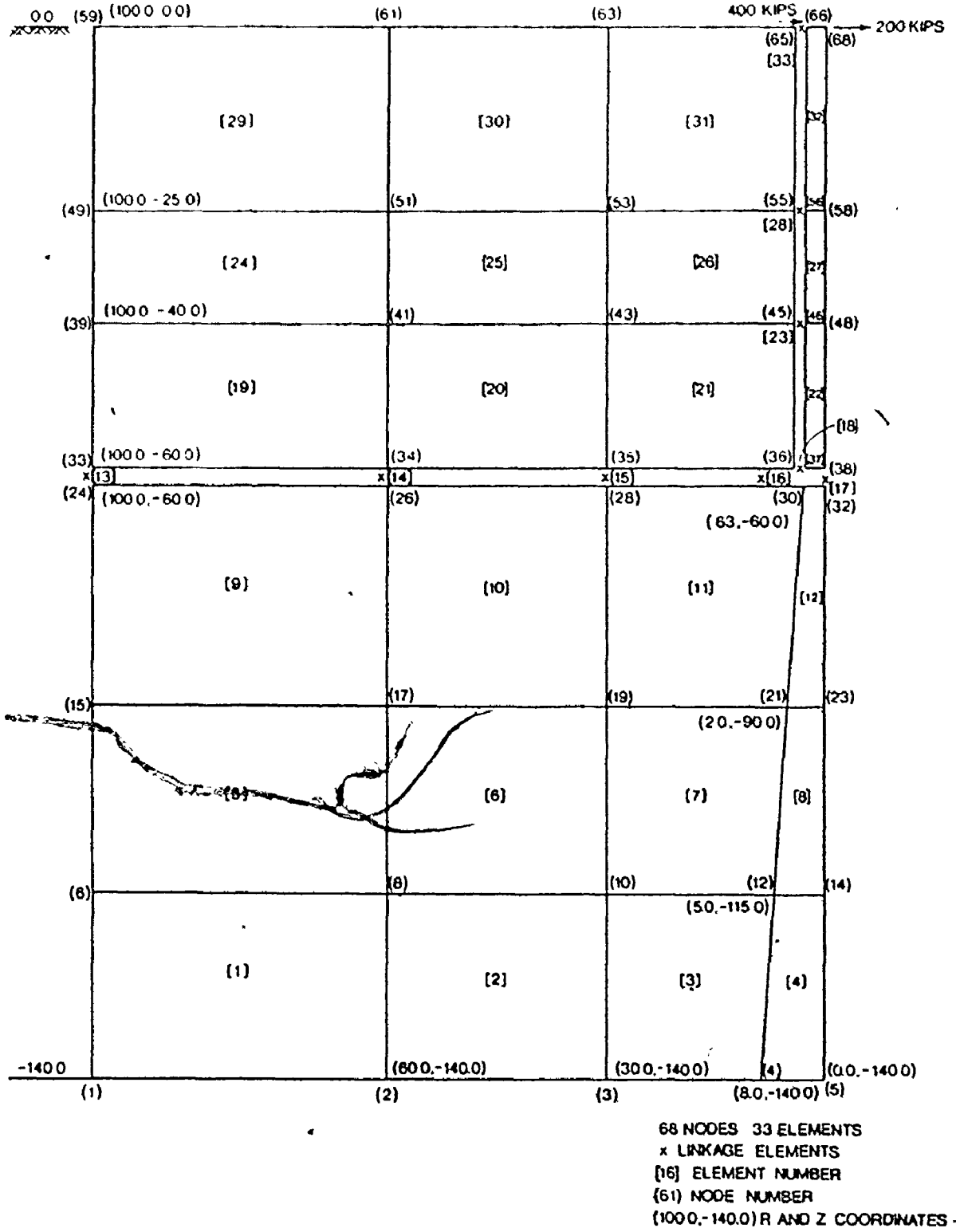

FIG. 5-4 SOIL-PILE SYSTEM WITH LINKAGE ELEMENTS

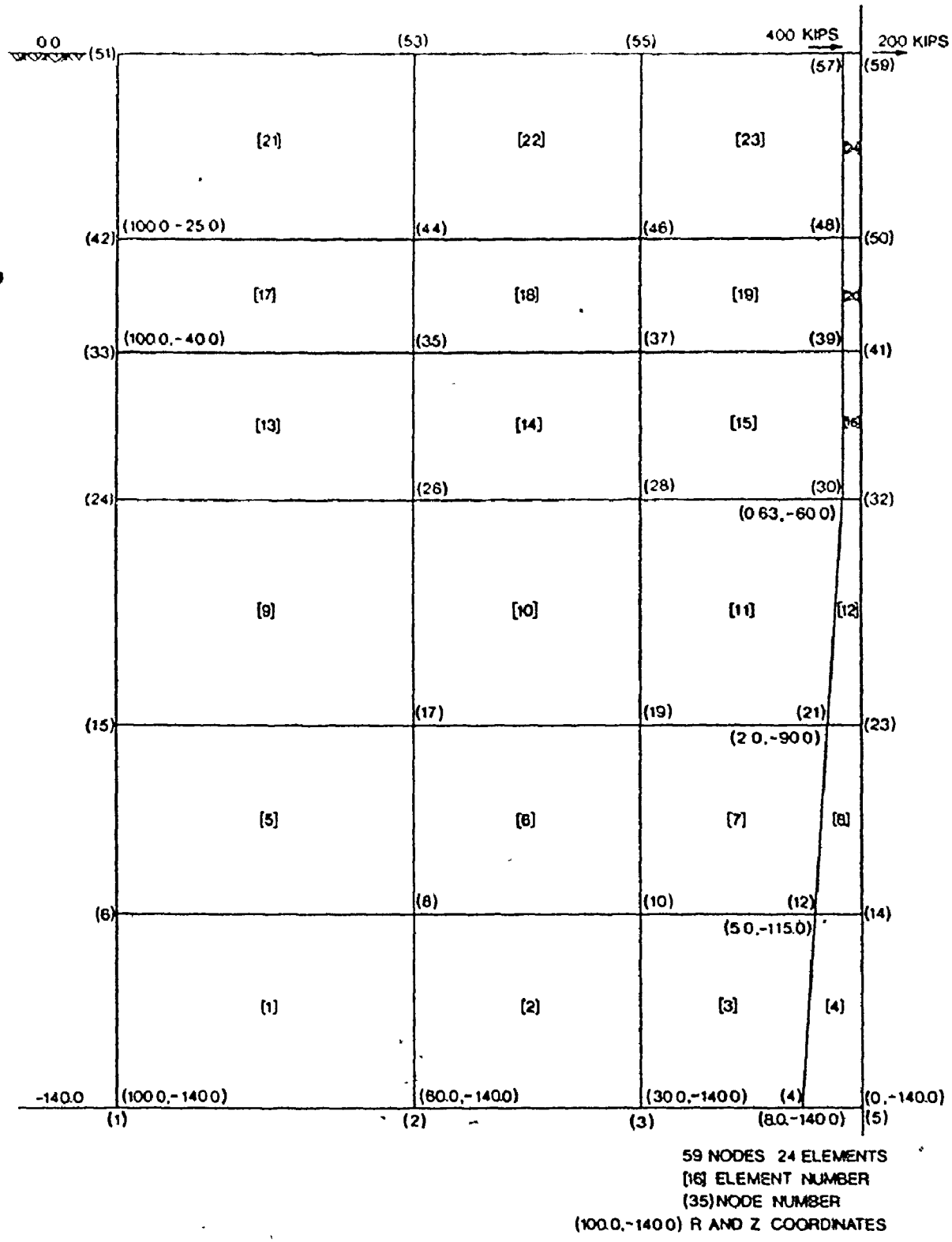

FIG. 5-5 SOIL-PILE SYSTEM WITHOUT LINKAGE ELEMENTS

amounts to the assumption that there is no slip of the pile with respect to the soil and thus the relative movement of the pile and the soil is neglected. Four specific cases were compared:

(1) A structure with linkage element stiffness of 1×10^{10} lb/ft;

(2) A structure with linkage element stiffness of 1×10^{8} lb/ft;

(3) A structure with linkage element stiffness of 0.1 lb/ft; and

(4) A structure neglecting interface slip.

In order to better represent the behaviour of piles, it would be more appropriate to use bending elements or a finer element discretization. Both modifications would require a much larger computer storage. For this reason, using bending elements or a finer mesh was not possible. As the soil stresses were low for the loading considered, it was assumed that the stiffness of the linkage element remained constant throughout the loading. Figure 5-6 shows a comparison of the variation of stresses along the radial (horizontal) and axial (vertical) directions along the length of the pile for $\theta=0°$. The stresses in all four cases were practically identical, with cases 1 and 4 closest, since the pile is acting essentially as a cantilever taking all the loading. There is a change in nature of the stress at a depth of 21 feet and this may be because bending is not properly represented and the soil properties alter at the interface levels. The radial displacements for $\theta=0°$ vary along the pile as shown in Figure 5-7a. There was some increase in the radial displacements when the interface slip was accounted for. The relative displacements between the pile and the soil along the interface are given in Figure 5-7b. For case 1, the relative displacements were practically

that was a -to-rigid The

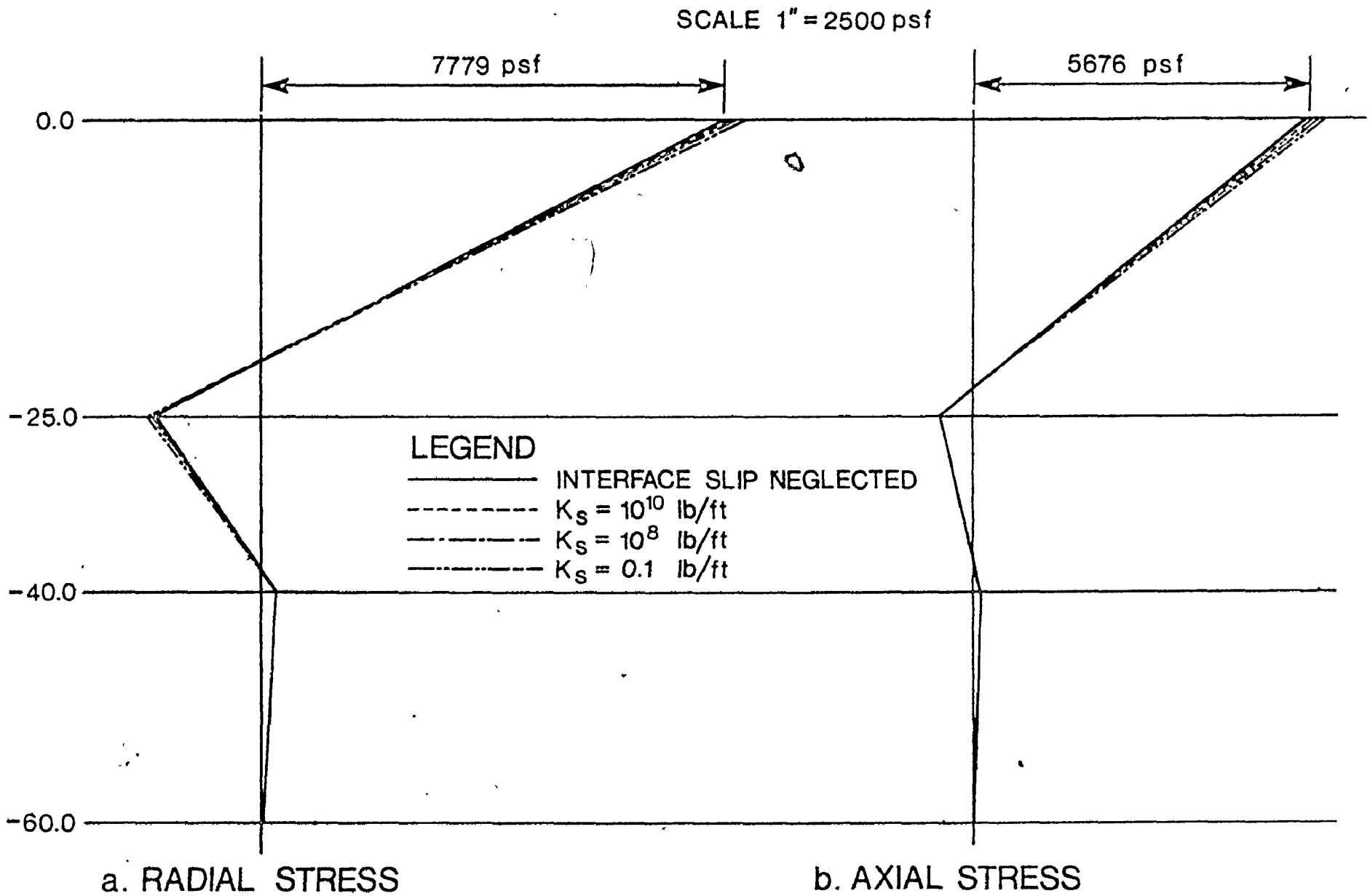

FIG. 5-6 RADIAL AND AXIAL STRESSES ALONG PILE AXIS

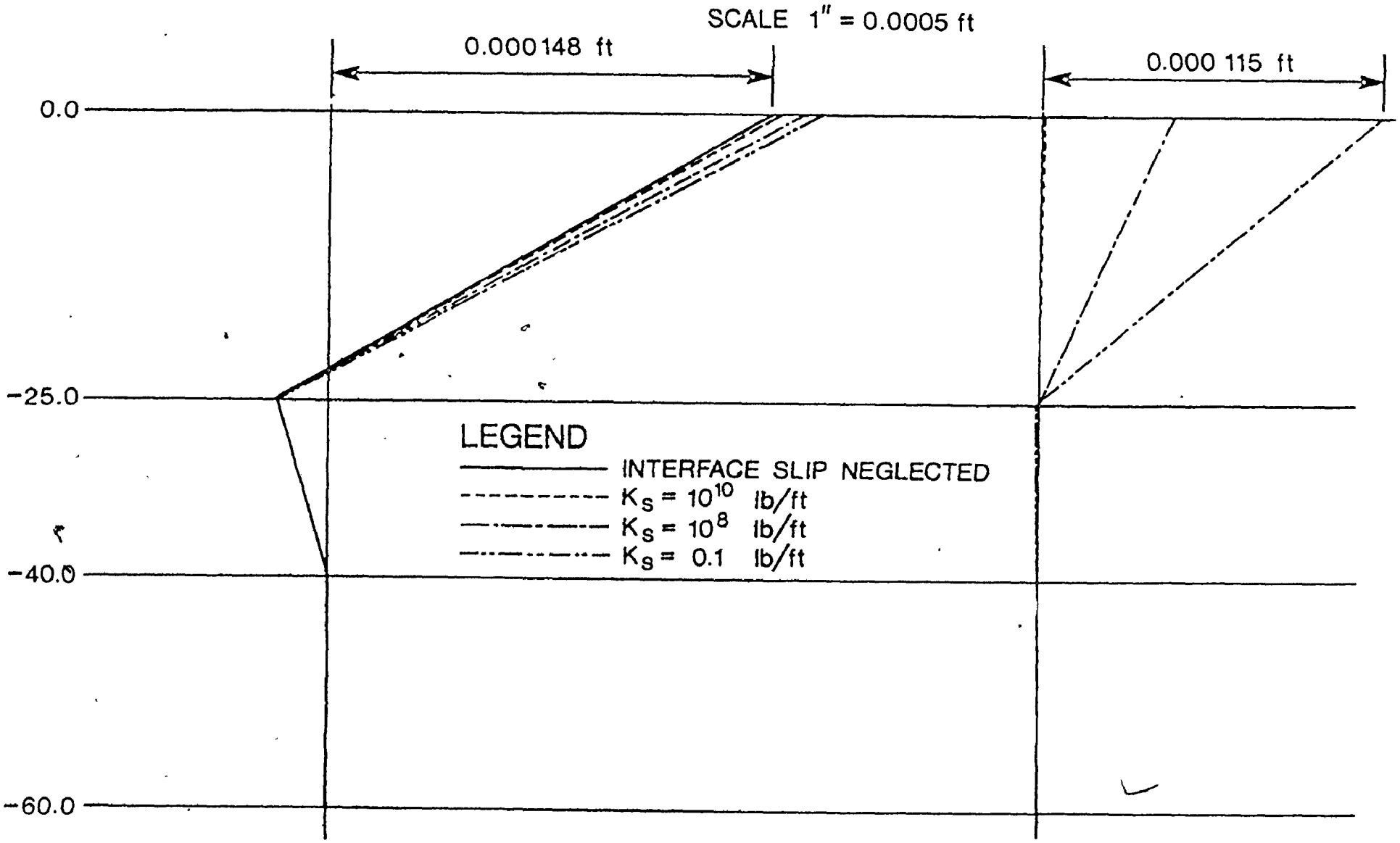

a. ABSOLUTE RADIAL DISPLACEMENT

b. RELATIVE RADIAL DISPLACEMENT OF PILE WITH RESPECT TO SOIL

FIG. 5-7 ABSOLUTE AND RELATIVE RADIAL DISPLACEMENTS ALONG PILE

relative displacement for case 2 was about 30% of the absolute displacement, while it was of the order of 75% for case 3. The axial displacements were found to be negligible. From these studies, the following conclusions were arrived at:

(1) The stresses and displacements decrease markedly with increasing depth and the lateral load has a fairly small influence at a depth of 25 ft. This agrees with the results obtained for piles and pile groups in research conducted at the Center for Highway Research, the University of Texas [4].

(2) The stresses in the pile are somewhat underestimated in an analysis neglecting the interface slip. The pore pressure developed in the soil due to the lateral load was not significant in any of the four cases.

(3) The relative displacements between the pile and the soil are considerable throughout the length of the pile when the stiffness of linkage elements was set to 0.1 lb/ft. The pile with a value of K_s equalling 10^8 lb/ft showed that it simulated a semi-rigid connection. When K_s was set to 10^{10} lb/ft, there existed a close-to-rigid connection between the pile and the soil. The natural frequencies of the soil-pile system, with dimensions identical to the system used in this analysis, were evaluated making use of the two approaches; first, using linkage elements with K_s equal to 10^{10} lb/ft, and then neglecting the interface slip. The variation between the corresponding frequencies for the two approaches differed by 1-2% as shown in Table 8-4 under Section 8-F. Similarly, good comparison was found for piles in clays. All these findings indicate that the value of 10^{10} lb/ft was suitable as the stiffness of the linkage element in order to ensure a near rigid connection between the pile and the soil.

CHAPTER VI

THE MASS MATRIX FOR AXISYMMETRIC STRUCTURE AND THE EIGENVALUE PROBLEM

6-A INTRODUCTION

When the displacements of an elastic structure are time-dependent, in addition to the stiffness property, both the inertial and the damping properties of the structure are called into play. The inertia or mass is an essential property in the dynamic behaviour of the structure. The inertial and damping forces may be replaced by equivalent static forces using the well-known D'Alembert principle [44].

There are two basic types of mass matrices, namely, the consistent mass matrix and the lumped mass matrix. The stiffness matrix relates the strain energy of an element to its nodal displacements. In the same way the mass matrix serves to relate the kinetic energy to the nodal velocities. If the displacement functions used in the evaluation of the mass matrix are the same as those used in the formulation of the stiffness matrix, then the kinetic energy of the element is consistent with its potential energy. The resulting mass matrix is called the consistent mass matrix, which may be derived by the application of Hamilton's principle [71] as given in Appendix C-4. The lumped mass matrix may be formulated using the direct method of

computing the mass of the volume tributory to any particular node, the resulting mass matrix being diagonal.

In general the use of the consistent mass matrix needs excessive computational effort. Therefore, it is justified only if the results so obtained show improved accuracy. The validity of the two types of mass matrices was studied by solving the eigenvalue problem.

6-B MASS MATRIX FOR TRIANGULAR RING ELEMENTS

The dynamic analysis of an axisymmetric structure requires the formulation of the mass matrix. For the triangular ring element, it is possible to derive a consistent mass matrix by applying Hamilton's principle [71]. The lumped mass matrix for this element may be formed by means of a direct method of accounting for the contributions of the element volume to the three nodes.

6-B-1 Consistent Mass Matrix

The consistent mass matrix for an axisymmetric structure with constant density throughout each element may be obtained from the relationship

$$[m] = \rho\, [C^{-1}]^T \left(\int_{vol} [A]^T\, [A]\, dvol \right) [C^{-1}] \qquad (6:1)$$

as derived in Appendix C-4. The matrix $[C^{-1}]$ is the same as the one used in the stiffness matrix formulation and given in Appendix C-1. The

matrix [A] is known from Equation 4:4 and may be written

$$[A] = \begin{bmatrix} 1 & r & z & 0 & 0 & 0 & 0 & 0 & 0 \\ 0 & 0 & 0 & 1 & r & z & 0 & 0 & 0 \\ 0 & 0 & 0 & 0 & 0 & 0 & 1 & r & z \end{bmatrix} \qquad (6:2)$$

For unit angle (1 radian) the quantity within the parantheses in Equation 6:1 becomes

$$\int_{vol} [A]^T [A] \, r \, dr \, dz$$

which contains the integral λ_1, being the volume of the element and also additional axisymmetric integrals λ_7 to λ_{11}. These integrals may be evaluated using Green's Lemma and are found to be lengthy expressions. However, as in the case of λ_1 to λ_6, there are simplified forms for these additional integrals. The values of λ_9 to λ_{11} so obtained are approximate but valid so long as the dimensions of the element are small compared to the radius. The simplified forms of these integrals λ_7 to λ_{11} are also included in Appendix C-2.

The consistent mass matrix formulated using Equation 6:1 does not include any term in n, the number of the harmonic and thus remains a constant for the structure. This is of importance for it need be computed only once in the program.

6-B-2 Lumped Mass Matrix

The lumped mass matrix for a triangular ring element can be directly formulated if it is possible to judge the relative contributions

of the mass of the element volume to its three nodes. In the case of a plane triangular element the lumped mass matrix is formed by lumping the mass of the element at the nodes in three equal parts. This lumped mass matrix may also be obtained by first formulating the consistent mass matrix and then adding all off-diagonal terms to the diagonal term in each row. In the case of the triangular axisymmetric ring element, the contributions of the mass to the three nodes are not equal as they are at different radii. However, the lumped mass matrix may be formed by adding the off-diagonal terms to the diagonal terms in each row of the consistent mass matrix derived in Section 6-B-1. The lumped mass matrix is found to satisfy the following relationship:

$$m_i : m_j : m_k = (2\ r_i+r_j+r_k) : (r_i+2\ r_j+r_k) : (r_i+r_j+2\ r_k) \qquad (6:3)$$

where m_i, m_j and m_k are the contributions of the element mass at nodes i, j, and k of the triangular ring.

The mass of the volume of the triangular ring element per unit angle is

$$m = \rho\ \lambda_1 \qquad (6:4)$$

where ρ is the mass density and the axisymmetric integral λ_1 is the volume of the element. The contribution of the mass to the node i may be expressed as

$$m_i = \frac{2\ r_i+r_j+r_k}{4(r_i+r_j+r_k)}\ \rho\ \lambda_1 = \frac{\rho A}{12}\ (2\ r_i+r_j+r_k) \qquad (6:5)$$

The lumped mass matrix for the triangular ring element is given in Appendix C-5, and it is independent of the number of the harmonic. The validity of this matrix is checked by computing the frequencies of the axisymmetric structure.

6-C MASS MATRIX FOR A QUADRILATERAL ELEMENT

The quadrilateral element used in the analysis consists of four triangular ring subelements as shown in Figure 4-1c. The mass matrix is the same in all harmonics and for the quadrilateral ring element this may be formed by systematically adding the mass matrices for the triangular subelements as in the case of the stiffness matrix. However, the condensation of the mass matrix is not possible [16] and thus the possibility of formulating such a consistent mass matrix for a quadrilateral element may be ruled out. The lumped mass matrix for this quadrilateral is a diagonal matrix of order 15, three of the diagonal terms referring to the interior node. The mass associated with the interior node is distributed to the four exterior nodes in the ratio of their radii. The resulting mass matrix is diagonal and of order 12 and is given in Appendix C-5. The validity of this lumped mass matrix is also checked by computing the frequencies of the axisymmetric structure.

6-D EIGENVALUE PROBLEM

In dynamic problems the lumped mass approach is used more often as this leads to great simplifications in the analysis. The mass

matrix in the lumped mass approach is diagonal and this provides some significant economies. Therefore, if once it can be ensured that the results obtained by the use of the lumped mass matrix are reliable, there is no reason why a consistent mass approach should even be required. One way to study the reliability of the mass matrices is to solve the eigenvalue problem for the natural frequencies. Once the suitability of the lumped mass approach in axisymmetric problems is established, the same may be used in all dynamic problems.

6-D-1 Computer Program for Eigenvalues and Eigenvectors

A computer program (PRITZ) suitable for the computation of eigenvalues and eigenvectors of very lage banded matrices in CDC machines (CDC 6400) was prepared. The original program PRITZ was developed at the University of British Columbia for IBM Machines [58]. Many modifications and changes were completed to ensure its reliability when used in CDC machines. The program works on the Ritz iteration procedure [23] and is quite efficient when more than a few eigenvalues are required and especially when close eigenvalues are found. The banded property of the matrix is utilized in saving computer storage and the computation time. The program allows for variable dimensioning and as a result storage areas may be acquired dynamically. The method is a fast converging one and there is the need for only a very few iterations.

The program has been checked by solving for the natural frequencies of a ten story building with their masses lumped at floor

levels. The building considered is shown in Figure 6-1a and it has 30 columns which are uniform throughout the height. The mass at each floor level was taken as 1500 kips and the moment of inertia of each column about its weaker axis was 225.5 in^4. The stiffness of the columns in each story was found to be 12280 kips per ft , as the story height was constant being 11 ft. The natural frequencies of the building and the mode shapes are as shown in Figure 6-1b. The results of this analysis were found to be identical with those obtained using other established techniques.

6-E NATURAL FREQUENCIES AND VECTORS OF AN AXISYMMETRIC STRUCTURE

The natural frequencies of an axisymmetric structure are worked out in order to check the validity of the mass matrices. The structure considered was a cylindrical bar 4 ft in diameter and 4 ft long. One end of the bar is fixed and the other end is left free as shown in Figure 6-2a. The structure was discretized into axisymmetric ring elements of different configurations as per Systems 1 to 4 shown in Figure 6-2b. Systems 1 to 3 consist of triangular ring elements whereas System 4 makes use of quadrilateral ring elements. The natural frequencies and mode shapes were worked out for Systems 1 to 3 by means of both the consistent as well as the lumped mass approaches in the program PRITZ. For System 4 only the lumped mass approach was possible. The natural frequencies of the bar for uncoupled longitudinal vibrations were also worked out by solving the general differential equation of motion given by Equation A:12 (Appendix A-1) [82]. The

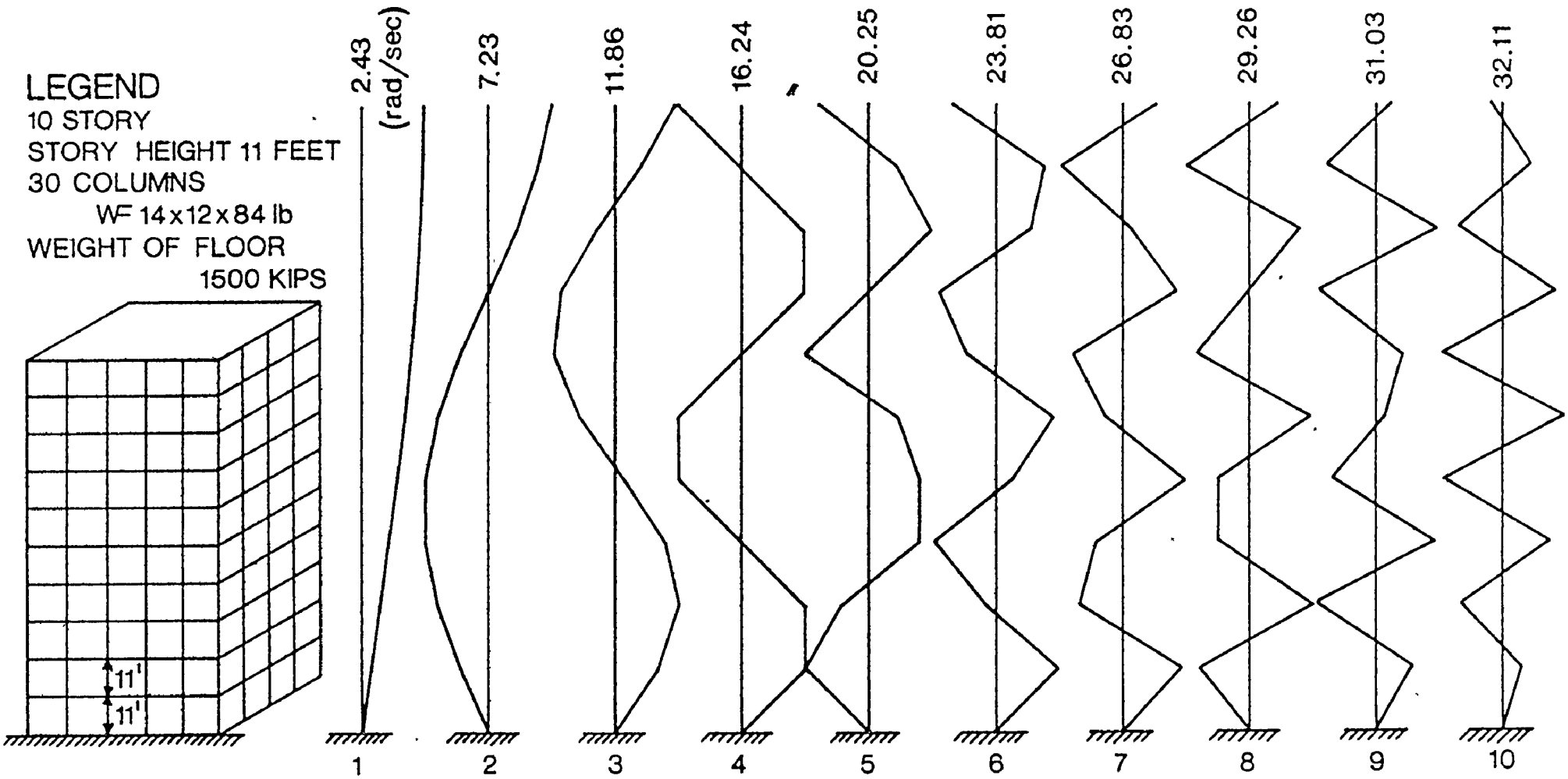

TEN STORY BUILDING

b. FREQUENCIES AND MODE SHAPES

FIG. 6-1 FREQUENCIES AND MODE SHAPES OF A TEN STORY BUILDING

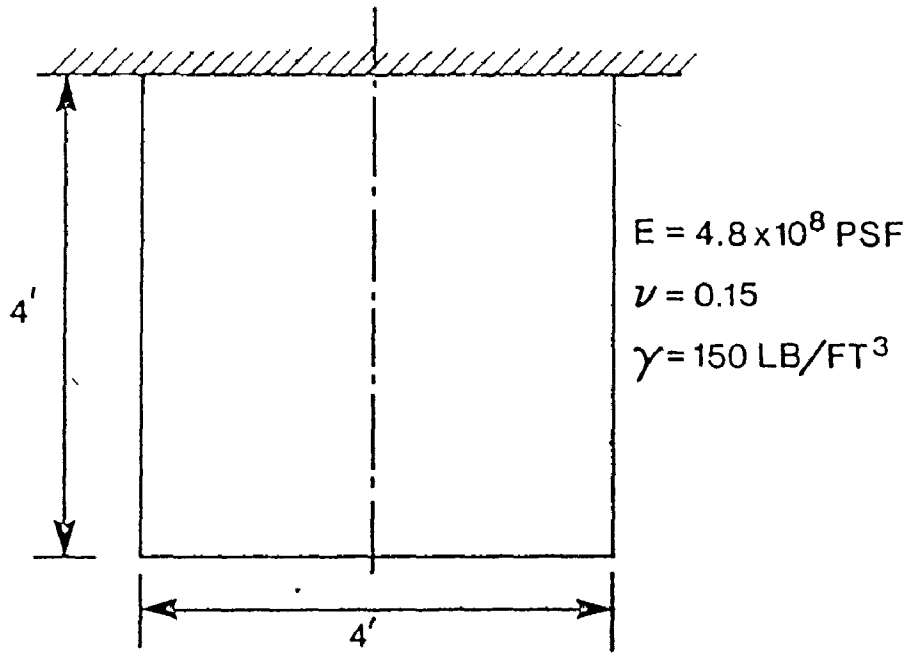

a. FIXED-FREE CYLINDER

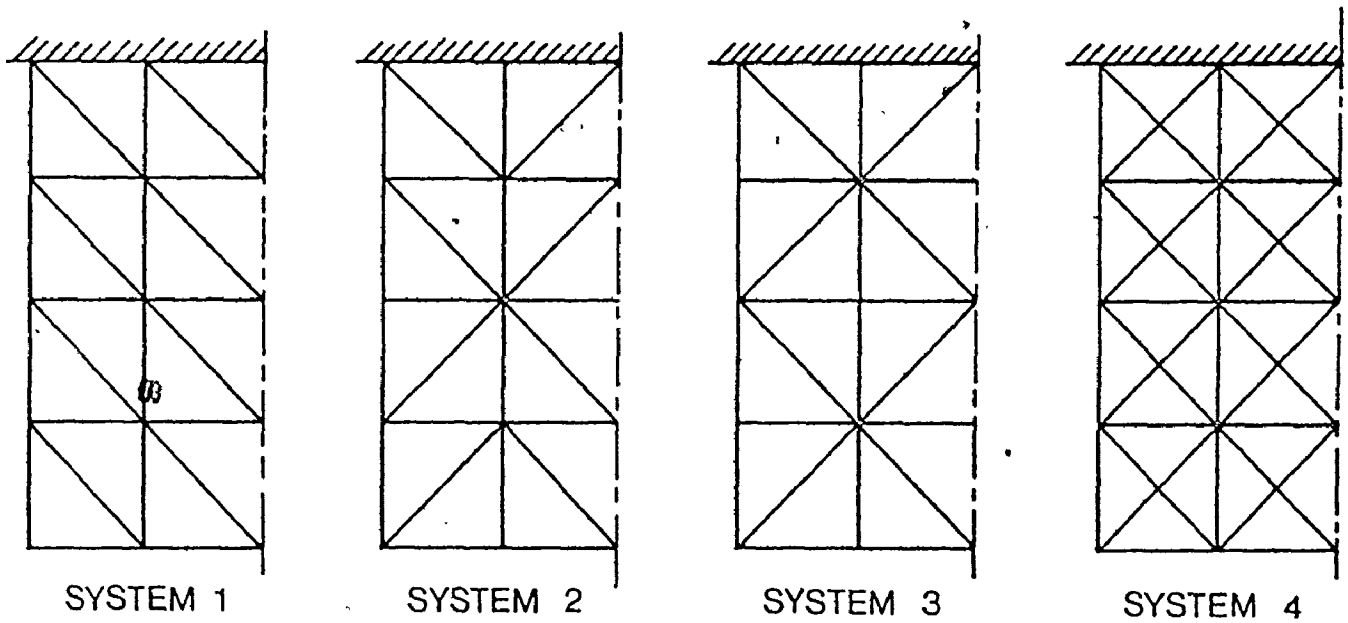

b. VARIOUS FINITE ELEMENT SYSTEMS USED FOR FREQUENCY ANALYSIS

FIG. 6-2 CYLINDER ILLUSTRATING SOLUTIONS FOR FREQUENCIES OF AXISYMMETRIC STRUCTURE

values of the natural frequencies for all these cases are given in Table 6-1 for comparison purposes.

It is of interst to note that the fundamental frequency has been given within ($\simeq$ 5%) of the correct value by each system irrespective of whether consistent or lumped masses were used. The results obtained for each higher frequency in Systems 1 to 3 by means of the lumped mass approach were within a narrow range of values. It is obvious that the type of element discretization affected the results obtained for natural frequencies only marginally when the lumped mass was utilized. On the other hand there is a wide variation in the values obtained in various systems for each higher frequency when the consistent mass approach is applied. The results of the analyis using consistent masses are very sensitive to the shapes and locations of elements. The natural frequencies obtained by the use of the consistent mass matrix are found to be upper bounds to the exact solution. The same conclusions have been reached in earlier research by Archer [3] for two-dimensional structures. The results obtained for System 4 using quadrilateral ring elements show that the lumped mass approach is acceptable when quadrilateral ring elements are used. The results for Systems 3 and 4 show similarity when the lumped approach is used.

From these studies it can be inferred that the use of a consistent mass matrix is undesirable for axisymmetric structures for the reasons mentioned below:

(1) The consistent mass method does not give reliable natural frequencies and the values are upper bound solutions. A

TABLE 6-1

NATURAL FREQUENCIES FOR FIXED-FREE CYLINDER
(rad/sec)

MODE	CONSISTENT ELEMENT			LUMPED ELEMENT				CLOSED-FORM VALUES
	1	2	3	1	2	3	4	
1	3991	4025	4024	3992	3969	3966	3979	4205
2	9910	10011	9882	8400	8233	8268	7926	9980
3	10653	11444	11307	10091	9486	9101	9006	
4	12711	13134	13026	12328	12125	11279	11139	12615
5	13390	15145	15682	12795	12942	11553	11494	
6	14408	15982	16007	13514	13297	12783	12863	
7	15201	18377	17595	13995	13920	13489	13095	
8	17537	18639	22057	15272	14171	15436	14300	16650
9	17933	23214	23112	15180	15398	15736	15511	
10	18335	23494	25358	17385	17532	17441	15805	21019

lumped mass representation having the same number of equations for the eigenvalue problem as the consistent mass approach gives more accurate natural frequencies [16,24].

(2) The results obtained using the consistent mass matrix are very sensitive to the element discretization.

(3) The use of consistent mass matrices calls for excessive computational effort.

(4) In dynamic problems using the finite element method, the storage capacity of the computer becomes increasingly important. With the lumped mass approach, there is considerable saving in computer storage without too much effect on the accuracy.

(5) The lumped mass approach leads to great simplification in the subsequent dynamic analysis.

In all wave propagation problems, the lumped mass formulation is advocated [13,16]. It may be concluded that the lumped mass approach is a reliable method for finding natural frequencies of axisymmetric structures and that the use of both triangular and quadrilateral ring elements is acceptable.

6-F PRACTICAL EXAMPLE - NATURAL FREQUENCIES OF A SOIL-PILE SYSTEM

The experimental program to determine the natural frequencies of a soil-pile system can best be done using dynamic field tests, but they are time-consuming and prohibitively costly. However, there is

one such test done by Alpan [1] on a prestressed concrete pile of 30 by 30 cm. in cross section and an embedded length of 4.7 m. The upper part of the pile is encased in a rigid reinforced concrete block and the top of the pile may be assumed to undergo no rotation. In fact complete fixity could not be achieved and only an appreciable degree of fixity (80%) could be ensured. The basic data for the soil layers were obtained from a planned subsoil exploration which revealed that the upper 3.5 m of the subsoil consisted of a highly plastic clay overlying fine sand. The details of the soil-pile system are shown in Figure 6-3.

The horizontal displacements of the pile head were measured by deflectometers while two accelerometers were mounted on the block to register the horizontal motions following dynamic excitation. Dynamic free vibration tests were conducted by inducing free oscillations and these tests furnished the damped natural frequency of the fixed pile as 12.2 Hz (i.e., a period of 0.082 sec) and the logarithmic decrement (with respect to time) of 0.054 corresponding to 5.4% critical damping. As the damping is small, the difference between the damped and undamped natural frequencies is small. Assuming the pile to be a beam on elastic supports the frequency was computed by Alpan as 14.3 Hz corresponding to a period of 0.070 sec.

The frequencies of a soil-pile system comprised of an equivalent circular concrete pile were worked out using the program PRITZ. The equivalent axisymmetric structure analyzed is shown in Figure 6-4. The fundamental frequency of the soil-pile system is 11.5

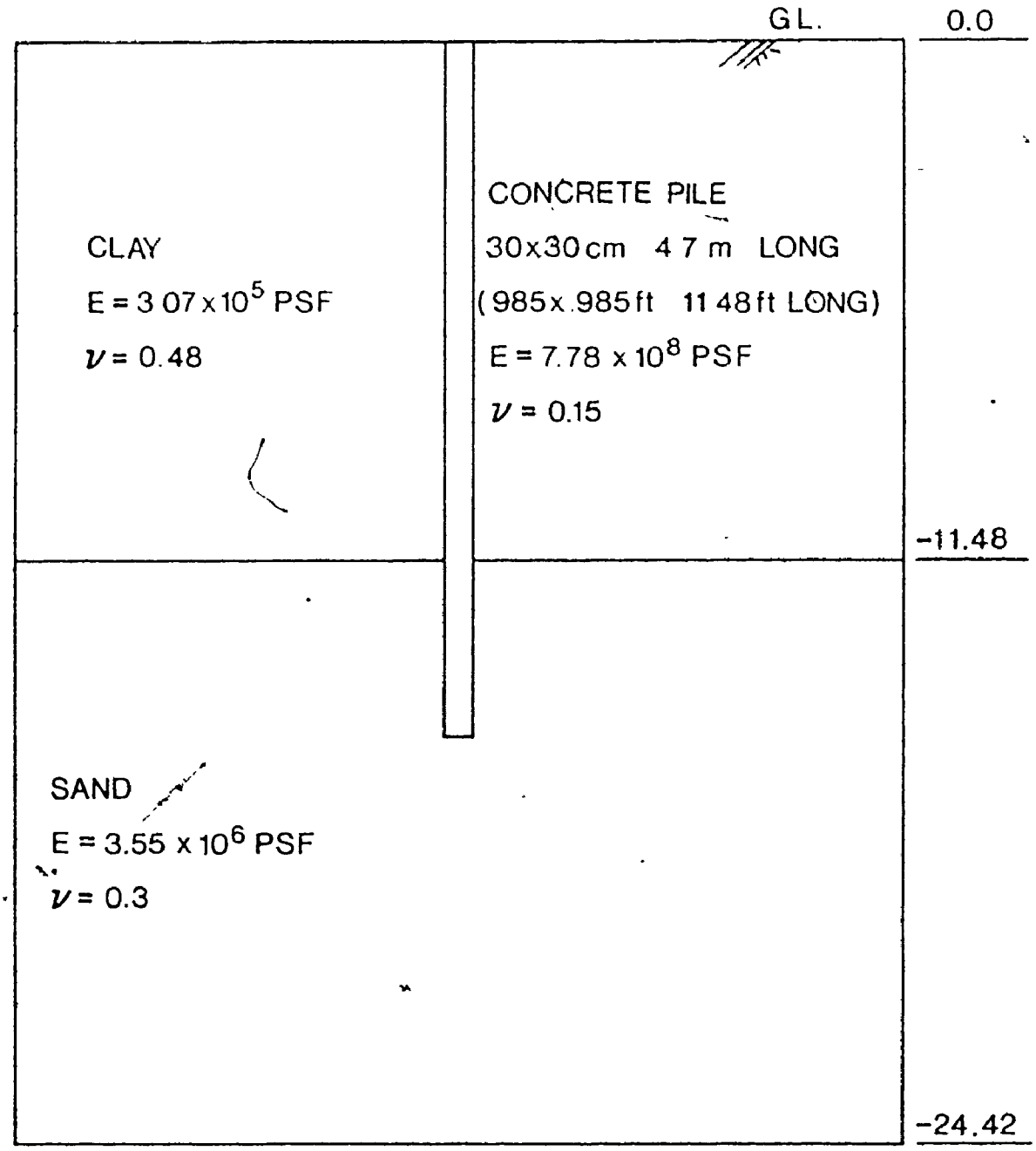

FIG. 6-3 DETAILS OF PILE AND SOIL LAYERS IN DYNAMIC FIELD TEST [1]

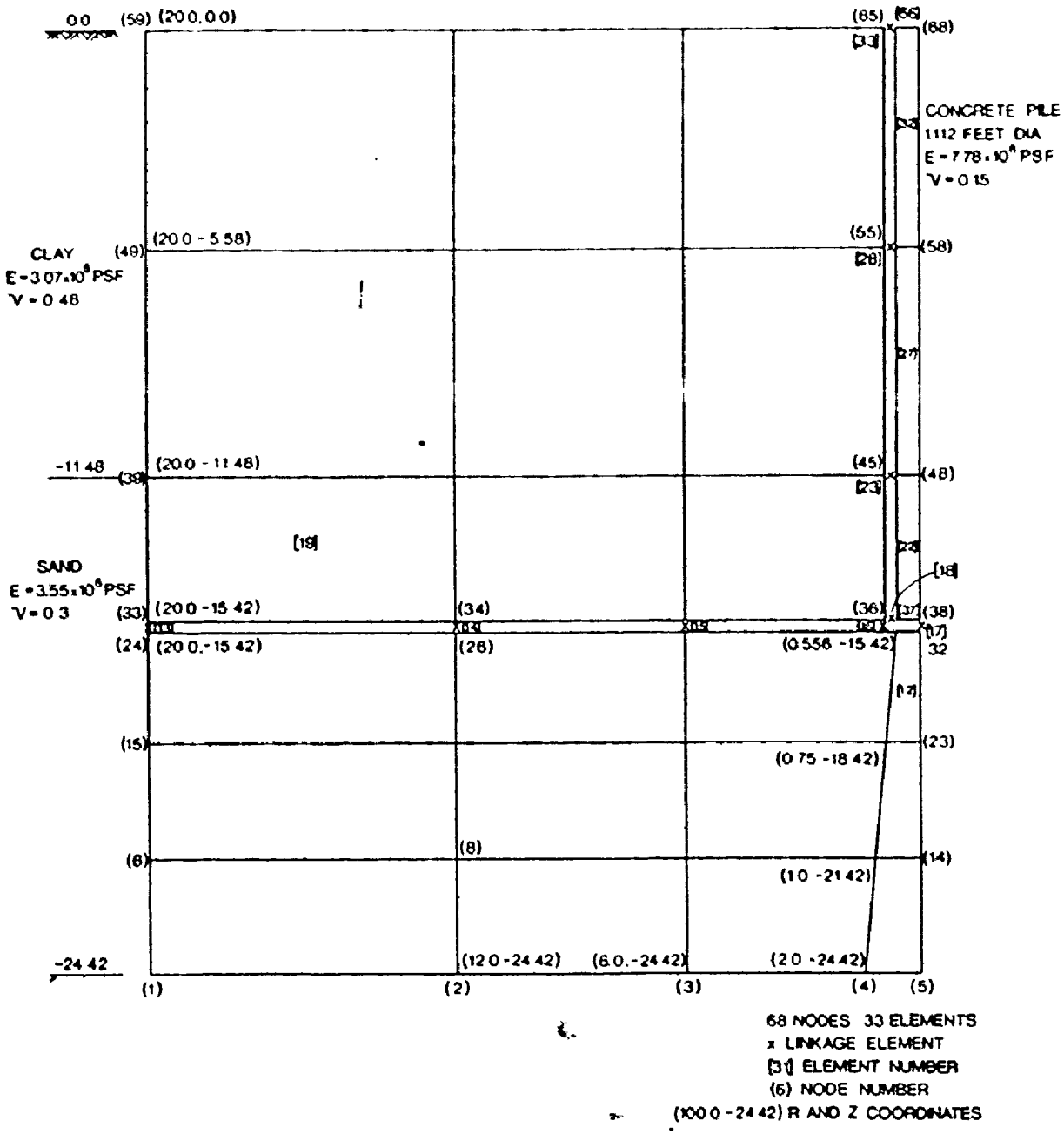

FIG. 6-4 DESCRIPTION OF THE SOIL-PILE SYSTEM IN THE EIGENVALUE PROBLEM

Hz and the corresponding period is 0.087 sec. The natural frequency of the pile alone neglecting the pile-soil interaction is 60 Hz and this corresponds to a period of 0.017 sec. The results are summarized in Table 6-2.

TABLE 6-2

FUNDAMENTAL FREQUENCIES AND PERIODS

OF A SOIL-PILE SYSTEM

	Frequency (Hz)	Period (sec)
Dynamic field test of pile (damped)	12.2	0.0820
Reference Figure 6-3 [1] (undamped)	12.22	0.0819
Pile as a beam on elastic supports [1]	14.3	0.0700
Axisymmetric soil-pile system using program PRITZ (Reference Figure 6-4)	11.5	0.0870
Pile independent of soil support	60.0	0.0170

From these studies, it could be concluded that the fundamental period of the soil-pile system should be computed by including the interaction between the pile and the soil.

CHAPTER VII

DYNAMIC ANALYSIS OF AXISYMMETRIC STRUCTURES UNDER NONSYMMETRIC LOADING

7-A INTRODUCTION

Until the early 1950's, the evaluation of the dynamic response of structures had been accomplished by means of an empirical constant termed the seismic coefficient. The force acting on any element or member of the structure was computed as the product of its weight and the seismic coefficient. As the various elements moved in ways different from one another, this simplification did not give reliable results. In the past few years, a new approach has been developed in order to analyze the behaviour of structures during dynamic loading; that is known as the full dynamic analysis. Although there are still a number of problems yet to be solved, the method is found to be of immense use in a detailed structural analysis.

In the first attempts to deal with dynamic analysis problems, the structure analyzed was a lumped parameter idealization involving the assumption that the mass is concentrated at discrete points. By lumping the mass at the nodes, the equilibrium conditions prevailing on the system may be written as a finite number of ordinary differential

equations rather than the partial differential equations required to describe the distributed mass system. When these equations using the lumped mass approximation are written in matrix form, the resulting mass matrix is diagonal. The consistent mass approach can be used, but in general they are found to increase the computational problem without much improving accuracy. On the other hand, the lumped mass approach results in reasonable accuracy and a considerable saving in computer storage and time [13, 24].

In order to accomplish the dynamic analysis of structures, one of two procedures, namely, the modal superposition method or the step-by-step analysis may be used. The modal analysis [6,41] involves the solution of the eigenvalue problem which is represented by the free vibrations of the system. This method uncouples the response of the system so that the response in each mode may be computed independently of the others. The step-by-step methods [56, 60, 62, 68, 95] involve the direct numerical integration of the equilibrium equations in their original form without transformation to the principal coordinates of the system.

Though the modal analysis is quite suitable for the dynamic analysis and yields the required accuracy, the solution of the eigenvalue problem and the transformation to the principal coordinates are major computational problems. The method is suitable only for the case of linear structural behaviour.

In the step-by-step method, all modes are automatically accounted for. It is suitable for nonlinear material behaviour and any

number of degrees of freedom may be used. Therefore, the step-by-step method has been chosen as the procedure for the dynamic analysis of structures in this work.

The step-by-step procedure suitable for an axisymmetric structure subjected to nonsymmetric excitation has never been presented earlier. The formulation in this Chapter is applicable to the most general problem of nonsymmetric excitation in an axisymmetric structure.

7-B STEP-BY-STEP METHOD OF DYNAMIC ANALYSIS

The numerical analysis of the coupled differential equations of motion have been investigated by various researchers including Newmark [60], Melin [56] and Penzien [68]. However, it is found that the step-by-step dynamic analysis procedure formulated by Wilson and Clough [95] is the most suitable in this case as it can be applied to a variety of problems including inelastic systems. In this method, from the known values of displacement, velocity and acceleration at any time $t - \Delta t$, it is possible to compute these quantities at time t, where Δt is a small increment in time. In the time interval Δt, the acceleration may be taken to vary either linearly or parabolically. The mid-acceleration method developed by Penzien [68] may also be used in a similar way.

7-B-1 Derivation of Step-By-Step Equations

The equations of motion of a discrete system with viscous damping at time t may be written in matrix form:

$$[M]\{\ddot{u}\}_t + [C]\{\dot{u}\}_t + [K]\{u\}_t = \{f\}_t \qquad (7:1)$$

where $\{f\}_t$ is the vector of external forces acting on the system, $\{u\}_t$, $\{\dot{u}\}_t$ and $\{\ddot{u}\}_t$ are the vectors of displacements, velocities and accelerations on the system and [M], [C] and [K] are the mass, damping and stiffness matrices. The solution of the set of differential equations may be obtained by means of a sequence of repeating matrix operations, by assuming some form of variation for the accelerations in the small time interval.

1. Linear Acceleration Method

If it is assumed that the accelerations associated with each degree of freedom of the discrete system varies linearly within a time increment Δt, then the expressions for velocities and displacements at time t may be stated as [95]

$$\{\dot{u}\}_t = \{\dot{u}\}_{t-\Delta t} + \frac{\Delta t}{2}\{\ddot{u}\}_{t-\Delta t} + \frac{\Delta t}{2}\{\ddot{u}\}_t \qquad (7:2)$$

$$\{u\}_t = \{u\}_{t-\Delta t} + \Delta t\,\{\dot{u}\}_{t-\Delta t} + \frac{\Delta t^2}{3}\{\ddot{u}\}_{t-\Delta t} + \frac{\Delta t^2}{6}\{\ddot{u}\}_t \qquad (7:3)$$

Substituting these expressions in Equation 7:1, the accelerations at time t may be written

$$\{\ddot{u}\}_t = [F]\left(\{f\}_t - [C]\{a\} - [K]\{b\}\right) \qquad (7:4)$$

where

$$[F] = \left([M] + \frac{\Delta t}{2}[C] + \frac{\Delta t^2}{6}[K]\right)^{-1} \qquad (7:5\text{-a})$$

$$\{a\} = \{\dot{u}\}_{t-\Delta t} + \frac{\Delta t}{2}\{\ddot{u}\}_{t-\Delta t} \qquad (7:5\text{-b})$$

$$\{b\} = \{u\}_{t-\Delta t} + \Delta t\ \{\dot{u}\}_{t-\Delta t} + \frac{\Delta t^2}{3}\ \{\ddot{u}\}_{t-\Delta t} \qquad (7:5\text{-c})$$

Finally the velocities and displacements at the end of the interval may be obtained as

$$\{\dot{u}\}_t = \{a\} + \frac{\Delta t}{2}\ \{\ddot{u}\}_t \qquad (7:6)$$

$$\{u\}_t = \{b\} + \frac{\Delta t^2}{6}\ \{\ddot{u}\}_t \qquad (7:7)$$

If the initial velocities and displacements are given as $\{\dot{u}\}_0$ and $\{u\}_0$, then the starting vector of accelerations may be found using the relationship

$$\{\ddot{u}\}_0 = [M]^{-1}\ (\{f\}_0 - [C]\ \{\dot{u}\}_0 - [K]\ \{u\}_0) \qquad (7:8)$$

Then by repeated application of Equations 7:4, 7:6 and 7:7, the response of the system may be computed.

2. Proportional Damping

The damping in the structure is usually represented by some simplified means. By assuming proportional damping, the damping matrix may be expressed as a linear combination of the mass and stiffness matrices.

$$[C] = \alpha\ [M] + \beta\ [K] \qquad (7:9)$$

where α and β are empirical constants, their units being sec^{-1} and sec^{+1} respectively. Then the matrix [F] in Equation 7:5-a may be rewritten

$$[F] = \left\{(1 + \alpha\ \frac{\Delta t}{2})\ [M] + (\beta\ \frac{\Delta t}{2} + \frac{\Delta t^2}{6})\ [K]\right\}^{-1}, \qquad (7:10)$$

3. Time Step for Computation

The time step Δt for computation should be selected with due consideration to the dynamic properties of the structure. One method is to compute all significant mode shapes and the corresponding periods. Then a value less than 0.1 times the smallest significant period may be chosen. In case the smallest significant period is an unknown, then it is required to try different values for the time step and use the value which is the largest among all those which give stable solutions.

7-B-2 Load Vector for the Earthquake Problem

It is possible to specify the applied load associated with each degree of freedom to be an independent function of time. However, in most practical problems, the load vector may be of a simple form

$$\{f\}_t = \xi \{P\} \tag{7:11}$$

where $\{P\}$ is the constant vector which gives the relative values of the various forces in the system and ξ is a time-dependent scalar multiplier.

In earthquake problems, the load vector may be stated as

$$\{f\}_t = - [M] \{\ddot{u}_g\} \tag{7:12}$$

where $\{\ddot{u}_g\}$ is the vector of earthquake accelerations. Equation 7:12 may be applied to the most general case of earthquake loading where each element in the vector $\{\ddot{u}_g\}$ is different from any other because of the spatial variations in seismic motions described in Chapter III. However, if these spatial variations in seismic motions are not

accounted for as in the case of a building with small lateral dimensions resting on a rigid foundation at a distant site, then Equation 7:12 may be reduced as

$$\{f\}_t = -\ddot{u}_{g1}(t)\,(m_1 \;\; 0 \;\; 0 \;\; m_2 \;\; 0 \;\; 0 \ldots\ldots m_n \;\; 0 \;\; 0)^T$$

$$-\ddot{u}_{g2}(t)\,(0 \;\; m_1 \;\; 0 \;\; 0 \;\; m_2 \;\; 0 \ldots\ldots 0 \;\; m_n \;\; 0)^T \qquad (7:13)$$

$$-\ddot{u}_{gv}(t)\,(0 \;\; 0 \;\; m_1 \;\; 0 \;\; 0 \;\; m_2 \ldots\ldots 0 \;\; 0 \;\; m_n)^T$$

where n is the number of degrees of freedom and $\ddot{u}_{g1}(t)$, $\ddot{u}_{g2}(t)$ and $\ddot{u}_{gv}(t)$ are the three components of accelerations, namely, in the E-W, N-S and vertical directions.

7-C MID-ACCELERATION METHOD

The response of a structure may be computed at regular intervals of time using the mid-acceleration method which has been proposed by Penzien [68] for the analysis of elasto-plastic structures. In this technique, if the values of displacements, velocities and accelerations are known at the beginning of an interval, t-Δt, then their values may be computed at the end of the interval, t, using the mid-acceleration which is the acceleration at time $t - \frac{\Delta t}{2}$. Let $\{f\}_b$, $\{u\}_b$, $\{\dot{u}\}_b$ and $\{\ddot{u}\}_b$ be the load, displacement, velocity, and acceleration vectors at the beginning of the time interval and the corresponding quantities be $\{f\}_m$, $\{u\}_m$, $\{\dot{u}\}_m$ and $\{\ddot{u}\}_m$ midway during the time interval, then the following relationships hold:

$$\{\dot{u}\}_m = \{\dot{u}\}_b + \frac{\Delta t}{2}\{\ddot{u}\}_b$$

$$\{u\}_m = \{u\}_b + \frac{\Delta t}{2}\{\dot{u}\}_b + \frac{\Delta t^2}{8}\{\ddot{u}\}_b \tag{7:14}$$

From the motions defined by Equation 7:1, the mid-acceleration may be computed using the equation:

$$\{\ddot{u}\}_m = [M]^{-1}\left(\{f\}_b - [C]\{\dot{u}\}_m - [K]\{u\}_m\right) \tag{7:15}$$

The end values of velocities and displacements are

$$\{\dot{u}\}_e = \{\dot{u}\}_b + \Delta t\{\ddot{u}\}_m$$

$$\{u\}_e = \{u\}_b + \Delta t\{\dot{u}\}_b + \frac{\Delta t^2}{2}\{\ddot{u}\}_m \tag{7:16}$$

Finally, the vector of accelerations at the end of the time interval may be evaluated using the relationship

$$\{\ddot{u}\}_e = [M]^{-1}\left(\{f\}_m - [C]\{\dot{u}\}_e - [K]\{u\}_e\right) \tag{7:17}$$

In the case of earthquake loading, Equations 7:15 and 7:17 may be rewritten

$$\{\ddot{u}\}_m = -\{\ddot{u}_g\}_b - [M]^{-1}\left([C]\{\dot{u}\}_m + [K]\{u\}_m\right) \tag{7:18}$$

$$\{\ddot{u}\}_e = -\frac{(\{\ddot{u}_g\}_b + \{\ddot{u}_g\}_e)}{2} - [M]^{-1}\left([C]\{\dot{u}\}_e + [K]\{u\}_e\right) \tag{7:19}$$

By using proportional damping these equations may be reduced

$$\{\ddot{u}\}_m = -\{\ddot{u}_g\}_b - \alpha\{\dot{u}\}_m - [M]^{-1}[K]\left(\beta\{\dot{u}\}_m + \{u\}_m\right) \tag{7:20}$$

$$\{\ddot{u}\}_e = -\frac{(\{\ddot{u}_g\}_b + \{\ddot{u}_g\}_e)}{2} - \alpha\{\dot{u}\}_e - [M]^{-1}[K]\left(\beta\{\dot{u}\}_e + \{u\}_e\right) \tag{7:21}$$

7-D COMPUTER PROGRAMS FOR DYNAMIC ANALYSIS

In order to accomplish the dynamic analysis of axisymmetric structures under the most general case of nonsymmetric loading, two programs have been developed. The principles of the step-by-step procedure described in Section 7-B are utilized in formulating the first program, while the other makes use of the mid-acceleration method indicated in Section 7-C.

7-D-1 Program STEPP Using the Step-By-Step Procedure

The program STEPP facilitates the computation of the dynamic responses of an axisymmetric structure under nonsymmetric excitation at regular intervals of time, Δt. An outline of the method and the various equations involved are presented in Section 7-B. The program uncouples the problem into a series of analyses in different harmonics and whenever results are to be printed out, the solutions in the various harmonics are algebraically added up. The series of operations involved in the program are given in Figure 7-1. The initial operations in the program are the same as those in the program PORAX, described in Section 5-D so far as the stiffness matrix formulation in each of the various harmonics is concerned. In addition the mass matrix [M] is prepared, depending upon whether the lumped or consistent mass approach is adopted. The lumped mass approach is more desirable, for the various reasons explained in Section 6-E. The next step is to feed in data such as the earthquake records, the constants α and β required to define the proportional damping matrix [C] and the time intervals, Δt, for the computation and ΔT for printing results, ΔT being a multiple of

INPUT DATA: PROBLEM NUMBER (N1), NUMBER OF NODES (N2), NUMBER OF ELEMENTS (N3), NUMBER OF FIRST AND SECOND TYPE HARMONICS (N4,N5), NUMBER OF SETS OF INITIAL PROPERTIES (N8), DRAINAGE CONDITION INDICATOR (N10), INDICATOR FOR LUMPED OR CONSISTENT MASS (N11), n AND TYPE OF EACH HARMONIC (NHAR (I), NTYPE (I)), NODAL DEGREES OF FREEDOM ((ND(I,J), J=1,4), I=1,N2), AND NODAL COORDINATES

SUBROUTINE CNUN DETERMINES THE NUMBER OF UNKNOWNS

FOR EACH ELEMENT, READ ITS NODES AND PROPERTIES E, ν AND UNIT WEIGHT (UW). SUBROUTINE CCODE ASSIGNS CODE NUMBERS FOR EACH DEGREE OF FREEDOM AND SUBROUTINE TRAN COMPUTES AND STORES ELEMENT DETAILS

SUBROUTINE CWIDTH DETERMINES 1/2 BANDWIDTH N6 OF THE STIFFNESS MATRIX [K]

SUBROUTINE MASSY COMPUTES THE MASS MATRIX [M], WHICH IS DIAGONAL IF LUMPED OR OF 1/2 BANDWIDTH N6 IF CONSISTENT.

I=1

FOR THE I^{TH} HARMONIC, SUBROUTINE STIFF COMPUTES ELEMENT STIFFNESS MATRICES. FOR POREPRESSURE CASE, ONLY QUADRILATERAL ELEMENTS ARE POSSIBLE AND EFFECTIVE STRESS PARAMETERS $\bar{E}$ AND $\bar{\nu}$ SHALL BE USED. FINALLY STIFF ASSEMBLES THE GLOBAL STIFFNESS MATRIX WHICH IS BANDED.

I=N4+N5 — NO → I=I+1

YES

INPUT DATA:CONSTANTS α AND β FOR PROPORTIONAL DAMPING, NUMBER OF RECORDS, TIME INTERVAL FOR PRINTING, TIME INTERVAL Δt FOR COMPUTATION

I=1

SUBROUTINE FMAT COMPUTES $[F] = \{(1+\alpha\frac{\Delta t}{2})[M] + (\beta\frac{\Delta t}{2} + \frac{\Delta t^2}{6})[K]\}^{-1}$

I=N4+N5 — NO → I=I+1

YES

SUBROUTINE STEP COMPUTES ACCELERATIONS, VELOCITIES AND DISPLACEMENTS AT REGULAR INTERVALS, Δt.

INITIAL: $\{u\}_o = \{\dot{u}\}_o = 0 \quad \{\ddot{u}\}_o = -\{\ddot{u}_g\}$

STEP BY STEP: $\{a\}$ AND $\{b\}$ USING EQUATION (7:5)
$\{\ddot{u}\}_t$ USING EQUATION (7:4), AND
$\{\dot{u}\}_t$ AND $\{u\}_t$ FROM EQUATIONS (7:6) AND (7:7)

ADD FOR VARIOUS HARMONICS WHENEVER PRINTING

CALL CSTREL AND CSTRN TO COMPUTE STRESSES

Δt. The subroutine FMAT computes the lower triangular matrix [L] such that $[L] * [L]^T = [F]^{-1}$, where [F] is defined by Equation 7:5-a. This procedure is repeated for each harmonic and the matrix [L] in each is stored on a file. The routine STEP computes the accelerations, velocities and displacements in each harmonic at regular intervals of time, Δt. For the case of earthquake loading, the initial conditions are $\{\dot{u}\}_0 = \{u\}_0 = \{0\}$ and $\{\ddot{u}\}_0 = -\{\ddot{u}_g\}_0$. From these known initial conditions and the record at time Δt, the responses at time Δt are computed using the step-by-step equations given in Section 7-B. Repeating this procedure, the responses at the end of any interval are worked out from known responses at the commencement of the interval and the input earthquake record. Whenever it is required to print out accelerations and/or displacements at any locations defined by the node numbers and the circumferential coordinates θ, the program carries out algebraic additions of results obtained in various harmonics. If stresses are also to be printed out, the routine STEP needs to call subroutines CSTREL and CSTRN.

For a structure consisting of 26 nodes and 8 quadrilateral elements and involving 54 unknowns, it takes only 39 seconds per harmonic to perform the dynamic analysis and print results at 101 regular intervals, the time required for each step being less than 0.1 second.

7-D-2 Program MSTEPP Utilizing Mid-Acceleration Method

The dynamic analysis of an axisymmetric structure subjected to nonsymmetric excitation may be carried out using the program MSTEPP

based on the mid-acceleration method outlined in Section 7-C. The sequence of operations involved are presented in the form of a flow chart as in Figure 7-2. The operations in the program MSTEPP are the same as those in STEPP until calling the subroutine FMAT. Then, the program calls routine MFMAT which computes the lower triangular matrix [L] where $[L] * [L]^T = [M]$. When the mass matrix is diagonal, it is enough to compute the diagonal matrix $[M]^{-1}$. The subroutine MSTEP computes the accelerations, velocities and displacements at the end of interval Δt from known responses at the commencement of the interval and the earthquake record. The initial responses are $\{\dot{u}\}_o = \{u\}_o = \{0\}$ and $\{\ddot{u}\}_o = - \{\ddot{u}_g\}_o$ for the case of earthquake loading. The accelerations $\{\ddot{u}\}_m$ at the mid-interval of time Δt are computed and they are utilized for the computation of responses at the end of the interval as described in Section 7-C. Whenever printing, the program adds up the responses in the various harmonics for the desired locations. The routine MSTEP calls other subroutines CSTREL and CSTRN if stresses are to be computed.

For the structure consisting of 26 nodes, 8 quadrilateral elements and 54 unknowns, the computation takes 38 seconds for the analysis and printing results at 101 regular intervals of time Δt, the time for each step being less than 0.1 second.

7-E EXAMPLE - THREE-DIMENSIONAL RESPONSE OF A WATER TANK

A reinforced concrete water tank circular in cross section and resting on firm ground at a location far from the earthquake source is

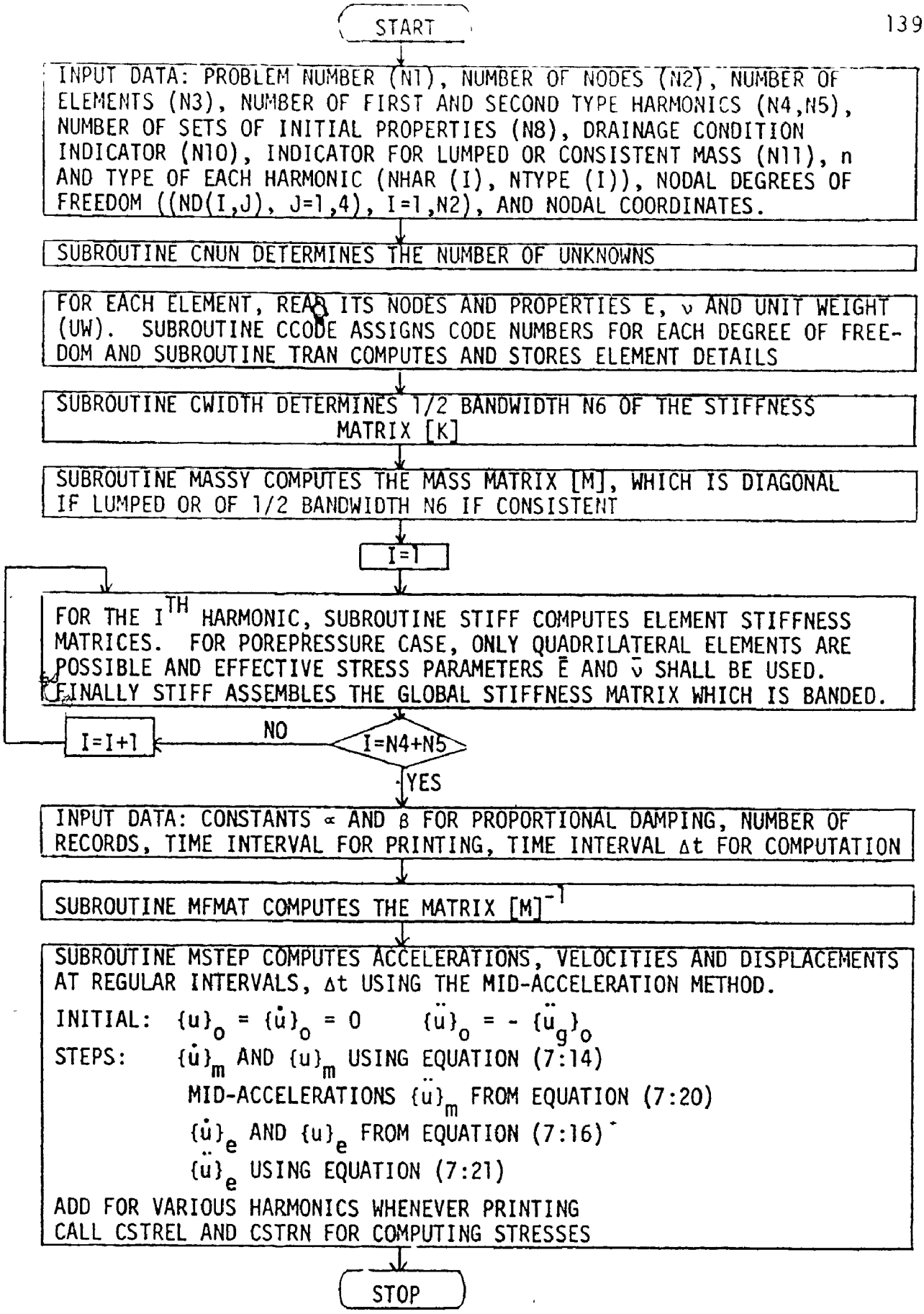

FIG. 7-2 FLOW CHART FOR AXISYMMETRIC DYNAMIC ANALYSIS USING MID-

chosen as an example for the three-dimensional analysis. At this site the shear waves may be considered vertically propagating and there is no need to consider the simultaneous effect of Rayleigh waves. There is no horizontal time lag and thus nearby stations at the same level have equal responses. The inner dimensions of the tank are 40 ft in diameter and 11 ft 3 in. in height and the various details are shown in Figure 7-3a. As the purpose of this analysis was only to get an indirect check on the dynamic programs, only the excitation during the first one second was considered. The responses of the tank when empty as a result of the first 1 second of the E-W and N-S components of the Olympia earthquake, 1949 are computed, the E-W direction being taken as the reference (θ=0) as in Figure 7-3b. In order to present the results in a simple form, the relative accelerations at a point A (21.0, θ=45°, 12.25) are considered and this corresponds to the relative accelerations of node 1 for θ=45°. The E-W component of the earthquake ($\ddot{x}_1$) may be represented as a dynamic excitation in the first symmetric harmonic (n=1) and then the N-S component ($\ddot{x}_2$) becomes the excitation in antisymmetric harmonic (m=1) as indicated in Figure 7-3b. The loads in the first symmetric harmonic are

$$\begin{aligned} \ddot{F}_r &= \ddot{x}_1 \cos\theta \\ \ddot{F}_\theta &= \ddot{x}_1 \sin\theta \end{aligned} \qquad (7:22)$$

and those in the first antisymmetric harmonic are

$$\begin{aligned} \ddot{F}_r &= \ddot{x}_2 \sin\theta \\ \ddot{F}_\theta &= \ddot{x}_2 \cos\theta \end{aligned} \qquad (7:23)$$

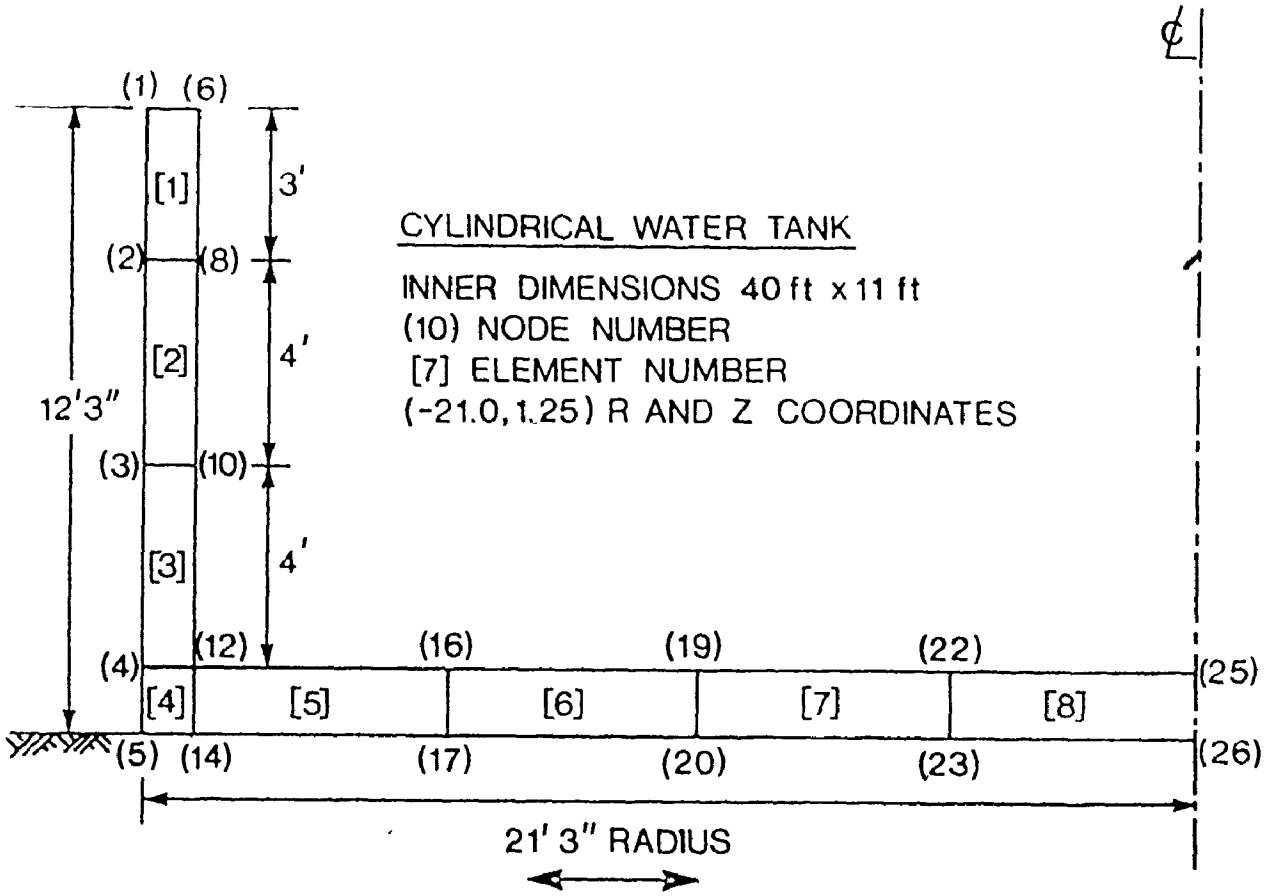

a. CYLINDRICAL WATER TANK

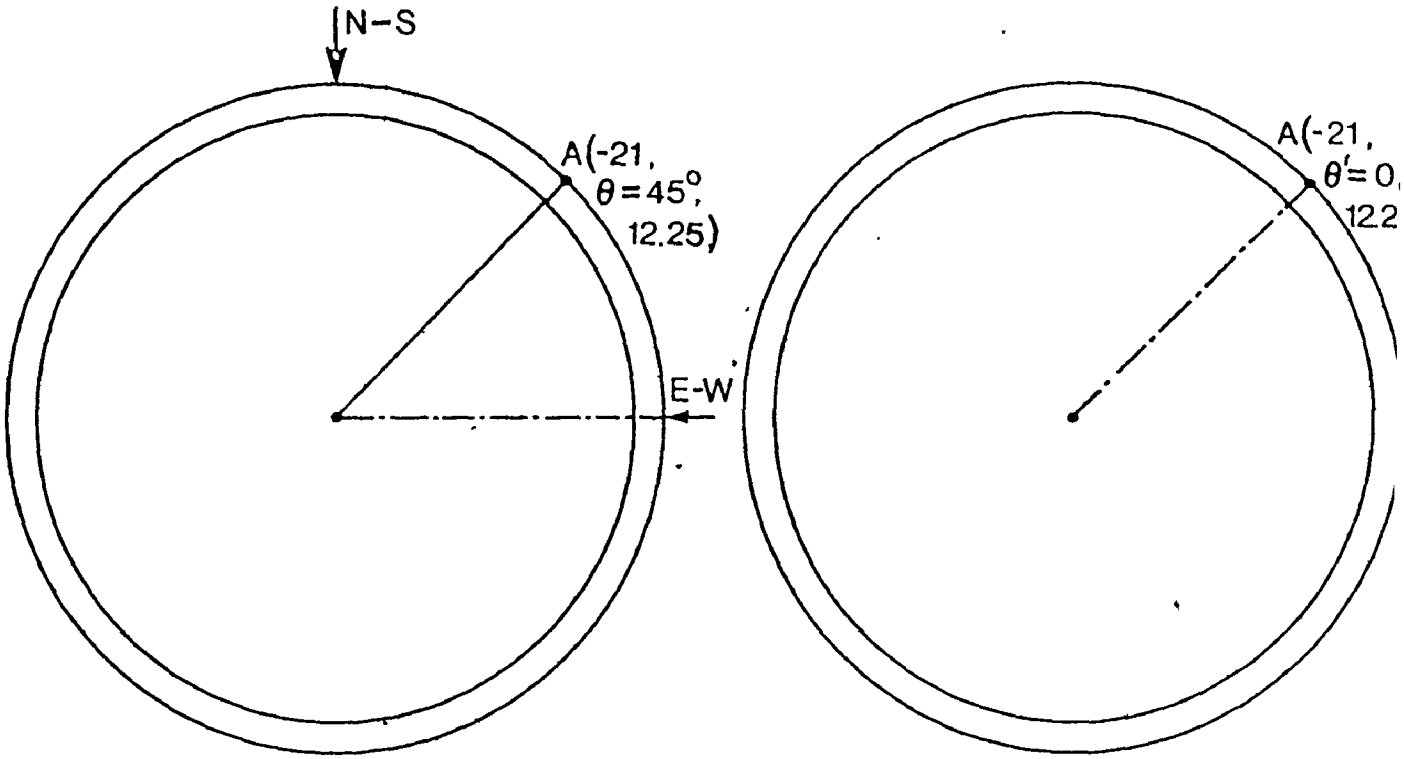

b. ORIGINAL COORDINATES

c. NEW COORDINATES

7-2 WATER TA REFEF A

The relative accelerations of node 1 in all the three directions are found to be $\ddot{u}_1$, $\ddot{v}_1$ $(=\ddot{u}_1)$ and $\ddot{w}_1$ in the first symmetric harmonic and $\ddot{u}_2$, $\ddot{v}_2$ $(=\ddot{u}_2)$ and $\ddot{w}_2$ in the first antisymmetric harmonic. Then the responses of the point A are

$$\begin{aligned} \ddot{u}_A &= \ddot{u}_1 \cos 45° + \ddot{u}_2 \sin 45° \\ \ddot{v}_A &= \ddot{u}_1 \sin 45° + \ddot{u}_2 \cos 45° \\ \ddot{w}_A &= \ddot{w}_1 \cos 45° + \ddot{w}_2 \sin 45° \end{aligned} \qquad (7:24)$$

The results obtained for $\ddot{u}_A$, $\ddot{v}_A$ and $\ddot{w}_A$ using the step-by-step procedure (Program STEPP) are shown in Figure 7-4 and those from the mid-acceleration method (Program MSTEPP) are presented in Figure 7-5. The radial and the circumferential responses of the point A have been found identical as indicated in Equation 7:24. The vertical component is found to be insignificant. The results using the two techniques produced slightly different results, well within the accuracy of the step-by-step methods.

Solution Using New Coordinates

At this stage it is of some interest to investigate the responses of the point A from another angle as it can give an indirect program check. Instead of taking E-W direction as the reference, a plane through A is taken as the reference as in Figure 7-3c and the angle θ' $(\theta' = \theta - 45°)$ is measured with respect to this plane. The coordinates of the point A are $(21.0, \theta' = 0, 12.25)$ and the relative accelerations of A are studied with reference to the new reference line. The E-W and N-S components of the Olympia earthquake, 1949 for the first 1 second are considered and the loadings in the first symmetric harmonic are:

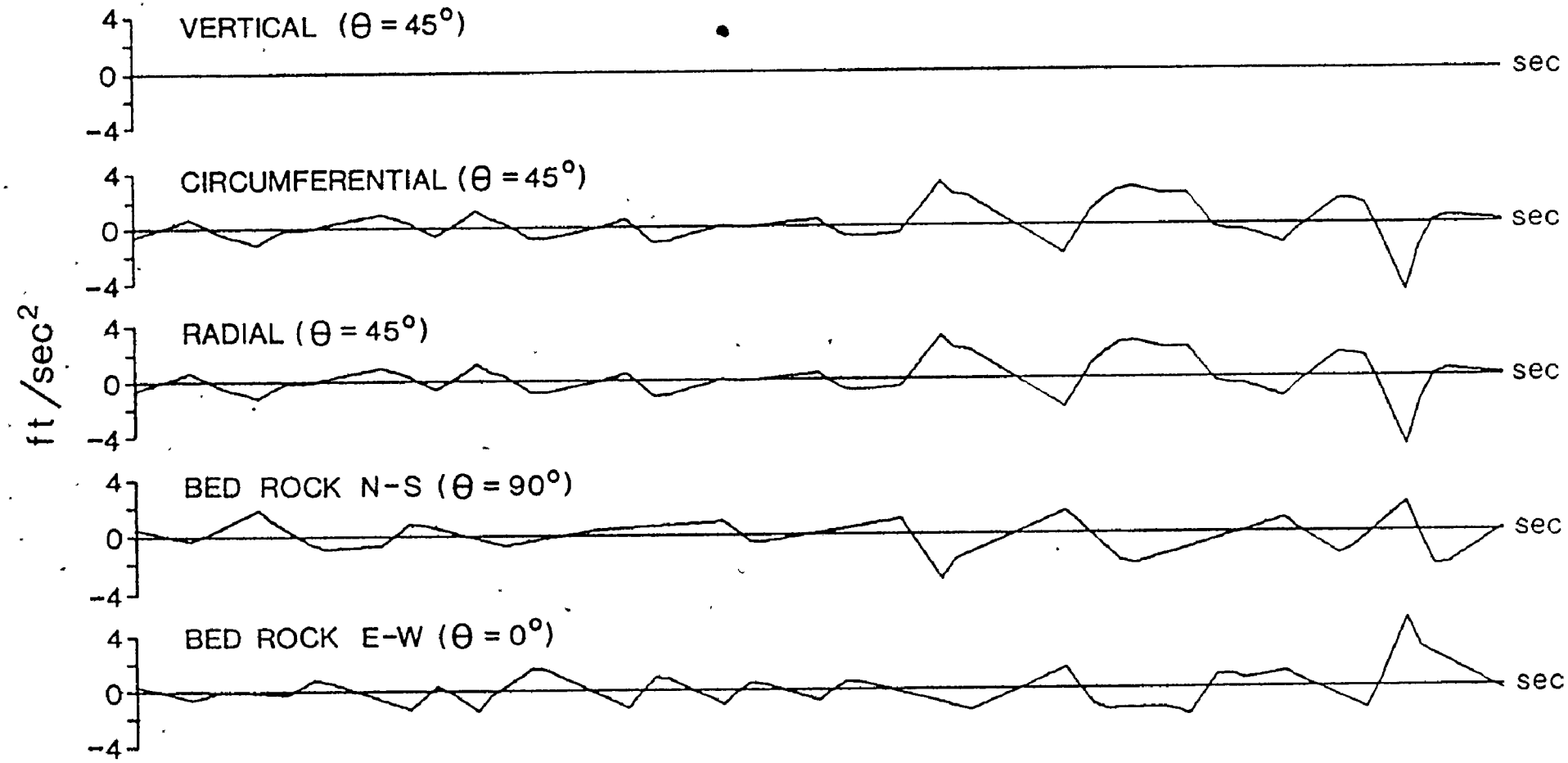

FIRST 1 SECOND DURING OLYMPIA EARTHQUAKE, 1949

FIG. 7-4 RESPONSES OF A WATER TANK USING STEP-BY-STEP ANALYSIS

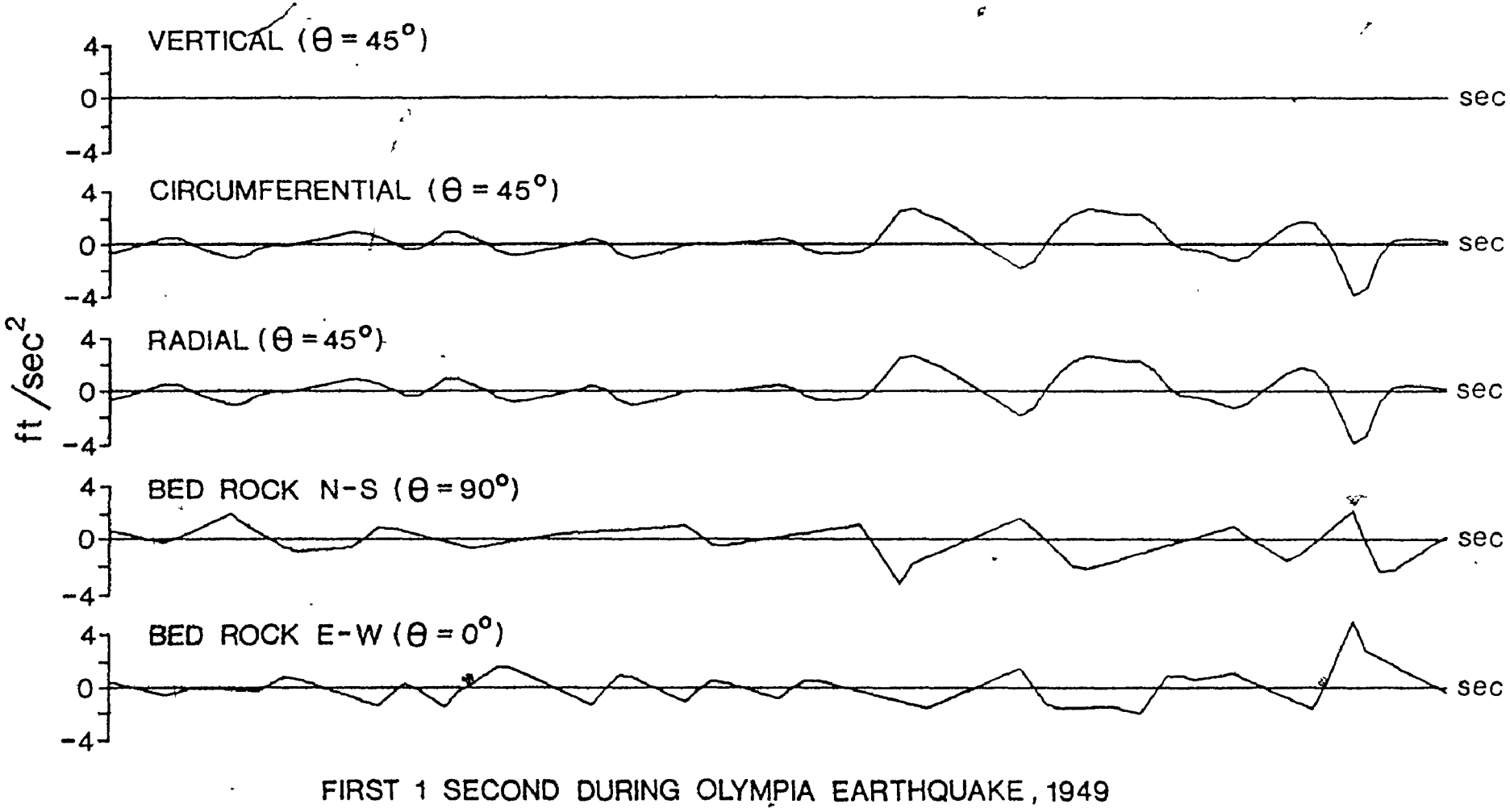

FIG.7-5 RESPONSES OF A WATER TANK USING MID-ACCELERATION METHOD

$$\ddot{F}_r = \frac{1}{\sqrt{2}} (\ddot{x}_1 + \ddot{x}_2) \cos \theta'$$

$$\ddot{F}_\theta = \frac{1}{\sqrt{2}} (\ddot{x}_1 - \ddot{x}_2) \sin \theta' \qquad (7:25)$$

Similarly, the loadings in the first antisymmetric harmonic are

$$\ddot{F}_r = \frac{1}{\sqrt{2}} (-\ddot{x}_1 + \ddot{x}_2) \sin \theta'$$

$$\ddot{F}_\theta = \frac{1}{\sqrt{2}} (\ddot{x}_1 + \ddot{x}_2) \cos \theta' \qquad (7:26)$$

The relative accelerations of node 1 in all the three directions are $\ddot{u}_1'$, $\ddot{v}_1'$ and $\ddot{w}_1'$ in the first symmetric harmonic while those in the first antisymmetric harmonic are $\ddot{u}_2'$, $\ddot{v}_2'$ and $\ddot{w}_2'$. Then the responses of the point A are

$$\ddot{u}_A = \ddot{u}_1'$$

$$\ddot{v}_A = \ddot{v}_2' \qquad (7:27)$$

$$\ddot{w}_A = \ddot{w}_1'$$

First the computations were carried out in these new coordinates using the program STEPP. The responses of A obtained in the new coordinates were identical to those in the original coordinates and the results were a mechanical reproduction of Figure 7-4; so there was no need to show them separately. The solution in new coordinates were also obtained using the program MSTEPP which gave results identical to those in original coordinates and shown in Figure 7-5. These results

give an analytical check for both these programs.

7-F COMPARISON BETWEEN THE STEP-BY-STEP PROCEDURE AND THE MID-ACCELERATION METHOD

The two methods using the step-by-step procedure and the mid-acceleration method are suitable for the dynamic analysis of structures in general and also axisymmetric structures. The results indicate that there are smooth transitions in the response diagram when the mid-acceleration method is employed. Though it may be said that each program is characteristic in its own way, the mid-acceleration method is deemed to give more accurate results as it makes use of the acceleration at the mid-interval in the response calculations. The mid-acceleration method involves more computations; yet the time required for both procedures are of the same order. A major advantage in using the mid-acceleration method for large structures lies in the fact that no storage space is required to locate the matrix [F] defined in Equation 7:5-a. However, it is found that the mid-acceleration method meets with numerical problems when dealing with complicated problems such as the soil-pile system as indicated in the following discussion.

In the step-by-step method using the program STEPP, the computation for accelerations at the end of the time interval Δt involved multiplication by the matrix [F]. The mid-acceleration method (Program MSTEPP) involved the multiplication by $[M]^{-1}$, the inverse of the mass matrix, twice for each time step; first to get

the mid-accelerations and then to determine the end accelerations. For almost all structures, the ratios of the diagonal terms of the matrix $[F]^{-1}$ to the corresponding diagonal terms of the stiffness matrix [K] are found to be roughly of the same order. However, the ratios of the diagonal terms of the matrix [M] to the corresponding diagonal terms of the matrix [K] are of the same order only in the case of simple structures. In the soil-pile system, the density of concrete and soil are of the same order, whereas the moduli varied from 2.64×10^6 psf for the soil to 4.32×10^8 psf for concrete. Further the mass of an axisymmetric ring element varied with the square of the radius while the stiffness varied linearly with it. Thus, the ratio of the mass term to the corresponding stiffness term for a pile element was very small and insignificant compared to the ratio for a soil element, especially when it was at a large radial distance. Table 7-1 shows the comparison of diagonal terms of matrices $[F]^{-1}$, [M] and [K] corresponding to nodes 59 and 68 of the soil-pile system (Figure 5-4). The operation with the matrix $[M]^{-1}$ in the mid-acceleration method involved quantities which differed drastically in order and resulted in serious computational errors. In the computation, using the mid-acceleration method, the solution for the soil-pile system became unstable even in the first step.

TABLE 7-1

COMPARISON BETWEEN THE DIAGONAL TERMS

OF MATRICES $[F]^{-1}$, [M] AND [K]

Node	K	M	F^{-1}	F^{-1}/K	M/K
59					
RADIAL	5.36×10^{9}	72463	1.503×10^{5}	2.80×10^{-4}	1.35×10^{-5}
CIRCUM-FERENTIAL	5.65×10^{9}	72463	15.12×10^{5}	2.68×10^{-4}	1.28×10^{-5}
AXIAL	2.10×10^{9}	72463	6.33×10^{5}	3.02×10^{-4}	3.44×10^{-5}
68					
RADIAL	2.14×10^{9}	7.58	5.73×10^{5}	2.67×10^{-4}	3.53×10^{-9}
CIRCUM-FERENTIAL	2.26×10^{9}	7.58	6.04×10^{5}	2.67×10^{-4}	3.36×10^{-9}
AXIAL	$.841 \times 10^{9}$	7.58	2.14×10^{5}	2.67×19^{-4}	9.03×10^{-9}

CHAPTER VIII

THE RESPONSE OF SOIL-PILE SYSTEMS DURING EARTHQUAKES

8-A INTRODUCTION

In order to compute the responses of a soil-pile system during earthquakes, the first step is to clearly define the dimensions of the system and specify the forces that excite it. In existing methods for the dynamic analysis of similar systems, the spatial variations in seismic motions are not accounted for and fixed vertical boundaries for the soil layers are assumed at large distances from the center line, usually of the order of 30 times the total thickness of the layers [25,45]. Records of ground motions during earthquakes provide convincing evidence of the spatial variations in motions and the important effects of the local soil conditions. A realistic analysis of the soil-pile system calls for consideration of these spatial variations and allowing continuity at the boundaries of the system.

As illustrated in Chapters 2 and 3, the spatial variations in seismic motions depend on various factors such as the focal depth and epicentral distance, relative contributions of different types of waves and soil properties. At a site far from the source, the combined effect of shear and Rayleigh waves need not be accounted for because of the difference in their velocities and the corresponding difference in their

arrival times. Further the shear waves at this site may be considered to be vertically propagating, thus causing variations in motions only in the vertical direction. There is no significant error in this situation by neglecting the angle of incidence and the resulting horizontal time lag. On the other hand when a nearby site is under consideration, it is essential to include the angle of incidence of shear waves as well as the relative contributions of both shear and Rayleigh waves. This time lag in the horizontal direction becomes an important factor, especially when large structures are involved [9,14,18].

The dimensions of the soil-pile system are decided upon so as to ensure that the boundary accelerations are not influenced by the presence of the pile and then it is possible to assume "free field" conditions at these boundaries, being the sides and the base of the system. Using the concepts of spatial variations in seismic motions described in Chapter 3, the absolute boundary accelerations may be computed. Once these boundary values are known, what remains is a computational procedure which can evaluate the unknown responses of the interior locations including the top of the pile (pile cap), satisfying compatibility at the boundary and equilibrium of the system.

8-B EVALUATION OF BOUNDARY ACCELERATIONS OF THE SYSTEM

The computation of the responses of a soil-pile system to travelling seismic waves requires the boundary accelerations as input data. From the available information on the pile and the soil layers, it

is possible to define the dimensions of the pile-soil systems and then compute the absolute accelerations at the boundary.

8-B-1 Dimensions of The Soil-Pile System

The dimensions of the soil-pile system are chosen so that the construction or presence of the pile has no influence on the boundaries of the system. At some distance from the pile this is a valid assumption and by defining the dimensions of the system with due regard to this aspect, it is possible to have free field conditions existing at the boundary. The length of the pile, the total depth of the soil layers and the shear wave velocities which depend on it and the predominant period of ground motions are important factors in defining the dimensions of the system. These dimensions should be suitable for assuming free field conditions at the boundary and at the same time should not result in a very large system which might increase the total computational work. It is sometimes assumed [17] that if the wave length of the advancing motion is greater than four times the span of the structure, the base motions are fairly uniform. Further it may be considered that two stations, which are at a distance apart of 1/4 of the wave length, have motions independent of each other. For the usual depths of soil strata, the shear wave velocity is of the order of 1000 fps and if the predominant period of the earthquake motion is 0.3 - 0.4 sec., the wave length works out to be 300 - 400 ft and the radius of the system works out as 75-100 ft. The radius of the soil-pile system was chosen, taking into consideration all of these factors, as 100 ft. Often the depth of

soil - pile system may be limited to the total depth of the soil layers. However, if the base rock is far below, the depth of the system may be taken as 2 - 2.5 times the length of the pile. For the 60 ft long pile shown in Figure 8-1a the radius of the soil-pile system is taken as 100 ft and the depth of 140 ft adopted coincides with the total depth of the soil layers.

8-B-2 Boundary Accelerations

The accelerations at any time, t, at the various locations along the boundary are different and they may be computed at the desired locations using the principles of spatial motions described in Chapter 3. In the final dynamic analysis, the nonsymmetric excitation on the system is separated into a series of analyses and therefore the required input data in the analysis are the radial, circumferential and axial components of the boundary accelerations in each significant harmonic at regular intervals of time. Figure 8-1a shows the nodes of the system at which the boundary accelerations are to be specified. Of these, nodes 1-5, 15, 24, 49 and 59 lie on the interfaces between the different soil layers while the remaining nodes, namely 6, 33 and 39 are in between. As for example, the computation of acceleration coefficients at node 15 in the various harmonics at any time t is described. In order to accomplish this, it is necessary to consider the boundary accelerations at all points along the nodal ring 15 as shown in Figure 8-1b. The program SPARES for the computation of spatial motions gives the accelerations at all desired locations along the nodal ring 15 in cartesian coordinates. It is

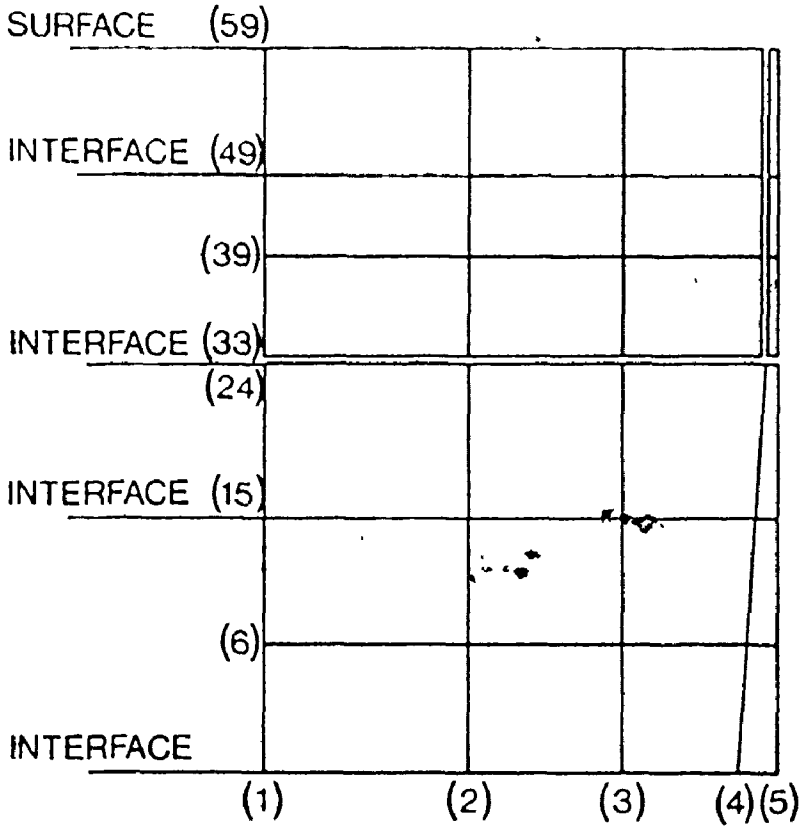

a. BOUNDARY NODES OF THE SYSTEM

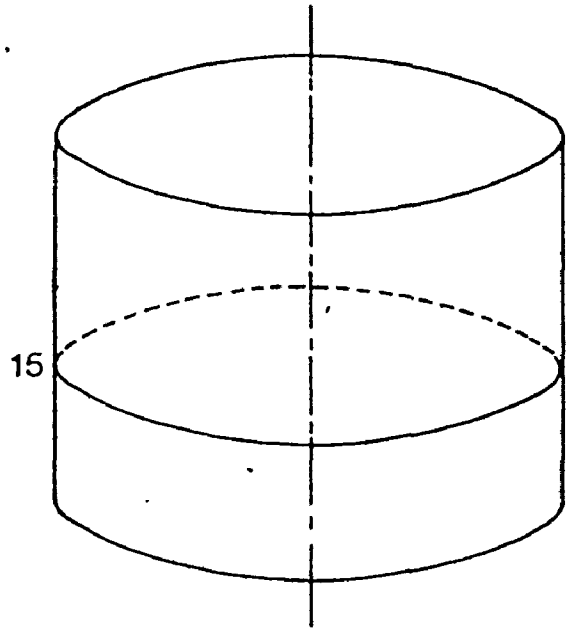

b. NODAL RING 15

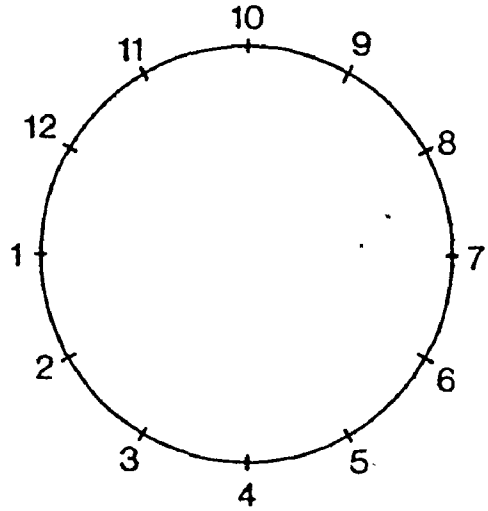

c. SELECTED POINTS ALONG NODAL RING

FIG. 8-1 BOUNDARY NODES AND SELECTED POINTS ALONG NODAL RINGS

possible to transform these motions into cylindrical coordinates using trigonometric functions. Once the cylindrical components of accelerations at any time t at all points along the nodal ring 15 are known, then it is possible to find the acceleration coefficients in each significant harmonic at that time. Thereafter the radial, circumferential and axial boundary accelerations at any point along the nodal ring 15 at time t may be expressed as

$$\ddot{u}(t) = \sum_{n=0}^{\infty} \ddot{u}_{rn}(t) \cos n\theta + \sum_{m=1}^{\infty} \ddot{u}_{rm}(t) \sin m\theta$$

$$\ddot{v}(t) = \sum_{n=1}^{\infty} \ddot{u}_{\theta n}(t) \sin n\theta + \sum_{m=1}^{\infty} \ddot{u}_{\theta m}(t) \cos m\theta \qquad (8:1)$$

$$\ddot{w}(t) = \sum_{n=0}^{\infty} \ddot{u}_{zn}(t) \cos n\theta + \sum_{m=1}^{\infty} \ddot{u}_{zm}(t) \sin m\theta$$

where the coefficients $\ddot{u}_{rn}(t)$, $\ddot{u}_{rm}(t)$ etc. may be evaluated by integrating the general expressions for accelerations along the nodal ring 15. For instance, the expressions for these coefficients are:

$$\ddot{u}_{ro}(t) = \frac{1}{2\pi} \int_{-\pi}^{\pi} \ddot{u}_r(t)\, d\theta$$

$$\ddot{u}_{rn}(t) = \frac{1}{\pi} \int_{-\pi}^{\pi} \ddot{u}_r(t) \cos n\theta\, d\theta$$

$$\ddot{u}_{rm}(t) = \frac{1}{\pi} \int_{-\pi}^{\pi} \ddot{u}_r(t) \sin m\theta\, d\theta$$

$$\ddot{u}_{\theta n}(t) = \frac{1}{\pi} \int_{-\pi}^{\pi} \ddot{u}_\theta(t) \sin n\theta\, d\theta \qquad (8:2\text{-a})$$

$$\ddot{u}_{\theta m}(t) = \frac{1}{\pi} \int_{-\pi}^{\pi} \ddot{u}_{\theta}(t) \cos m\theta \, d\theta$$

$$\ddot{u}_{zo}(t) = \frac{1}{2\pi} \int_{-\pi}^{\pi} \ddot{u}_{z}(t) \, d\theta$$

$$\ddot{u}_{zn}(t) = \frac{1}{\pi} \int_{-\pi}^{\pi} \ddot{u}_{z}(t) \cos n\theta \, d\theta$$

$$\ddot{u}_{zm}(t) = \frac{1}{\pi} \int_{-\pi}^{\pi} \ddot{u}_{z}(t) \sin m\theta \, d\theta \qquad (8:2\text{-b})$$

where $\ddot{u}_r(t)$, $\ddot{u}_\theta(t)$ and $\ddot{u}_z(t)$ are the general expressions for the cylindrical components of accelerations at time t along the nodal ring 15. However, it is not feasible to find a general expression for the accelerations along the nodal ring 15 and therefore an averaging procedure is adopted.

8-B-3 Averaging Procedure

As it is not possible to use a general expression for accelerations along a nodal ring and find the required acceleration coefficients at the node in the various harmonics by means of integration, the accelerations at a few selected points are first determined. Any number of points may be selected and it is convenient to use 12 or 8 points, so that the averaging is adequate. The radial, circumferential and axial components of accelerations at time t at these 12 selected points, spaced at regular angular distances of 30° as shown in Figure 8-1c,

along the nodal ring 15 are worked out. Then the coefficients of accelerations in the various harmonics at node 15 are computed by means of the averaging procedure. The acceleration coefficients in the various harmonics are given by Equation 8:3 and these are the discretized forms of the expressions given by Equation 8:2.

$$\ddot{u}_{ro}(t) = \frac{1}{12} \sum_{i=1}^{12} \ddot{u}_{ri}(t)$$

$$\ddot{u}_{rn}(t) = \frac{1}{\pi\, n} \sum_{i=1}^{12} \ddot{u}_{ri}(t) \{\sin (30in - 15n)^{\circ} - \sin (30in - 45n)^{\circ}\}$$

$$\ddot{u}_{rm}(t) = \frac{1}{\pi\, m} \sum_{i=1}^{12} \ddot{u}_{ri}(t) \{\cos (30im - 45m)^{\circ} - \cos (30im - 15m)^{\circ}\}$$

$$\ddot{u}_{\theta n}(t) = \frac{1}{\pi\, n} \sum_{i=1}^{12} \ddot{u}_{\theta i}(t) \{\cos (30in - 45n)^{\circ} - \cos (30in - 15n)^{\circ}\}$$

$$\ddot{u}_{\theta m}(t) = \frac{1}{\pi\, m} \sum_{i=1}^{12} \ddot{u}_{\theta i}(t) \{\sin (30im - 15m)^{\circ} - \sin (30im - 45m)^{\circ}\} \qquad (8:3)$$

$$\ddot{u}_{zo}(t) = \frac{1}{12} \sum_{i=1}^{12} \ddot{u}_{zi}(t)$$

$$\ddot{u}_{zn}(t) = \frac{1}{\pi\, n} \sum_{i=1}^{12} \ddot{u}_{zi}(t) \{\sin (30in - 15n)^{\circ} - \sin (30in - 45n)^{\circ}\}$$

$$\ddot{u}_{zm}(t) = \frac{1}{\pi\, m} \sum_{i=1}^{12} \ddot{u}_{zi}(t) \{\cos (30im - 45m)^{\circ} - \cos (30im - 15m)^{\circ}\}$$

8-B-4 Program for Computing Boundary Accelerations

The program SPARES used for the computation of spatial variations in seismic motions is extended to evaluate the boundary accelerations of the soil-pile system. For example, the accelerations in cartesian coordinates at the 12 points along the nodal ring 15 are given at any time t by the program SPARES. The extension is carried out by adding a subroutine AXIS which uses these boundary accelerations in cartesian coordinates, transforms them into cylindrical coordinates and finally, using the averaging procedure explained in Section 8-B-3, gives the components of acceleration at node 15 in the various harmonics.

The program has been used to determine the acceleration coefficients in the various harmonics and it is found that non-zero motions are found in harmonics (0,1), (1,1), (1,2), (2,1), (10,1), (11,1), (11,2), (12,1), etc. where the first term in parantheses gives the value of n while the second term denotes the symmetric (1) or antisymmetric (2) harmonic. However, the significant responses are only in the first four harmonics listed, namely (0,1), (1,1), (1,2) and (2,1). Therefore, only the terms in these four harmonics need be accounted for and the insignificant higher order terms may be deleted.

When the site is far away from the earthquake source there is no horizontal time lag and a simple subroutine AXES added to program SPARES gives the components of accelerations in the three harmonics, (0,1), (1,1) and (1,2).

8-C DERIVATION OF THE EQUATIONS OF MOTION FOR THE SOIL-PILE SYSTEM

The equations of motion in matrix notation of a discrete system with viscous damping at time t may be expressed in terms of absolute responses:

$$[M]\,\{\ddot{U}\}_t + [C]\,\{\dot{U}\}_t + [K]\,\{U\}_t = \{0\} \tag{8:4}$$

where $\{\ddot{U}\}_t$, $\{\dot{U}\}_t$ and $\{U\}_t$ are the vectors of absolute accelerations, velocities and displacements for the system and [M], [C] and [K] are the mass, damping and stiffness matrices. In the case of the soil-pile system, the responses at the boundary nodes $\{\ddot{U}_g\}_t$, $\{\dot{U}_g\}_t$ and $\{U_g\}_t$ are available from solving the wave propagation problem. Therefore, only the unknown responses of the interior nodes of the system need be computed and the total response vectors may be partitioned as

$$\{\ddot{U}\}_t = \left\{\begin{matrix} \ddot{U}_i \\ \hline \ddot{U}_g \end{matrix}\right\}_t$$

$$\{\dot{U}\}_t = \left\{\begin{matrix} \dot{U}_i \\ \hline \dot{U}_g \end{matrix}\right\}_t \tag{8:5}$$

$$\{U\}_t = \left\{\begin{matrix} U_i \\ \hline U_g \end{matrix}\right\}_t$$

where $\{\ddot{U}_i\}_t$, $\{\dot{U}_i\}_t$ and $\{U_i\}_t$ correspond to the interior nodes and $\{\ddot{U}_g\}_t$, $\{\dot{U}_g\}_t$ and $\{U_g\}_t$ are the known boundary responses of the system. When the

system undergoes displacements at the boundary nodes, there will be corresponding displacements at the remaining interior nodes of the system to balance the system and let it assume the displaced position. The total displacement vector for the interior nodes may be written:

$$\{U_i\}_t = \{u\}_t + \{U_{gg}\}_t \tag{8:6}$$

in which $\{u\}_t$ is the vector of dynamic displacements and $\{U_{gg}\}_t$ is the vector of balancing displacements. The boundary nodal displacements $\{U_g\}_t$ and the balancing displacements $\{U_{gg}\}_t$ at the interior nodes are such that the system can remain in that distorted position without any application of forces at the interior nodes, i.e.,

$$[K_{11} \mid K_{12}] \left\{ \begin{array}{c} U_{gg} \\ \hline U_g \end{array} \right\}_t = \{0\} \tag{8:7}$$

The balancing displacements $\{U_{gg}\}_t$ may be computed as follows:

Each boundary nodal degree of freedom is given a unit displacement, one at a time, while keeping all other nodal degrees of freedom on the boundary fixed. The displacements of the interior nodes due to this unit displacement are computed. If there are NUB nodal degrees of freedom on the boundary and NUI nodal degrees of freedom in the interior, then considering all the boundary nodes the balancing displacements may be expressed as

$$\{U_{gg}\}_t = [H] \{U_g\}_t \tag{8:8}$$

where [H] is a matrix of order (NUI * NUB). Then Equation 8:7 may be

rewritten

$$([K_{11}]\ [H] + [K_{12}])\ \{U_g\}_t = \{0\} \tag{8:9}$$

The equations of motion given by Equation 8:4 may be partitioned into two sets of equations, namely, those corresponding to the interior nodes and the nodes on the boundary.

$$\left[\begin{array}{c|c} M_{11} & M_{12} \\ \hline M_{21} & M_{22} \end{array}\right] \left\{\begin{array}{c} \ddot{U} \\ \hline \ddot{U}_g \end{array}\right\}_t + \left[\begin{array}{c|c} C_{11} & C_{12} \\ \hline C_{21} & C_{22} \end{array}\right] \left\{\begin{array}{c} \dot{U} \\ \hline \dot{U}_g \end{array}\right\}_t + \left[\begin{array}{c|c} K_{11} & K_{12} \\ \hline K_{21} & K_{22} \end{array}\right] \left\{\begin{array}{c} U \\ \hline U_g \end{array}\right\}_t = \left\{\begin{array}{c} 0 \\ \hline 0 \end{array}\right\} \tag{8:10}$$

As the responses on the boundary of the system are initially known, there is no need to consider the second set of equations and hence they may be deleted. The equations of motion associated with the interior nodes may be stated

$$[M_{11}]\{\ddot{U}\}_t + [M_{12}]\{\ddot{U}_g\}_t + [C_{11}]\{\dot{U}\}_t + [C_{12}]\{\dot{U}_g\}_t + [K_{11}]\{U\}_t + [K_{12}]\{U_g\}_t = \{0\} \tag{8:11}$$

which may be rewritten

$$[M_{11}]\{\ddot{u}\}_t + [C_{11}]\ \{\dot{u}\}_t + [K_{11}]\{u\}_t =$$

$$-[M_{11}]\{\ddot{U}_{gg}\}_t - [M_{12}]\{\ddot{U}_g\}_t - [C_{11}]\{\dot{U}_{gg}\}_t - [C_{12}]\{\dot{U}_g\}_t - [K_{11}]\{U_{gg}\}_t - [K_{12}]\{U_g\}_t \tag{8:12}$$

Using lumped masses and proportional damping and also making note of the relationships established in Equation 8:9, Equation 8:12 reduces to

$$[M_{11}]\{\ddot{u}\}_t + [C_{11}]\{\dot{u}\}_t + [K_{11}]\{u\}_t = -[M_{11}][H]\{\ddot{U}_g\}_t - \alpha[M_{11}][H]\{\dot{U}_g\}_t \tag{8:13}$$

The vectors $\{\ddot{U}_g\}_t$ and $\{\dot{U}_g\}_t$ depend on the ground motions and the usual value of α for soils is of the order of 0.01 second^{-1}. The natural period of ground increases with depth of soil layers above the bed rock and its approximate value is found from the relationship [64]:

$$T_G = 4 \sum \frac{h_i}{\beta_i} \tag{8:14}$$

where h_i and β_i are the depth and shear wave velocity of the ith layer. Among the systems considered, the highest period works out as 1.49 sec. for the dry sand strata and this corresponds to a frequency of 4.22 radians/sec. In response spectrum analysis, the maximum acceleration and maximum velocity are found using the expressions:

$$\begin{aligned} \dot{u}_{max} &\simeq S_v \\ \ddot{u}_{max} &\simeq \omega S_v \end{aligned} \tag{8:15}$$

The relationship between the acceleration and velocity at any time is of the same order and, therefore, it may be written:

$$\left\{\dot{U}_g\right\}_t \simeq \frac{1}{\omega}\left\{\ddot{U}_g\right\}_t \tag{8:16}$$

The term corresponding to damping in the right hand side of Equation 8:13 is approximately 0.0025 of the inertia term and looses significance. Thus, this damping term is negligible to the inertia term in the equation and may be deleted. It is interesting to note from Equation 8:13 that the

general form of the equations of motion are not changed and the only difference between the travelling seismic waves solution and the rigid base solution lies in the magnitude of the time-dependent exciting forces. Once these exciting forces are specified, the methods developed in Chapter 7 may be adopted to evaluate the dynamic responses. Finally, the absolute responses of the interior nodes may be computed using the relationship given by Equation 8:6.

8-D PROGRAM FOR COMPUTING RESPONSE OF SOIL-PILE SYSTEMS TO SEISMIC WAVES

In order to accomplish the dynamic analysis of a soil-pile system, a program WAVAX has been developed making use of the principles described in Chapters 2 and 3 and Sections 8-A to 8-C. The program consists of two parts:

(1) The first part computes the free-field boundary accelerations for the soil-pile system and these form the input data for the second part of the program.

(2) The second part makes use of the boundary accelerations as input and computes the responses at the various nodes within the system, satisfying the equilibrium of the system and compatibility at its boundary.

The series of operations involved in the program WAVAX are presented in the form of a flow chart in Figure 8-2.

PART 1

COMPUTATION OF BOUNDARY RESPONSES OF SOIL-PILE SYSTEM: DIMENSIONS AND PROPERTIES OF SOIL LAYERS, EARTHQUAKE RECORDS AND SPATIAL (r, θ AND z) COORDINATES OF BOUNDARY NODES ARE INPUT DATA

↓

COMPUTE BOUNDARY NODAL RESPONSES OF SOIL-PILE SYSTEM USING PROGRAM SPARES; THE ROUTINE AXIS OR AXES CALCULATES THE BOUNDARY ACCELERATION COEFFICIENTS IN THE NECESSARY HARMONICS AND STORES THEM ON FILE IN AN ORDER IN WHICH THEY ARE REQUIRED IN PART 2: FULL FINITE ELEMENT DYNAMIC PROGRAM

↓

PART 2

FINITE ELEMENT DYNAMIC PROGRAM

INPUT DATA: PROBLEM NUMBER (N1), NUMBER OF NODES (N2), NUMBER OF ELEMENTS (N3), NUMBER OF FIRST AND SECOND TYPE HARMONICS (N4,N5), NUMBER OF SETS OF INITIAL PROPERTIES (N8), DRAINAGE CONDITION INDICATOR (N10), INDICATOR FOR LUMPED OR CONSISTENT MASS (N11), n AND TYPE OF HARMONIC (NHAR(I), NTYPE(I)), NODAL DEGREES OF FREEDOM (ND(I,J), J=1,4), I=1,N2), BOUNDARY NODES, NODAL COORDINATES AND ELEMENT DETAILS.

↓

SUBROUTINES CNUN COMPUTES THE NUMBER OF UNKNOWNS, CCODE ASSIGNS CODE NUMBERS, CWIDTH DETERMINES ½ BAND WIDTH N6 OF STIFFNESS MATRIX, MASSY ASSEMBLES THE MASS MATRIX [M] AND STIFF COMPUTES THE STIFFNESS MATRIX [K] IN EACH HARMONIC

↓

INPUT DATA: CONSTANTS α AND β FOR PROPORTIONAL DAMPING, TIME INTERVAL FOR PRINTING AND TIME INTERVAL Δt FOR COMPUTATION

↓

I=1

↓

SUBROUTINE FFMAT COMPUTES $[M_{11}]$ AND $[K_{11}]$ IN EQUATION 8:13 AND DETERMINES

$$[F] = \{(1 + \alpha \frac{\Delta t}{2})[M_{11}] + (\beta \frac{\Delta t}{2} + \frac{\Delta t^2}{6})[K_{11}]\}^{-1}$$

↓

I=I+1 ← NO — I=N4+N5

↓ YES

SUBROUTINE FSTEP COMPUTES ABSOLUTE ACCELERATIONS, VELOCITIES AND DISPLACEMENTS AT REGULAR TIME INTERVALS, Δt.

INITIAL: $\{\dot{U}_i\}_0 = \{U_i\}_0 = \{\dot{u}\}_0 = \{u\}_0 = 0 \quad \{\ddot{U}_i\}_0 = \{\ddot{u}\}_0 = [H]\{\ddot{U}_g\}_0$

STEP-BY-STEP: $\{a\}$ AND $\{b\}$ by EQUATION 7:5

$\{\ddot{u}\}_t$ USING EQUATION 7:4, WHERE $\{f\}_t = [H]\{\ddot{U}_g\}_t$

$\{\dot{u}\}_t$ AND $\{u\}_t$ FROM EQUATIONS 7:6 AND 7:7

$\{\ddot{U}_{gg}\}_t$ $\{\dot{U}_{gg}\}_t$ AND $\{U_{gg}\}_t$ USING EQUATION 8:8

$\{U_i\}_t$ USING EQUATION 8:6

ADD FOR VARIOUS HARMONICS WHENEVER PRINTING

CALL CSTREL AND CSTRN TO COMPUTE STRESSES

8-D-1 Part 1 - Boundary Accelerations

The first part of the program WAVAX is an extension of the program SPARES by making suitable modifications and adding two subroutines AXIS and AXES. When the site is nearby to the earthquake source, the program first computes the accelerations in cartesian coordinates at the 12 selected points along the various nodal rings at each time interval, Δt. These accelerations are transformed into cylindrical coordinates and by an averaging procedure as outlined in Sections 8-B-3 and 8-B-4, the acceleration coefficients for all time intervals in the harmonics (0,1), (1,1), (1,2) and (2,1) are computed in that order (Subroutine AXIS). These coefficients in all the three directions (r, θ, and z) at each boundary node and each time interval are written on a file (TAPE 11) in the order in which they are called from Part 2 as input data.

When the site considered is far from the earthquake source, there is no horizontal time lag and no need to compute the accelerations at points along a nodal ring as all of them have identical response. The acceleration coefficients in cylindrical coordinates in the three harmonics, namely, (0,1), (1,1) and (1,2) are computed (Subroutine AXES) and written on a file (TAPE 11) in the order in which they are required as input data in Part 2.

The only details which are carried from Part 1 to Part 2 are:

(1) The total number of harmonics to be considered, being 4 for the nearby site and 3 for the distant site.

(2) The time interval for computation, Δt and the time interval for printout, ΔT.

(3) The total number of recorded time intervals.

(4) The acceleration coefficients in the various harmonics, recorded on file 11.

8-D-2 Part 2 - Response of the Soil-Pile System

Once the coefficients of absolute (total) accelerations in the various harmonics at the boundary are computed, the program WAVAX gets into the second part of evaluating the responses of the entire system. The total responses at the boundary for the entire period of time are known at regular intervals. As the motions at a few nodes of the system are known and the remaining are to be computed, this is a problem of mixed conditions and therefore the stiffness matrices [K] in the various harmonics need modification. The dynamic analysis is accomplished by means of the step-by-step integration procedure using the linear acceleration method. The subroutine FFMAT computes the matrix [H] defined by Equation 8:8 and the lower triangular matrix [L], where $[L] * [L]^T = [F]^{-1}$, [F] being given by Equation 7:5. The procedure is repeated for each harmonic and the matrices [H] and [L] are stored on a file. The routine FSTEP computes the balancing accelerations and corresponding velocities from known acceleration coefficients at the boundary at any time interval using Equation 8:8. Once the excitation forces defined by the right hand side of Equation 8:13 are computed, the program works out the [illegible] mic r [illegible] In [illegible] to arrive at the abs [illegible] at

the interior nodes, the dynamic responses and balancing responses are added up algebraically as in Equation 8:6. Repeating this procedure, the absolute responses at the end of any time interval are obtained from the known responses at the beginning of the time interval and the record of boundary acceleration coefficients. Whenever results are to be printed out, the values obtained from the various harmonics for any location, defined by a node number and the circumferential coordinate θ, are algebraically added up. If stresses are also to be printed out, the routine FSTEP calls subroutines CSTREL and CSTRN. In calculating strains and stresses at any time, the absolute displacements are used.

The time required for the computation of responses of the system to seismic waves is just over two times that required to get the rigid base solutions. For a system with 68 nodes and 33 elements (24 quadrilateral and 9 linkage elements), the solution requires about 60 seconds to compute the boundary accelerations at 500 intervals for a nearby site, while the same work needs only about 35 seconds for a far away site. The final dynamic analysis requires about 0.7 second per time interval. The calculation of stresses and strains at any time interval takes about 2 seconds. However, usually it is adequate to compute stresses at relatively large intervals of time.

8-E ILLUSTRATIVE EXAMPLES

In order to study and compare the dynamic behavior of piles during earthquakes in different types of soil under different conditions, two soil-pile systems were considered. The types of soil in these systems were clay and sand r tively and the dimensions and properties of the

pile were kept identical in each system to facilitate comparisons. It was also assumed that bed rock is located at a depth of 140 ft and that there are four distinct soil layers in each system. The dimensions of the soil-pile system are shown in Figure 8-3 (same as Figure 5-4). The stiffness of the linkage element was set to 10^{10} lb/ft. If the element failed the stiffness could be set to a small value. However this was not done in the present dynamic problems because of limitations in computer storage and very large increases in computation time. The responses of these soil-pile systems to the peak acceleration during different earthquakes were considered. The influence of focal depth and the epicentral distance was also accounted for by considering both near and distant sites.

8-E-1 Properties of the Pile Founded in Sand

The case of a pile founded in sand presents a complex problem and the elastic properties of a sand stratum depend on the shape and size of sand particles, the relative density of the sand and the confining pressures acting at each point within the sand. For a pile driven into sand, the problem is further complicated due to changes in soil properties which occur during the driving process. In order to get a reasonably accurate representation of the physical properties and the arrangement of soil strata and the location of the ground water table, a soil exploration is usually carried out. Though the soil exploration may

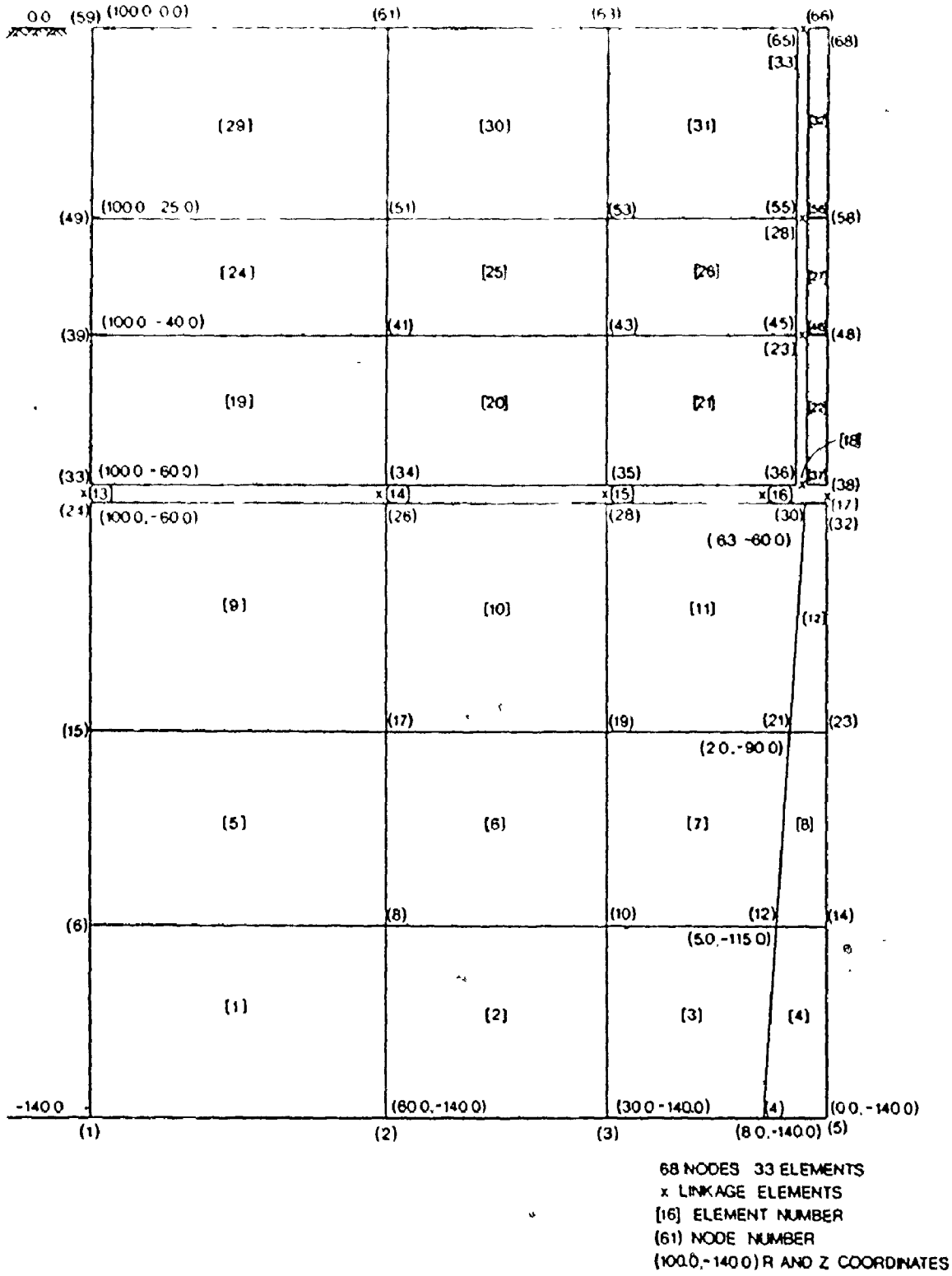

FIG. 8-3 DIMENSIONS OF THE SOIL-PILE SYSTEM

be performed by soil boring, and soil samples can be taken out, usually the samples of granular materials are disturbed. However, it is possible to make use of the results of the Standard Penetration tests done in the vicinity of the pile and predict the soil parameters such as the relative density, the angle of internal friction and the unit weight. Table 8-1 gives relationships between the penetration resistance and various parameters.

The shear modulus of sand in psi may be calculated using the relationship given by Hardin and Drnevich [34,35], being,

$$G = 1230\,(\bar{\sigma}_0)^{1/2}\,\frac{(2.973 - e)^2}{(1+e)} \qquad (8:17)$$

where $\bar{\sigma}_0$ is the mean principal effective stress given in psi.
The damping in the system may be assumed as 5% critical based on the available test results [1]. The Poisson's ratio may be obtained using the relationship [63]

$$\nu = 0.2 + 0.3 \quad 1 - \frac{1}{16}\{\sqrt{\log_{10}(.7G) - 2}\}^2 \qquad (8:18)$$

where G is the shear modulus of the soil in psi.

The properties of the soil layers and the pile for the system in sand are given in Table 8-2, for both dry and saturated conditions. The shear modulus of sand has been computed using the relationship given by Equation 8:17.

TABLE 8-1

RELATIONSHIPS BETWEEN SOIL PARAMETERS

AND PENETRATION RESISTANCE, N

(N in blows/ft)

SAND

N^+	0-4	4-10	10-30	30-50	>50
Description	Very Loose	Loose	Medium	Dense	Very Dense
Relative Density (D_r %)	0-15	15-35	35-65	65-85	85-100
**Angle of internal friction, ϕ (deg)	25-30	27-32	30-35	35-40	38-43
Unit weight, γ (lb/ft^3)	70-100	90-115	110-130	110-140	130-150

+Corrected value [30]

** $\phi = 25 + 0.15\ D_r$ for sands with more than 5% fines [57]

$\phi = 30 + 0.15\ D_r$ for sands with less than 5% fines [57]

TABLE 8-2

MATERIAL PROPERTIES OF SOIL-PILE SYSTEM IN SAND

ITEM	G	e	ν	ϕ	DENSITY γ lb/ft^3	MODULUS OF RIGIDITY, G lb/ft^2	MODULUS OF ELASTICITY, E lb/ft^2	SHEAR WAVE VELOCITY β, fps
SAND LAYER 1	2.65	.71	.3	38	96.7 (dry)	12,80,000	33,25,000	652
					122.7 (sat.)	10,15,000	26,40,000	515
SAND LAYER 2	2.72	.68	.33	41	101.1 (dry)	24,53,000	65,24,000	884
					126.4 (sat.)	19,43,000	51,68,000	704
SAND LAYER 3	2.71	.63	.33	41	103.7 (dry)	35,47,000	94,35,000	1050
					127.8 (sat.)	28,14,000	74,85,000	842
SAND LAYER 4	2.80	.57	.35	42	110.1 (dry)	48,23,000	130,24,000	1388
					133.9 (sat.)	38,41,000	103,70,000	961
BED ROCK			.40	42	145.0			6000
PILE			.15		150.0		4320,00,000	

8-E-2 Properties of the Bored Pile in Clay

The construction of a pile in clay is usually accomplished by excavating a hole by means of augering and then having the pile cast-in-situ. It has been reported by Skempton [85] that the water content in the soil adjacent to the pile increases during excavation and that the extent of this change is limited to an annular shaft. This local disturbance has very little effect on the elastic properties of the clay layers and so there is no difficulty in estimating these quantities. The Poisson's ratio for clays ranges from 0.45 to 0.48 and a value of 0.48 may always be used. The shear modulus of clays has been given by [34,35]:

$$G = 1230\,(\bar{\sigma}_o)^{1/2}\,\frac{(2.973 - e)^2}{(1+e)}\,(OCR)^K \qquad (8:19)$$

where G and $\bar{\sigma}_o$ are in psi and OCR is the overconsolidation ratio. The value of K depends on the plasticity index and it varies from 0-0.50 for varying plasticity index values from 0-100.

Table 8-3 shows the properties of clay assumed for both dry and saturated conditions.

8-F NATURAL FREQUENCIES

The natural frequencies of the two soil-pile systems have been determined. It was interesting to note that the soil-pile system in which the slip elements were assumed to have a stiffness of 10^{10} lb/ft and the system neglecting the slip between the pile and the soil gave very close natural frequencies. This was a good indication that the value of 10^{10} lb/ft assumed

TABLE 8-3

MATERIAL PROPERTIES OF SOIL-PILE SYSTEM IN CLAY

ITEM	G	e	ν	φ	DENSITY γ lb/ft³	MODULUS OF RIGIDITY, G lb/ft²	MODULUS OF ELASTICITY, E lb/ft²	SHEAR WAVE VELOCITY β, fps
CLAY LAYER 1	2.81	1.70	.48	10	65.0 (dry)	4,18,000	12,37,000	455
					104.2 (sat.)	4,24,000	12,55,000	462
CLAY LAYER 2	2.75	1.42	.48	10	70.8 (dry)	8,70,000	25,75,000	629
					107.2 (sat.)	7,70,000	22,77,000	480
CLAY LAYER 3	2.73	0.98	.48	10	86.0 (dry)	21,25,000	62,90,000	892
					116.7 (sat.)	18,04,000	53,41,000	705
CLAY LAYER 4	2.70	1.10	.48	10	80.2 (dry)	20,80,000	61,60,000	914
					112.8 (sat.)	16,70,000	49,55,000	691
BED ROCK			.40	42	145.0			6000
PILE			.15		150.0		4320,00,000	

as the stiffness of the linkage element was appropriate. The first few natural frequencies of the soil-pile systems in sand and clay for the various assumptions are given in Table 8-4.

TABLE 8-4

NATURAL FREQUENCIES OF SOIL-PILE SYSTEMS
(rad/sec)

MODE	PILE IN SAND		PILE IN CLAY	
	Linkage Element*	No Linkage	Linkage Element*	No Linkage
1	19.45	19.53	16.40	15.72
2	23.11	23.20	19.75	20.30
3	33.62	33.92	27.45	28.00
4	38.22	38.00	30.05	30.40
5	44.01	44.00	35.02	35.01
6	49.15	49.55	37.30	37.75
7	50.60	50.70	40.40	40.35
8	52.25	52.50	43.45	43.55

*Linkage element stiffness is 10^{10} lb/ft.

8-G GENERAL RESULTS

The response analysis of the soil-pile system during earthquakes has been determined using the program WAVAX, which computes the boundary accelerations and then uses the boundary acceleration coefficients in the various harmonics for the final response computations. The location of a pile at various epicentral distances and the corresponding values for the relative contributions of the shear and Rayleigh waves to the seismic motion have been considered. For comparison purposes, the pile in dry sand is considered for four specific cases:

(1) Pile at a location near the source - travelling wave solution; contribution of Rayleigh waves considered as 25% with the remaining contribution from the inclined propagation of shear waves.

(2) Pile at a location near the source - travelling wave solution; inclined propagation of shear waves.

(3) Pile at a distant location - travelling wave solution; vertical propagation of shear waves.

(4) Pile at a distant location - rigid base solution; assumption that all points on the boundary of the soil-pile system move simultaneously.

Three different earthquakes were used in this study:

(1) Olympia Earthquake, 1949;

(2) El Centro Earthquake, 1940;

(3) accelerograms from the Pacoima Dam site recorded during the San Fernando Earthquake, 1971. (There is some question about the accuracy of these particular records, but they are adopted here for comparison purposes.)

The Olympia Earthquake was considered as an example of a moderate shock while the El Centro Earthquake was severe. The accelerograms from the Pacoima Dam site during the San Fernando Earthquake referred to as the San Fernando Earthquake, showed that there was a severe shock. Therefore, these three earthquakes were considered to be representative of a range of ground shaking, and the responses of the pile cap have been chosen to facilitate comparisons of the pile's dynamic behaviour. Figure 8-4 shows the accelerations of the pile cap for the four cases during the San Fernando Earthquake. It was found that the rigid base solution gave an underestimate of the response. The maximum acceleration using the rigid base solution was 14.22 ft/sec^2 while the maximum accelerations using the travelling wave solution are 22.12, 20.65 and 18.30 ft/sec^2 respectively for cases 1, 2 and 3. The comparisons were similar for the other two earthquakes, and Table 8-5 shows the absolute maximum accelerations of the pile cap for the four cases during the three earthquakes. The absolute maximum acceleration at the base rock level, and also the absolute maximum acceleration at the surface above the dry sand layers at a distant are included in this table for comparison purposes. This data

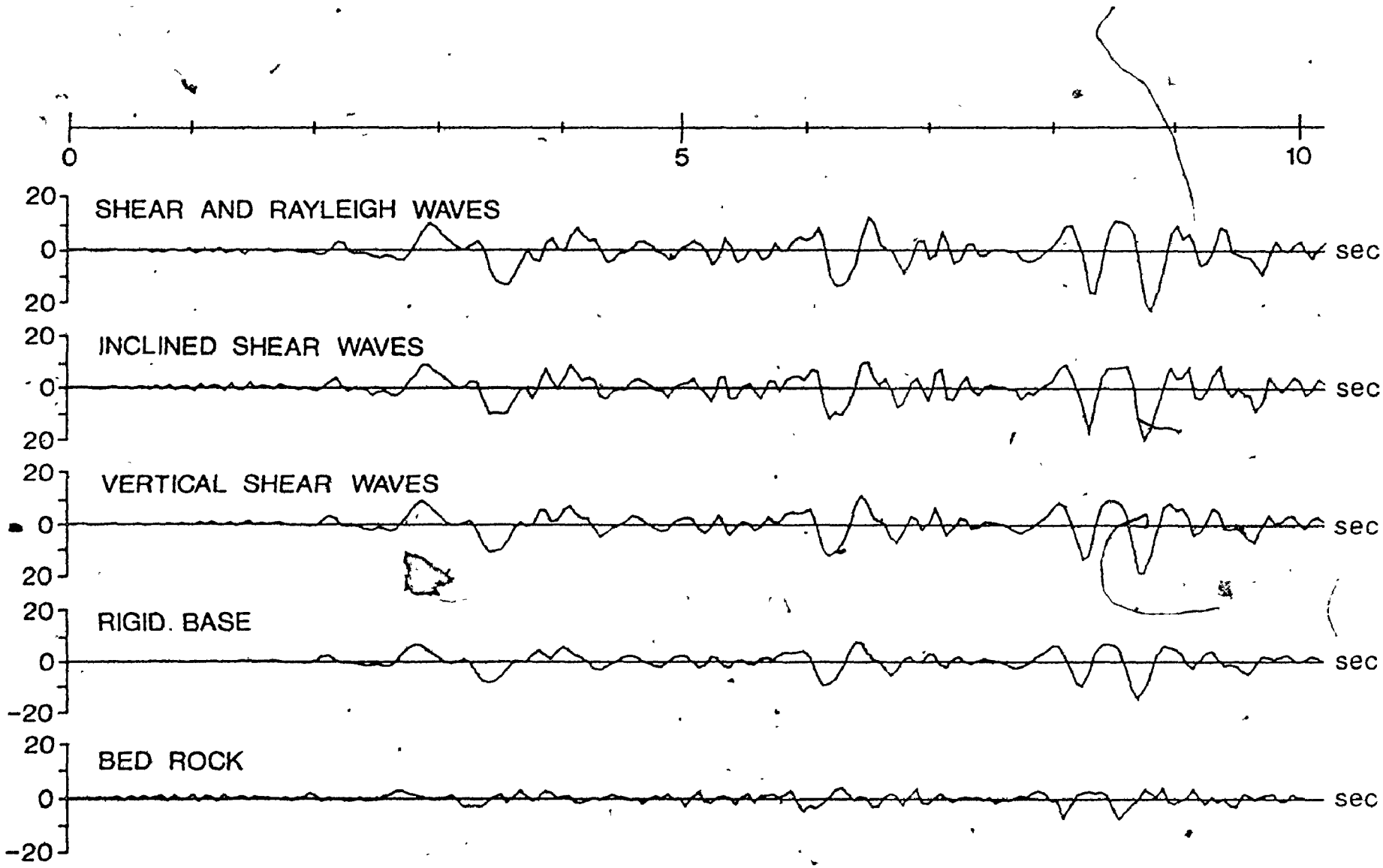

INPUT MOTION AT BED ROCK LEVEL
FIRST 10 SECONDS DURING THE SAN FERNANDO EARTHQUAKE

FIG. 8-4 COMPARISON OF RESPONSES OF CAP FOR PILE FOUNDED IN SAND UNDER DIFFERENT ASSUMPTIONS

TABLE 8-5

ABSOLUTE MAXIMUM ACCELERATIONS

OF THE PILE CAP, ft/sec^2

EARTHQUAKE	Case 1	Case 2	Case 3	Case 4	Base Rock	Surface at distant location (input)
Olympia, 1949	2.81	2.50	2.35	1.82	1.53	4.94
El Centro, 1940	5.53	5.09	4.47	3.42	3.11	10.17
San Fernando, 1971. (Pacoima Dam)	22.12	20.65	18.30	14.22	12.35	40.30

indicates the importance of adopting a travelling wave solution to estimate the response of the soil-pile system.

By comparing the responses of the pile cap for cases 1, 2 and 3 in Table 8-5, it can be seen that the responses of the pile cap increased as anticipated when the epicentral distance decreased. The increase was found to be of the order of 10-15% when inclined shear wave propagation alone was considered. When the contribution (25%) of Rayleigh waves was also accounted for, the increase at a relatively nearby site was 20-25% compared to those at the distant location. A comparison of the surface response at the distant location, and the corresponding response of the pile cap shows that the presence of the pile in dry sand reduces the responses; the responses of the cap were about 0.44 to 0.47 times the corresponding ground response.

Figure 8-5 shows the responses of the pile cap in the E-W, N-S and vertical directions at the nearby location during the San Fernando Earthquake, for case 1 which included Rayleigh waves. The corresponding responses for this site neglecting the contribution of Rayleigh waves (Case 2) are shown in Figure 8-6. As anticipated the vertical component is more prominent when the contribution of Rayleigh waves is accounted for. The 3-D responses of the pile cap at the distant site (Case 3) are given in Figure 8-7 and they show that the vertical component is insignificant.

The components $\ddot{u}_1$ and $\ddot{u}_2$ in the E-W and N-S directions have magnitudes of the same order, and for a section at $\theta = 45°$, the radial and circumferential accelerations are the greatest, being:

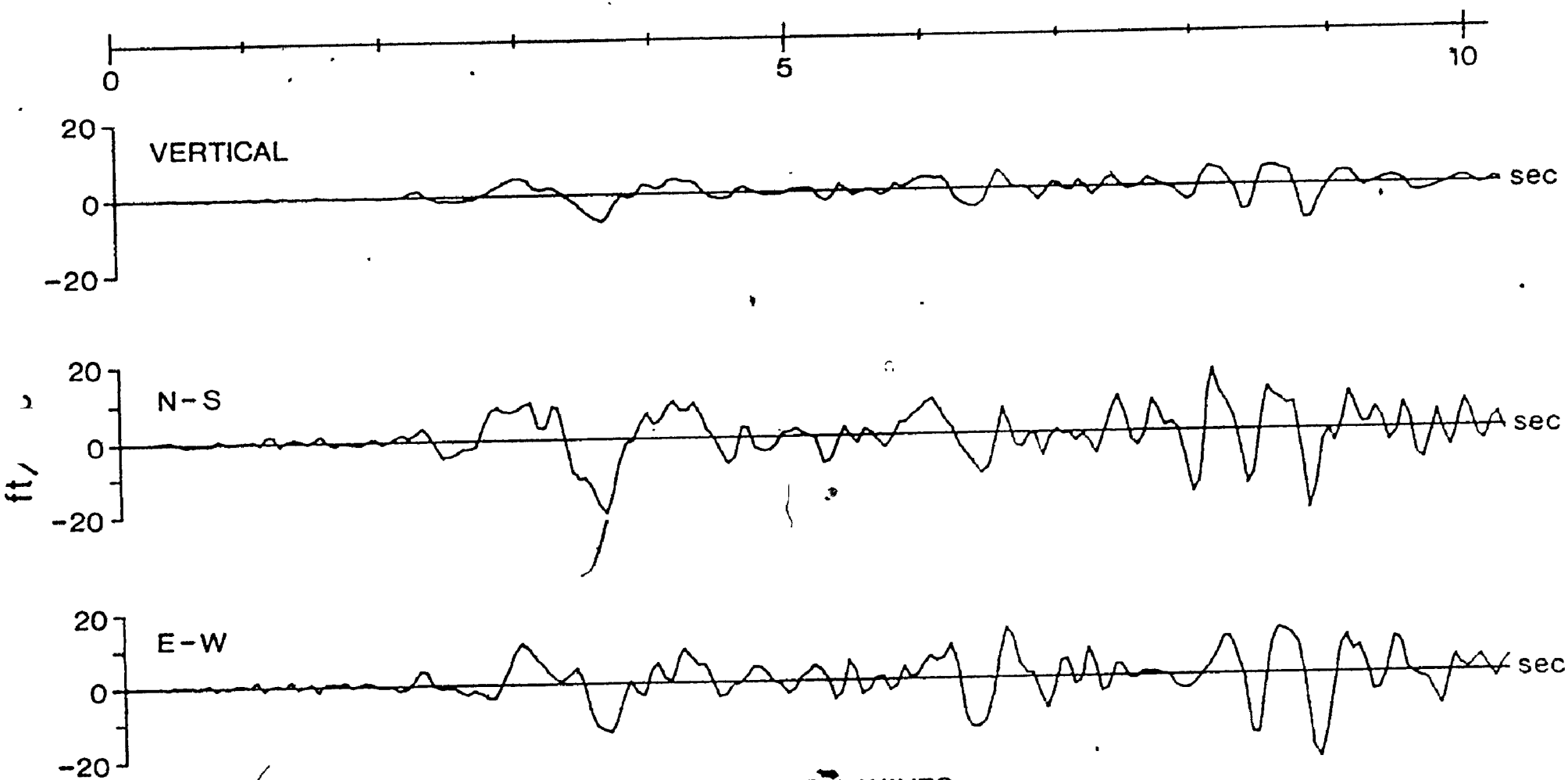

NEARBY SITE: SHEAR AND RAYLEIGH WAVES
INPUT MOTION AT BED ROCK LEVEL
FIRST 10 SECONDS DURING THE SAN FERNANDO EARTHQUAKE

FIG. 8-5 RESPONSES OF CAP FOR PILE FOUNDED IN DRY SAND AT NEAR SITE DUE TO RAYLEIGH WAVES AND INCLINED SHEAR WAVES

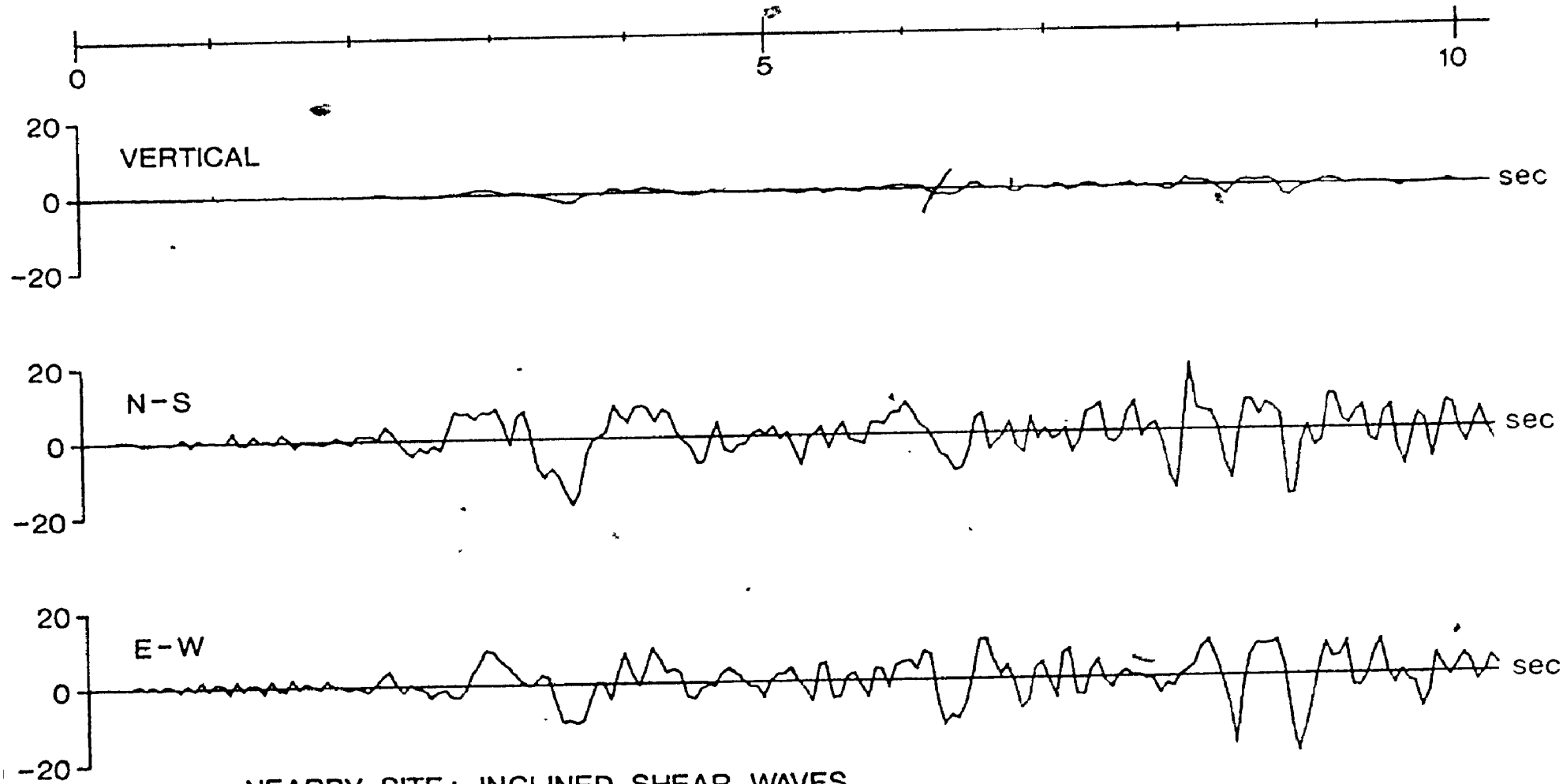

NEARBY SITE: INCLINED SHEAR WAVES
INPUT MOTION AT BED ROCK LEVEL
FIRST 10 SECONDS DURING THE SAN FERNANDO EARTHQUAKE

FIG. 8-6 RESPONSES OF CAP FOR PILE FOUNDED IN DRY SAND AT NEAR SITE DUE TO INCLINED SHEAR WAVES

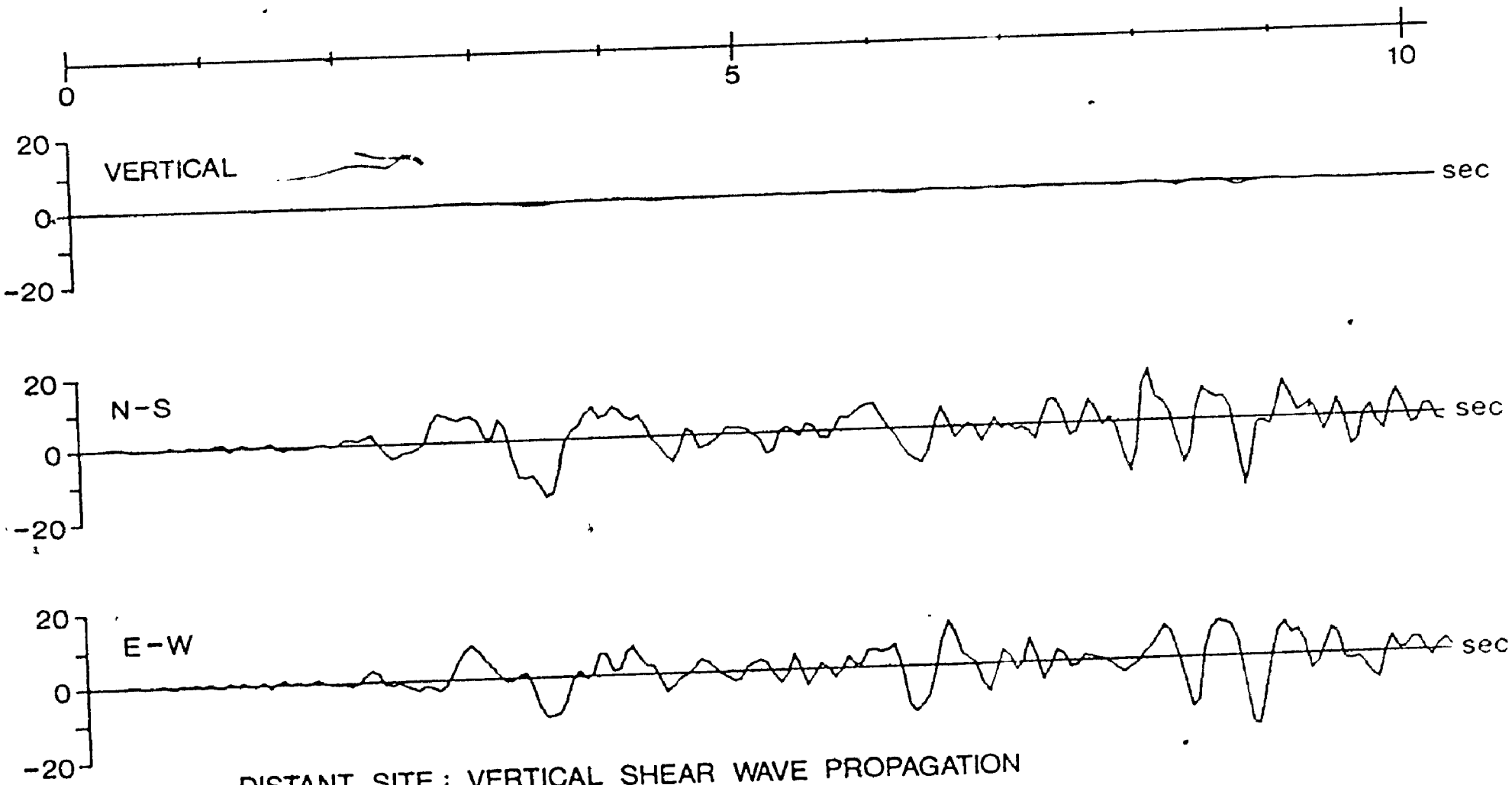

DISTANT SITE : VERTICAL SHEAR WAVE PROPAGATION
INPUT MOTION AT BED ROCK LEVEL
FIRST 10 SECONDS DURING THE SAN FERNANDO EARTHQUAKE

FIG. 8-7 RESPONSES OF CAP FOR PILE FOUNDED IN DRY SAND AT DISTANT SITE

$$\ddot{u}_r(t) = (\ddot{u}_1 + \ddot{u}_2) \frac{1}{\sqrt{2}}$$

$$\ddot{u}_\theta(t) = (\ddot{v}_1 + \ddot{v}_2) \frac{1}{\sqrt{2}} \qquad (8.17)$$

The stresses at the various nodes of the soil-pile system were determined and a general stress concentration was found at and underneath the tip of the pile. The highest stresses were found in areas near the pile tip and there was a general decrease in stresses with increasing radius. For example, the stress at node 6 was only about 1% of the corresponding stress at node 14. Figure 8-8 shows the variation of the principal stresses along two radii through nodes 6 and 1 respectively at a time of 6.31 seconds which corresponds to a peak during the San Fernando Earthquake.

In general, the stresses decreased with increased depth from ground level, and this could be attributed to the earthquake amplification due to soil layering. Figure 8-9 shows the variation in the principal stresses with depth along the vertical through node 1 at a time of 6.31 seconds during the San Fernando Earthquake. There was a decrease in the stresses in the vicinity of the surface as a result of less confining action.

8-G-1 Piles in Sand

When the ground water table rises and finally coincides with the ground level, the sand layers become saturated and as a result, the soil properties alter. The saturation always reduces the moduli and

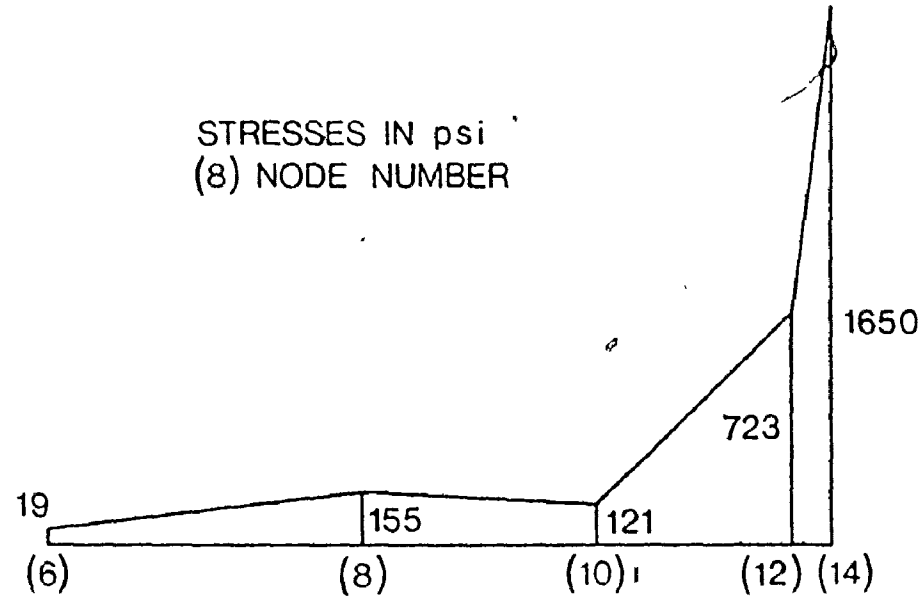

a. PRINCIPAL STRESSES ALONG RADIUS THROUGH NODE 6

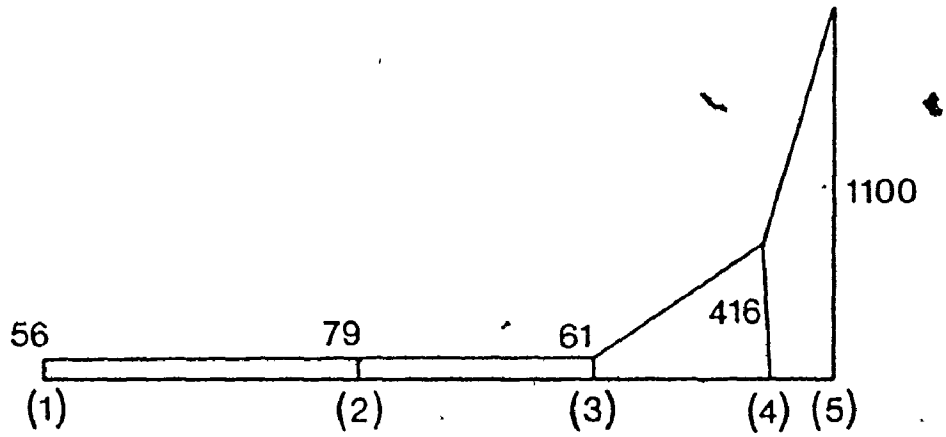

b. PRINCIPAL STRESSES ALONG RADIUS THROUGH NODE 1

FIG. 8-8 VARIATION OF PRINCIPAL STRESSES ALONG RADII (Stresses correspond to a time of 6.31 seconds during san fernando earthquake (pacoima dam), 1971

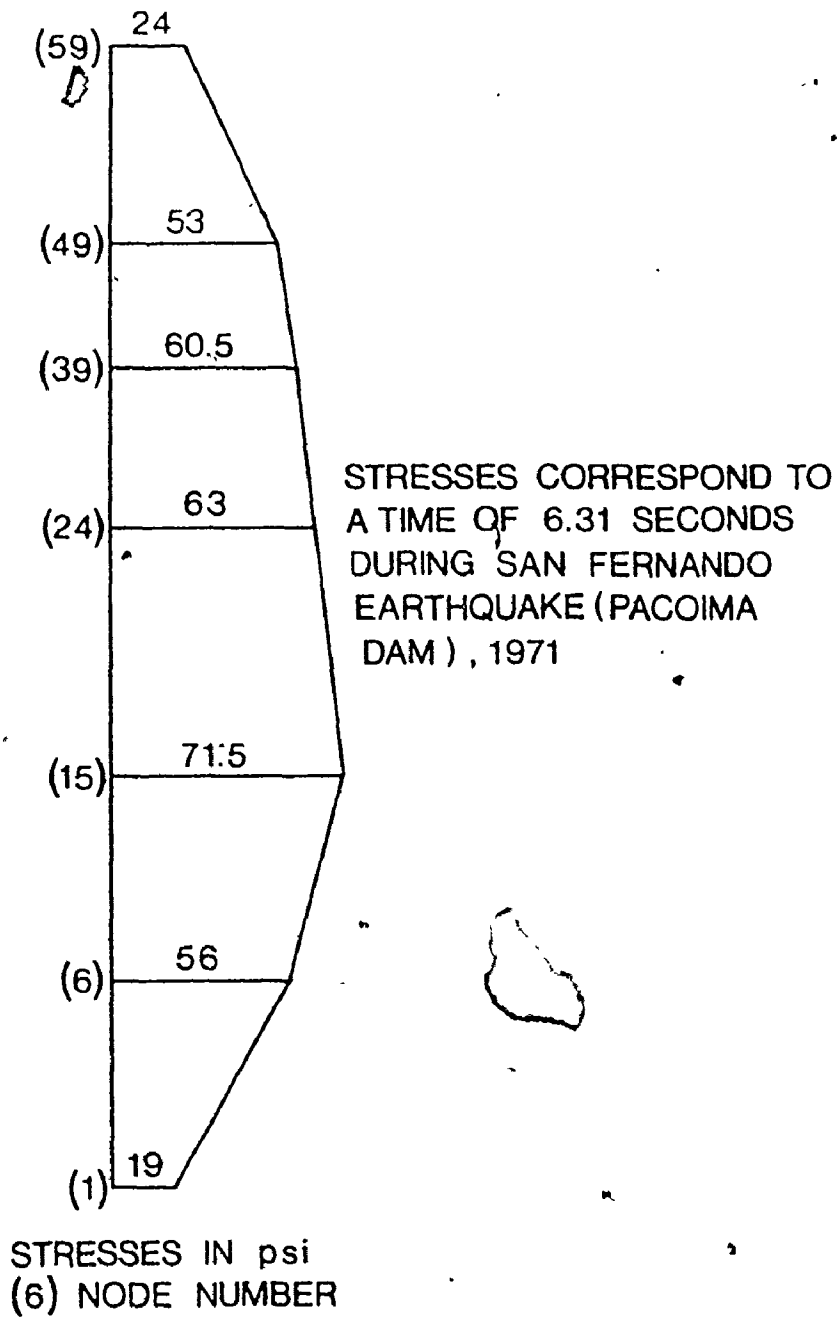

FIG. 8-9 VARIATION OF PRINCIPAL STRESSES ALONG VERTICAL THROUGH NODE 1

the shear wave velocities in the soils, and the impedance factors which are important parameters alter. Figure 8-10 shows the responses of the pile cap for the pile in saturated sand during the San Fernando Earthquake. The saturation of sands around and underneath the pile increases the responses of the system. For the pile in sand under consideration, the increase worked out to be of the order of 25%.

The pore pressures were computed assuming that no volume change occured in the sand during the earthquake. This is considered a reasonable assumption because of the sudden nature of most seismic excitation. High pore pressures developed and these were largest underneath the pile; the pore pressures in elements 3, 4, 7, 8, 11 and 12 were the highest, and correspondingly nodes 5, 14 and 23 were locations of pore pressure concentration. There was a steady increase in pore pressure with time, and the decrease in the ratio of the effective principal stress to the pore pressure was taken as a guide for studying the liquefaction potential of the sand. The value at node 5 reduced from 0.396 at the beginning to zero at a time of 9.31 seconds during the San Fernando Earthquake. This behavior is shown in Figure 8-11 and indicates that the saturated sand liquefied during this earthquake [77]. Similar liquefaction effects on saturated sands have been reported during strong motion earthquakes [2, 79, 84]. During the Alaskan Earthquake [84] there was considerable damage to pile systems such as bridge supports due to the liquefaction of sands. Heavy damage also occured to pile-sand systems, with piles 15 to 60 ft long, as a result of sand liquefaction during the Niigata Earthquake [79]. The liquefaction of loose deposits has caused foundation failures during many strong motion earth-

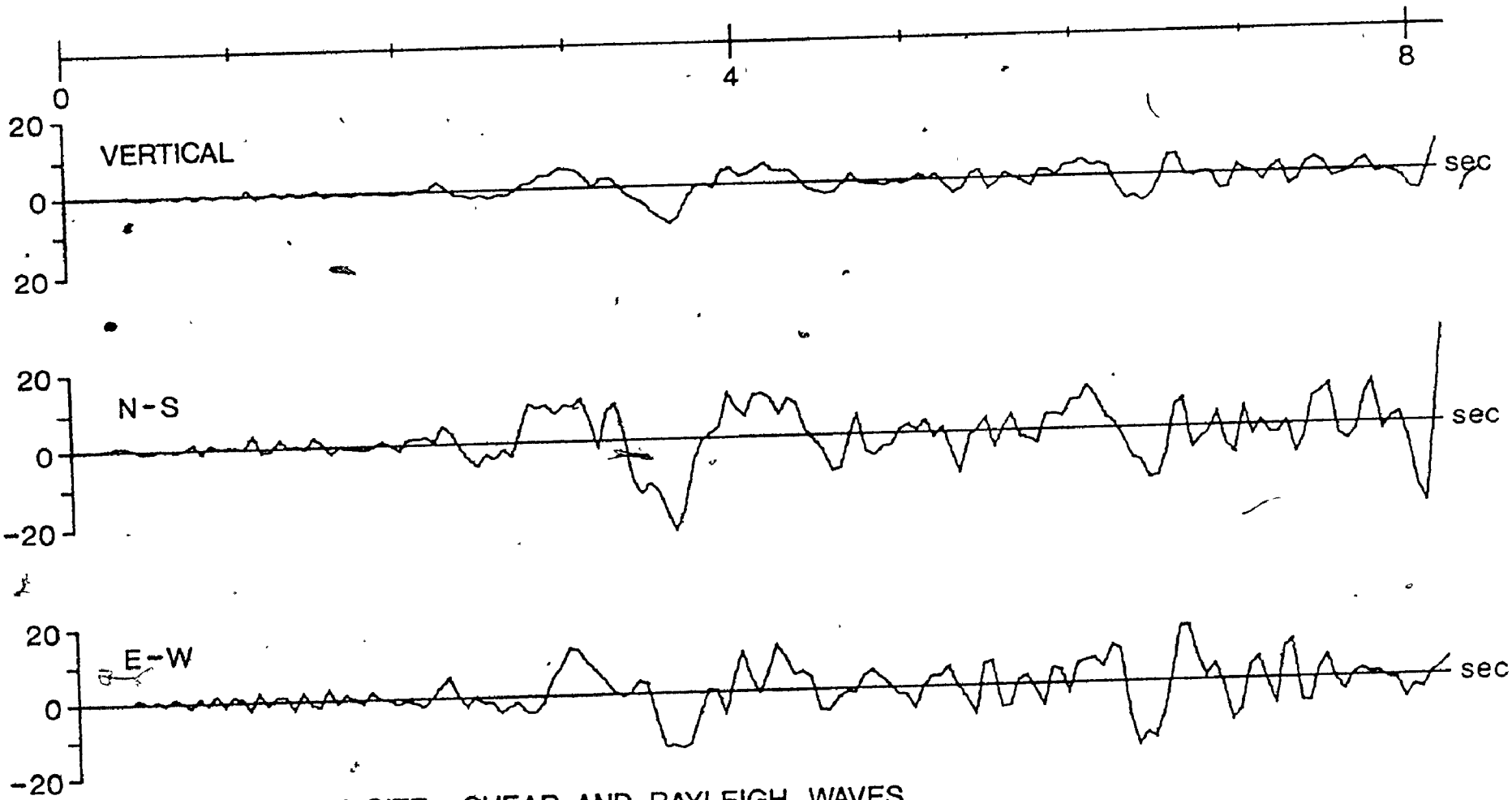

NEARBY SITE: SHEAR AND RAYLEIGH WAVES
INPUT MOTION AT BED ROCK LEVEL
FIRST 8 SECONDS DURING THE SAN FERNANDO EARTHQUAKE

FIG. 8-10 RESPONSES OF CAP FOR PILE FOUNDED IN SATURATED SAND

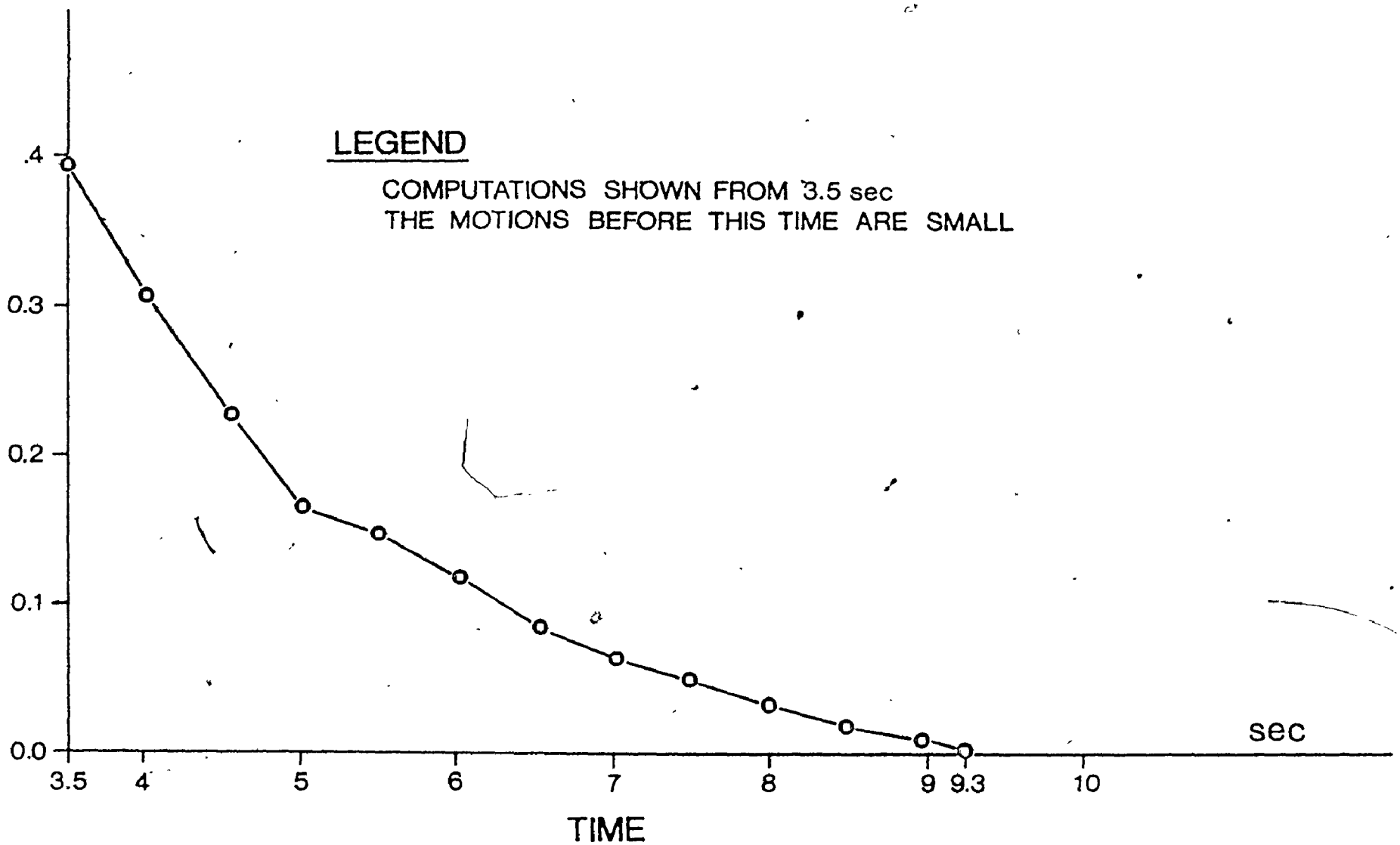

FIG. 8-11 DECREASE IN THE RATIO OF EFFECTIVE PRINCIPAL STRESS TO PORE PRESSURE WITH TIME IN SATURATED SANDS UNDERNEATH A CONCRETE PILE, SAN FERNANDO EARTHQUAKE 1971

8-G-2 Piles in Clay

For the soil-pile system in dry clay at a nearby site, the responses of the pile cap are shown in Figure 8-12, while the corresponding responses when the clay is saturated are given by Figure 8-13. As in the case of sands, the saturation resulted in a decrease of the shear wave velocities in the clay layers. However, it was found that as a result of saturation, there was a reduction in the response amplification and thus saturation proved beneficial to the system. In the case of the soil-pile system under consideration, the decrease in the responses due to saturation was of the order of 30%. There was a general tendency for the development of higher stresses around and underneath the pile. The pore pressures developed in the clay layers were not significant.

8-H DISCUSSION

The seismic response of a structure depends upon the motions of the ground on which it rests. If a structure is supported on piles, then the exciting forces transmitted to the structure are the responses of the piles. The existence of piles reduced these input motions to the structure irrespective of the type of the soil and decreased the predominant frequency of the input motions. The motions of shorter periods on the ground scarcely appeared in the motions on the pile cap, which vibrated with a longer period. This period was found to be the predominant period of the soil-pile system. For the systems in clays as well as those in sands, the presence of a pile had beneficial effects. The piles in sand showed the responses to be about 0.4-0.5 of the

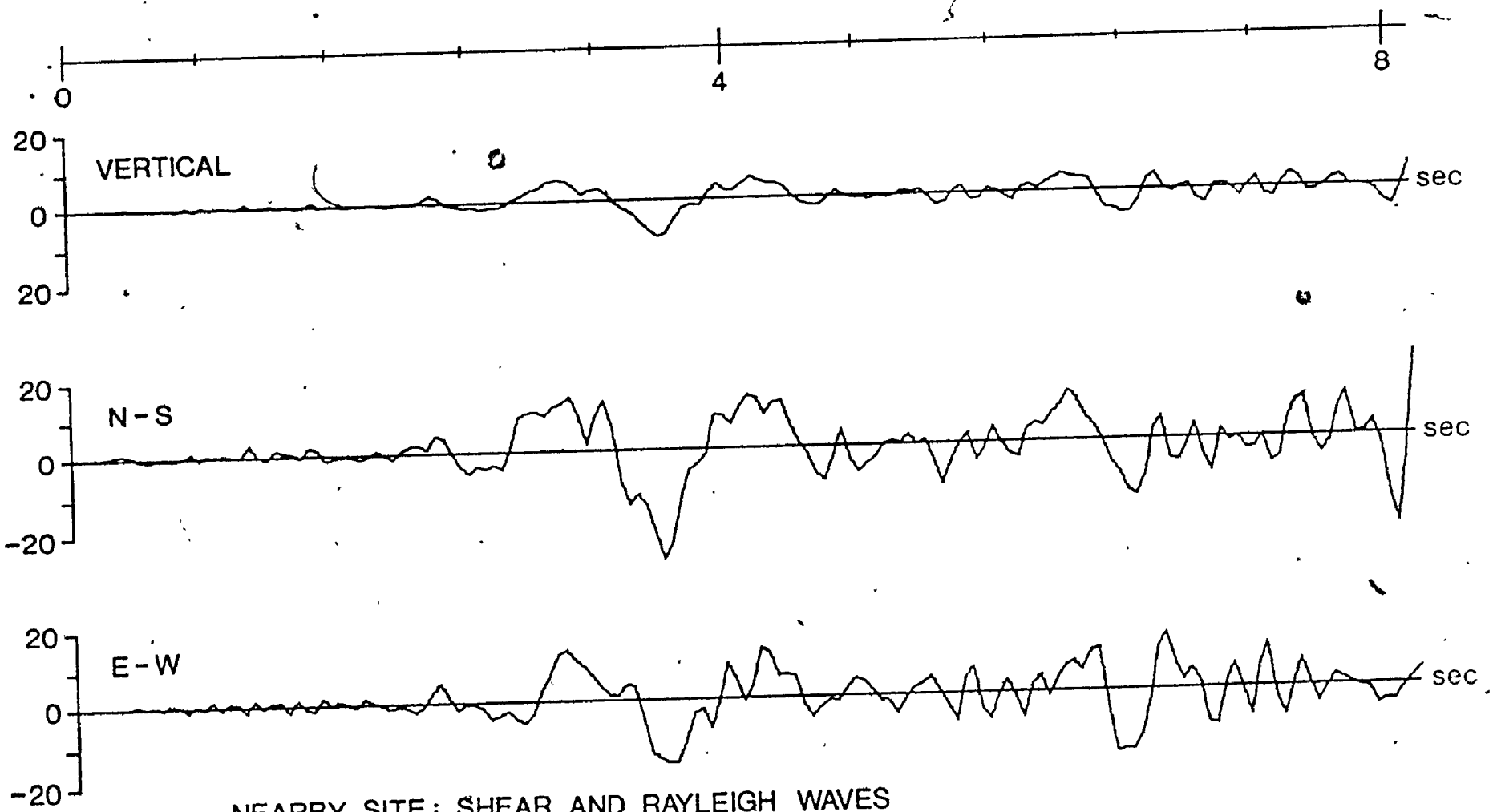

NEARBY SITE: SHEAR AND RAYLEIGH WAVES
INPUT MOTION AT BED ROCK LEVEL
FIRST 8 SECONDS DURING THE SAN FERNANDO EARTHQUAKE

FIG. 8-12 RESPONSES OF CAP FOR PILE FOUNDED IN DRY CLAY

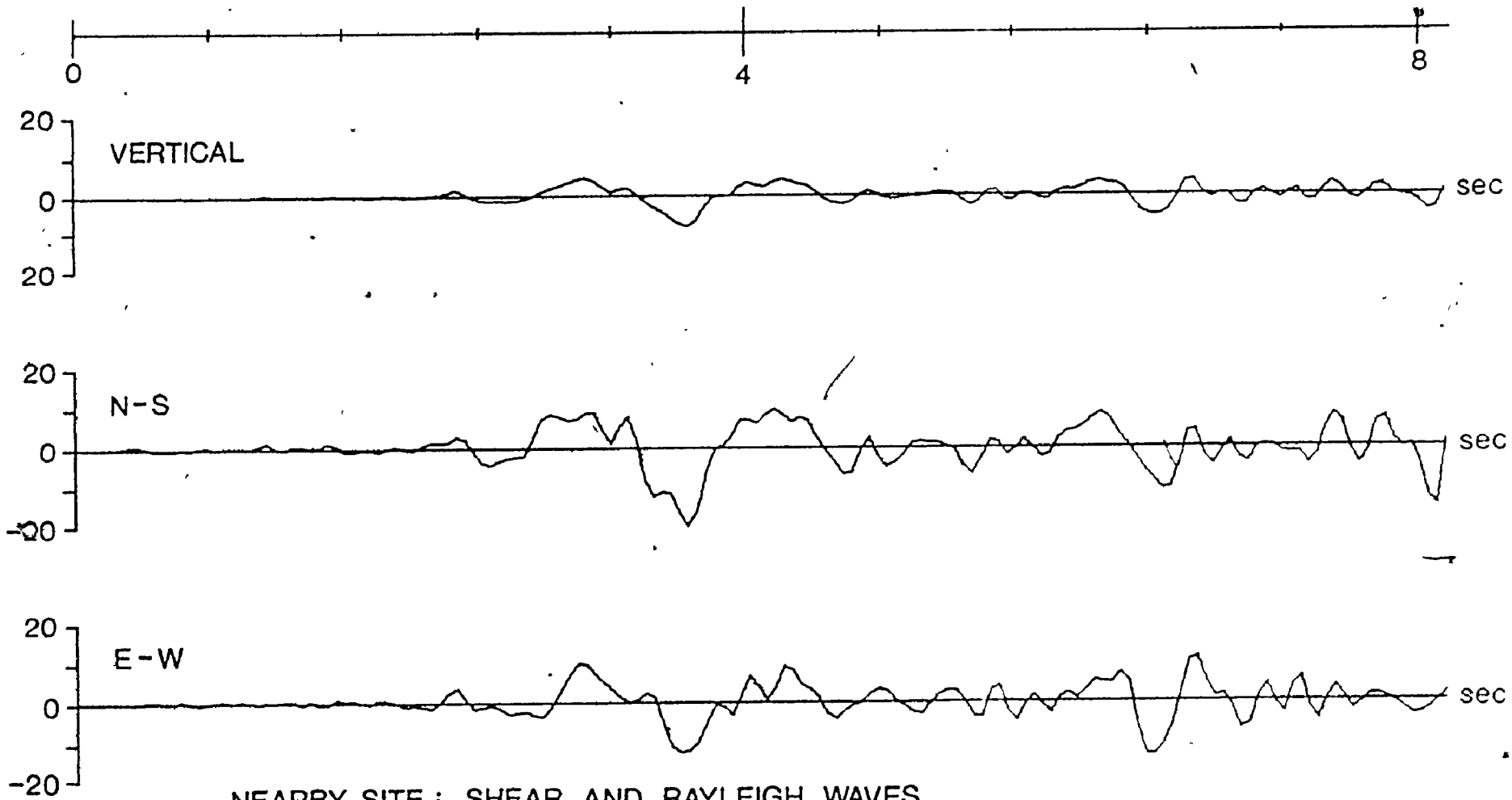

NEARBY SITE : SHEAR AND RAYLEIGH WAVES
INPUT MOTION AT BASE ROCK LEVEL
FIRST 8 SECONDS DURING THE SAN FERNANDO EARTHQUAKE

FIG. 8-13 RESPONSES OF CAP FOR PILE FOUNDED IN SATURATED CLAY

corresponding ground responses had there been no pile. The value varied from 0.38-0.55 in the case of a pile in clay. It may be generalized that the presence of piles roughly halved the input responses to the structure.

An important feature was the effect of saturation on different types of soils. In locations where the soils were predominantly clays, the rise in the ground water table had a beneficial effect on the responses. Further, high pore pressures did not build up in the clay layers. On the other hand, saturation was found to have a damaging effect in the case of sands; resulting in an increase in the responses of the system. High pore pressures developed around and underneath the pile resulting in liquefaction of the sands. These results are in general agreement with the damage reports available from various earthquakes [2,52,79,84].

CHAPTER IX

CONCLUSIONS

In the computation of the seismic response of structures, the effects of travelling seismic waves are usually accounted for by assuming that the earthquake energy is only carried by vertically propagating shear waves, or that the structure rests on a rigid, uniform base. A survey of field observations and computations by geophysicists shows that the direction of wave propagation is inclined for most sites where seismic effects are significant. Many strong motion records for near sites reveal that a part of these motions is associated with surface waves. For this reason, the spatial variations in seismic motions were studied taking into account the inclined propagation of shear waves and the presence of Rayleigh waves which are the most important surface waves. Certain assumptions were made with regard to the relative contributions of these waves, the angle of incidence, the decomposition of waves at soil interfaces and the time lags in motions for various site distances. The inclined shear wave propagation was accounted for by extending the method of multiple reflections and refractions. The Rayleigh wave amplification was considered in the frequency domain by assuming that these waves are uniformly spread in the anticipated range of phase velocities. It is possible to furnish the seismic motion records in the three directions for any point, defined by its spatial coordinates. As a first step the earthquake amplification due to soil layering was com-

puted, and it was found to be greater in magnitude than when vertical propagation of shear waves is assumed.

The response of various pile-soil systems to travelling seismic waves was determined by finding the absolute accelerations at their boundaries and then making use of these boundary responses in the full finite element dynamic analysis assuming that the soil behaves linearly. This is a rather complicated problem because of the nonsymmetric nature of the loading. However, it was possible to accomplish this by considering the spatial variations as a set of loadings in different harmonics.

These results indicated that the rigid boundary solution, assuming that the boundary accelerations of the system and base motions were equal, gave an underestimate of the responses. The travelling wave solutions showed an increase of about thirty percent for distant sites, while the increase was of the order of fifty percent for nearby sites, where the relative contributions of Rayleigh waves and shear waves were considered.

As anticipated from field observations, the construction of structures on piles was found to have a beneficial effect during earthquakes. The responses transferred through the pile to the structure were roughly half of those transferred through the soil in the absence of a pile. The information gained from the single pile studies is invaluable for understanding the behaviour of more complicated systems such as groups of piles and structures resting on them.

The effect of saturated sands and cohesive soils on pile-soil was and it was found that liquefaction of saturated

sands surrounding a pile during earthquakes is a critical problem. The saturated clays did not show a similar liquefaction tendency. These results are in close agreement with field observations.

Four major areas in which the present research could be extended are:

1) Computation of earthquake acceleration records at the foundation locations of structures with large lateral extent. These structures will have significant spatial variations in their input accelerations, particularly when they are supported on independent footings or flexible foundations. It is anticipated that the response of such structures to these accelerations will indicate the importance of spatial variations in seismic motions.
2) Expand the method of analysis to include nonlinear material behaviour, particularly for the soils.
3) Apply the solution technique to examine the response behaviour of pile groups. This will require a large and efficient computer.
4) There are many additional problems involving soil-structure systems in which the methods can be utilized. For instance, it is possible to consider large axisymmetric structures such as smoke stacks, reactor pressure vessels and towers, with their foundations and surrounding soil, for complicated static and dy-

namic loading conditions.

While the methods and solutions in this work are somewhat idealized, particularly with regard to the assumption of linear elastic soils, it is believed that they provide a clear understanding of the behaviour of soil-structure systems during earthquakes.

BIBLIOGRAPHY

1. Alpan, I., "The Dynamic Response of Pile Foundations to Lateral Forces", *Proceedings of the Fifth World Conference on Eathquake Engineering*, Rome, 1973, Preprint No. 229.

2. Ambraseys, N. and Sarma, S., "Liquefaction of Soils Induced by Earthquakes", *Bulletin of the Seismological Society of America*, Vol. 59, No. 2, April, 1969, pp 651-664.

3. Archer, J.S., "Consistent Mass Matrix for Distributed Mass Systems", *Journal of the Structural Division*, ASCE, Vol. 89, No. ST4, Proc. Paper 3591, August 1963, pp 161-178.

4. Awoshika, K. and Reese, L.C., "Analysis of Foundation with Widely Spaced Battered Piles", *Center of Highway Research Report No. 117-3F*, The University of Texas, Austin, 1971.

5. Biot, M.A., "Theory of Propagation of Elastic Waves in a Fluid-Saturated Porous Solid", *Journal of the Acoustical Society of America*, Vol. 28, March 1956, pp 168-191.

6. Bishplinghoff, R.L., Ashley, H. and Halfman, R.L., *Aeroelasticity*, Addison-Wesley Publishing Company, Inc., Cambridge, Massachusetts, 1955.

7. Carneiro, F.L.L.B. and Barcellos, A., "Concrete Tensile Strength", Bulletin 13, *RILEM*, Paris, March, 1953, pp 97-123.

8. Chandra, U., "Angles of Incidence of S Waves", *Bulletin of the Seismplogical Society of America*, Vol. 62, No. 4, August 1972, pp 903-915.

9. Chopra, A.K., Dibaj, M., Clough, R.W., Penzien, J. and Seed, H.B., "Earthquake Analysis of Earth Dams", *Proceedings of the Fourth World Conference on Earthquake Engineering*, Santiago, Vol. 3, A-5, 1969, pp 55-72.

10. Christian, J.T., "Two-Dimensional Analysis of Stress and Strain in Soils", *Report No. I*, Report to U.S. Army Engineer Waterways Experiment Station, Vicksburg, Mississippi, 1965.

11. Christian, J.T., "Undrained Stress Distribution by Numerical Methods", *Journal of the Soil Mechanics and Foundations Division*, ASCE, Vol. 94, No. SM6, Proc. Paper 6243, November 1968, pp 1333-1345.

12. Christian, J.T. and Boehmer, J.W., "Plane Strain Consolidation by Finite Elements", *Journal of the Soil Mechanics and Foundation Division*, ASCE, Vol. 96, No. SM4, Proc. Paper 7437, July 1970, pp 1435-1457.

13. Clough, R.W., "Analysis of Structural Vibrations and Dynamic Response", *Recent Advances in Matrix Methods of Structural Analysis and Design*, University of Alabama Press, Huntsville, 1971, pp 441-486.

14. Clough, R.W. and Chopra, A.K., "Earthquake Stress Analysis in Earth Dams", *Journal of the Engineering Mechanics Division*, ASCE, Vol. 92, Proc. Paper 4793, No. EM2, April 1966, pp 197-211.

15. Clough, R.W. and Rashid, Y., "Finite Element Analysis of Axisymmetric Solids", *Journal of the Engineering Mechanics Division*, ASCE, Vol. 91, No. EM1, Proc. Paper 4229, February 1965, pp 71-85.

16. Desai, C.S. and Abel, J.F., *Introduction to the Finite Element Method*, Van Nostrand Reinhold Company, New York, 1972.

17. Dezfulian, H. and Seed, H.B., "Response of Non-uniform Soil Deposits to Travelling Seismic Waves", *Journal of the Soil Mechanics and Foundation Division*, ASCE, Vol. 97, Proc. Paper 7808, No. SM1, January 1971, pp 27-46.

18. Dibaj, M. and Penzien, J., "Response of Earth Dams to Travelling Seismic Waves", *Journal of the Soil Mechanics and Foundation Division*, ASCE, Vol. 95, No. SM2, Proc. Paper 6453, March 1969, pp 541-560.

19. *Earthquake Resistant Regulations*, A World List, Uniform Building Code 1970, Section 2314, pp 393-403.

20. Ellison, R.D., "An Analytical Study of the Mechanics of Single Pile Foundations", *Ph.D. Thesis*, Carnegie-Mellon University, Pittsburgh, December 1968.

21. Ellison, R.D., D'Appolonia, E. and Thiers, G.R., "Load-Deformation Mechanism for Bored Piles", *Journal of the Soil Mechanics and Foundation Division*, ASCE, Vol. 97, No. SM4, Proc. Paper 8052, April 1971, pp 661-678.

22. Ewing, W.M., Jardetzky, W.S. and Press, F., *Elastic Waves in Layered Media*, McGraw-Hill Book Company, Inc., New York, 1957.

23. Faddeev, D.K. and Faddeva, V.N., *Computational Methods of Linear Algebra*, W.H. Freeman and Company, San Francisco, 1963.

24. Felippa, C.A., "Refined Finite Element Analysis of Linear and Non-Linear Two-Dimensional Structures", *SMRR No. 66-22*, University of California, Berkeley, October 1966.

25. Finn, W.D.L., Emery, J.J. and Reimer, R.B., "The Effect of Foundation Soils on Seismic Response of Structures", *Proceedings of the First Canadian Conference on Earthquake Engineering*, Vancouver, 1971, pp 128-141.

26. Finn, W.D.L., Miller, R.I.S. and Emery, J.J., "Seismic Interaction Between Foundations and Structures", *Proceedings of the Third South East Asian Conference on Soil Engineering*, Hong Kong, November 1972, pp 273-280.

27. Finn, W.D.L. and Reimer, R.B., "Effect of Soil Structure Interaction on Seismic Response", *Proceedings of the Third European Symposium on Earthquake Engineering*, Sofia, 1970, pp 243-251.

28. Fleming, J.F., Screwvala, F.N. and Kondner, R.L., "Foundation Superstructure Interaction Under Earthquake Motion", *Proceedings of the Third World Conference on Earthquake Engineering*, New Zealand, 1965, Vol. 1, pp 22.

29. Frocht, M.M., *Photoelasticity*, Vol. 2, John Wiley and Sons, New York, 1948.

30. Gibbs, H.J. and Holtz, W.G., "Research on Determining the Density of Sands by Spoon Penetration Testing". *Proceedings of 4th International Conference on Soil Mechanics and Foundation Engineering*, London, Vol. 1, 1957, pp 35-39.

31. Gibson, R.E., "Some Results Concerning Displacement and Stresses in a Non-homogeneous Elastic Half-Space", *Geotechnique*, Vol. 17, 1967, pp 58-67.

32. Goodman, R.E., Taylor, R. and Brekke, T.L., "A Model for the Mechanics of Jointed Rock", *Journal of Soil Mechanics and Foundations Division*, ASCE, Vol. 94, No. SM3, Proc. Paper 5937, May 1968, pp 637-659.

33. Gutenberg, B., "Effects of Ground on Earthquake Motion", *Bulletin of the Seismological Society of America*, Vol. 47, No. 3, July 1957, pp 221-251.

34. Hardin, B.O. and Drnevich, V.P., "Shear Modulus and Damping in Soils: Measurement and Parameter Effects", *Journal of the Soil Mechanics and Foundations Division*, ASCE, Vol. 98, No. SM6, Proc. Paper 8977, June 1972, pp 603-624.

35. Hardin, B.O. and Drnevich, V.P., "Shear Modulus and Damping in Soils: Design Equations and Curves", *Journal of the Soil Mechanics and Foundations Division*, ASCE, Vol. 98, No. SM7, Proc. Paper 9006, July 1972, pp 667-692.

36. Harr, M.E., *Foundation of Theoretical Soil Mechanics*, McGraw-Hill Book Company, Inc., New York.

37. Haskell, N.A., "The Dispersion of Surface Waves on Multilayered Media", *Bulletin of the Seismological Society of America*, Vol. 43, No. 1, January 1953, pp 17-34.

38. Herrin, E., et al, "1968 Seismological Tables for P Waves", *Bulletin of the Seismological Society of America*, Vol. 58, No. 4, August 1968, pp 1193-1241.

39. Herrmann, L.R., "Elasticity Equations for Incompressible and Nearly Incompressible Materials by a Variational Theorem", *AIAA Journal*, Vol. 3, No. 10, December 1965, pp 1896-1900.

40. Heslop, W.G., "Some Theoretical Aspects of the Split Cylinder Tension Test for Concrete", *Internal Report*, Department of Civil Engineering, University of British Columbia, Vancouver, 1969.

41. Housner, G.W., "Behaviour of Structures During Earthquakes", *Journal of the Engineering Mechanics Division*, ASCE, Vol. 85, No. EM4, Proc. Paper 2220, October 1959, pp 109-129.

42. Housner, G.W., "Intensity of Earthquake Ground Shaking Near the Causative Fault", *Proceedings of the Third World Conference on Earthquake Engineering*, New Zealand, 1965, Vol. 3, pp 94-115.

43. Hudson, D.E., "Strong Motion Records from the San Fernando Earthquakes", *Report No. EERL 71-02*, "Engineering Features of the San Fernando Earthquake", P.C. Jennings, ed., Earthquake Engineering Research Laboratory, June 1971.

44. Hurty, W.C. and Rubinstein, M.F., *Dynamics of Structures*, Prentice-Hall, Inc., Englewood Cliffs, N.J., 1964.

45. Idriss, I.M., "Finite Element Analysis for the Seismic Response of Earth Dams", *Journal of the Soil Mechanics and Foundations Division*, ASCE, Vol. 94, No. SM3, Proc. Paper 5929, May 1968, pp 617-636.

46. Idriss, I.M. and Seed, H.B., "An Analysis of Ground Motions During the 1957 San Francisco Earthquake", *Bulletin of the Seismological Society of America*, Vol. 58, No.6, December 1968, pp 2013-2032.

47. Idriss, I.M., Seed, H.B. and Dezfulian, H., "Influence of Geometry and Material Properties on the Seismic Response of Soil Deposits", *Proceedings of the Fourth World Conference on Earthquake Engineering, Santiago, Chile*, Vol. 1, Session A2, 1969, pp 53-67.

48. Irons, B.M., Comment on "Stiffness Matrices for Sector Element", by I.R. Raju and A.K. Rao, *AIAA Journal*, Vol.7, 1969, pp 156-157.

49. Isenberg, J., Lee, Li-Chih and Agbabian, M.C., "Response of Structures to Combined Blast Effects", *Transportation Engineering Journal*, ASCE, Vol. 99, No. TE4, Proc. Paper 10166, November 1973, pp 887-908.

50 Kanai, K., "Some New Problems of Seismic Vibration of Structure", *Proceedings of the 3rd World Conference on Earthquake Engineering*, New Zealand, Vol. II, 1965, pp 260-275.

51. Kawamata, S. and Shioya, S., "Application of Finite Element Method to Non-Symmetric Problems of Solids of Revolution", *Recent Researches of Structural Mechanics*, Uno Shoten, Tokyo, 1968, pp 159-174.

52. Kishida, H., "Characteristics of Liquefied Sands During Mino-Owari, Tohnakai and Fukui Earthquakes", *Soils and Foundations*, Vol. 9, No. 1, 1969.

53. Kobayashi, H. and Kagami, H., "A Method for Local Seismic Intensity Zoning Maps", *Proceedings of the International Conference on Microzonation for Safer Construction Research and Application*, Vol. 2, Seattle, Washington, October - November 1972, pp 513-528.

54. Lambe, T. and Whitman, R.V., *Soil Mechanics*, John Wiley and Sons, New York, 1969.

55. McCamy, K., Meyer, R.P. and Smith, T.J., "Generally Applicable Solutions of Zoeppritz' Amplitude Equations", *Bulletin of the Seismological Society of America*, Vol. 52, No.4, October 1962, pp 923-955.

56. Melin, J.W., "Numerical Integration by the Beta Method", *Proceedings*, ASCE Conference on Electronic Computation, Kansas City, November 1958.

57. Meyerhof, G.G., "Formula for Standard Penetration Blow Count vs Relative Density", *Proceedings of the 4th International Conference on Soil Mechanics and Foundation Engineering*, Vol. 3, 1957, pp 110.

58. Miller, I., Radomske, B. and Bird, C., "Solution of the Eigenproblem AX = λBX", *Internal Report*, Department of Civil Engineering Computing Center, The University of British Columbia, Vancouver, 1973.

59. *National Building Code of Canada*, 1970, Part 4, Subsection 4.1.7.

60. Newmark, N.M., "A Method of Computation for Structural Dynamics", *Journal of the Engineering Mechanics Division*, ASCE, Vol. 85, No. EM3, Proc. Paper 2094, July 1959, pp 67-94.

61. Newmark, N.M. and Rosenbleuth, E., *Fundamentals of Earthquake Engineering*, Prentice-Hall, Inc., Englewood Cliffs, N.J., 1971.

62. Nickell, R.E., "A Survey of Direct Integration Methods in Structural Dynamics", Brown University, Providence, R.I.

63. Ohsaki, Y. and Iwasaki, R., "On Dynamic Shear Moduli and Poisson's Ratios of Soil Deposits", *Soils and Foundations*, Vol. 13, No. 4, December 1973, pp 61-73.

64. Okamoto, S., *Introduction to Earthquake Engineering*, John Wiley & Sons, Inc., New York, 1973.

65. Oliver, J. and Ewing, M., "Higher Modes of Continental Rayleigh Waves", *Bulletin of the Seismological Society of America*, Vol. 47, No. 3, July, 1957, pp 187-203.

66. Parmalee, R.A., "Building Foundation Interaction Effects", *Journal of the Engineering Mechanics Division*, ASCE, Vol. 93, No. EM2, Proc. Paper 5200, April 1967, pp 131-152.

67. Parmalee, R.A., et al, "Seismic Effects of Structures Supported on Piles Extending Through Deep Sensitive Clays", *Report No. 92*, Report to the California State Division of Highways, August 1964.

68. Penzien, J., "Elasto-Plastic Response of Idealized Multi-story Structures Subjected to Strong Motion Earthquakes", *Proceedings of the 2nd World Conference on Earthquake Engineering*, Tokyo, 1960, Vol. 2, pp 739-760.

69. Pho, H.T. and Behe, L., "Extended Distances and Angles of Incidence of P Waves", *Bulletin of the Seismological Society of* Vol. 62, No. 4, August 1972, pp 885-902.

70. Pichumani, R. and D'Appolonia, E., "Theoretical Distribution of Loads Among the Piles in a Group", *Proceedings of the Third Pan American Conference on Soil Mechanics and Foundation Engineering*, Venezuela, July 1967.

71. Pipes, L.A. and Harvill, L.R., *Applied Mathematics for Engineers and Physicists*, McGraw-Hill Book Company, Inc., New York, N.Y., 1970.

72. Rainer, J.H., "Method of Analysis of Structure-Ground Interaction in Earthquakes", Division of Building Research, National Research Council of Canada, *Technical Paper No. 340*, Ottawa, April 1971.

73. Randall, M.J., "A Revised Travel Time Table for S", *Geophysical Journal*, No. 22, 1971, pp 229-234.

74. Lord Rayleigh, "On Waves Propagated Along the Plane Surface of an Elastic Solid", *Proceedings* 17, London Mathematical Society, pp 4-11.

75. Richart, F.E., Woods, R.D. and Hall, J.R., *Vibrations of Soils and Foundations*, Prentice-Hall, Inc., Englewood Cliffs, N.J., 1970.

76. Scavuzzo, R.J., Bailey, J.L. and Raftopoulos, D.D., "Lateral Structure Interaction with Seismic Waves", *Journal of Applied Mechanics*, Vol. 38, No. 1, March 1971, pp 125-134.

77. Scott, R.F., "San Fernando Earthquake, 9 February 1971 Preliminary Soil Engineering Report", *Report No. EERL 71-02*, "Engineering Features of the San Fernando Earthquake", C.C. Jennings, ed., Earthquake Engineering Research Laboratory, June 1971.

78. Seed, H.B., "The Influence of Local Soil Conditions on Earthquake Damage", *Soil Dynamics Specialty Conference*, 7th International Conference on Soil Mechanics and Foundation Engineering, Mexico City, Mexico, August 1969.

79. Seed, H.B. and Idriss, I.M., "Analysis of Soil Liquefaction: Niigata Earthquake", *Journal of the Soil Mechanics and Foundation Division*, ASCE, Vol. 93, No. SM3, Proc. Paper 5233, May 1967, pp 83-108.

80. Seed, H.B., Idriss, I.M. and Kiefer, F.W., "Characteristics of Rock Motions During Earthquakes", *EERC Report No. 68-5*, Earthquake Engineering Research Center, University of California, Berkeley, Calif., September 1968.

81. Seefired, K.J., Gesund, H. and Pincus, G., "An Experimental Investigation of the Strain Distribution in the Split Cylinder Test", *Journal of Materials*, ASTM, Vol. 2, No. 4, December 1967, pp 703-718.

82. Seto, W.W., *Theory and Problems of Mechanical Vibrations*, Schaum Publishing Company, New York, N.Y., 1964.

83. Sezawa, K., "Dispersion of Elastic Waves Propagated on the Surface of Stratified Bodies and on Curved Surfaces", *Bulletin of the Earthquake Research Institute*, Vol. 3, 1927, pp 1-18.

84. Shannon and Wilson, Inc., *Anchorage Area Soil Studies, Alaska*, Report to the U.S. Army Engineer District, Anchorage, Alaska.

85. Skempton, A.W., "Cast in situ Bored Piles in London Clay", *Geotechnique*, Vol. 9, 1959, pp 153-173.

86. Sokolnikoff, I.S., *The Mathematical Theory of Elasticity*, McGraw-Hill Book Company, Inc., New York, N.Y., 1956, pp 79.

87. Suzuki, T., "On the Angle of Incidence of the Initial Motion Observed at Hongo and Mitaka", *Bulletin of the Earthquake Research Institute*, Vol. 10, 1932, pp 517-535.

88. Thomson, W.T., "Transmission of Elastic Waves Through a Stratified Solid Medium", *Journal of Applied Physics*, Vol. 21, February 1950, pp 89-93.

89. Timoshenko, S. and Goodier, J.N., *Theory of Elasticity*, McGraw-Hill Book Company, Inc., New York, N.Y., 1951.

90. Trifunac, M.D., "Response Envelope Spectrum and Interpretation of Strong Earthquake Ground Motion", *Bulletin of the Seismological Society of America*, Vol. 61, No. 2, April 1971, pp 343-356.

91. Trifunac, M.D. and Brune, J.N., "Complexity of Energy Release During the Imperial Valley, California Earthquake of 1940", *Bulletin of the Seismological Society of America*, Vol. 60, No. 1, February 1970, pp 137-160.

92. Tsai, N.C., "Influence of Local Geology on Earthquake Ground Motion", *Ph.D. Thesis*, California Institute of Technology, Pasadena, California, 1969.

93. Wiegel, R.L., ed., *Earthquake Engineering*, Prentice-Hall, Inc., Englewood Cliffs, N.J., 1970.

94. Wilson, E.L., "Structural Analysis of Axisymmetric Solids", *AIAA Journal*, 1965, pp 2269-74.

95. Wilson, E.L. and Clough, R.W., "Dynamic Response by Step-by-Step Analysis", *Proceedings*, Symposium on the Use of Computers in Civil Engineering, held in Lisbon, Portugal, Paper No. 45, October 1962, pp 45.1 - 45.14.

96. Yamahara, H., "Ground Motions during Earthquakes and the Input Loss of Earthquake Power to an Excitation of Buildings", *Soils and Foundations*, Vol. 10, No. 2, June 1970, pp 145-161.

97. Zeevaert, L., "Strong Ground Motions Recorded During Earthquakes of May the 11th and 19th, 1962 in Mexico City", *Bulletin of the Seismological Society of America*, Vol. 54, No. 1, February 1964, pp 209-231.

98. Zienkiewicz, O.C., *The Finite Element Method in Engineering Science*, McGraw-Hill Book Company Inc., London, England, 1971.

APPENDIX A

SOIL LAYER RESPONSE DUE TO THE PROPAGATION OF RAYLEIGH WAVES

This appendix outlines a method to evaluate the transfer functions for layer response during an earthquake as a result of the propagation of Rayleigh waves through a layered soil system. The Thomson-Haskell matrix formulation technique is extended to solve the problem of the seismic response of soil layers.

A-1 EQUATIONS OF MOTION FOR AN ELASTIC MEDIUM

In order to derive the equations of motion for an elastic medium it is required to consider the equilibrium of a small element as shown in Figure A-1 [75,89]. The equations of motion may be written in terms of stresses, assuming that there are no body forces

$$\rho \frac{\partial^2 u}{\partial t^2} = \frac{\partial \sigma_{xx}}{\partial x} + \frac{\partial \tau_{xy}}{\partial y} + \frac{\partial \tau_{xz}}{\partial z}$$

$$\rho \frac{\partial^2 v}{\partial t^2} = \frac{\partial \tau_{xy}}{\partial x} + \frac{\partial \sigma_{yy}}{\partial y} + \frac{\partial \tau_{yz}}{\partial z} \qquad \text{(A:1)}$$

$$\rho \frac{\partial^2 w}{\partial t^2} = \frac{\partial \tau_{xz}}{\partial x} + \frac{\partial \tau_{yz}}{\partial y} + \frac{\partial \sigma_{zz}}{\partial z}$$

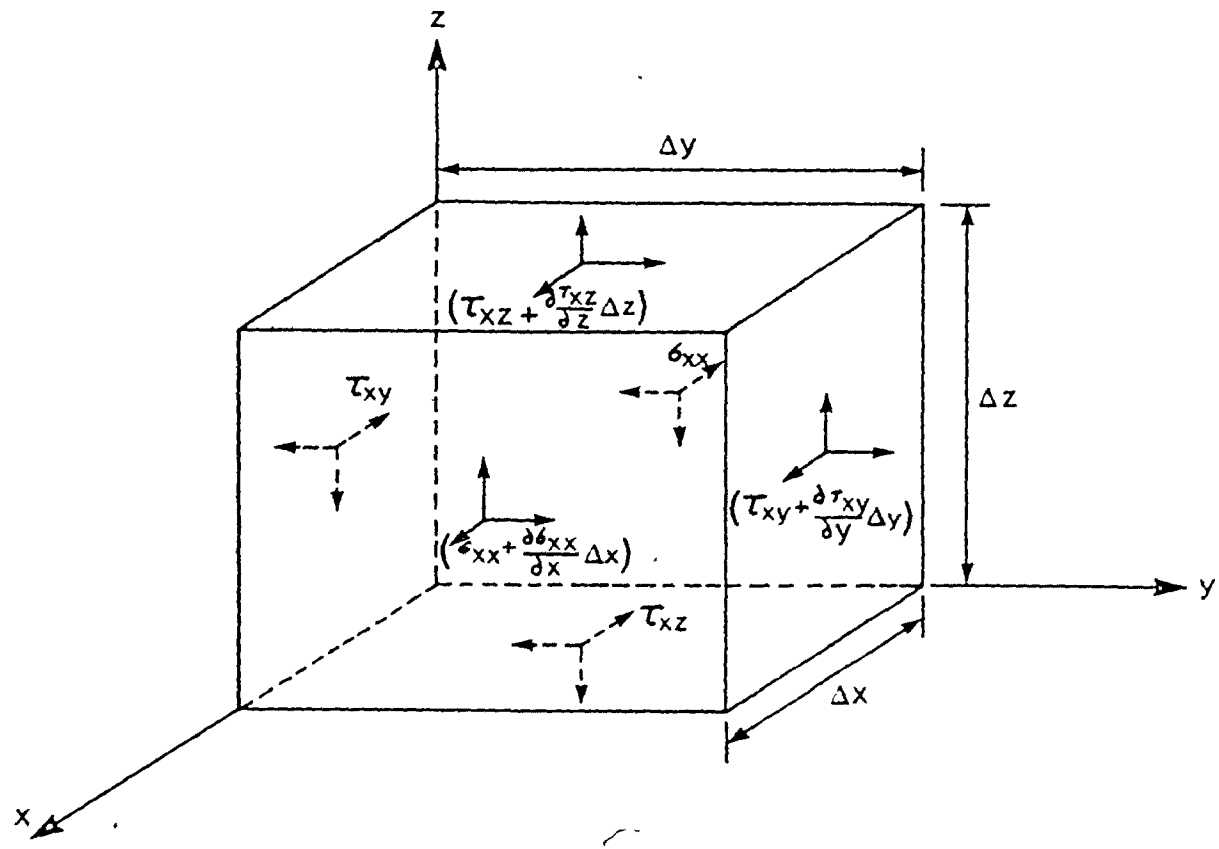

FIG. A-1 STRESSES ON AN ELEMENT

The relationships between stresses and displacements are

$$\begin{aligned}
\sigma_{xx} &= \lambda e + 2 G \epsilon_{xx} \\
\sigma_{yy} &= \lambda e + 2 G \epsilon_{yy} \\
\sigma_{zz} &= \lambda e + 2 G \epsilon_{zz} \\
\tau_{xy} &= G \gamma_{xy} \\
\tau_{yz} &= G \gamma_{yz} \\
\tau_{xz} &= G \gamma_{xz}
\end{aligned} \tag{A:2}$$

where

$$e = \epsilon_{xx} + \epsilon_{yy} + \epsilon_{zz}$$

$$\lambda = \frac{\nu E}{(1+\nu)(1-2\nu)} \quad \text{and} \quad G = \frac{E}{2(1+\nu)}$$

Strains and rotations may be written in terms of displacements

$$\begin{aligned}
\epsilon_{xx} &= \frac{\partial u}{\partial x} \\
\epsilon_{yy} &= \frac{\partial v}{\partial y} \\
\epsilon_{zz} &= \frac{\partial w}{\partial z} \\
\gamma_{xy} &= \frac{\partial v}{\partial x} + \frac{\partial u}{\partial y} \\
\gamma_{yz} &= \frac{\partial w}{\partial y} + \frac{\partial v}{\partial z} \\
\gamma_{xz} &= \frac{\partial u}{\partial z} + \frac{\partial w}{\partial x} \\
\bar{\omega}_x &= \frac{1}{2}\left[\frac{\partial w}{\partial y} - \frac{\partial v}{\partial z}\right] \\
\bar{\omega}_y &= \frac{1}{2}\left[\frac{\partial u}{\partial z} - \frac{\partial w}{\partial x}\right] \\
\bar{\omega}_z &= \frac{1}{2}\left[\frac{\partial v}{\partial x} - \frac{\partial u}{\partial y}\right]
\end{aligned} \tag{A:3}$$

where $\bar{\omega}$ is the rotation about each axis and e is the volume expansion. From Equations A:1 to A:3, the following relationships may be established:

$$\rho \frac{\partial^2 u}{\partial t^2} = (\lambda + G) \frac{\partial e}{\partial x} + G \nabla^2 u$$

$$\rho \frac{\partial^2 v}{\partial t^2} = (\lambda + G) \frac{\partial e}{\partial y} + G \nabla^2 v \qquad \text{(A:4)}$$

$$\rho \frac{\partial^2 w}{\partial t^2} = (\lambda + G) \frac{\partial e}{\partial z} + G \nabla^2 w$$

Differentiating e with respect to x

$$\frac{\partial e}{\partial x} = \frac{\partial}{\partial x} \left(\frac{\partial u}{\partial x} + \frac{\partial v}{\partial y} + \frac{\partial w}{\partial z}\right)$$

$$= \left(\frac{\partial^2 u}{\partial x^2} + \frac{\partial^2 u}{\partial y^2} + \frac{\partial^2 u}{\partial z^2}\right) + \frac{\partial}{\partial y} \left(\frac{\partial v}{\partial x} - \frac{\partial u}{\partial y}\right) + \frac{\partial}{\partial z} \left(\frac{\partial w}{\partial x} - \frac{\partial u}{\partial z}\right)$$

$$= \nabla^2 u + 2 \frac{\partial \bar{\omega}_z}{\partial y} - 2 \frac{\partial \bar{\omega}_y}{\partial z} \qquad \text{(A:5)}$$

or

$$\nabla^2 u = \frac{\partial e}{\partial x} - 2 \frac{\partial \bar{\omega}_z}{\partial y} + 2 \frac{\partial \bar{\omega}_y}{\partial z} \qquad \text{(A:6)}$$

The substitution of Equation A:6 into A:4 yields

$$\rho \frac{\partial^2 u}{\partial t^2} = (\lambda + 2G) \frac{\partial e}{\partial x} + 2G \frac{\partial \bar{\omega}_y}{\partial z} - 2G \frac{\partial \bar{\omega}_z}{\partial y} \qquad \text{(A:7-a)}$$

and in a similar way

$$\rho \frac{\partial^2 v}{\partial t^2} = (\lambda + 2G) \frac{\partial e}{\partial y} + 2G \frac{\partial \bar{\omega}_z}{\partial x} - 2G \frac{\partial \bar{\omega}_x}{\partial z} \qquad \text{(A:7-b)}$$

$$\rho \frac{\partial^2 w}{\partial t^2} = (\lambda + 2G) \frac{\partial e}{\partial z} + 2G \frac{\partial \bar{\omega}_x}{\partial y} - 2G \frac{\partial \bar{\omega}_y}{\partial x} \qquad \text{(A:7-c)}$$

For a plane wave travelling in the x direction, the particle displacements are not dependent on the y direction. Thus, the displacements u and w depend on x and z and hence they may be written in terms of two potential functions $\phi(x,z)$ and $\psi(x,z)$ such that

$$u = \frac{\partial\phi}{\partial x} + \frac{\partial\psi}{\partial z}$$

$$w = \frac{\partial\phi}{\partial z} - \frac{\partial\psi}{\partial x} \qquad \text{(A:8)}$$

The dilatation and rotation also may be expressed as functions of ϕ and ψ

$$e = \frac{\partial u}{\partial x} + \frac{\partial w}{\partial z} = \frac{\partial}{\partial x}\left(\frac{\partial\phi}{\partial x} + \frac{\partial\psi}{\partial z}\right) + \frac{\partial}{\partial z}\left(\frac{\partial\phi}{\partial z} - \frac{\partial\psi}{\partial x}\right) = \nabla^2\phi$$

$$2\bar{\omega}_y = \frac{\partial u}{\partial z} - \frac{\partial w}{\partial x} = \frac{\partial}{\partial z}\left(\frac{\partial\phi}{\partial x} + \frac{\partial\psi}{\partial z}\right) - \frac{\partial}{\partial x}\left(\frac{\partial\phi}{\partial z} - \frac{\partial\psi}{\partial x}\right) = \nabla^2\psi \qquad \text{(A:9)}$$

By substituting values of e and $\bar{\omega}_y$ from Equation A:9, Equations A:7-a and A:7-c may be written

$$\rho\frac{\partial}{\partial x}\left(\frac{\partial^2\phi}{\partial t^2}\right) + \rho\frac{\partial}{\partial z}\left(\frac{\partial^2\psi}{\partial t^2}\right) = (\lambda + 2G)\frac{\partial}{\partial x}(\nabla^2\phi) + G\frac{\partial}{\partial z}(\nabla^2\psi)$$

$$\rho\frac{\partial}{\partial z}\left(\frac{\partial^2\phi}{\partial t^2}\right) - \rho\frac{\partial}{\partial x}\left(\frac{\partial^2\psi}{\partial t^2}\right) = (\lambda + 2G)\frac{\partial}{\partial z}(\nabla^2\phi) - G\frac{\partial}{\partial x}(\nabla^2\psi) \qquad \text{(A:10)}$$

The relationships given by Equation A:10 are satisfied if

$$\frac{\partial^2\phi}{\partial t^2} = \left(\frac{\lambda + 2G}{\rho}\right)\nabla^2\phi = \alpha^2\nabla^2\phi$$

$$\frac{\partial^2\psi}{\partial t^2} = \left(\frac{G}{\rho}\right)\nabla^2\psi = \beta^2\nabla^2\psi \qquad \text{(A:11)}$$

The x dependence on the two functions $\phi(x,z)$ and $\psi(x,z)$ may be determined using the wave equation for x-direction motion of the wave

$$\frac{\partial^2 u}{\partial t^2} = c^2 \frac{\partial^2 u}{\partial x^2} \tag{A:12}$$

which may be resolved by the method of separation of variables

$$u = [C_1 \exp(ikx) + C_2 \exp(-ikx)][C_3 \exp(ikct) + C_4 \exp(-ikct)] \tag{A:13-a}$$

A solution that allows the amplitude of the wave becoming infinite as x increases is not acceptable; also, if only the wave that travels in the positive direction of the x axis is considered, then

$$u = C \exp[ik(ct-x)] \tag{A:13-b}$$

A close look at the relationship between ϕ, ψ and x reveals that the term in x in either ϕ or ψ is $\exp[ik(ct-x)]$. Then ϕ and ψ may be expressed

$$\begin{aligned} \phi &= F(z) \exp[ik(ct-x)] \\ \psi &= G(z) \exp[ik(ct-x)] \end{aligned} \tag{A:14}$$

If the expressions for ϕ and ψ in Equation A:14 are substituted in Equation A:11, the resulting expressions are:

$$\begin{aligned} -\frac{k^2c^2}{\alpha^2} F(z) &= -k^2 F(z) + F''(z) \\ -\frac{k^2c^2}{\beta^2} G(z) &= -k^2 G(z) + G''(z) \end{aligned} \tag{A:15}$$

or

$$F''(z) - k^2 (1 - c^2/\alpha^2)\, F(z) = 0$$

$$G''(z) - k^2 (1 - c^2/\beta^2)\, G(z) = 0 \qquad \text{(A:16)}$$

where $F''(z)$ and $G''(z)$ are derivatives with respect to z. Letting

$$q^2 = k^2 (1 - c^2/\alpha^2)$$

$$s^2 = k^2 (1 - c^2/\beta^2) \qquad \text{(A:17)}$$

the solutions of Equation 16 are

$$F(z) = C_1 \exp(-qz) + C_2 \exp(qz)$$

$$G(z) = C_3 \exp(-sz) + C_4 \exp(sz) \qquad \text{(A:18)}$$

and then

$$\Phi = [C_1 \exp(-qz) + C_2 \exp(qz)] \exp[ik(ct-x)]$$

$$\Psi = [C_3 \exp(-sz) + C_4 \exp(sz)] \exp[ik(ct-x)] \qquad \text{(A:19)}$$

From Equation A:17,

$$q = ik\, r_a$$

$$s = ik\, r_b \qquad \text{(A:20)}$$

where

$$r_a = [(c^2/\alpha^2) - 1]^{1/2} \qquad \text{if } c > \alpha$$

$$= -i[1 - (c^2/\alpha^2)]^{1/2} \qquad c < \alpha \qquad \text{(A:21-a)}$$

and

$$r_b = [(c^2/\beta^2) - 1]^{1/2} \qquad \text{if } c > \beta$$

$$= -i[1 - (c^2/\beta^2)]^{1/2} \qquad c < \beta \qquad \text{(A:21-b)}$$

Substituting for Φ and ψ in Equation A:9 from the expressions in Equation A:19,

$$e = \nabla^2\Phi = (q^2-k^2)[C_1\exp(-qz) + C_2\exp(qz)]\exp[ik(ct-x)]$$

$$\bar{\omega}_y = \frac{1}{2}\nabla^2\psi = \frac{1}{2}(s^2-k^2)[C_3\exp(-sz) + C_4\exp(sz)]\exp[ik(ct-x)] \qquad \text{(A:22)}$$

which may be rewritten

$$e = [\Delta' \exp(-ik\, r_a z) + \Delta'' \exp(ik\, r_a z)]\exp[ik(ct-x)]$$

$$\bar{\omega}_y = [\omega' \exp(-ik\, r_b z) + \omega'' \exp(ik\, r_b z)]\exp[ik(ct-x)] \qquad \text{(A:23)}$$

where

$$\Delta' = -C_1\, k^2c^2/\alpha^2$$

$$\Delta'' = -C_2\, k^2c^2/\alpha^2$$

$$\omega' = -C_3\, k^2c^2/2\beta^2 \qquad \text{(A:24)}$$

and $$\omega'' = -C_4\, k^2c^2/2\beta^2$$

The functions Φ and ψ take the forms

$$\Phi = -\frac{\alpha^2}{k^2c^2}[\Delta' \exp(-ik\, r_a z) + \Delta'' \exp(ik\, r_a z)]\exp[ik(ct-x)]$$

$$\psi = -\frac{2\beta^2}{k^2c^2}[\omega' \exp(-ik\, r_b z) + \omega'' \exp(ik\, r_b z)]\exp[ik(ct-x)] \qquad \text{(A:25)}$$

The term in Δ' represents a plane wave propagated in the +x direction with amplitude diminishing exponentially in the +z direction when r_a is imaginary and one with its direction of propagation making an angle of $\cot^{-1} r_a$ with the +z direction when r_a is real. Similarly, the term in Δ'' corresponds to a plane wave propagated in the +x direction with amplitude increasing in the +z direction when r_a is imaginary and one with its direction of propagation making an angle of $\cot^{-1} r_a$ with the -z direction when r_a is real. These remarks are applicable to the terms in ω' and ω'' when r_a is replaced by r_b.

The displacements u and w are found from Equation A:8 with substitution for Φ and ψ from Equation A;25

$$u = \frac{\partial\Phi}{\partial x} + \frac{\partial\psi}{\partial z} = \frac{i\alpha^2}{kc^2}[\Delta' \exp(-ik\, r_a z)+\Delta'' \exp(ik\, r_a z)]\exp[ik(ct-x)]$$

$$+ \frac{2i\beta^2 r_b}{kc^2}[\omega' \exp(-ik\, r_b z)-\omega'' \exp(ik\, r_b z)]\exp[ik(ct-x)] \tag{A:26}$$

$$w = \frac{\partial\Phi}{\partial z} - \frac{\partial\psi}{\partial x} = -\frac{i\alpha^2 r_a}{kc^2}[-\Delta' \exp(-ik\, r_a z)+\Delta'' \exp(ik\, r_a z)]\exp[ik(ct-x)]$$

$$- \frac{2i\beta^2}{kc^2}[\omega' \exp(-ik\, r_b z)+\omega'' \exp(ik\, r_b z)]\exp[ik(ct-x)]$$

The dimensionless quantities for velocities ($\dot{u}/c$) and $\dot{w}/c$) are

$$\dot{u}/c = -\frac{\alpha^2}{c^2}[\Delta' \exp(-ik\, r_a z)+\Delta'' \exp(ik\, r_a z)]\exp[ik(ct-x)]$$

$$- \frac{2\beta^2 r_b}{c^2}[\omega' \exp(-ik\, r_b z)-\omega'' \exp(ik\, r_b z)]\exp[ik(ct-x)] \tag{A:27-a}$$

$$\dot{w}/c = \frac{\alpha^2 r_a}{c^2}[-\Delta' \exp(-ik\ r_a z)+\Delta'' \exp(ik\ r_a z)]\ \exp[ik(ct-x)]$$

$$+ \frac{2\beta^2}{c^2}\ [\omega' \exp(-ik\ r_b z)+\omega'' \exp(ik\ r_b z)]\exp[ik(ct-x)] \qquad \text{(A:27-b)}$$

which may be rewritten

$$\dot{u}/c = \frac{\alpha^2}{c^2}\ [-(\Delta'+\Delta'')\ \cos(kr_a z) + i(\Delta'-\Delta'')\ \sin(kr_a z)]\ \exp[ik(ct-x)]$$

$$+rr_b[-(\omega'-\omega'')\ \cos(kr_b z) + i(\omega'+\omega'')\ \sin(kr_b z)]\ \exp[ik(ct-x)]$$

(A:28)

$$\dot{w}/c = \frac{\alpha^2 r_a}{c^2}[-(\Delta'-\Delta'')\ \cos(kr_a z) + i(\Delta'+\Delta'')\ \sin(kr_a z)]\ \exp[ik(ct-x)]$$

$$+r[(\omega'+\omega'')\ \cos(kr_b z) - i(\omega'-\omega'')\ \sin(kr_b z)]\ \exp[ik(ct-x)]$$

where

$$r = 2\ \beta^2/c^2 \qquad \text{(A:29)}$$

From Equation A:2

$$\sigma_{zz} = \rho[(\alpha^2 - 2\ \beta^2)\ \frac{\partial u}{\partial x} + \alpha^2\ \frac{\partial w}{\partial z}]$$

$$\tau_{xz} = \rho\ \beta^2\ (\frac{\partial u}{\partial z} + \frac{\partial w}{\partial x}) \qquad \text{(A:30)}$$

The various derivatives are obtained by differentiating u and w in Equation A:26

$$\frac{\partial u}{\partial x} = \frac{\alpha^2}{c^2}\,[(\Delta' + \Delta'')\cos(kr_a z) - i(\Delta' - \Delta'')\sin(kr_a z)]\exp[ik(ct-x)]$$

$$+ \frac{2\beta^2}{c^2}\,r_b[(\omega' - \omega'')\cos(kr_b z) - i(\omega' + \omega'')\sin(kr_b z)]\exp[ik(ct-x)]$$

$$\frac{\partial w}{\partial z} = \frac{\alpha^2}{c^2}\,r_a^2[(\Delta' + \Delta'')\cos(kr_a z) - i(\Delta' - \Delta'')\sin(kr_a z)]\exp[ik(ct-x)]$$

$$- \frac{2\beta^2 r_b}{c^2}[(\omega' - \omega'')\cos(kr_b z) - i(\omega' + \omega'')\sin(kr_b z)]\exp[ik(ct-x)]$$

(A:31)

$$\frac{\partial u}{\partial z} = \frac{\alpha^2}{c^2}\,r_a[(\Delta' - \Delta'')\cos(kr_a z) - i(\Delta' + \Delta'')\sin(kr_a z)]\exp[ik(ct-x)]$$

$$+ \frac{2\beta^2 r_b^2}{c^2}[(\omega' + \omega'')\cos(kr_b z) - i(\omega' - \omega'')\sin(kr_b z)]\exp[ik(ct-x)]$$

$$\frac{\partial w}{\partial x} = \frac{\alpha^2}{c^2}\,r_a[(\Delta' - \Delta'')\cos(kr_a z) - i(\Delta' + \Delta'')\sin(kr_a z)]\exp[ik(ct-x)]$$

$$- \frac{2\beta^2}{c^2}[(\omega' + \omega'')\cos(kr_b z) - i(\omega' - \omega'')\sin(kr_b z)]\exp[ik(ct-x)]$$

Substituting for the derivatives in Equation A:30 the stresses may be written

$$\sigma_{zz} = -\rho\alpha^2(r-1)[(\Delta' + \Delta'')\cos(kr_a z) - i(\Delta' - \Delta'')\sin(kr_a z)]\exp[ik(ct-x)]$$

$$-\rho c^2 r^2 r_b[(\omega' - \omega'')\cos(kr_b z) - i(\omega' + \omega'')\sin(kr_a z)]\exp[ik(ct-x)]$$

(A:32

$$\tau_{xz} = \rho\alpha^2 r r_a[(\Delta' - \Delta'')\cos(kr_a z) - i(\Delta' + \Delta'')\sin(kr_z z)]\exp[ik(ct-x)]$$

$$-\rho c^2 r(r-1)[(\omega' + \omega'')\cos(kr_b z) - i(\omega' - \omega'')\sin(kr_a z)]\exp[ik(ct-x)] \qquad \text{(A:32-b)}$$

It may be noted that the term exp[ik(ct-x)] is common in all the expressions for the velocites and the stresses and hence may be included in terms such as $(\Delta' + \Delta'')$, $(\Delta' - \Delta'')$, etc. Then the velocities and the stresses are

$$\dot{u}/c = -(\alpha/c)^2 \cos(kr_z z)\,(\Delta' + \Delta'') + i(\alpha/c)^2 \sin(kr_z z)\,(\Delta' - \Delta'')$$

$$-rr_b \cos(kr_b z)\,(\omega' - \omega'') + i\, rr_b \sin(kr_b z)\,(\omega' + \omega'')$$

$$\dot{w}/c = i(\alpha/c)^2 r_a \sin(kr_a z)\,(\Delta' + \Delta'') - (\alpha/c)^2 r_a \cos(kr_a z)\,(\Delta' - \Delta'')$$

$$-ir \sin(kr_b z)\,(\omega' - \omega'') + r\cos(kr_b z)\,(\omega' + \omega'') \qquad \text{(A:33)}$$

$$\sigma = -\rho\alpha^2(r-1)\cos(kr_a z)\,(\Delta' + \Delta'') + i\rho\alpha^2(r-1)\sin(kr_a z)\,(\Delta' - \Delta'')$$

$$-\rho c^2 r^2 r_b \cos(kr_b z)\,(\omega' - \omega'') + i\rho c^2 r^2 r_b \sin(kr_b z)\,(\omega' + \omega'')$$

$$\tau = -i\rho\alpha^2 r r_a \sin(kr_a z)\,(\Delta' + \Delta'') + \rho\alpha^2 r r_a \cos(kr_a z)\,(\Delta' - \Delta'')$$

$$+i\rho c^2 r(r-1)\sin(kr_b z)\,(\omega' - \omega'') - \rho c^2 r(r-1)\cos(kr_b z)\,(\omega' + \omega'')$$

A-2 THOMSON-HASKELL MATRIX FORMULATION

For layered soil strata, the phase velocity, c, of plane Rayleigh waves depends on the frequency, ω, of the source of excitation [22]. Thus, the first step in the computation for Rayleigh waves is the calculation of the phase velocity and a convenient procedure for accomplishing this in the case of elastic layers overlying an elastic half space has been formulated by Thomson [88] and Haskell [37]. A brief outline of the matrix formulation is presented below:

The various layers and interfaces are shown in Figure A-2. The details for the mth layer are obtained by adding a suffix m to various quantities

ρ_m	=	density
h_m	=	thickness of layer
β_m	=	shear wave velocity
α_m	=	dilatational wave velocity
$k = \omega/c = 2\pi/L$	=	wave number
L	=	wave length

$$r_{am} = \begin{cases} +[(c/\alpha_m)^2 - 1]^{1/2} & \text{if } c > \alpha_m \\ -i[1 - (c/\alpha_m)^2]^{1/2} & c < \alpha_m \end{cases}$$

$$r_{bm} = \begin{cases} +[(c/\beta_m)^2 - 1]^{1/2} & \text{if } c > \beta_m \\ -i[1 - (c/\beta_m)^2]^{1/2} & c < \beta_m \end{cases}$$

$$r_m = 2(\beta_m/c)^2$$

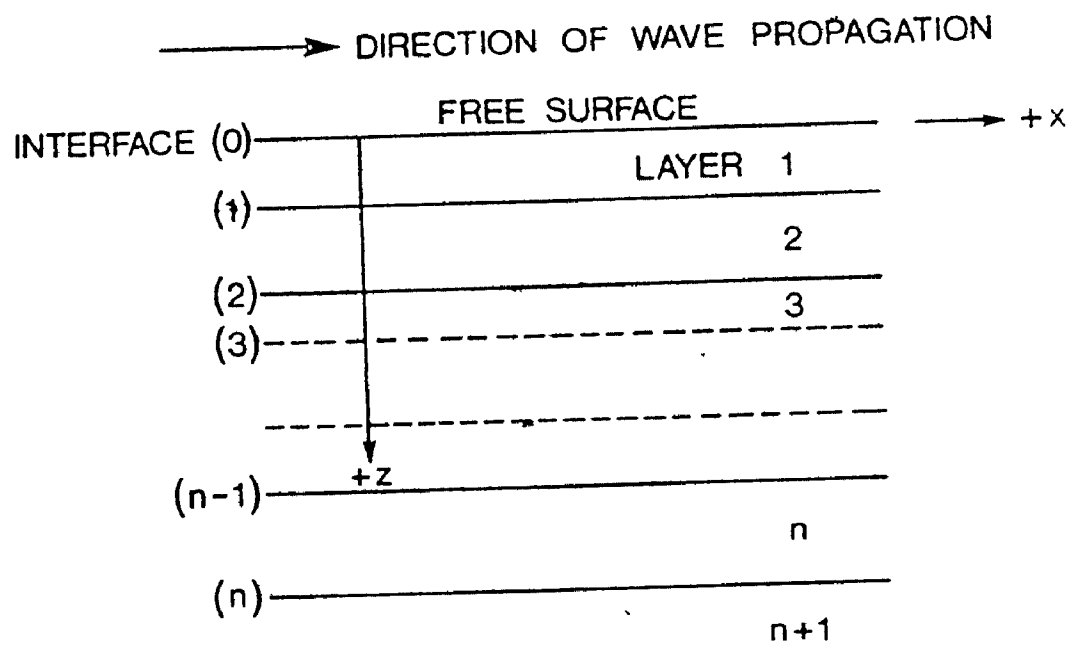

FIG. A-2 LAYERS, INTERFACES AND DIRECTION OF RAYLEIGH WAVE PROPAGATION

The periodic solutions of the elastic equations of motion for the mth layer are obtained from Equation A:23.

$$e_m = [\Delta_m' \exp(-ik\, r_{am} z) + \Delta_m'' \exp(ik\, r_a z)]\exp[ik(ct-x)]$$

$$\omega_m = [\omega_m' \exp(-ik\, r_{bm} z) + \omega_m'' \exp(ik\, r_b z)]\exp[ik(ct-x)] \qquad \text{(A:34)}$$

The expressions for the displacements and the stress components corresponding to Equation A:34 may be reproduced from Equation A:33. At an interface between two layers the four quantities must be continuous. The resulting equations for the bottom of the layer ($z = h_m$) are

$$(\dot{u}_m/c,\ \dot{w}_m/c,\ \sigma_m,\ \tau_m) = [D_m](\Delta_m'+\Delta_m'',\ \Delta_m'-\Delta_m'',\ \omega_m'-\omega_m'',\ \omega_m'+\omega_m'') \qquad \text{(A:35)}$$

where $[D_m]$ is the matrix

$$\left[\begin{array}{c|c|c|c}
-(\alpha_m/c)^2 \cos P_m & i(\alpha_m/c)^2 \sin P_m & -r_m r_{bm} \cos Q_m & i r_m r_{bm} \sin Q_m \\
i(\alpha_m/c)^2 r_{am} \sin P_m & -(\alpha_m/c)^2 r_{am} \cos P_m & -i r_m \sin Q_m & r_m \cos Q_m \\
-\rho_m \alpha_m^2 (r_{m-1}) \cos P_m & i\rho_m \alpha_m^2 (r_{m-1}) \sin P_m & -\rho_m c^2 r_m^2 r_{bm} \cos Q_m & i\rho_m c^2 r_m^2 r_{bm} \sin Q_m \\
-i\rho_m \alpha_m^2 r_m r_{am} \sin P_m & \rho_m \alpha_m^2 r_m r_{am} \cos P_m & i\rho_m c^2 r_m (r_{m-1}) \sin Q_m & -\rho_m c^2 r_m (r_{m-1}) \cos Q_m
\end{array}\right] \qquad \text{(A:36)}$$

with $P_m = k\, r_{am}\, h_m$ and $Q_m = k\, r_{bm}\, h_m$.

At the top of the layer where $z = 0$, the relevant equations are

$$(\dot{u}_{m-1}/c,\ \dot{w}_{m-1}/c,\ \sigma_{m-1},\ \tau_{m-1}) = [E_m](\Delta_m'+\Delta_m'',\ \Delta_m'-\Delta_m'',\ \omega_m'-\omega_m'',\ \omega_m'+\omega_m'') \qquad \text{(A:37)}$$

where $[E_m]$ is the matrix

$$\begin{bmatrix} -(\alpha_m/c^2) & 0 & -r_m r_{bm} & 0 \\ 0 & -(\alpha_m/c)^2 r_{am} & 0 & r_m \\ -\rho_m \alpha_m^2 (r_{m-1}) & 0 & -\rho_m c^2 r_m^2 r_{bm} & 0 \\ 0 & \rho_m \alpha_m^2 r_m r_{am} & 0 & -\rho_m c^2 r_m (r_{m-1}) \end{bmatrix} \qquad \text{(A:38)}$$

The relationship between the state vectors at the top and bottom of the mth layer is expressed by the equation

$$(\dot{u}_m/c,\ \dot{w}_m/c,\ \sigma_m,\ \tau_m)=[D_m][E_m^{-1}](\dot{u}_{m-1}/c,\ \dot{w}_{m-1}/c,\ \sigma_{m-1},\ \tau_{m-1}) \qquad \text{(A:39)}$$

where $[E_m^{-1}]$ is the inverse of $[E_m]$ and is the matrix

$$\begin{bmatrix} -2(\beta_m/\alpha_m)^2 & 0 & (\rho_m \alpha_m^2)^{-1} & 0 \\ 0 & c^2(r_{m-1})/\alpha_m^2 r_{am} & 0 & (\rho_m \alpha_m^2 r_{am})^{-1} \\ (r_{m-1}) r_m^{-1} r_{bm}^{-1} & 0 & -(\rho_m c^2 r_m r_{bm})^{-1} & 0 \\ 0 & 1 & 0 & (\rho_m c^2 r_m)^{-1} \end{bmatrix} \qquad \text{(A:40)}$$

and the elements of the matrix $[a_m] = [D_m]\ [E_m^{-1}]$ are given in Equation A:41.

$$(a_m)_{11} = r_m \cos P_m - (r_{m-1}) \cos Q_m$$

$$(a_m)_{12} = i[(r_{m-1})r_{am}^{-1} \sin P_m + r_m r_{\beta m} \sin Q_m]$$

$$(a_m)_{13} = -(\rho_m c^2)^{-1} (\cos P_m - \cos Q_m)$$

$$(a_m)_{14} = i\,(\rho_m c^2)^{-1} (r_{am}^{-1} \sin P_m + r_{\beta m} \sin Q_m)$$

$$(a_m)_{21} = -i[r_m r_{am} \sin P_m + (r_{m-1})\, r_{\beta m}^{-1} \sin Q_m]$$

$$(a_m)_{22} = -(r_{m-1}) \cos P_m + r_m \cos Q_m$$

$$(a_m)_{23} = i\,(\rho_m c^2)^{-1} (r_{am} \sin P_m + r_{\beta m}^{-1} \sin Q_m)$$

$$(a_m)_{24} = (a_m)_{13} \qquad \text{(A:41)}$$

$$(a_m)_{31} = \rho_m c^2\, r_m\, (r_{m-1})(\cos P_m - \cos Q_m)$$

$$(a_m)_{32} = i\,\rho_m c^2[(r_{m-1})^2\, r_{am}^{-1} \sin P_m + r_m^2\, r_{\beta m} \sin Q_m]$$

$$(a_m)_{33} = (a_m)_{22}$$

$$(a_m)_{34} = (a_m)_{12}$$

$$(a_m)_{41} = i\,\rho_m c^2\, [r_m^2\, r_{am} \sin P_m + (r_{m-1})^2\, r_{\beta m}^{-1} \sin Q_m]$$

$$(a_m)_{42} = (a_m)_{31}$$

$$(a_m)_{43} = (a_m)_{21}$$

$$(a_m)_{44} = (a_m)_{11}$$

By repeated applications of Equation A:39 the following sets of equations may be established.

$$(\dot{u}_m/c, \dot{w}_m/c, \sigma_m, \tau_m) = [a_m](\dot{u}_{m-1}/c,\ \dot{w}_{m-1}/c,\ \sigma_{m-1},\ \tau_{m-1})$$

$$= [a_m][a_{m-1}](\dot{u}_{m-2}/c,\ \dot{w}_{m-2}/c,\ \sigma_{m-2},\ \tau_{m-2})$$

$$= [a_m][a_{m-1}][a_{m-2}](\dot{u}_{m-3}/c,\ \dot{w}_{m-3}/c,\ \sigma_{m-3},\ \tau_{m-3}) \qquad \text{(A:42)}$$

$$= [a_m][a_{m-1}][a_{m-2}]\ldots[a_1](\dot{u}_0/c,\ \dot{w}_0/c,\ \sigma_0,\ \tau_0)$$

Letting $[A_m] = [a_m][a_{m-1}][a_{m-2}]\ldots.[a_1]$

$$(\dot{u}_m/c,\ \dot{w}_m/c,\ \sigma_m,\ \tau_m) = [A_m]\ (\dot{u}_0/c,\ \dot{w}_0/c,\ \sigma_0,\ \tau_0) \qquad \text{(A:43)}$$

and for the bottommost layer n

$$(\dot{u}_n/c,\ \dot{w}_n/c,\ \sigma_n,\ \tau_n) = [A]\ (\dot{u}_0/c,\ \dot{w}_0/c,\ \sigma_0,\ \tau_0) \qquad \text{(A:44)}$$

by letting $[A] = [A_n]$

Using the inverse of Equation A:37 for the $(n+1)^{th}$ layer which is rock

$$(\Delta'_{n+1}+\Delta''_{n+1},\ \Delta'_{n+1}-\Delta''_{n+1},\ \omega'_{n+1}-\omega''_{n+1},\ \omega'_{n+1}+\omega''_{n+1}) = [E^{-1}_{n+1}][A]\ (\dot{u}_0/c, \dot{w}_0/c, \sigma_0, \tau_0) \qquad \text{(A:45)}$$

In general the surface is stress free and in the case of the earthquake excitation, it may be assumed that there are no sources at infinity. If $[J]$ is the matrix product $[E^{-1}_{n+1}][A]$, then Equation A:45 becomes

$$(\Delta'_{n+1},\ \Delta'_{n+1},\ \omega'_{n+1},\ \omega'_{n+1}) = [J]\ (\dot{u}_0/c,\ \dot{w}_0/c,\ \sigma_0,\ \tau_0) \qquad \text{(A:46)}$$

By eliminating Δ'_{n+1} and ω'_{n+1} in Equation A:46

$$\dot{u}_o/\dot{w}_o = \frac{J_{22} - J_{12}}{J_{11} - J_{21}} = \frac{J_{42} - J_{32}}{J_{31} - J_{41}} \tag{A:47}$$

Using Equation A:40, it is possible to write Equation A:47 in the form

$$-(\dot{u}_o/\dot{w}_o) = F_1/F_2 = F_3/F_4 \tag{A:48}$$

where

$$\begin{aligned}
F_1 &= r_n\, r_{an}\, A_{12} + (r_{n-1})\, A_{22} - r_{an}\, A_{32}/\rho_n c^2 + A_{42}/\rho_n c^2 \\
F_2 &= r_n\, r_{an}\, A_{11} + (r_{n-1})\, A_{21} - r_{an}\, A_{31}/\rho_n c^2 + A_{41}/\rho_n c^2 \\
F_3 &= -(r_{n-1})\, A_{12} + r_n\, r_{bn}\, A_{22} + A_{32}/\rho_n c^2 + r_{bn}\, A_{42}/\rho_n c^2 \\
F_4 &= -(r_{n-1})\, A_{11} + r_n\, r_{bn}\, A_{21} + A_{31}/\rho_n c^2 + r_{bn}\, A_{41}/\rho_n c^2
\end{aligned} \tag{A:49}$$

In the case of Rayleigh waves, the amplitude diminishes with depth and thus r_{an} and r_{bn} must be imaginary. Thus, the phase velocity must be less than the shear wave velocity in the base rock, β_{n+1}. Then all terms in F_1 and F_4 are real and all terms in F_2 and F_3 are imaginary. The ratio $\dot{u}_o/\dot{w}_o$ is always imaginary implying that there exists a phase difference of 90° between the horizontal and vertical displacement components.

A-3 COMPUTATIONAL PROCEDURE FOR WAVE NUMBER

The numerical computation of the wave number k corresponding to the phase velocity, c, of Rayleigh waves shall be carried out by a trial and error process. The steps involved in the procedure shall be systematically followed.

1) From available data, tabulate quantities such as Poisson's ratio, mass density, layer thickness and wave velocities of each layer.

2) It is usually convenient to take the thickness h_1 of the first layer as the unit of length, ρ_1 as the unit of density and β_1 as the unit of velocity. The properties of other layers may be expressed in dimensionless form. Then the result of the computation will be a relationship between dimensionless quantities kh_1 and c/β_1.

3) For any phase velocity c, compute the quantities r_m, r_{am} and r_{bm}, P_m, Q_m, etc. for each layer.

4) It is possible to make a preliminary estimate of the value of k for the chosen value of c such that this value may be within an order of magnitude of the correct value. For this purpose, Sezawa's curves [83] for the two-layer case or curves provided by Oliver and Ewing [65] may be used. If the computation is carried out on a computer, k may be given unit value to start with.

5) With the chosen value of c and the assumed value of k, work out the functions F_1, F_2, F_3 and F_4 in Equation (A:49) and the ratios F_1/F_2 and F_3/F_4.

6) If $(F_1/F_2 - F_3/F_4)$ is very small in magnitude compared to F_1/F_2 or F_3/F_4, then the assumed value for k is acceptable.

7) If the difference is significant, then try other values of k and repeat the procedure until it establishes k for the chosen c.

APPENDIX B

FEATURES OF THE IDEALIZED INCLINED PROPAGATION OF SHEAR WAVES

The direction of shear wave propagation is not truly vertical and it has been observed that the angle of incidence of the wave at the surface depends on the surface layer velocity, the epicentral distance of the station and the focal depth. The nature and the magnitude of the emitted waves depend on the incident angle. It is noteworthy that the motions vary not only with the elevations but also with the horizontal distances. The details of the angle of incidence, the emitted waves and the time lags in seismic motions are outlined in this appendix.

B-1 ANGLE OF INCIDENCE OF SHEAR WAVES

The angles of incidence of shear waves in a surface layer with a shear wave velocity of 11200 ft/sec have been computed and are available as a set of tables [8]. These results are based on a theoretical model of the earth and are not quite suitable for nearby locations. However, they are considered to be qualitatively reasonable. The shortest epicentral distance for which these tables are presented is 1350 miles. At this distance, the value for the angle of incidence assumes values of 36.21, 35.67 and 34.67 degrees for focal depths of 0, 25, and 65 miles. It is apparent that the

value has only little dependence on focal depth. Further, the sine of the angle of incidence in a layer is proportional to the wave velocity in it. By allowing a factor of 1.5, the angle of incidence may be assumed as 54 degrees for nearby locations. Then the shear wave velocity $\bar{\beta}$ corresponding to 1° incidence is

$$\underset{\text{(ft/sec)}}{\bar{\beta}} = 11200\ (\sin 1^\circ / \sin 54^\circ) = 240 \qquad \text{(B:1)}$$

The angle of incidence of the shear wave, θ_1 in the surface layer with a wave velocity β_1 is

$$\underset{\text{(degrees)}}{\theta_1} = \sin^{-1}\ (.000072\ \beta_1 \text{ in ft/sec}) \qquad \text{(B:2)}$$

For small angles of incidence, a simplified formula may be used.

$$\underset{\text{(degrees)}}{\theta_1} = \frac{\beta_1 \text{ in ft/sec}}{240} \quad \text{for nearby sites} \qquad \text{(B:3-a)}$$

$$= 0 \quad \text{for distant sites} \qquad \text{(B:3-b)}$$

B-2 AMPLITUDE AND NATURE OF EMITTED WAVES

When a shear wave meets an interface with an angle of inclination to the normal, there are four resultant waves as shown in Figure B-1a. The relationship between the angles at which the resultant waves leave the interface depends on the wave velocities in the two layers.

$$\frac{\sin \theta_1}{\beta_1} = \frac{\sin \theta_2}{\beta_2} = \frac{\sin \theta_3}{\alpha_1} = \frac{\sin \theta_4}{\alpha_2} \qquad \text{(B:4)}$$

where θ_1, θ_2, θ_3 and θ_4 are the angles measured between the normal to

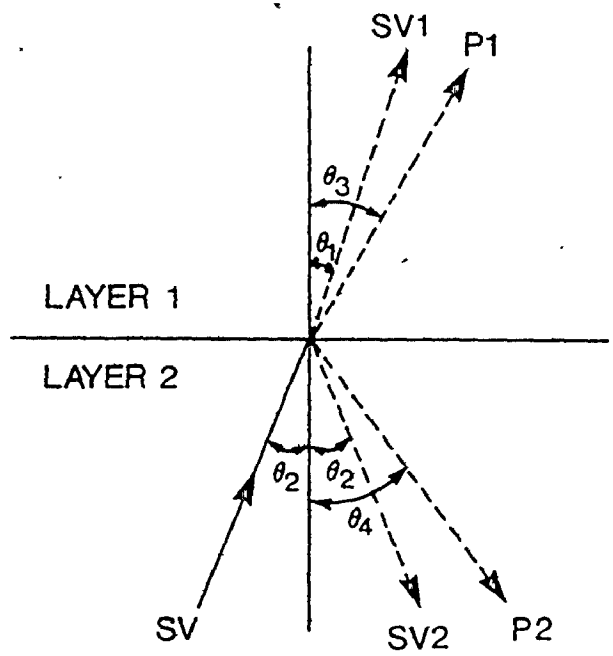

a. DECOMPOSITION OF SHEAR WAVE AT INTERFACE BETWEEN TWO ELASTIC MEDIA

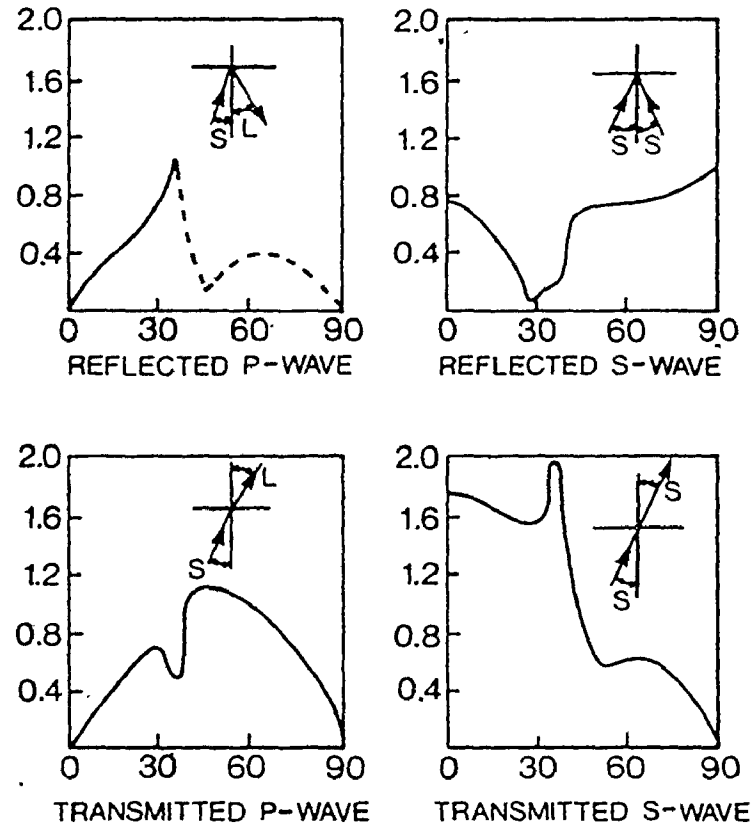

b. RELATION BETWEEN AMPLITUDE RATIO OF EMITTED WAVES AND INCIDENT ANGLE

FIG. B-1 DECOMPOSITION OF SHEAR WAVES WITH INCIDENT ANGLE

the interface and the directions of motions of the transmitted shear wave, the reflected shear wave, the transmitted P-wave and the reflected P-wave respectively. Figure B-1b shows the correlation between the amplitudes of incident and emitted waves when $\beta_2 = 2\beta_1$ [55,75]. When the angle of incidence of a shear wave is small, the amplitude ratios of P-waves become less significant.

If the earthquake response of a layered soil system as a result of the inclined propagation of shear waves is to be computed accurately, then each emitted wave and its inclination at successive reflections and transmissions shall be accounted. This process is not only cumbersome but also impractical. However, because of the relatively low values for the angle of incidence, there is no appreciable error introduced by neglecting the emitted P-waves. Thus, the problem is simplified to one of the wave propagation of shear waves. An idealized path of the shear wave propagation through layered soils is shown in Figure 3-3a.

B-3 VERTICAL TIME LAG IN SHEAR WAVE MOTION

A plane shear wave signal propagating on the xz plane with an angle of incidence reaches two locations at different timings. The time difference in the arrival of the wave at these locations is the vertical time lag between them. Thus, the upward moving wave first reaches the location O_k in Figure 3-3b and a part of the wave is transmitted into the $k-1^{th}$ layer. This transmitted wave proceeds along O_k-O' and reaches O' when all the locations with no time lag with respect to O' such as O_{k-1} get

excited. The vertical time lag between stations O_k and O_{k-1} is the time required for the wave to travel the distance from O_k to O', being $h_k \cos \theta_k$. As the wave velocity in the kth layer is β_k, the time taken by the wave to travel this distance is

$$t_{vk} = \frac{h_k \cos \theta_k}{\beta_k} \tag{B:6}$$

Then t_{vk} is the time lag in the arrival of shear waves between two locations on the same vertical and lying on the top and bottom interfaces of the layer k. It is of interest to note that the magnitudes of time lags for the upward and downward motions in a layer are equal as shown in Figure 3-3b.

B-4 HORIZONTAL TIME LAG IN SHEAR WAVE MOTION

When a shear wave propagates on a plane with an angle of inclination with the vertical, two locations on this plane at the same level and at a horizontal distance apart have a time lag in their motions. For example, locations O_k and P_k which are on the xz plane in Figure 3-3 are at the same level and at a distance d_p apart. Then the motion at O_k at any time t is that at P_k at time $(t + t_{hp})$ where t_{hp} is the time lag between O_k and P_k for wave motions on the xz plane. This horizontal time lag between these two locations is the time required for the wave to travel from the isolag* through O_k to the isolag through P_k. The horizontal time lag t_{hp} between any

*(locus of points having the same time lag in motion)

two stations such as O_k and P_k depends on the distance d_p between them, and $(\sin \theta_1/\beta_1)$ where θ_1 is the angle of incidence in the surface layer and β_1 is the wave velocity in surface layer.

$$t_{hp} = d_p \frac{\sin \theta_1}{\beta_1} \tag{B:7}$$

Once the layered soil system and the wave motions are defined, then the time lag between horizontally equidistant locations remains a constant irrespective of their elevations. Thus, the time lag is a constant for the following pairs of locations in Figure 3-2, namely O_{k-1} and P_{k-1} and O_k and P_k.

APPENDIX C

MATRICES, INTEGRALS AND DERIVATION OF MATRIX EQUATIONS FOR POREPRESSURE PROBLEMS IN AXISYMMETRIC STRUCTURES

Some of the important matrices and all the axisymmetric integrals used in both the static and dynamic analysis of axisymmetric structures under nonsymmetric loading are given in this appendix. The derivation of the matrix equations required to apply the procedure to porepressure problems is also included.

C-1 MATRICES RELATING STRESSES, STRAINS AND DISPLACEMENTS

The matrices [D], [B], $[C^{-1}]$, and $([B]^T[D][B])$ used in the axisymmetric structure analysis are defined

$$[D] = \frac{\nu E}{(1+\nu)(1-2\nu)} \begin{bmatrix} \frac{1-\nu}{\nu} & 1 & 1 & 0 & 0 & 0 \\ 1 & \frac{1-\nu}{\nu} & 1 & 0 & 0 & 0 \\ 1 & 1 & \frac{1-\nu}{\nu} & 0 & 0 & 0 \\ 0 & 0 & 0 & \frac{1-2\nu}{2\nu} & 0 & 0 \\ 0 & 0 & 0 & 0 & \frac{1-2\nu}{2\nu} & 0 \\ 0 & 0 & 0 & 0 & 0 & \frac{1-2\nu}{2\nu} \end{bmatrix} \quad \text{(C:1)}$$

(isotropic)

where

E - Young's modulus

ν - Poisson's ratio

$$[B] = \begin{bmatrix} 0 & 1 & 0 & 0 & 0 & 0 & 0 & 0 & 0 \\ \frac{1}{r} & 1 & \frac{z}{r} & \underline{\frac{n}{r}} & \underline{n} & \underline{n\frac{z}{r}} & 0 & 0 & 0 \\ 0 & 0 & 0 & 0 & 0 & 0 & 0 & 0 & 1 \\ 0 & 0 & 1 & 0 & 0 & 0 & 0 & 1 & 0 \\ \underline{-\frac{n}{r}} & \underline{-n} & \underline{-n\frac{z}{r}} & -\frac{1}{r} & 0 & -\frac{z}{r} & 0 & 0 & 0 \\ 0 & 0 & 0 & 0 & 0 & 1 & \underline{-\frac{n}{r}} & \underline{-n} & \underline{-n\frac{z}{r}} \end{bmatrix} \qquad (C:2)$$

where

r and z are the coordinates

n is the harmonic

Note:- The matrix is applicable to symmetric harmonic

For antisymmetric harmonic, all underlined elements shall be changed in sign.

$$[C]^{-1} = \frac{1}{||A||} \times$$

$$\begin{bmatrix}
r_j z_k - r_k z_j & 0 & 0 & r_k z_i - r_i z_k & 0 & 0 & r_i z_j - r_j z_i & 0 & 0 \\
z_j - z_k & 0 & 0 & z_k - z_i & 0 & 0 & z_i - z_j & 0 & 0 \\
r_k - r_j & 0 & 0 & r_i - r_k & 0 & 0 & r_j - r_i & 0 & 0 \\
0 & r_j z_k - r_k z_j & 0 & 0 & r_k z_i - r_i z_k & 0 & 0 & r_i z_j - r_j z_i & 0 \\
0 & z_j - z_k & 0 & 0 & z_k - z_i & 0 & 0 & z_i - z_j & 0 \\
0 & r_k - r_j & 0 & 0 & r_i - r_k & 0 & 0 & r_j - r_i & 0 \\
0 & & r_j z_k - r_k z_j & 0 & 0 & r_k z_i - r_i z_k & 0 & 0 & r_i z_j - r_j z_i \\
0 & & z_j - z_k & 0 & 0 & z_k - z_i & 0 & 0 & z_i - z_j \\
0 & & r_k - r_j & 0 & 0 & r_i - r_k & 0 & 0 & r_j - r_i
\end{bmatrix} \qquad (C:3)$$

where

$$||A|| = r_i(z_j - z_k) + r_j(z_k - z_i) + r_k(z_i - z_j)$$

$$\{[B]^T\,[D]\,[B]\} = \frac{\nu E}{(1+\nu)(1-2\nu)} \times$$

$\frac{m_1+m_2n^2}{r^2}$	$(\frac{1}{\nu}+m_2n^2)\frac{1}{r}$	$(m_1+m_2n^2)\frac{z}{r^2}$	$\frac{(m_1+m_2)n}{r^2}$	$\frac{m_1 n}{r}$	$(m_1+m_2)\frac{nz}{r^2}$	0	0	$\frac{1}{r}$
	$\frac{2}{\nu}+m_2n^2$	$(\frac{1}{\nu}+m_2n^2)\frac{z}{r}$	$(\frac{n}{\nu}+m_2n)\frac{1}{r}$	$\frac{n}{\nu}$	$(\frac{n}{\nu}+m_2n)\frac{z}{r}$	0	0	2
		$m_2+(m_1+m_2n^2)\frac{z^2}{r^2}$	$(m_1+m_2)\frac{nz}{r^2}$	$\frac{m_1 nz}{r}$	$(m_1+m_2)\frac{nz}{r^2}$	0	m_2	$\frac{z}{r}$
			$\frac{m_1n^2+m_2}{r^2}$	$\frac{m_1n^2}{r}$	$(m_1n^2+m_2)\frac{z}{r^2}$	0	0	$\frac{n}{r}$
				m_1n^2	$m_1n^2\frac{z}{r}$	0	0	n
					$m_2+(m_1n^2+m_2)\frac{z^2}{r^2}$	$\frac{-m_2n}{r}$	$-m_2n$	$(1-m_2)\frac{nz}{r}$
	(S Y M M E T R I C)					$\frac{m_2n^2}{r^2}$	$\frac{m_2n^2}{r^2}$	$\frac{m_2n^2z}{r^2}$
							$m_2(1+n^2)$	$\frac{m_2n^2z}{r}$
								$m_1+\frac{m_2n^2z^2}{r^2}$

(C:4)

where ν = Poisson's ratio, $m = (1/\nu-1)$ and $m = (1/\nu-2)$

This matrix holds for symmetric harmonics; for antisymmetric harmonics, the corresponding matrix is obtained if all underlined elements are changed in sign.

C-2 AXISYMMETRIC INTEGRALS

There are eleven axisymmetric integrals λ_1 to λ_{11} which are often used in the analysis of axisymmetric structures. Only the first six are needed in the static program, while all of them are required in the dynamic analysis. The absolute forms of these integrals are evaluated using Green's Lemma and these are lengthy expressions. However, there are simplified expressions for these integrals which are approximate in the case of λ_4, λ_5, λ_6 and λ_9 to λ_{11}. These approximations are valid under the assumption that the dimension of the cross section of the element is small compared to its radius of revolution. The simplified forms are:

$$\lambda_1 = A\,\bar{r}$$

$$\lambda_2 = A$$

$$\lambda_3 = A\,\bar{z}$$

$$\lambda_4 = A/\bar{r}$$

$$\lambda_5 = A\,\bar{z}/\bar{r}$$

$$\lambda_6 = \frac{A}{12\,\bar{r}}\left[(z_i + z_j)^2 + (z_j + z_k)^2 + (z_k + z_i)^2\right]$$

$$\lambda_7 = \frac{A}{12}\left[(r_i + r_j)^2 + (r_j + r_k)^2 + (r_k + r_i)^2\right] \qquad \text{(C:5)}$$

$$\lambda_8 = A\bar{z}\bar{r}$$

$$\lambda_9 = \frac{A}{24}\left[(r_i + r_j)^3 + (r_j + r_k)^3 + (r_k + r_i)^3\right]$$

$$\lambda_{10} = \frac{A\bar{z}}{12}[(r_i + r_j)^2 + (r_j + r_k)^2 + (r_k + r_i)^2], \text{ and,}$$

$$\lambda_{11} = \frac{A\bar{r}}{12}[(z_i + z_j)^2 + (z_j + z_k)^2 + (z_k + z_i)^2]$$

where

$$2A = r_i(z_j - z_k) + r_j(z_k - z_i) + r_k(z_i - z_j)$$

$$\bar{r} = \frac{1}{3}(r_i + r_j + r_k) \qquad \text{(C:6)}$$

and

$$\bar{z} = \frac{1}{3}(z_i + z_j + z_k)$$

The exact integrals are:

$$\lambda_1 = \iint r\,dr\,dz = -\oint r z\,dr = -\left[\frac{a_1}{2}(r_j^2 - r_i^2) + \frac{b_1}{3}(r_j^3 - r_i^3) + \frac{a_2}{2}(r_k^2 - r_j^2) + \frac{b_2}{3}(r_k^3 - r_j^3) + \frac{a_3}{2}(r_i^2 - r_k^2) + \frac{b_3}{3}(r_i^3 - r_k^3)\right] \qquad \text{(C:7)}$$

$$\lambda_2 = \iint dr\,dz = -\oint z\,dr = -\left[a_1(r_j - r_i) + \frac{b_1}{2}(r_j^2 - r_i^2) + a_2(r_k - r_j) + \frac{b_2}{2}(r_k^2 - r_j^2) + a_3(r_i - r_k) + \frac{b_3}{2}(r_i^2 - r_k^2)\right] \qquad \text{(C:8)}$$

$$\lambda_3 = \iint z\,dr\,dz = -\oint \frac{z^2}{2}\,dr = -\Bigg[\frac{a_1^2}{2}(r_j-r_i) + \frac{a_1 b_1}{2}(r_j^2 - r_i^2)$$

$$+ \frac{b_1^2}{6}(r_j^3-r_i^3) + \frac{a_2^2}{2}(r_k-r_j) + \frac{a_2 b_2}{2}(r_k^2-r_j^2)$$

$$+ \frac{b_2^2}{6}(r_k^3-r_j^3) + \frac{a_3^2}{2}(r_i-r_k) + \frac{a_3 b_3}{2}(r_i^2-r_k^2)$$

$$+ \frac{b_3^2}{6}(r_i^3-r_k^3)\Bigg] \qquad \text{(C:9)}$$

$$\lambda_4 = \iint \frac{1}{r}\,dr\,dz = -\oint \frac{z}{r}\,dr = -\Bigg[a_1 \ln\left(\frac{r_j}{r_i}\right) + b_1(r_j-r_i) + a_2 \ln\left(\frac{r_k}{r_j}\right)$$

$$+ b_2(r_k-r_j) + a_3 \ln\left(\frac{r_i}{r_k}\right) + b_3(r_i-r_k)\Bigg] \qquad \text{(C:10)}$$

$$\lambda_5 = \iint \frac{z}{r}\,dr\,dz = -\oint \frac{z^2}{2r}\,dr = -\Bigg[\frac{a_1^2}{2}\ln\left(\frac{r_j}{r_i}\right) + a_1 b_1(r_j-r_i) + \frac{b_1^2}{4}(r_j^2-r_i^2)$$

$$+ \frac{a_2^2}{2}\ln\left(\frac{r_k}{r_j}\right) + a_2 b_2(r_k-r_j) + \frac{b_2^2}{4}(r_k^2-r_j^2)$$

$$+ \frac{a_3^2}{2}\ln\left(\frac{r_i}{r_k}\right) + a_3 b_3(r_i-r_k) + \frac{b_3^2}{4}(r_i^2-r_k^2)\Bigg] \qquad \text{(C:11)}$$

$$\lambda_6 = \iint \frac{z^2}{r}\, drdz = -\oint \frac{z^3}{3r}\, dr = -\Bigg[\frac{a_1^3}{3}\ln\left(\frac{r_j}{r_i}\right) + a_1^2 b_1\,(r_j - r_i) + \frac{a_1 b_1^2}{2}(r_j^2 - r_i^2) + \frac{b_1^3}{9}(r_j^3 - r_i^3) + \frac{a_2^3}{3}\ln\left(\frac{r_k}{r_j}\right) + a_2^2 b_2\,(r_k - r_j) + \frac{a_2 b_2^2}{2}(r_k^2 - r_j^2) + \frac{b_2^3}{9}(r_k^3 - r_j^3) + \frac{a_3^3}{3}\ln\left(\frac{r_i}{r_k}\right) + a_3^2 b_3\,(r_i - r_k) + \frac{a_3 b_3^2}{2}(r_i^2 - r_k^2) + \frac{b_3^3}{9}(r_i^3 - r_k^3)\Bigg] \qquad \text{(C:12)}$$

$$\lambda_7 = \iint r^2\, drdz = -\oint r^2\, zdr = -\Bigg[\frac{a_1}{3}(r_j^3 - r_i^3) + \frac{b_1}{4}(r_j^4 - r_i^4) + \frac{a_2}{3}(r_k^3 - r_j^3) + \frac{b_2}{4}(r_k^4 - r_j^4) + \frac{a_3}{3}(r_i^3 - r_k^3) + \frac{b_3}{4}(r_i^4 - r_k^4)\Bigg] \qquad \text{(C:13)}$$

$$\lambda_8 = \iint zrdrdz = -\oint \frac{rz^2}{2}\, dr = -\Bigg[\frac{a_1^2}{4}(r_j^2 - r_i^2) + \frac{a_1 b_1}{3}(r_j^3 - r_i^3) + \frac{b_1^2}{8}(r_j^4 - r_i^4) + \frac{a_2^2}{4}(r_k^2 - r_j^2) + \frac{a_2 b_2}{3}(r_k^3 - r_j^3) + \frac{b_2^2}{8}(r_k^4 - r_j^4) + \frac{a_3^2}{4}(r_i^2 - r_k^2) + \frac{a_3 b_3}{3}(r_i^3 - r_k^3) + \frac{b_3^2}{8}(r_i^4 - r_k^4)\Bigg] \qquad \text{(C:14)}$$

$$\lambda_9 = \iint r^3 \, drdz = - \oint r^3 z \, dr = - \left[\frac{a_1}{4}(r_j^4 - r_i^4) + \frac{b_1}{5}(r_j^5 - r_i^5) + \frac{a_2}{4}(r_k^4 - r_j^4) + \frac{b_2}{5}(r_k^5 - r_j^5) + \frac{a_3}{4}(r_i^4 - r_k^4) + \frac{b_3}{5}(r_i^5 - r_k^5) \right] \quad \text{(C:15)}$$

$$\lambda_{10} = \iint r^2 z \, drdz = - \oint \frac{r^2 z^2}{2} \, dr = - \left[\frac{a_1^2}{6}(r_j^3 - r_i^3) + \frac{a_1 b_1}{4}(r_j^4 - r_i^4) + \frac{b_1^2}{10}(r_j^5 - r_i^5) + \frac{a_2^2}{6}(r_k^3 - r_j^3) + \frac{a_2 b_2}{4}(r_k^4 - r_j^4) + \frac{b_2^2}{10}(r_k^5 - r_j^5) + \frac{a_3^2}{6}(r_i^3 - r_k^3) + \frac{a_3 b_3}{4}(r_i^4 - r_k^4) + \frac{b_3^2}{10}(r_i^5 - r_k^5) \right] \quad \text{(C:16)}$$

and,

$$\lambda_{11} = \iint r z^2 \, drdz = - \oint \frac{r z^3}{3} \, dr = - \left[\frac{a_1^3}{6}(r_j^2 - r_i^2) + \frac{a_1^2 b_1}{3}(r_j^3 - r_i^3) + \frac{a_1 b_1^2}{4}(r_j^4 - r_i^4) + \frac{b_1^3}{15}(r_j^5 - r_i^5) + \frac{a_2^3}{6}(r_k^2 - r_j^2) + \frac{a_2^2 b_2}{3}(r_k^3 - r_j^3) + \frac{a_2 b_2^2}{4}(r_k^4 - r_j^4) + \frac{b_2^3}{15}(r_k^5 - r_j^5) + \frac{a_3^3}{6}(r_i^2 - r_k^2) + \frac{a_3^2 b_3}{3}(r_i^3 - r_k^3) + \frac{a_3 b_3^2}{4}(r_i^4 - r_k^4) + \frac{b_3^3}{15}(r_i^5 - r_k^5) \right] \quad \text{(C:17)}$$

where

$$a_1 = z_i - b_1 r_i \qquad b_1 = \frac{z_j - z_i}{r_j - r_i} \quad \text{(C:18)}$$

$$a_2 = z_j - b_2 r_j \qquad b_2 = \frac{z_k - z_j}{r_k - r_j} \quad \text{(C:19)}$$

$$a_3 = z_k - b_3 r_k \qquad b_3 = \frac{z_i - z_k}{r_i - r_k} \quad \text{(C:20)}$$

When any radius is zero, the corresponding logarithm becomes infinite; however, the limit of such terms as determined using L'Hospital's rule is zero. Whenever a radius is zero, the corresponding logarithmic term should be deleted. When two radial coordinates of an element are equal, apparently a and b constants become infinite. In these cases, the line integration is not required and the constants should be set to zero.

For the triangular ring element with coordinates (2,1), (7,3) and (4,7), the values of these integrals were obtained using both the lengthy expressions as well as the simplified forms. These are given in Table C-1 for comparison purposes.

TABLE C-1

COMPARISON BETWEEN THE EXACT AXISYMMETRIC INTEGRALS AND THEIR SIMPLIFIED FORMS

Element	Integral	Exact Value	Value Obtained Using The Simplified Expressions
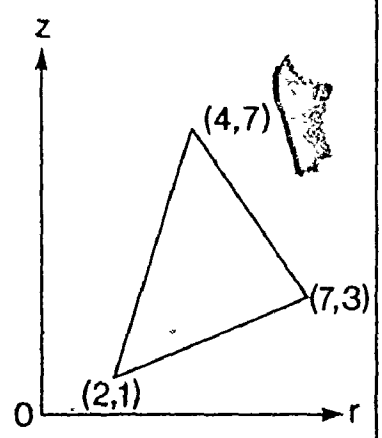	λ_1	56.33	56.33
	λ_2	13.00	13.00
	λ_3	47.68	47.68
	λ_4	3.1	3.00
	λ_5	11.12	11.00
	λ_6	45.45	45.00
	λ_7	257.83	257.83
	λ_8	210.67	210.67
	λ_9	1237.02	1232.83
	λ_{10}	968.40	945.39
	λ_{11}	863.10	845.00

C-3 AXISYMMETRIC FINITE ELEMENT FORMULATION FOR NONSYMMETRIC LOADING IN INCOMPRESSIBLE MATERIALS

The finite element program suitable for nonsymmetric loading of axisymmetric structures with incompressible materials involves total and effective stresses and strains. The total stresses $\{\sigma\}$, the effective stresses $\{\bar{\sigma}\}$, the pore fluid stresses $\{\zeta\}$ and the strains $\{\varepsilon\}$ may be expressed as

$$\{\sigma\}^T = (\sigma_{rr}, \sigma_{\theta\theta}, \sigma_{zz}, \tau_{rz}, \tau_{r\theta}, \tau_{z\theta}) \tag{C:21}$$

$$\{\bar{\sigma}\}^T = (\bar{\sigma}_{rr}, \bar{\sigma}_{\theta\theta}, \bar{\sigma}_{zz}, \tau_{rz}, \tau_{r\theta}, \tau_{z\theta}) \tag{C:22}$$

$$\{\zeta\}^T = (\zeta, \zeta, \zeta, 0, 0, 0) \tag{C:23}$$

$$\{\varepsilon\}^T = (\varepsilon_{rr}, \varepsilon_{\theta\theta}, \varepsilon_{zz}, \gamma_{rz}, \gamma_{r\theta}, \gamma_{z\theta}) \tag{C:24}$$

If the initial state of strain is $\{\varepsilon_0\}$, then

$$\{\bar{\sigma}\} = [D]\,(\{\varepsilon\} - \{\varepsilon_0\}) \tag{C:25}$$

where [D] is given by Equation C:1 by replacing the stress constants E and ν by $\bar{E}$ and $\bar{\nu}$.

If the applied surface loads are $\{p\}$ and body forces $\{\bar{b}\}$, $\{u\}$ are the generalized displacements and δ indicates an arbitrarily small increment, then

$$\int_s (\delta\{u\})^T\{p\}\, ds + \int_{vol} (\delta\{u\})^T\{b\}dvol = \int_{vol} (\delta\{\varepsilon\})^T\{\sigma\}dvol$$
$$= \int_{vol} (\delta\{\varepsilon\})^T\{\bar{\sigma}\}\, dvol$$
$$+ \int_{vol} (\delta\{\varepsilon\})^T\{\zeta\}dvol \qquad (C:26)$$

is the principle of virtual work.

For the triangular element,Equation C:26 may be rewritten

$$\int_s (\delta\{u_N\})^T[C^{-1}]^T[A]^T\{p\}ds + \int_{vol} (\delta\{u_N\})^T[C^{-1}]^T[A]^T\{b\}dvol$$

$$= \int_{vol} (\delta\{u_N\})^T[C^{-1}]^T[B]^T\{\bar{\sigma}\}\, dvol - \int_{vol} (\delta\{u_N\})^T[C^{-1}]^T[B]\{\zeta\}dvol \qquad (C:27)$$

which may be reduced to

$$[C^{-1}]^T(\int_s [A]^T\{p\}ds + \int_{vol} [A]^T\{b\}dvol)$$

$$= \int_{vol} [C^{-1}]^T[B]^T[D](\{\varepsilon\} - \{\varepsilon_0\})dvol + \int_{vol} [C^{-1}]^T[B]\{\zeta\}dvol \qquad (C:28)$$

or

$$[C^{-1}]^T(\int_s [A]^T\{p\}ds + \int_{vol} [A]\{b\}dvol + [B]^T[D]\{\varepsilon_0\}dvol)$$

$$= [C^{-1}]^T(\int_{vol} [B]^T[D][B]dvol)[C^{-1}]\{u_N\} + [C^{-1}]^T \int_{vol} [B]^T\{\zeta\}dvol) \qquad (C:29)$$

Let $\{F_N\}$ denote left half side of Equation C:29 and then

$$\{F_N\} = [k]\{u_N\} + [C^{-1}]^T \int_{vol} [B]^T\{\zeta\}dvol \qquad (C:30)$$

In the usual finite element method, the pore fluid stresses are not part of the analysis and then Equation C:30 reduces to

$$\{F_N\} = [k]\{u_N\} \tag{C:31}$$

which is same as Equation 4:13 derived in Section 4-C.

The porepressure ζ within the element is a constant and therefore

$$\frac{\{\zeta\}}{\zeta} = (1 \quad 1 \quad 1 \quad 0 \quad 0 \quad 0) \tag{C:32}$$

Using Equation C:2 for [B], the term due to porepressure in Equation C:31 may be written in terms of $[\bar{B}]$, where

$$[\bar{B}] = [B]^T \frac{\{\zeta\}}{\zeta} \tag{C:33}$$

For the axisymmetric case, $[\bar{B}]$ is given by

$$\underset{1\times 9}{[\bar{B}]^T} = \left[\frac{1}{r} \quad 2\frac{z}{r} \quad \underline{\frac{n}{r}} \quad \underline{n} \quad \underline{\frac{nz}{r}} \quad 0 \quad 0 \quad 1\right] \tag{C:34}$$

and this holds for the case of symmetric harmonics. The same relationship is applicable to antisymmetric harmonic if all underlined terms in Equation C:34 are changed in sign.

The unknowns in the problem are the nodal displacements and the pore pressure. As these quantities are quite different in magnitude, there is a possibility that the matrix equations are ill-conditioned. This problem can be avoided by bringing the two quantities nearer in magnitude. This is achieved by dividing the porepressure by the bulk

modulus $K_B = \bar{E}/3(1-2\,\bar{\nu})$. Then the unknowns are the nodal displacements and H_N, where

$$H_N = \frac{\zeta}{K_B} \tag{C:35}$$

Equation C:30 may then be written as

$$\underset{9\times1}{\{F_N\}} = \underset{9\times9}{[k]}\ \underset{9\times1}{\{u_N\}} + \underset{9\times1}{[k']}\ H_N \tag{C:36}$$

where

$$[k'] = K_B\left([C^{-1}]^T \int_{vol} [\bar{B}]\,dvol\right) \tag{C:37}$$

As there are ten unknowns, there is an additional equation and this is formed by restricting the volume change, e_N. From Equation C:2

$$e_N = \varepsilon_{rr} + \varepsilon_{\theta\theta} + \varepsilon_{zz} = \left[\frac{1}{r}\quad 2\frac{z}{r}\quad \underline{\frac{n}{r}}\quad \underline{n}\quad \underline{\frac{nz}{r}}\quad 0\quad 0\quad 1\right]\left[C^{-1}\right]\{u_N\} \tag{C:38}$$

Equation C:38 holds for loading in the symmetric harmonic while for the antisymmetric harmonic, the underlined terms in Equation C:38 should be changed in sign. Multiplying both sides of Equation C:38 by K_B, the bulk modulus and integrating over the volume

$$K_B \int_{vol} e_N\,dvol = [k']^T\{u_N\} \tag{C:39}$$

where

$$\int_{vol} e_N\,dvol$$

is the specified volume change in the element. For incompressibility this equals zero, but it is possible to specify any volume change.

Combining Equations C:36 and C:39,

$$\left[\begin{array}{c|c} k & k' \\ \hline k'^T & 0 \end{array}\right] \left\{\begin{array}{c} u_N \\ \hline H_N \end{array}\right\} = \left\{\begin{array}{c} F_N \\ \hline K_B \int_{vol} e_N dvol \end{array}\right\} \qquad \text{(C:40)}$$

As there is a zero on the diagonal, triangular ring elements pose a problem in the solution. However, this computational problem can be overcome if quadrilateral elements are used and the porepressure in each element is assumed a constant. There are sixteen unknowns out of which three are the displacements of the interior node. The resulting equations may be written in matrix form:

$$\left\{\begin{array}{c} F_1 \\ \hdashline K_B \int_{vol} e_N dvol \\ \hline F_2 \end{array}\right\} = \left[\begin{array}{c:c|c} k_{11} & & k_{12} \\ (13x13) & & (13x3) \\ \hdashline & 0 & \\ \hline k_{21} & & k_{22} \\ (3x13) & & (3x3) \end{array}\right] \left\{\begin{array}{c} u_1 \\ \hdashline H_N \\ \hline u_2 \end{array}\right\} \qquad \text{(C:41)}$$

which may be condensed as outlined in Section 4-D. The resulting stiffness matrix $[k^*]$ after condensation has no zero on its diagonal.

C-4 HAMILTON'S PRINCIPLE FOR EVALUATING MASS MATRICES

The loads, displacements, velocities, strains and stresses are time-dependent in dynamic problems. Hamilton's principle [71] states that the motion of the dynamic system takes place in such a manner that

$$\delta \int_{t_1}^{t_2} L \, dt = 0 \qquad \text{(C:42)}$$

where L is the Lagrangian function which shall have stationary values at times t_1 and t_2. The Lagrangian function L is given by

$$L = T - U - W \qquad \text{(C:43)}$$

where T is the kinetic energy, U is the strain energy stored in the deflected element and W is the work done by the forces. The kinetic energy T is

$$T = \frac{1}{2} \int_{vol} \rho \; \{\dot{u}\}^T \{u\} \, dvol \qquad \text{(C:44)}$$

From Equations 4:10, 4:11 and C:44, the Lagrangian functional L may be expressed as

$$L = \frac{1}{2} \int_{vol} \rho \; \{\dot{u}\}^T \{u\} \, dvol - \frac{1}{2} \int_{vol} \{\varepsilon\}^T [D] \left(\{\varepsilon\} - \{\varepsilon_0\}\right) dvol$$

$$- \frac{1}{2} \int_{vol} \{u\}^T \{b\} \, dvol - \frac{1}{2} \int_{s} \{u\}^T \{p\} \, ds \qquad \text{(C:45)}$$

where {b} are the body forces, {p} are the surface forces and $\{\varepsilon_0\}$ are the initial strains within the element. For the finite element, the Lagrangian functional may be rewritten

$$L = \frac{1}{2}\left[\int_{vol} \rho\{\dot{u}_N\}^T[C^{-1}]^T[A]^T[A][C^{-1}]\{\dot{u}_N\}dvol\right.$$

$$- \int_{vol} \{u_N\}^T[C^{-1}]^T[B]^T[D][B][C^{-1}]\{u_N\}dvol$$

$$\left. -\{u_N\}^T[C^{-1}]^T \left(\int_{vol} [A]^T\{b\}dvol + \int_{s}[A]^T\{p\}ds + \int_{vol} [B]^T[D]\{\varepsilon_0\}dvol\right)\right]$$

(C:46)

The derivative of the term containing mass density ρ in Equation C:46 may be integrated by parts and then setting limits.

$$\int_{t_1}^{t_2} \delta\{\dot{u}_N\}^T \int_{vol} \rho[C^{-1}]^T[A]^T[A][C^{-1}]\{u_N\}dvol\ dt$$

$$= \left[(\delta\{u_N\})^T \int_{vol} \rho[C^{-1}]^T[A]^T[A][C^{-1}]\{u_N\}dvol\right]_{t_1}^{t_2}$$

$$- \int_{t_1}^{t_2} (\delta\{u_N\})^T \int_{vol} \rho[C^{-1}]^T[A]^T[A][C^{-1}]\{\ddot{u}_N\}dvol\ dt \quad \text{(C:47)}$$

The first term in the right hand side of Equation C:47 is zero because the Lagrangian has stationary values at t_1 and t_2. Then from Equations C:42, C:46, and C:47

$$\delta \int_{t_1}^{t_2} L\, dt = - \int_{t_1}^{t_2} (\delta\{u_N\})^T \left[\int_{vol} \rho[C^{-1}]^T[A]^T[A][C^{-1}]dvol\ \{\ddot{u}_N\} \right.$$

$$+ \int_{vol} [C^{-1}]^T[B]^T[D][B][C^{-1}]dvol\ \{u_N\}$$

$$\left. - [C^{-1}]^T \left(\int_S [A]^T\{p\}ds + \int_{vol} [A]^T\{b\}dvol - \int_{vol} [B][D]\{\varepsilon_0\}dvol \right) \right] \tag{C:48}$$

which reduces to

$$\rho[C^{-1}]^T\left(\int_{vol} [A]^T[A]dvol\right)[C^{-1}]\{\ddot{u}_N\} + [C^{-1}]^T\left(\int_{vol} [B]^T[D][B]dvol\right)[C^{-1}]\{u_N\}$$

$$=[C^{-1}]^T \left(\int_S [A]^T\{p\}ds + \int_{vol} [A]^T\{b\}dvol + \int_{vol} [B]^T[D]\{\varepsilon_0\}dvol \right) \tag{C:49}$$

for an element with constant density throughout the element; or

$$[m]\ \{\ddot{u}_N\} + [k]\ \{u_N\} = \{F_N\} \tag{C:50}$$

C-5 LUMPED MASS MATRIX FOR AN AXISYMMETRIC RING ELEMENT

Triangular Ring Element

$$[m] = \frac{\rho A}{12} \begin{bmatrix} \bar{R}_i & & & & & & & & \\ & \bar{R}_i & & & & & & & \\ & & \bar{R}_i & & & & & & \\ & & & \bar{R}_j & & & & & \\ & & & & \bar{R}_j & & & & \\ & & & & & \bar{R}_j & & & \\ & & & & & & \bar{R}_k & & \\ & & & & & & & \bar{R}_k & \\ & & & & & & & & \bar{R}_k \end{bmatrix} \qquad (C:51)$$

where

ρ is the mass density

A is the area of cross section

$\bar{R}_i = (2r_i + r_j + r_k)$ $\quad \bar{R}_j = (r_i + 2r_j + r_k)$ and $\bar{R}_k = (r_i + r_j + 2r_k)$

Quadrilateral Ring Element

$$[m] = \begin{bmatrix} m_1 & & & & & & & & & & & \\ & m_1 & & & & & & & & & & \\ & & m_1 & & & & & & & & & \\ & & & m_2 & & & & & & & & \\ & & & & m_2 & & & & & & & \\ & & & & & m_2 & & & & & & \\ & & & & & & m_3 & & & & & \\ & & & & & & & m_3 & & & & \\ & & & & & & & & m_3 & & & \\ & & & & & & & & & m_4 & & \\ & & & & & & & & & & m_4 & \\ & & & & & & & & & & & m_4 \end{bmatrix} \qquad (C:52)$$

where

$m_1+m_2+m_3+m_4$ = total mass of the element

and

m_1, for instance, is given by

$$m_1 = \frac{\rho}{48}\left[A_1(9r_1+5r_2+r_3+r_4) + A_4(9r_1+r_2+r_3+5r_4) + \frac{2r_1}{(r_1+r_2+r_3+r_4)}\left\{A_1(3r_1+3r_2+r_3+r_4) + A_2(r_1+3r_2+3r_3+r_4) + A_3(r_1+r_2+3r_3+3r_4) + A_4(3r_1+r_2+r_3+3r_4)\right\}\right] \qquad (C:53)$$